Transport properties of helical Luttinger liquids

Dissertation zur Erlangung des naturwissenschaftlichen Doktorgrades der Julius-Maximilians-Universität Würzburg

vorgelegt von

Florian Geißler

aus Bamberg

Würzburg 2017

Eingereicht am: .....
bei der Fakultät für Physik und Astronomie

1. Gutachter: .....
2. Gutachter: .....
3. Gutachter: .....
der Dissertation

Vorsitzende(r): .....

1. Prüfer: .....
2. Prüfer: .....
3. Prüfer: .....
im Promotionskolloquium

Tag des Promotionskolloquiums: .....

Doktorurkunde ausgehändigt am: .....

Zusammenfassung

Mit der Vorhersage und der experimentellen Entdeckung von topologischen Isolatoren wurde die Grundlage für eine vollkommen neue Art von elektronischen Bauelementen geschaffen. Diese neue Klasse von Materialien zeichnet sich gegenüber herkömmlichen Metallen und Halbleitern durch besondere Transporteigenschaften der Probenoberfläche aus, wobei elektrische Leitung in Randkanälen an den topologischen Grenzflächen des Systems stattfindet. Eine spezielle Form des zweidimensionalen topologischen Isolators stellt der Quanten-Spin-Hall-Zustand dar, welcher in bestimmten Materialien mit starker Spin-Bahn-Kopplung beobachtet werden kann. Die hier auftretenden eindimensionalen Leitungskanäle sind von helikaler Natur, was bedeutet, dass die Orientierung des Spins eines Elektrons und seine Bewegungsrichtung fest miteinander gekoppelt sind. Aufgrund von Symmetrien wie Zeitumkehr ist elastische Rückstreuung an eventuell vorhandenen Störstellen in solchen helikalen Kanälen verboten, sodass elektrische Leitung als nahezu ballistisch betrachtet werden kann. Prinzipiell bieten sich dadurch neue Möglichkeiten zur Konstruktion von energieeffizienten Transistoren, "Spintronik"-Bauelementen, oder zur Erzeugung von speziellen Zuständen, die für den Betrieb eines Quantencomputers benutzt werden könnten.

Die vorliegende Arbeit beschäftigt sich mit den allgemeinen Transporteigenschaften von eindimensionalen, helikalen Randzuständen. Neben dem oben erwähnten topologischen Schutz gibt es zahlreiche Störquellen, die inelastische Rückstreuprozesse induzieren. Die wichtigsten davon werden im Rahmen dieser Dissertation beleuchtet. Entscheidend wirkt hierbei oft die Rolle von Elektron-Elektron-Wechselwirkungen, welche in eindimensionalen Systemen generell von großer Bedeutung ist.

Zunächst werden bewährte Techniken der Festkörperphysik wie etwa Abelsche Bosonisierung (mithilfe derer Wechselwirkungen in einer Raumdimension exakt berücksichtigt werden können), die Theorie von Luttinger Flüssigkeiten, oder die störungstheoretische Renormierungsgruppenanalyse rekapituliert. Diese Methoden werden im Weiteren benutzt, um die Korrekturen zum Leitwert eines helikalen Transportkanals zu berechnen, welche aufgrund von ausgewählten Störungen auftreten können. Ein Fokus liegt hierbei auf dem Zusammenspiel von Wechselwirkungen und Rashba Spin-Bahn-Kopplung als Quelle inelastischer Ein-Teilchen- oder Zwei-Teilchen-Rückstreuung. Mikroskopische Details wie etwa die Existenz einer Impulsobergrenze, welche das Energiespektrum beschränkt, oder die Anwesenheit von wechselwirkungsfreien Spannungskontakten, sind dabei von grundsätzlicher Bedeutung. Die charakteristische Form der vorhergesagten Korrekturen kann dazu dienen, die Struktur und die mikroskopischen Vorgänge im Inneren einer Quanten-Spin-Hall-Probe besser zu verstehen. Ein weiterer grundlegender Mechanismus ist Rückstreuung verursacht durch magnetische Momente. Aus der entsprechenden Analyse der Korrekturen zur Leitfähigkeit ergeben sich interessante Übereinstimmungen mit aktuellen Experimenten in InAs/GaSb Quantentrögen.

Summary

The prediction and the experimental discovery of topological insulators has set the stage for a novel type of electronic devices. In contrast to conventional metals or semiconductors, this new class of materials exhibits peculiar transport properties at the sample surface, as conduction channels emerge at the topological boundaries of the system. In specific materials with strong spin-orbit coupling, a particular form of a two-dimensional topological insulator, the quantum spin Hall state, can be observed. Here, the respective one-dimensional edge channels are helical in nature, meaning that there is a locking of the spin orientation of an electron and its direction of motion. Due to the symmetry of time-reversal, elastic backscattering off interspersed impurities is suppressed in such a helical system, and transport is approximately ballistic. This allows in principle for the realization of novel energy-efficient devices, "spintronic" applications, or the formation of exotic bound states with non-Abelian statistics, which could be used for quantum computing.
The present work is concerned with the general transport properties of one-dimensional helical states. Beyond the topological protection mentioned above, inelastic backscattering can arise from various microscopic sources, of which the most prominent ones will be discussed in this Thesis. As it is characteristic for one-dimensional systems, the role of electron-electron interactions can be of major importance in this context. First, we review well-established techniques of many-body physics in one dimension such as perturbative renormalization group analysis, (Abelian) bosonization, and Luttinger liquid theory. The latter allow us to treat electron interactions in an exact way. Those methods then are employed to derive the corrections to the conductance in a helical transport channel, that arise from various types of perturbations. Particularly, we focus on the interplay of Rashba spin-orbit coupling and electron interactions as a source of inelastic single-particle and two-particle backscattering. It is demonstrated, that microscopic details of the system, such as the existence of a momentum cutoff, that restricts the energy spectrum, or the presence of non-interacting leads attached to the system, can fundamentally alter the transport signature. By comparison of the predicted corrections to the conductance to a transport experiment, one can gain insight about the microscopic processes and the structure of a quantum spin Hall sample. Another important mechanism we analyze is backscattering induced by magnetic moments. Those findings provide an alternative interpretation of recent transport measurements in InAs/GaSb quantum wells.

Contents

1. Introduction and motivation

In 1965, G. Moore, cofounder of the Intel corporation, observed that transistors develop fast enough such that every year twice as many of them can be squeezed on a single chip [Moo65]. As a consequence, both the computational speed and the memory of electronic devices double in a comparable time interval, while at the same time the size of the devices is shrinking. Due to continuous progress in the manufacturing process as well as falling unit costs, Moore anticipated, that such an exponential growth of the transistor count might continue for years to come. Indeed, this trend known as "Moore's law" turned out to reflect the technological progress very accurately. Chip developers, mostly dominated by Intel, managed to keep pace with – or deliberately follow – Moore's law up to now. This constant increase of computational power helped to realize what in 1965 was imagined to be "wonders as home computers", or "personal portable communications equipment" [Moo65, Moo75] at a very short time scale. Transistors are at the heart of computer architecture. A transistor is a basic semiconductor device with the function of amplifying or switching currents in electronic circuits. Modern specimen are usually metal–oxide–semiconductor field-effect transistors (MOSFET), based on silicon. Many of such transistors, put together on a flat semiconductor plate (mostly silicon as well) in the form of logical gates, form an integrated circuit, or "chip". They are the fundamental components of any advanced electronic device, such as (micro-)processors and memory chips. In 2016, a cutting-edge commercial single-chip processor, such as for example the Intel Broadwell-EP Xeon, contains up to 7.2 billion transistors with features of only a few nanometers [Alc16].

This notwithstanding, the pursuit of Moore's law is expected to hit a natural barrier, and come to a halt very soon, approximately within the next decade [Wal16, Sim16]. This is due to the fundamental problem of heat dissipation in the integrated circuits. With transistors being more and more densely packed on the chip panel, waste heat is harder to get rid of. Beyond a certain limit, energy leakage in the transistors will simply cause the device to melt down. Also, at very small scales quantum effects come into play, that in general render conventional transistors ineffective. In a pessimistic scenario, chip technology then would stagnate in the near future. To prevent such a thing from happening, chip producers are eagerly searching for innovations to press ahead with current computer technology. Present challenges demand for mostly mobile devices, supplied by battery, that are expected to be long-lived, and to process an enormous amount of incoming and outgoing information. Microchips of the next generation need to be faster, more energy-efficient, and more compact. Concepts like autonomous driving, virtual reality, intelligent wearables and implants, or also improved encryption or artificial intelligence, will be slowed down drastically, if not even become impossible, without further technological progress. In particular, the field of machine learning relies heavily on hardware-based innovations, as employed techniques like the simulation of artificial neuronal networks are

very power-consuming. A number of recent achievements was possible owing to improved chip technology. For instance, with the help of a newly developed custom chip, the Google software "AlphaGo" was for the first time able to beat the world's top Go-player in a historical encounter in the spring of 2016 [Kni16, Fra16]. Similar learning algorithms are used to create smart machines, that are already capable of outperforming humans in visually recognizing objects in photos and videos, or acoustically comprehend and translate spoken language, at real time [Lin15]. To keep this successful trend going, new ideas of boosting computer technology beyond Moore's law have to be explored. Two paths to achieve this, are to substantially advance the existing technology, for example, by the use of novel materials or spintronic devices, or to change the paradigms of computing as a whole, such as the idea of quantum computing. One class of materials which has appeared to be a promising prospect for both the approaches mentioned above, is represented by topological insulators. In a two-dimensional quantum spin Hall insulator, for instance, one-dimensional helical edge states emerge, that are protected against elastic backscattering by symmetry, and as a consequence, electronic transport is almost ballistic. With heat dissipation minimized that way, one can imagine very energy-efficient circuits made of suchlike topological materials, which in addition provide a high electron mobility. Furthermore, the peculiar locking of spin and momentum of each edge electron allows, in principle, to inject and control spin currents. A hypothetical spintronics device could then operate with spin currents, where the information is transferred by accumulations of spins, instead of electric charges. The basic concept of a spin transistor was hereby explored by Datta and Das [DD90]. Parts of the running device with a zero net charge current, do not radiate any magnetic fields, again boosting the energy performance. Eventually, when combining topological insulators with superconductivity, exotic bound states can emerge at the interfaces, that could in principle be used to perform quantum computing (see more about this point at the end of this Thesis).

1.1. 2D QSH insulators

Matter is generally considered to be in a topologically non-trivial phase, if its electronic surface and bulk properties are significantly different, in contrast to the topologically trivial cases of conventional insulators, semiconductors or metals. In particular, a topological insulator (TI) is characterized by an insulating bulk, and metallic states at its surface. Such systems became first prominent by the experimental discovery and theoretical description of the integer and fractional quantum Hall effect (QHE) [KDP80, Hal82, TSG82, Lau83]. The corresponding state of matter can be classified by means of topological invariants [TKND82, MB07]. Starting from 2005, it was realized that similar topologically insulating phases can arise even in the absence of magnetic fields (different from the QHE), but from strong intrinsic spin-orbit interactions. The existence of metallic edge states is hereby protected by the underlying symmetry of time-reversal (TRS), or by the crystal symmetry itself [Fu11]. Such quantum spin Hall (QSH) insulators were predicted [KM05b, KM05a, BHZ06, FK07, LHQ$^+$08], and later experimentally observed in quantum wells of HgTe/CdTe [KWB$^+$07], as well as in InAs/GaSb bilayers [KDS11, SND$^+$14]. In HgTe/CdTe-based systems, a topologically non-trivial state arises due to an inversion

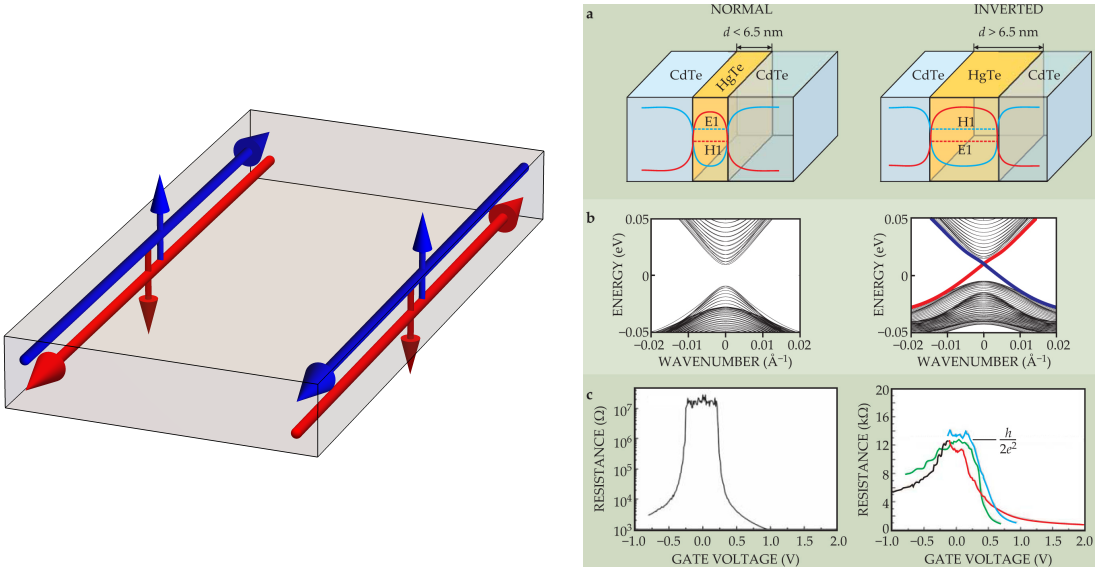

Figure 1.1.: (Left hand side) Sketch of a 2D QSH system. At the 1D boundaries of the sample, helical edge states emerge, with the electron spin locked to the direction of motion. They represent the only transport channels if the Fermi energy is within the bulk band gap. (Right hand side) Formation of a QSH state in HgTe/CdTe quantum wells. Reproduced from Ref. [QZ10], with the permission of the American Institute of Physics. (a) If the central HgTe layer exceeds a given width, a band inversion of the conductance and valence band leads to a topologically non-trivial QSH state. (b) Edge states with an almost linear energy dispersion arise in the band gap. (c) Those can be identified from the longitudinal conductance or resistance of the sample in a transport experiment. For energies within the gap, one finds a small, and quantized resistance in the QSH regime, compared to a very large resistance in the non-topological, insulating regime.

of conductance and valence bands, in case the central HgTe layer exceeds a critical width (see Fig. 1.1). Here, we put the focus on two-dimensional (2D) quantum spin Hall insulators, that feature one-dimensional (1D) edge states at the boundaries of the sample. Note that also three-dimensional (3D) topological insulators, for instance represented by materials such as $Bi_{1-x}Sb_x$, have become the subject of intensive studies in the last years [FKM07, HQW+08].

By virtue of spin-orbit interaction effects, the edge states of a 2D QSH system are of helical nature, meaning that the spin of an electron is strongly coupled to its direction of motion. In the absence of perturbations, the spin is quantized along an axis pointing out of plane. This peculiar helical character, in combination with time-reversal symmetry, results in a protection against elastic backscattering and leads to almost ballistic transport properties (see a further discussion in Sec. 3.3). Furthermore, the energy dispersion relation of the edge electrons is found to be almost linear in momentum, suggesting quasi-relativistic physics. When tuning the Fermi energy such as to lie within the bulk band gap of the 2D QSH system, electronic transport is carried only by the 1D helical edge channels, where each channel contributes the same quantum of e^2/h to the total conductance. The corresponding quantization of the latter can be observed in a transport experiment,

and represents the most important signature of the topological state (see Fig. 1.1). As we discuss in this Thesis, various types of inelastic backscattering mechanisms, that are consistent with TRS, are expected to generate corrections to the quantized value of the conductance in a realistic system, as a function of the applied temperature or the bias voltage. In HgTe/CdTe quantum wells, such corrections have not yet been observed conclusively, but instead, the conductance was found to be almost constant with temperature [KWB$^+$07, RBB$^+$09]. Some possible issues could be: (i) backscattering effects are simply too weak to be identified in the measurements, possibly due to an effective screening of electron interactions in this material, (ii) the use of relatively high currents (bias voltages) hides the temperature dependence of the conductance, (iii) conductance fluctuations mask the measured signal. Those arise for instance from impurity scattering (quantum interference), or potential fluctuations due to trap states and charge accumulations at the interface layers. To overcome such experimental challenges, various approaches are taken: Revised sample fabrication processes such as wet etching, material modifications in the form of strain engineering (which can enhance the bulk band gap), or gate-dependent interface gating can help to improve the quality of the measurement result [BKLB16].
For InAs/GaSb-based quantum wells, on the other hand, some promising observations of correlated electron effects have been made [LWF$^+$15], see more in Chap. 5.

1.2. Selected applications of TIs

To illustrate the potential capacities of topological insulators, we here give a few examples for applications in future devices. First, let us understand how it is possible to generate basic spin currents from all-electric fields in a 2D QSH sample with multiple terminals, as was originally pointed out by the authors of Ref. [KM05a]. Under the assumption that transport between the different contacts of the system is ballistic, one can make use of the Landau-Büttiker formalism [But86, But88]. The charge or spin current, flowing out of (positive sign) or into (negative sign) a terminal with label i and applied bias V_i, is given by [DSS16]

$$I_i^{\mathrm{S/C}} = \sum_j \left(G_{ji}^{\mathrm{S/C}} V_i - G_{ij}^{\mathrm{S/C}} V_j \right). \tag{1.1}$$

Here, the superscripts indicate spin- and charge-related quantities, respectively. The transmission between two contacts is given by the (spin or charge) conductance $G^{\mathrm{S/C}}$, where time-reversal symmetry requires that $G_{ij}^{\mathrm{C}} = G_{ji}^{\mathrm{C}}$ and $G_{ij}^{\mathrm{S}} = -G_{ji}^{\mathrm{S}}$. Let us first consider a simple two-terminal setup, as depicted in Fig. 1.2, top panel. By inspection of the helical conductance channels, and taking into account both the upper and the lower edge, we see that

$$G_{ij}^{\mathrm{C}} = \frac{e^2}{h} \begin{pmatrix} 0 & 2 \\ 2 & 0 \end{pmatrix}_{ij}, \qquad G_{ij}^{\mathrm{S}} = 0. \tag{1.2}$$

There is no net spin transport from the left to the right contact, as the sample provides the same number of channels for both spin directions. Once a positive bias voltage is applied

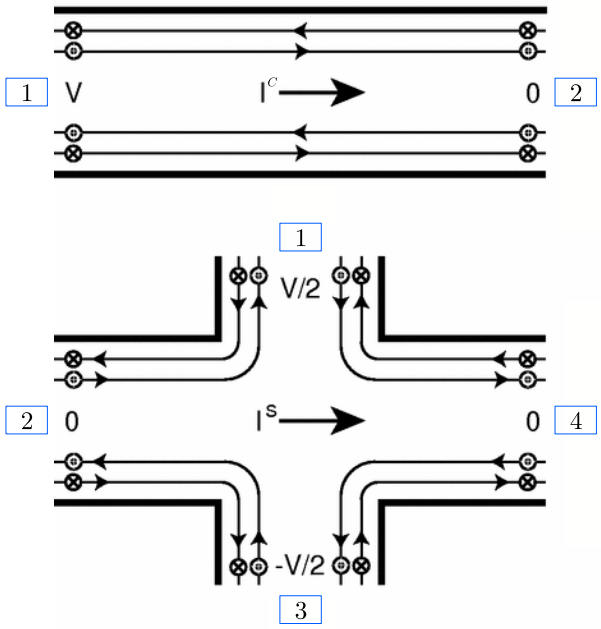

Figure 1.2.: Schematic of a two-terminal (top) and four-terminal (bottom) QSH sample. Edge channels with the electron spins pointing upwards (downwards) are indicated by arrows with dots (crosses). Framed numbers symbolize the terminal labels. Given the plotted voltage drops, a charge current flows to the right in the two-terminal device. For the four-terminal setup, on the other hand, not only a charge current runs from top to bottom, but also a spin current flows to the right. Figure adapted with permission from Ref. [KM05a]. Copyrighted by the American Physical Society.

to the left hand side contact, charge flows to the right, and we obtain with Eq. (1.1),

$$\begin{aligned} I_1^{\mathrm{C}} &= -I_2^{\mathrm{C}} = \frac{2e^2 V}{h}, \\ I_1^{\mathrm{S}} &= I_2^{\mathrm{S}} = 0. \end{aligned} \tag{1.3}$$

Next, we take a look at the four-terminal device presented in Fig. 1.2, bottom panel. The transmission matrices now have the form [KM05a]

$$G_{ij}^{\mathrm{C}} = \frac{e^2}{h} \begin{pmatrix} 0 & 1 & 0 & 1 \\ 1 & 0 & 1 & 0 \\ 0 & 1 & 0 & 1 \\ 1 & 0 & 1 & 0 \end{pmatrix}_{ij}, \qquad G_{ij}^{\mathrm{S}} = \frac{e}{4\pi} \begin{pmatrix} 0 & 1 & 0 & -1 \\ -1 & 0 & 1 & 0 \\ 0 & -1 & 0 & 1 \\ 1 & 0 & -1 & 0 \end{pmatrix}_{ij}. \tag{1.4}$$

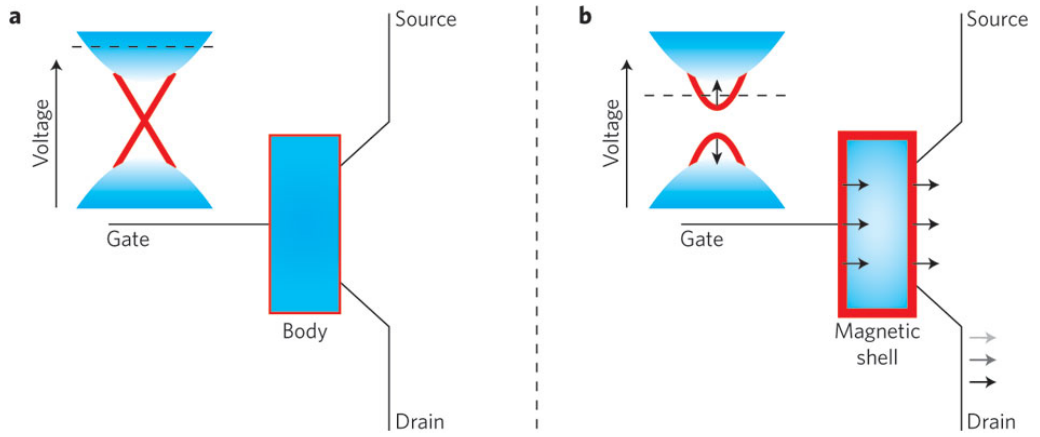

Figure 1.3.: Idea of a TI-based transistor according to Ref. [CYO+12]. A 3D TI doped with a small number of magnetic atoms is used as a transistor body. (a) If the Fermi energy is outside the band gap, transport is carried out by plenty of bulk electrons, and the device behaves like an ordinary metal. (b) If the Fermi energy lies within the bulk band gap, only the surface electrons contribute to electronic transport. They then interact with the magnetic adatoms to form a ferromagnetic shell, and a subgap opens in the energy spectrum. By tuning the gate voltage, the device can operate in different modes, and act as a current switch or spin filter. Figure reprinted by permission from Macmillan Publishers Ltd: [Wra12], copyright 2012.

Applying a bias voltage between the top and the bottom contact, we identify the outgoing and incoming charge and spin currents to be

$$\begin{aligned} I_1^{\mathrm{C}} &= -I_3^{\mathrm{C}} = \frac{e^2 V}{h}, \\ I_2^{\mathrm{S}} &= -I_4^{\mathrm{S}} = \frac{eV}{4\pi}, \\ I_2^{\mathrm{C}} &= I_4^{\mathrm{C}} = I_1^{\mathrm{S}} = I_3^{\mathrm{S}} = 0. \end{aligned} \tag{1.5}$$

As expected, a charge current $I^{\mathrm{C}} = e^2 V/h$ flows from top to bottom. Interestingly, at the same time, a net spin current of $I^{\mathrm{S}} = eV/4\pi$ runs from the left to the right terminal in this setup. Due to spin-momentum locking of the material, and the presence of helical edge states, the electric potential forces the spin-up electrons to accumulate at the right hand side contact. With this basic idea, spin currents can not only be generated, but also detected – a spin current injected between the left and right terminals will vice versa induce a voltage bias drop between the top and bottom contacts.

This concept gives prospects to spintronics applications of topological insulators. In particular, combinations of 3D TIs with magnetic components have appeared to be a promising approach [FW16]. Starting from the electrical detection of charge-current induced spin polarizations at the surface of 3D topological insulators [LvR+14], recent experiments have, for instance, also confirmed the optical control of such spin polarizations [SBGV+16], or the spin-charge conversion in topological surface states, where spin currents were injected with the help of spin pumping techniques [SNK+14, RSOF+16].

Eventually, let us briefly present the idea of a TI-based transistor, as it was for instance pioneered in Ref. [CYO+12]. The authors there use a 3D TI, doped with a very small amount of magnetic Manganese atoms, as a transistor body (see Fig. 1.3). The key idea is the following: If the gate voltage is tuned such that the Fermi energy is outside the TI band gap, bulk electrons are the dominant contributors to electronic transport, and the device behaves like an ordinary semiconductor. As there is a great number of free electrons in this case, the few magnetic impurities are effectively screened. On the other hand, if the Fermi energy is tuned such as to lie within the band gap of the topological insulator, only a small number of surface electrons remain available for transport. Those surface electrons now become spin-polarized due to an interaction with the magnetic impurities, and form a ferromagnetic shell. As a consequence, a small subgap opens within the band gap of the TI (see right hand side of Fig. 1.3). From this analysis it can be understood, that by variation of the applied gate voltage, the device can operate in an effectively metallic or insulating mode, but also in an intermediate regime, where transport takes place via spin-polarized surface states. The presented structure therefore meets all the requirements for the versatile use as a conventional, or a spin transistor.

1.3. Scope of this Thesis

Motivated by the interesting and promising properties of 2D topological insulators, as described above, this Thesis is dedicated to the study of the transport properties of one-dimensional helical states. Despite the topological protection against elastic backscattering, we demonstrate, that various inelastic backscattering processes are possible, or even inevitable at the helical edge. We investigate the corresponding corrections to the conductance, or the breakdown of the latter for certain types of strong perturbations. All the predicted effects on the conductance could in principle be observed in a transport experiment. We furthermore discuss the microscopic sources to induce such backscattering mechanisms, and their behaviour in the presence of electron interactions. In contrast to higher-dimensional systems, interactions in 1D have a great impact on the electronic properties. At the same time, well-established techniques of many-body physics, such as bosonization, allow us to obtain analytical results even for strong interactions. The analysis of transport in 1D helical liquids is therefore also about correlated electron effects. As elastic backscattering is typically suppressed by TRS, the proper treatment of inelastic electron interactions appears to be not only of quantitative, but also of qualitative importance. Those aspects are of crucial interest for the understanding of 1D systems, and for future applications in real materials. For instance, by comparing experimentally observed corrections to the conductance with theoretical predictions, one can obtain information about the microscopic processes, and the structure of a material.
The Thesis is organized as follows: In Chap. 2 we review the theory of (helical) Luttinger liquids, which describes 1D many-body systems including electron interactions, given that the energy-momentum relation can be linearized around the Fermi points. In addition, fundamental techniques such as bosonization, the operator product expansion, or the perturbative RG scheme are outlined. Subsequently, in Chap. 3, we turn to the calculation of the conductance, as the fundamental transport signature of the systems under considera-

tion. The lowest-order generic backscattering processes in the helical liquid are discussed. Chap. 4 is concerned with Rashba spin-orbit coupling (SOC) as a microscopic source of inelastic backscattering. We study the effects of a single impurity, and many disordered spin-orbit coupling impurities, and the respective corrections to the total conductance of the system. The profound ramifications of a momentum cutoff in the model are highlighted. Another important source of backscattering, in the form of magnetic moments (or Kondo impurities), is investigated in Chap. 5. There, we derive the explicit energy-dependence of the conductance in the presence of weak electron interactions, and compare it to a recent experiment in InAs/GaSb bilayers. Eventually, we conclude in Chap. 6, and give a brief outlook on hybrid structures of 2D topological insulators with superconductors. Throughout, we use simplified units by setting $\hbar = 1$, as well as $k_B = 1$.

2. Luttinger liquid theory

Systems of interacting fermions are a notoriously difficult challenge in many-body physics. In two and more spatial dimensions, such systems comply (in most cases) very well with the predictions of Fermi liquid theory, first developed by Landau [Lan57b, Lan57a]. Simply speaking, it states that the low-energy properties of the Fermi electron gas remains qualitatively the same in the presence or absence of interactions. The elementary excitations of the system are long-living quasiparticles, which can be conceived of as individual electrons dressed by particle-hole like excitations of the ground state. Such quasiparticles are still fermionic in nature, and move essentially freely in the metal. This finding allows to account for interactions in the Fermi gas by (diagrammatic) perturbation theory. In one dimension on the other hand, the physical picture is drastically altered. Excitations in 1D are always bosonic in nature, and interactions play a crucial role for the low-energy properties of the system. In contrast to the individual quasiparticles, only collective modes are possible, such as density waves or charge and current excitations. This can be understood pictorially from the fact that no particle can propagate freely without pushing its neighbor. Formally, perturbation theory fails due to a number of divergences of physical quantities, such as the susceptibility in response to an applied electromagnetic potential [Gia03]. As a consequence, there is need for a new model, the so-called Luttinger liquid (LL) theory.

It was realized early on, that a many-body system of interacting (relativistic) 1D fermions can be described, and solved exactly, by mapping it onto a model of free bosons [Tom50, Lut63, ML65]. This transformation is commonly called (Abelian) bosonization. The key idea was provided by Tomonaga in an article of 1950 [Tom50]. Here, the abstract states: "The fact implied by Bloch several years ago that in some approximate sense the behavior of an assembly of Fermi particles can be described by a quantized field of sound waves in the Fermi gas, where the sound field obeys Bose statistics, is proved in the one-dimensional case. This fact provides us with a new possibility of treating an assembly of Fermi particles in terms of the equivalent assembly of Bose particles, namely, the assembly of sound quanta." Tomonaga again refers to a much earlier article by Bloch from 1933 [Blo33], which presumably makes Bloch one of the first to explore the concept of bosonization. The resulting Tomonaga-Luttinger liquid model was later improved and refined significantly, by contributions of Haldane [Hal81a, Hal81b] and many others. Even though bosonization was primarily developed for one-dimensional systems, the concept can be generalized as well to interacting fermions in two dimensions and higher. This technique was used to demonstrate that there exist higher dimensional models, that, depending on the form of the interactions, do not exhibit the typical Fermi liquid, but a Luttinger liquid behaviour [Hal92, KHR93, YLD94].

2.1. Bosonization

2.1.1. General theory

We here recall the bosonization scheme for 1D spinless fermions, following the instructive Ref. [vS98], however, introducing both right- and left-movers from the beginning. Subsequently, we discuss the relation to spinful and helical systems. The bosonization transformation is generally based on a linearization of the energy dispersion, and the assumption of an unbounded spectrum with infinitely many states. As the latter leads to characteristic divergences of fundamental correlation functions, one accounts for this point by the implementation of a cutoff. If the energy dispersion is strictly linear, both the kinetic energy and the interaction terms will be mapped onto bosonic terms with yet again a linear spectrum, which corresponds to (effectively) free bosons. An exact solution of the free bosonic model is then possible. On the other hand, if the original fermionic spectrum is non-linear, bosonization can only succeed in transforming the system into another model of interacting bosons (meaning that bosonic excitations decay), and generally no significant progress is gained. Additionally, such non-linearities usually break particle-hole symmetry. The linear spectrum, as a prerequisite for bosonization, is clearly provided in a 1D gas of relativistic free fermions. In a many-body system of non-relativistic free fermions, the parabolic spectrum needs to be linearized around the Fermi energy (see Fig. 2.1.1). The validity of the model then is limited to a certain range of energy close to this expansion point, which is nevertheless expected to correctly describe the low-energy physics of interest. High energy states not compatible with this approximation have to be excluded by introducing a momentum cutoff, that truncates the spectrum. Note that a bosonization procedure in such a linearized system requires the introduction of "unphysical" positron states [vS98] that, however, do not change the low-energy physics. In order to enhance the power of bosonization, some effort was made to include non-linearities into the bosonization scheme perturbatively. Some findings are, that the low-energy properties still remain the same [Hal81b], and more generally, the Luttinger liquid theory could be considered a special case of a more fundamental non-linear theory [ISG12]. Here, we focus on systems whose energy spectrum is fairly linear in momentum, such as the edge states of 2D quantum spin Hall systems. In that case, there is no need for linearization and difficulties related to the influence of non-linearities do not appear. The implementation of a high-energy cutoff nevertheless remains a physical requirement, as the linear edge states exist only at energies inside the band gap of the topological insulator, while beyond, bulk states will become dominant.
The linear (or linearized) spectrum consists of two branches of opposite slope (chirality) $\pm v_F$, the Fermi surface being two mere points $\pm p_F$ (see Fig. 2.1.1). The kinetic energy is then given by (we here suppress the spin index for the moment)

$$H_0 = \sum_p \varepsilon(p) c_p^\dagger c_p, \tag{2.1}$$

with $\varepsilon(p) = v_F(\pm p - p_F)$. The sign identifies the two separated regions around the Fermi points for $p \gtrless 0$, respectively. Let us introduce the corresponding label $r = \pm 1$. We now

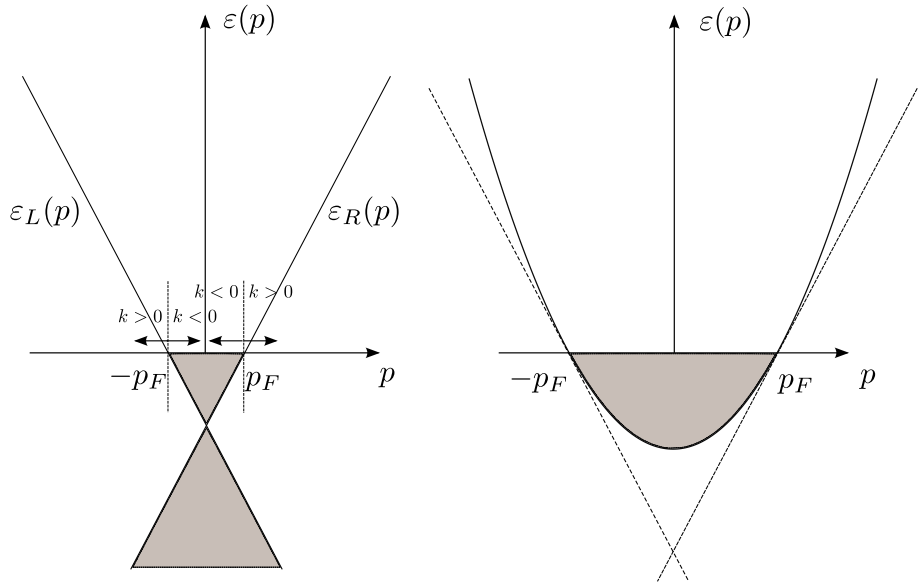

Figure 2.1.: Energy spectrum of the Luttinger liquid, featuring the two branches R/L that indicate right- and left-moving particles. The linear dispersion may either be given naturally (e.g. in the gap of a 2D topological insulator), or emerge from linearization of a parabolic spectrum (right hand side).

define a new momentum k by $p = r(k + p_F)$, such that [1]

$$H_0 = \sum_{k,r=\pm} \varepsilon_r(k) c^\dagger_{r(k+p_F)} c_{r(k+p_F)} = \sum_{k,r=\pm} \varepsilon_r(k) c^\dagger_{r,k} c_{r,k}, \tag{2.2}$$

and simply

$$\varepsilon_r(k) = v_F k. \tag{2.3}$$

Importantly, we have here defined fermionic creation operators for two different species of chiral fermions by the projection $c_{r,k} = c_{r(k+p_F)}$, and in doing so assumed that $|k| \ll p_F$. This defines so-called right-moving and left-moving fermions, where we use equivalently $r = \pm = R/L$. Explicitly, $c^\dagger_{R/L,k}$ creates a fermion with momentum k at one of the branches of chirality R/L. Note that in this notation, both right- and left-moving particles have the same energy dispersion (and do not differ by a sign). As we consider a system of length L, the momentum is in general a quantized number, [2] $k = \frac{2\pi}{L}(n_k - 1/2) = \Omega^{-1}(n_k - 1/2)$, with the volume of the system $\Omega = \frac{L}{2\pi}$ and the integer $n_k \in \mathbb{Z}$. For large systems we are

[1] It is also common to use an alternative parametrization for k, such that $\varepsilon_r(k) = r v_F k$ ([Gia03] etc.). Here, however, we follow closely the notation of Ref. [vS98]. In the later Sec. 4, we adopt a slightly different notation in the context of fermionic perturbation theory.

[2] The term proportional to $1/2$ stems from a choice of boundary conditions, which is an additional subtlety (confer [vS98]). Quite generally, there are periodicities $\psi_r(x) = \psi_r(x+nL)$, with $n \in \mathbb{Z}$, in the definition of $\psi_r(x)$, which can be considered an effective boundary condition $\psi_r(x + L/2) = \psi_r(x - L/2)e^{i\pi\delta_b}$, $\delta_b \in \{0, 1\}$ and $k = \Omega^{-1}(n_k - \frac{1}{2}\delta_b)$. In many cases, and we shall do so here, one chooses somewhat arbitrarily antiperiodic boundaries of the fermionic fields, $\delta_b = 1$, in which case the bosonized free

free to perform the continuum limit $\sum_k = \Omega \int \mathrm{d}k$.
Next, we can define real-space fermionic fields

$$\psi(x) = \frac{1}{\sqrt{\Omega}} \sum_p e^{ipx} c_p = \frac{1}{\sqrt{\Omega}} \sum_{r,k} e^{ir(k+p_F)x} c_{r,k} = \sum_r \psi_r(x) e^{irp_F x}, \tag{2.4}$$

$$\psi_r(x) = \frac{1}{\sqrt{\Omega}} \sum_k e^{irkx} c_{r,k}. \tag{2.5}$$

Here, $\psi(x)$ is the total, physical field, while $\psi_r(x)$ represents the chiral field. The physical requirement of $|k| \ll p_F$ implies, that the decomposed fields $\psi_r(x)$ vary slowly on a scale of $1/p_F$. For future reference, we also have $c_{r,k} = \frac{1}{2\pi\sqrt{\Omega}} \int \mathrm{d}x\, e^{-irkx} \psi_r(x)$. The kinetic energy of Eq. (2.2), in real space takes the form (here not yet normal-ordered, see below)

$$H_0 = \sum_{k,r=R,L} (v_F k) c^\dagger_{r,k} c_{r,k} = \frac{v_F}{2\pi} \sum_{r=R,L} \int_{-L/2}^{L/2} \mathrm{d}x\, \psi^\dagger_r(x)(-ir\partial_x)\psi_r(x). \tag{2.6}$$

Importantly, the field operators fulfill the fermionic anticommutation relations [3]

$$\begin{aligned} \{c_{r,k}, c^\dagger_{r',k'}\} &= \delta_{rr'}\delta_{kk'}, \\ \{c_{r,k}, c_{r',k'}\} &= \{c^\dagger_{r,k}, c^\dagger_{r',k'}\} = 0, \\ \{\psi_r(x), \psi^\dagger_{r'}(x')\} &= 2\pi\delta_{rr'}\delta(x-x'), \\ \{\psi_r(x), \psi_{r'}(x')\} &= \{\psi^\dagger_r(x), \psi^\dagger_{r'}(x')\} = 0. \end{aligned} \tag{2.7}$$

Here, we assumed $|x|, |x'| < L/2$. Note that the Dirac delta distribution only appears in the case of an unbounded spectrum of momenta, as can be seen from Eq. (A.1). If a momentum cutoff is introduced, the delta distribution will be smeared out and therefore, strictly speaking, the usual anticommutation rules do not hold anymore in real space, while in momentum space they remain well-defined. The above observation is a characteristic consequence of introducing a momentum cutoff, and applies to both fermions and bosons. As we show later, it can have physical implications in terms of backscattering.

Bosonization reorganizes the fermionic Fock space in terms of bosonic operators only. Let us briefly sketch the general concept along the lines of Ref. [vS98]. Presume that the vector $|\vec{N}\rangle$ is an eigenstate of the system with eigenvalue $\vec{N} = (N_R, N_L)$, so it contains exactly N_R particles on the right-moving branch, and N_L particles on the left-moving branch. Any of the $N = N_R + N_L$ particles can occupy one of the discrete energy levels, given by the discretization of momenta at finite system length. The set of all such states with the same eigenvalues is then called the N-particle Hilbert space $\mathcal{H}_{\vec{N}}$. The entire Fock

Hamiltonian takes a slightly more simple form. On the other hand, this choice gives an (unimportant) additional factor $e^{-ir\pi x/L}$ in the bosonization identity of Eq. (2.12), which is usually dropped in the limit or large L.

[3] In Ref. [vS98], the notation involves an extra factor of 2π, which comes down to the definition of the volume $\Omega = L/2\pi$. As a result, the fields $\psi_r(x)$ are then normalized to 2π instead of one. See the discussion of different notations below.

space $\mathcal{F}$, spanned by all possible $\{c^\dagger_{r,k},\, c_{r',k'}\}$ operators, can generally be rewritten as a sum of N-particle Hilbert spaces $\mathcal{F} = \sum_{\oplus \vec{N}} \mathcal{H}_{\vec{N}}$, where in each of the Hilbert spaces the particle number is conserved. Importantly, the particles in a state $|\vec{N}\rangle$ can be ordered in an arbitrary way. If the system is in its energetic minimum, so only the lowest energy levels are occupied, and excitations are absent, this defines the ground state $|\vec{N}\rangle_0$. For a general $|\vec{N}\rangle$, however, there will be excitations on each branch, that are particle-hole like or bosonic in nature, since the chiral particle number for the state $|\vec{N}\rangle$ is fixed. In other words, one can in general write $|\vec{N}\rangle = f(\{c^\dagger_{r,k} c_{r,k'}\})|\vec{N}\rangle_0$, where f only depends on bilinear combinations of the fermionic operators. This understood, one realizes that the Fock space can be reorganized in terms of particle-hole like operators, though it is still far from trivial to show that for any state, instead of $f(\{c^\dagger_{r,k} c_{r,k'}\})$, one can find another function $\tilde{f}(\{b^\dagger_{r,k}\})$ or $\tilde{f}(\{b_{r,k}\})$ that contains true bosonic operators, and that this set of states is complete. An exhaustive proof can be found in Refs. [Hal81b, vS98].
We now define bosonic creation and annihilation operators, that include all particle-hole like excitations of some positive momentum $q > 0$, and thus are of the form of density fluctuations,

$$\begin{aligned} b^\dagger_{r,q} &= \frac{i}{\sqrt{n_q}} \sum_k c^\dagger_{r,k+q} c_{r,k}, \\ b_{r,q} &= \frac{-i}{\sqrt{n_q}} \sum_k c^\dagger_{r,k-q} c_{r,k}. \end{aligned} \tag{2.8}$$

Again, $q = \Omega^{-1} n_q > 0$. Those operators satisfy the bosonic commutation relations

$$\begin{aligned} [b_{r,q}, b^\dagger_{r',q'}] &= \delta_{rr'}\delta_{qq'}, \\ [b_{r,q}, b_{r',q'}] &= [b^\dagger_{r,q}, b^\dagger_{r',q'}] = 0. \end{aligned} \tag{2.9}$$

The derivation of the above commutator in terms of fermionic operators, using Eq. (2.8), requires the careful treatment of normal-ordering (see below), and is related to the issue of anomalous commutators. For the development of a bosonization scheme, however, we can as well consider Eq. (2.9) the definition of a bosonic operator.
Such bosonic operators can eventually be used to define the bosonic field operators

$$\begin{aligned} \varphi^\dagger_r(x) &= -\sum_{q>0} \frac{1}{\sqrt{n_q}} e^{-iqrx} b^\dagger_{q,r} e^{-aq/2}, \\ \varphi_r(x) &= -\sum_{q>0} \frac{1}{\sqrt{n_q}} e^{iqrx} b_{q,r} e^{-aq/2}, \\ \phi_r(x) &= \varphi^\dagger_r(x) + \varphi_r(x) = -\sum_{q>0} \frac{1}{\sqrt{n_q}} e^{-aq/2} (e^{-iqrx} b^\dagger_{q,r} + e^{iqrx} b_{q,r}). \end{aligned} \tag{2.10}$$

The $\phi_r(x)$ are called chiral fields. In Eq. (2.10), we have introduced the parameter a as a cutoff on large momenta q. It is a common procedure for Lorentz-invariant theories to restrict the energy spectrum in order to regularize diverging sums and singularities of correlation functions [GNT04]. In principle, the cutoff should be sent to zero at some point to undo this modification. We will discuss later, however, that the existence of a cutoff is one

of the key characteristics of the bosonic theory. It is sometimes useful or even necessary to keep the cutoff finite in order to obtain physically meaningful results. We also find that the transport properties of the system can be affected by the presence of absence of a cutoff.

The bosonic fields are in general time-dependent. Assuming that the time-dependence is governed by the free bosonic Hamiltonian in Eq. (2.6), one can use the Heisenberg equation of motion to arrive at $c_{r,k}(t) = e^{-i\varepsilon(k)t}c_{r,k}$ (and $c^\dagger_{r,k}(t) = e^{i\varepsilon(k)t}c^\dagger_{r,k}$). Bosons then gain a time-dependence $b^\dagger_{r,q}(t) = e^{iv_F qt}b^\dagger_{r,q}$ (and $b_{r,q}(t) = e^{-iv_F qt}b_{r,q}$). For the bosonic chiral fields, we find a dependence only on the combination $\phi_r(x,t) = \phi_r(rx - v_F t)$.
Occasionally, we reformulate the model in imaginary time, $\tau = it$. Let us define $z = ix + v\tau$, as well as $\overline{z} = -ix + v\tau$, to rewrite the chiral fields in terms of the new coordinates $\phi_L(z)$ and $\phi_R(\overline{z})$. Here, we also abbreviate

$$z_r = -i(rx - vt) = -irx + v\tau, \tag{2.11}$$

so compared to the above notation it is $z_+ = \overline{z}$ and $z_- = z$.

To make a connection between fermionic and bosonic operators, we have to find an expression for the function $\tilde{f}$ in $|\vec{N}\rangle = \tilde{f}(\{b^\dagger_{r,k}\})|\vec{N}\rangle_0$. Such a bosonic reorganization of the Fock space allows for the derivation of the so-called bosonization identity, which is found to be [vS98] (we use $k_F = p_F$ at times for convenience)

$$\begin{aligned}\psi_r(x) &= F_r \left(\frac{2\pi}{L}\right)^{1/2} e^{ir\frac{2\pi}{L}(N_r - \frac{1}{2})x} e^{-i\varphi^\dagger_r(x)} e^{-i\varphi_r(x)} \\ &= F_r \left(\frac{1}{a}\right)^{1/2} e^{ir\frac{2\pi}{L}(N_r - \frac{1}{2})x} e^{-i\phi_r(x)}\end{aligned} \tag{2.12}$$

As was already observed in Eq. (2.7), the anticommutation rules for the fields defined in Eq. (2.12), in real space hold strictly only in the limit of vanishing cutoff [vS98].
To go from the first to the second line in Eq. (2.12), we used the field commutator derived in the next sections. Also note, that while the first line is normal-ordered, the second line is not and therefore diverges in the limit of $a \to 0$ (see more details in the next section).
An additional object is introduced here in the form of the Klein factor F_r. Those factors are crucial ingredients for bosonization, and act as ladder operators that connect Hilbert spaces $\mathcal{H}_{\vec{N}}$ with different particle number, by raising ($F^\dagger_r$) or lowering (F_r) the r-type fermion number by one. Klein factors are needed to ensure the correct anticommutation relations and preserve the fermionic character of the operator. They fulfill the commutation relations [vS98] $\{F_r, F^\dagger_r\} = 2\delta_{r,r'}$, so $F_r F^\dagger_r = F^\dagger_r F_r = 1$ as well as $\{F^\dagger_r, F^\dagger_{r'}\} = \{F_r, F_{r'}\} = 0$ if $r \neq r'$. Klein factors by construction commute with all bosonic operators and fields, which is why they are often considered of minor importance. Crucially however, they do not commute with the particle number operator, as

$$\begin{aligned}|N_r, F^\dagger_{r'}] &= \delta_{rr'} F^\dagger_{r'}, \\ |N_r, F_{r'}] &= -\delta_{rr'} F_{r'}.\end{aligned} \tag{2.13}$$

As mentioned already, it is an inherent problem of bosonization that divergences may occur. Usually, they result from the fact that there are sums over infinitely many single

particle states. Such sums can be regularized by introducing a momentum cutoff, which effectively corresponds to a short-distance cutoff in real space. To make sure that an operator O is defined in a controlled way, it needs to be normal-ordered, denoted ${}^*_*(\ldots){}^*_*$, which is defined by

$$ {}^*_*O{}^*_* = O - \langle O\rangle_0, \text{ if } O \in \{c^\dagger_{r,k}, c_{r',k'}\} \text{ or } O \in \{b^\dagger_{r,k}, b_{r',k'}\}. \tag{2.14}$$

The respective ground state expectation value is subtracted, which is defined by $\langle\ldots\rangle_0 = {}_0\langle\vec{0}|\ldots|\vec{0}\rangle_0$ for operators that have the form of a product of fermionic creation and annihilation operators, $O \in \{c^\dagger_{r,k}, c_{r',k'}\}$, and $\langle\ldots\rangle_0 = {}_0\langle\vec{N}|\ldots|\vec{N}\rangle_0$ for bosonic operators $O \in \{b^\dagger_{r,k}, b_{r',k'}\}$. The state $|\vec{0}\rangle_0$ is hereby defined to be the vacuum state (Fermi sea), with $c_{r,k}|\vec{0}\rangle_0 = 0$ for $k > 0$ and $c^\dagger_{r,k}|\vec{0}\rangle_0 = 0$ for $k \leq 0$. The lack of normal-ordering may be troublesome, for example, a shift of indices or relabelings in a momentum sum can run into problems if the summand is not normal-ordered [vS98]. Note that $|\vec{0}\rangle_0$ and $|\vec{N}\rangle_0$ can contain infinitely many particles. Therefore the ground state average above may diverge and normal-ordering is supposed to regularize the expression. For fermionic operators, $O \in \{c^\dagger_{r,k}, c_{r,k}\}$, fermion normal-ordering corresponds to moving all $c_{r,k}$ with $k > 0$, and all $c^\dagger_{r,k}$ with $k \leq 0$, to the right of all other operators. For bosonic operators, $O \in \{b^\dagger_{r,k}, b_{r',k'}\}$, we can still use the same notation ${}^*_*(\ldots){}^*_*$, since a boson normal-ordered expression is automatically fermion normal-ordered and vice versa [vS98]. Generally, for any such operators of this type, the average with respect to the ground state is $\langle {}^*_*O{}^*_*\rangle_0 = 0$.

Let us illustrate the importance of normal-ordering by deriving the essential commutator of Eq. (2.9) in terms of fermionic operators. With Eq. (2.8), we have

$$\begin{aligned}
[b_{r,q}, b^\dagger_{r',q'}] &= \delta_{rr'}\frac{1}{\sqrt{n_q n_{q'}}}\sum_{k,k'}[c^\dagger_{r,k-q}c_{r,k}, c^\dagger_{r,k'+q'}c_{r,k'}] \\
&= \delta_{rr'}\frac{1}{\sqrt{n_q n_{q'}}}\sum_{k}\left(c^\dagger_{r,k-q+q'}c_{r,k} - c^\dagger_{r,k-q}c_{r,k-q'}\right) \\
&= \delta_{rr'}\frac{1}{\sqrt{n_q n_{q'}}}\sum_{k}\big({}^*_*c^\dagger_{r,k-q+q'}c_{r,k}{}^*_* - {}^*_*c^\dagger_{r,k-q}c_{r,k-q'}{}^*_* \\
&\quad + \langle c^\dagger_{r,k-q+q'}c_{r,k}\rangle_0 - \langle c^\dagger_{r,k-q}c_{r,k-q'}\rangle_0\big) \\
&= \delta_{rr'}\delta_{qq'}\frac{1}{n_q}\sum_{k}\left(\langle c^\dagger_{r,k}c_{r,k}\rangle_0 - \langle c^\dagger_{r,k-q}c_{r,k-q}\rangle_0\right) = \delta_{rr'}\delta_{qq'}.
\end{aligned} \tag{2.15}$$

Note that in the second line above, it is in general not correct to perform the momentum shift $k \to k+q'$ in the second term, in which case the whole expression vanishes. This is because the terms are not yet normal-ordered properly, and infinities would be subtracted in an uncontrolled way [ML65, vS98, Gia03]. For $q \neq q'$, on the other hand, the products are already normal-ordered, because then $\langle c^\dagger_{r,k-q+q'}c_{r,k}\rangle_0 = 0$, and $\langle c^\dagger_{r,k-q}c_{r,k-q'}\rangle_0 = 0$. The only nonzero contribution therefore arises from the terms with $q = q'$. Within normal-ordered expressions, a momentum shift can be performed safely, such that there is a partial cancellation of terms. Eventually, the sum over the difference of ground state averages

yields a factor of n_q.
Eq. (2.15) represents an example of a so-called anomalous commutator [GNT04, Fra13]. In general, this term is used for a commutator that is nonzero only for a system with infinitely many particles, and zero otherwise. Anomalous commutators are behind alleged paradoxa such as the "chiral anomaly". Let us very briefly comment on the latter: In a one-dimensional system of fermions, the response to an applied electromagnetic fields is related to the retarded density-density correlation. In momentum space, this involves the commutator $[\rho_r(q), \rho_{r'}^\dagger(q')]$, where we use $\rho_r(q) = \sum_k c_{r,k-q}^\dagger c_{r,k}$, for the respective chirality r. A naive derivation of this commutator, that does not account for normal-ordering of the fermionic operators in a thorough way, gives zero, as one can directly observe from Eq. (2.15). Obviously, this result can not be correct from a physical point of view. On the other hand, when the system is described in terms of bosonic operators only, such difficulties do not occur, as by definition, the bosons obey the commutation rules of Eq. (2.9). The anomalous character of the involved commutators is therefore already built-in in this framework.

Next, we derive the bosonized form of the most important physical quantities of the Luttinger liquid. In the process, we recurrently encounter the normal-ordered particle number operator $N_r = \sum_k {}^*_* c_{r,k}^\dagger c_{r,k} {}^*_*$. The (chiral) density is calculated from Eqs. (2.8) and (2.10), and takes the form [4]

$$\begin{aligned}\rho_r(x) = {}^*_* \psi_r^\dagger(x)\psi_r(x) {}^*_* &= \frac{2\pi}{L}\sum_q e^{irqx} \sum_k {}^*_* c_{r,k-q}^\dagger c_{r,k} {}^*_* \\ &= \frac{2\pi}{L}\sum_{q>0} i\sqrt{n_q} {}^*_* (e^{irqx} b_{r,q} - e^{-irqx} b_{r,q}^\dagger) {}^*_* + \frac{2\pi}{L}\sum_k {}^*_* c_{r,k}^\dagger c_{r,k} {}^*_* \\ &\overset{a\to 0}{=} -r {}^*_* \partial_x \phi_r(x) {}^*_* + \frac{2\pi}{L} N_r. \end{aligned} \tag{2.16}$$

Note that the above identification is possible only at zero cutoff. This limit can be taken safely, since the expression is normal-ordered and no divergences are expected. If a is finite, this brings additional terms. Making a connection to the density, the bosonic field ϕ_r can be interpreted as an ordering field of the particles of chirality r [Gia03].
In an analogous way, the kinetic energy in Eq. (2.6) can be bosonized to [Hal81b, vS98]

$$\begin{aligned} H_0 &= \sum_{k,r=R,L} v_F k {}^*_* c_{r,k}^\dagger c_{r,k} {}^*_* = \sum_r \frac{v_F \pi}{L} N_r^2 + \sum_{r,q>0} v_F q {}^*_* b_{r,q}^\dagger b_{r,q} {}^*_* \\ &= \sum_r \frac{v_F\pi}{L} N_r^2 + \sum_r \frac{v_F}{2\pi} \int_{-L/2}^{L/2} \mathrm{d}x \, \frac{1}{2} {}^*_* (\partial_x \phi_r(x))^2 {}^*_* = \frac{v_F}{2\pi} \int_{-L/2}^{L/2} \mathrm{d}x \, \frac{1}{2} \Big({}^*_* \rho_R^2(x) + \rho_L^2(x) {}^*_* \Big). \end{aligned} \tag{2.17}$$

The key point here is that even though H_0 is quadratic in the fermion operators, it can as well be expressed in a form, that is quadratic in bosonic operators (which means quartic in fermions). How this comes about can be sketched in the following way. Acting with $b_{r,q}^\dagger$

[4] Here, $q = \Omega^{-1} n_q$ was chosen, which implies periodicity of the bosonic fields, $\phi_r(L/2) = \phi_r(-L/2)$, and of the bosonic density. This is not in contradiction with the choice of antiperiodic boundaries for the fermionic fields above [vS98].

on a N-particle eigenstate of H_0, produces another N-particle eigenstate of H_0 (particle number is conserved) with an additional particle-hole excitation, so the energy is increased by $v_F q$. In other words,

$$H_0 b^\dagger_{r,q}|N_r\rangle = (E_{N_r} + v_F q) b^\dagger_{r,q}|N_r\rangle, \tag{2.18}$$
$$b^\dagger_{r,q} H_0|N_r\rangle = b^\dagger_{r,q} E_{N_r}|N_r\rangle. \tag{2.19}$$

Here, E_{N_r} is the total kinetic energy of state $|N_r\rangle$. The last line above holds trivially. Combining the two equations, we find $[H_0, b^\dagger_{r,q}] = (v_F q) b^\dagger_{r,q}$, which implies that the kinetic energy represented in bosonic operators only should read $H_0 \simeq (v_F q) b^\dagger_{r,q} b_{r,q}$.
The term including operators N_r in Eq. (2.17) stems from normal-ordering, and reflects the ground state average ${}_0\langle\vec{N}|H_0|\vec{N}\rangle_0$. There are additional terms proportional to $(N_L \partial_x \phi_L(x) - N_R \partial_x \phi_R(x))$, that vanish after spatial integration due to the periodicity of the bosonic fields.

2.1.2. Bosonized interactions

The great power of bosonization becomes evident if electron-electron interactions are included. Interacting electrons of either chirality can be described by the operator [vS98]

$$\begin{aligned} H_{\text{int}} &= \frac{1}{2\pi}\int_{-L/2}^{L/2} \mathrm{d}x\ \frac{1}{2}\left[g_2 {}^*_*(\psi^\dagger_R \psi^\dagger_L \psi_L \psi_R)(x) {}^*_* + g_4 {}^*_*(\psi^\dagger_R \psi^\dagger_R \psi_R \psi_R)(x) {}^*_* + \{L \leftrightarrow R\}\right] \\ &= \frac{1}{2\pi}\int_{-L/2}^{L/2} \mathrm{d}x\ \left[g_2 {}^*_* \rho_R(x)\rho_L(x) {}^*_* + \frac{1}{2} g_4 {}^*_*(\rho^2_R(x) + \rho^2_L(x)\right] {}^*_*. \end{aligned} \tag{2.20}$$

Here we use the common "g-ology" [Sól79, GS88, Gia03] for the two possible interactions of particles of different (g_2), or the same (g_4) species. For simplicity, we assumed homogeneous and local (contact) interactions, which means constant g. Generally, the Pauli principle forbids fully local terms of the form g_4, but we shall keep the term here for illustrating purposes (see further discussion in Sec. 2.2.2).
From Eqs. (2.17) and Eq. (2.20), the kinetic and the interaction term can be combined in a simple form, coined the Luttinger liquid Hamiltonian H_{LL},

$$H_{\text{LL}} = H_0 + H_{\text{int}} = \frac{1}{2\pi}\int_{-L/2}^{L/2} \mathrm{d}x\ \frac{1}{4} {}^*_* \left[vK(\rho_R - \rho_L)^2 + \frac{v}{K}(\rho_R + \rho_L)^2 \right](x) {}^*_*, \tag{2.21}$$

with the standard Luttinger parameters

$$\begin{aligned} v &= \left((v_F + g_4)^2 - g_2^2 \right)^{1/2}, \\ K &= \left(\frac{v_F + g_4 - g_2}{v_F + g_4 + g_2} \right)^{1/2}. \end{aligned} \tag{2.22}$$

The parameter v can be considered a renormalized Fermi velocity, and K the effective strength of electron interactions. We observe that the g_4-term, associated with forward scattering of the electrons, does not have any other physical effect than adding to v_F.

Repulsive electron interactions are represented by $0 \leq K < 1$, while attractive electron interactions correspond to $K > 1$.
It is useful to combine both chiral fields to more physical, non-chiral field operators, which are related to the total charge and current density of the system. The Luttinger Hamiltonian of Eq. (2.21) then can be rewritten in terms of non-chiral fields by a Bogoljubov transformation of the boson creation and annihilation operators,

$$\begin{aligned} H_{\mathrm{LL}} &= \frac{1}{2\pi}\int_{-L/2}^{L/2} \mathrm{d}x\; vK :(\partial_x\theta(x))^2: + \frac{v}{K} :(\partial_x\phi(x))^2:, \\ \phi(x) &= -\frac{1}{2}\int^{x} \mathrm{d}x'\; (\rho_R(x') + \rho_L(x')), \\ \theta(x) &= \frac{1}{2}\int^{x} \mathrm{d}x'\; (\rho_R(x') - \rho_L(x')). \end{aligned} \tag{2.23}$$

The non-chiral fields ϕ and $\partial_x\theta/\pi$ have the form of canonical conjugate partners, as can be seen from their commutation relation (see next section). In the non-interacting limit, given by $K \to 1$ and $v \to v_F$, one realizes that the above Hamiltonian recovers the one of Eq. (2.17), as it should be.
Making a connection to the chiral fields in the interacting system, we obtain from Eq. (2.16), $\phi(x) = \frac{1}{2}(\phi_R(x) - \phi_L(x)) - \frac{\pi x}{L}(N_R + N_L)$ and $\theta(x) = -\frac{1}{2}(\phi_R(x) + \phi_L(x)) + \frac{\pi x}{L}(N_R - N_L)$. This means,

$$\phi_r(x) = r\phi(x) - \theta(x) + r\frac{2\pi x}{L}N_r. \tag{2.24}$$

In particular, with Eq. (2.16), the total charge density only depends of the field ϕ, whereas the other field θ can be associated with the current density,

$$\begin{aligned} \rho(x) &= \sum_r \rho_r(x) = \sum_r (-:\partial_x\phi(x):\, + r:\partial_x\theta(x):) = -2:\partial_x\phi(x):, \\ j(x) &= vK\sum_r r\rho_r(x) = vK\sum_r (-r:\partial_x\phi(x):\, + :\partial_x\theta(x):) = 2vK:\partial_x\theta(x):. \end{aligned} \tag{2.25}$$

In the definition of the current density, we have used here the renormalized velocity vK instead of the bare v_F. This important detail follows from charge conservation, as manifested in the continuity equation,

$$\partial_x j(x,t) + \partial_t \rho(x,t) = 0. \tag{2.26}$$

It defines the current density

$$j(x,t) = -\int^{x} \mathrm{d}x'\; \partial_t\rho(x',t) = 2:\partial_t\phi(x,t): = 2vK:\partial_x\theta(x,t):. \tag{2.27}$$

Above, we have used ρ from Eq. (2.25), and in the last step anticipated the important relation $\partial_t\phi = vK\partial_x\theta$, that is derived with the help of the commutators in Eq. (2.61).
While the kinetic energy in the non-interacting case of Eq. (2.17) could be split into a sum of a right-moving and a left-moving part, this seems not the case in the presence of interactions. We see that in Eq. (2.23), when going back to chiral fields, the mixed terms

of the form $\partial_x\phi_R(x)\partial_x\phi_L(x)$ do not vanish for finite interactions, $K \neq 1$, and the question arises whether the physical nature of the system, in the form of a characteristic separation into right- and left-movers, has been altered. This is not the case, as new chiral fields can be introduced for instance by [Gia03] $\phi_r = K\theta - \phi$, including the Luttinger parameter K, that will again allow for a chiral sum representation of the kinetic energy. Therefore, also in the presence of interactions, there exist excitations that propagate solely to the left or to the right.
These considerations reflect an important point we like to emphasize here. Via the electron densities, the non-chiral fields in Eq. (2.23) can be directly connected to the chiral fermionic operators. On the other hand, the chiral fields are introduced in Eq. (2.10) in terms of bosonic creation and annihilation operators, that can be defined in various ways. Obviously, one has a certain freedom in defining such operators, since the functions $\tilde{f}(\{b^\dagger_{r,k}\})$ to span the bosonic Hilbert space are not unique. Therefore, unfortunately, many different notations of the chiral bosonized fields and the chiral version of the bosonization identity exist (for instance [Hal81b, GNT04, KF92a]). Here, we are concerned only with the nomenclature of Refs. [vS98, Gia03] and a slightly modified version that was used in Refs. [CBD$^+$12, Dol12, GCT14], and that we shall adapt in the following chapters. The representation of physical quantities, such as the density or the current, in terms of non-chiral fields remains the same.

2.1.3. Chiral fields – notation of this Thesis

So far, we have followed closely the notation of Ref. [vS98], which led us to the above notion of the chiral fields $\phi_r(x)$. Let us temporarily put a label and write $\phi_r^{\text{Delft}}(x)$ to mark the according source of notation. In the following, we prefer to use yet a slightly different definition of bosonic operators, which results in new chiral fields $\phi_r^{\text{Delft}}(x) \to \phi_r^{\text{new}}(x) = f(\phi_r^{\text{Delft}}(x))$ with some function f. Assuming that the new fields can eventually be expressed in terms of the former ones studied above, we do not worry about the intermediate fields at all. Fixing now and for all $\phi_r(x) = \phi_r^{\text{Delft}}(x)$ to be the fields defined in Eq. (2.10), a redefinition of bosonic operators then corresponds to the replacement $\phi_r(x) \to f(\phi_r(x))$.
Following the Refs. [CBD$^+$12, Dol12, GCT14], we here choose to use the redefined chiral fields

$$\begin{aligned} \phi_r(x) &\to -r\phi_r(x), \\ \psi_r(x) &\to \psi_r(x)/\sqrt{2\pi}. \end{aligned} \tag{2.28}$$

The last line above renormalizes the fermionic fields to match Ref. [Gia03], which results in $\rho_r \to \rho_r/2\pi$ (e.g. in Eq. (2.21)), as well as $g_2 \to g_2/2\pi$, $g_4 \to g_4/2\pi$ in Eq. (2.22). For instance, we find then from Eq. (2.25),

$$\begin{aligned} \rho(x) &= -{}^*_*\partial_x\phi(x){}^*_*/\pi, \\ j(x) &= vK{}^*_*\partial_x\theta(x){}^*_*/\pi. \end{aligned} \tag{2.29}$$

With these redefined bosons, the density in Eq. (2.16) can be phrased as

$$\rho_r(x) \to ({}^*_*\partial_x\phi_r(x){}^*_* + \frac{2\pi}{L}N_r)/2\pi. \tag{2.30}$$

Again, keep in mind that it is not the density, a physical quantity, that changes, but only its representation in terms of redefined chiral bosonic fields. Moreover, the non-chiral fields to reproduce the Hamiltonian Eq. (2.23) are then given in terms of the chiral ones by $\phi_r(x) \to -\phi(x) + r\theta(x) - \frac{2\pi x}{L} N_r$, compare to Eq. (2.24). Explicitly, they read

$$\begin{aligned} \phi(x) &= -\frac{1}{2}(\phi_R(x) + \phi_L(x)) - \frac{\pi x}{L}(N_R + N_L), \\ \theta(x) &= \frac{1}{2}(\phi_R(x) - \phi_L(x)) + \frac{\pi x}{L}(N_R - N_L). \end{aligned} \tag{2.31}$$

Finally, the bosonization identity in this redefined language becomes with Eqs. (2.12) and (2.28),

$$\begin{aligned} \psi_r(x) &= F_r \left(\frac{1}{2\pi a}\right)^{1/2} e^{ir(k_F - \frac{\pi}{L} + \frac{2\pi}{L} N_r)x} e^{ir\phi_r(x)} \\ &= F_r \left(\frac{1}{2\pi a}\right)^{1/2} e^{ir(k_F - \frac{\pi}{L})x} e^{-i(r\phi(x) - \theta(x))}. \end{aligned} \tag{2.32}$$

The total fermionic field is then just $\psi(x) = \sum_r \psi_r(x)$, since the factor of $e^{irk_F x}$ is included already in Eq. (2.32). [5] The notation here is similar to the one used in Ref. [Gia03], but note some subtle differences (see App. B for details).

2.2. Spinless, spinful and helical Luttinger liquids

2.2.1. Kinetic energy and electron density

So far, we have considered the spinless Luttinger liquid, where the wavefunction ψ is a scalar, and can be written as the sum of both chiral fields $\psi(x) = \psi_R(x) + \psi_L(x) = \sum_r \psi_r(x)$ (compare with Eq. (2.4), where oscillating factors are included in ψ_r). Occasionally, the chirality is expressed in the form of components of a pseudo-spin, such that ψ becomes a vector $\vec{\psi}(x) = (\psi_R(x), \psi_L(x))^T$, to emphasize the analogy to a $1+1$ dimensional Dirac particle [AS10]. We have to replace then, for instance, in the kinetic energy of Eq. (2.6) the scalar r by the matrix σ_z. This notation, however, can be misleading, as one observes best from the spinless electron density,

$$\rho^{\text{spinless}}(x) = \psi^\dagger(x)\psi(x) = \sum_r \rho_r(x) + \psi_r^\dagger(x)\psi_{-r}(x). \tag{2.33}$$

This is different from $\vec{\psi}^\dagger(x)\vec{\psi}(x) = \rho_R(x) + \rho_L(x)$ in the above pseudo-spin vector notation. The last term in the density of Eq. (2.33) is called Friedel oscillations [Gia03, AS10].
Next, let us include an additional degree of freedom in the form of the electron spin, in which case the wavefunction truly becomes a two-dimensional object. This is the spinor

$$\vec{\psi}(x) = \begin{pmatrix} \psi_\uparrow(x) \\ \psi_\downarrow(x) \end{pmatrix} = \begin{pmatrix} \psi_{R,\uparrow}(x) + \psi_{L,\uparrow}(x) \\ \psi_{R,\downarrow}(x) + \psi_{L,\downarrow}(x) \end{pmatrix}. \tag{2.34}$$

[5] Note that from the previous definition in Eq. (2.12), using Eq. (2.24), we find the same identity in terms of non-chiral fields, as expected.

In addition to an index R/L, each field therefore has another index $\sigma = \uparrow, \downarrow = \pm 1/2$, and we can rewrite everything in terms of the two-index components $\psi_{r,\sigma}(x)$. It turns out, that most physical quantities can be expressed as a sum of two separate parts with opposite spin, which hints at the phenomenon of spin-charge separation in a spinful LL [Gia03]. For instance, the kinetic energy of Eq. (2.6) in the spinful basis can be written as

$$\begin{aligned} H_0 = H_{0\uparrow} + H_{0\downarrow} &= \frac{v_F}{2\pi} \int_{-L/2}^{L/2} \mathrm{d}x \; \vec{\psi}^\dagger(x)(-ir\partial_x)\mathbb{1}\vec{\psi}(x) \\ &= \frac{v_F}{2\pi} \sum_{r=R,L;\sigma=\uparrow,\downarrow} \int_{-L/2}^{L/2} \mathrm{d}x \; \psi^\dagger_{r,\sigma}(x)(-ir\partial_x)\psi_{r,\sigma}(x), \end{aligned} \tag{2.35}$$

while the total density is given by

$$\rho^{\text{spinful}}(x) = \vec{\psi}^\dagger(x)\vec{\psi}(x) = \sum_\sigma \rho_\sigma(x) = \sum_{r,\sigma} \rho_{r,\sigma}(x) + \psi^\dagger_{r,\sigma}(x)\psi_{-r,\sigma}(x). \tag{2.36}$$

Here, we defined $\rho_{r,\sigma}(x) = \psi^\dagger_{r,\sigma}(x)\psi_{r,\sigma}(x)$.

In this work, we are concerned with a special case of a spinful Luttinger liquid, that is the helical liquid. In such systems, the electron spin is strongly coupled to the direction of propagation, such that particles propagating to the right and left have opposite spin. The helical wavefunction then takes the form

$$\vec{\psi}(x) = \begin{pmatrix} \psi_{R,\uparrow}(x) \\ \psi_{L,\downarrow}(x) \end{pmatrix}. \tag{2.37}$$

Due to the locking of chirality and spin, one index is redundant, and can be dropped eventually. We shall therefore at times use the equivalent notation $\vec{\psi}(x) = (\psi_R(x), \psi_L(x))^T$ for the helical spinor. This is why for a number of applications, the helical liquid is considered an effectively spinless model. In general, however, the two have to be clearly distinguished, as the basis of the helical liquid is a two-component spinor, while the one of the spinless LL is a scalar (or a pseudo-spin vector). The kinetic energy in the helical basis takes the form

$$H_0 = \frac{v_F}{2\pi} \int_{-L/2}^{L/2} \mathrm{d}x \; \vec{\psi}^\dagger(x)(-i\sigma_z\partial_x)\vec{\psi}(x) = \frac{v_F}{2\pi} \sum_{r=R,L} \int_{-L/2}^{L/2} \mathrm{d}x \; \psi^\dagger_{r,\sigma_r}(x)(-ir\partial_x)\psi_{r,\sigma_r}(x). \tag{2.38}$$

Here, we wrote σ_r with $\sigma_+ = \uparrow$ and $\sigma_- = \downarrow$, to indicate spin-momentum locking. The Eq. (2.38) indeed resembles the spinless version of Eq. (2.6) with an additional, redundant index σ_r. On the other hand, we see that the total density of the helical liquid reads

$$\rho^{\text{helical}}(x) = \vec{\psi}^\dagger(x)\vec{\psi}(x) = \sum_r \rho_r(x). \tag{2.39}$$

As a genuine property of the helical liquid, Friedel oscillations of the density are absent, in contrast to the spinless LL. Important differences are as well embodied in the form of the electron interactions, as we discuss next.

2.2.2. Form of electron interactions

We expect Coulomb interactions between electrons to be present naturally in the 1D Luttinger liquid. Two types of interactions, g_2 and g_4, were already introduced for the spinless case in Eq. (2.20). Here, we would like to comment in more detail on the specific form of the interactions in the spinful and helical case. A similar discussion is given in Ref. [GCT15], App. A.
Quite generally, translational invariant two-body interactions among spinful electrons are described by terms of the form

$$\begin{aligned} H_{\text{int}} &= \sum_{\substack{r,r',r'',r''',\sigma,\sigma';\\ r+r'=r''+r'''}} \int \mathrm{d}x\, \mathrm{d}x'\, \psi^\dagger_{r,\sigma}(x)\psi^\dagger_{r',\sigma'}(x')U(x-x')\psi_{r'',\sigma'}(x')\psi_{r''',\sigma}(x) \\ &= \sum_{r,\sigma,\sigma'} \int \mathrm{d}x\, \mathrm{d}x'\, U(x-x')\big[\psi^\dagger_{r,\sigma}(x)\psi^\dagger_{r,\sigma'}(x')\psi_{r,\sigma'}(x')\psi_{r,\sigma}(x) \\ &\quad + \psi^\dagger_{r,\sigma}(x)\psi^\dagger_{-r,\sigma'}(x')\psi_{-r,\sigma'}(x')\psi_{r,\sigma}(x) + \psi^\dagger_{r,\sigma}(x)\psi^\dagger_{-r,\sigma'}(x')\psi_{r,\sigma'}(x')\psi_{-r,\sigma}(x)\big], \end{aligned} \tag{2.40}$$

with operators arranged in normal order [Hal81a, Hal81b, Sch97, BF04]. [6] We can identify three types of interactions, that correspond to terms g_4, g_2 and g_1 of the g-ology classification, as we see below. Throughout, we assume that the total spin is conserved in the interaction process, and moreover, conservation of chiral particle number stipulates that $r + r' = r'' + r'''$, leaving only the terms above. In the presence of a lattice, for example, this requirement is relaxed and one can think of umklapp scattering (at half filling) [Gia91, Gia03], with two right-movers scattered into two left-movers, and some momentum absorbed by the lattice. Such processes can as well be considered a generic interaction term.
For many-body systems containing plenty of electrons, we generally expect short-range interactions due to screening effects. In Fourier space, this means that the interaction potential only varies slowly with momentum. The parameters of the first two terms in Eq. (2.40) are approximately given by the Fourier component $U(q \approx 0)$, which illustrates the fact that such processes correspond to excitations within the same branch, whereas the last term depends on $U(q \approx \pm 2p_F)$, indicating an excitation across the Fermi surface. For simplicity, let us now assume contact (zero-range) interactions of the form $U(x - x') = U_0\delta(x - x')$, such that the interaction potential is constant in Fourier space. In the usual g-ology classification, instead of U_0, one introduces three independent parameters g_4, g_2 and g_1 for the three interaction terms in Eq. (2.40). While for bare Coulomb interactions, the interaction strengths are expected to be all equal, this is generally not true anymore for a realistic system. For instance, coupling of the wavefunctions in the one-dimensional edge states with states in the bulk of a 2D topological insulator, mediated by spin-orbit coupling, or some spin-dependent screening mechanisms within the edge, may cause different interaction potentials.

[6] If the fermionic operators are not arranged in a normal-ordered way but in the form of density-density interactions, this corresponds to additional single-particle terms (with two fermionic operators after anticommutations), a subtle difference that is usually ignored.

For general contact interactions, we thus rewrite Eq. (2.40) as $H_{\text{int}} = H_1 + H_2 + H_4$, with

$$H_1 = g_{1,\parallel/\perp} \sum_{r,\sigma,\sigma'} \int \mathrm{d}x\ \psi^\dagger_{r,\sigma}(x)\psi^\dagger_{-r,\sigma'}(x)\psi_{r,\sigma'}(x)\psi_{-r,\sigma}(x), \tag{2.41}$$

$$H_2 = g_{2,\parallel/\perp} \sum_{r,\sigma,\sigma'} \int \mathrm{d}x\ \psi^\dagger_{r,\sigma}(x)\psi^\dagger_{-r,\sigma'}(x)\psi_{-r,\sigma'}(x)\psi_{r,\sigma}(x), \tag{2.42}$$

$$H_4 = g_{4,\parallel/\perp} \sum_{r,\sigma,\sigma'} \int \mathrm{d}x\ \psi^\dagger_{r,\sigma}(x)\psi^\dagger_{r,\sigma'}(x)\psi_{r,\sigma'}(x)\psi_{r,\sigma}(x). \tag{2.43}$$

Here, we have replaced, in each of the Eqs. (2.41) to (2.43), the constant U_0 by the prefactors $g_{1,\parallel/\perp}$, $g_{2,\parallel/\perp}$ and $g_{4,\parallel/\perp}$, where the index $\parallel$ indicates parallel spins $\sigma = \sigma'$ and $\perp$ represents $\sigma = -\sigma'$. All the above processes are expected to be present in a generic spinful LL.
A very important constraint is given by the Pauli principle: It manifests itself in forbidding contact interactions of the type $g_{4,\parallel}$, since in Eq. (2.43) $\psi_{r,\sigma}(x)\psi_{r,\sigma}(x) = 0$. Moreover, we see that after fermionic anticommutation, $g_{1,\parallel}$ is of the same form as $g_{2,\parallel}$ but with a minus sign. Therefore they cancel each other in case of equal magnitude, such that then all the parallel interactions are absent in the spinful LL.
In the spinless system, for the very same reasons, g_4 contact interactions are zero and the only remaining term,

$$H^{\text{spinless}}_{\text{int}} = H_2 + H_1 = (g_2 - g_1) \sum_r \int \mathrm{d}x\ \psi^\dagger_r(x)\psi^\dagger_{-r}(x)\psi_{-r}(x)\psi_r(x) \simeq 0, \tag{2.44}$$

vanishes as well if both couplings are of comparable strength. Therefore, we expect no contact interactions at all in the spinless LL [KF92a, SMHG99, Mas05].
In the helical liquid, however, spin momentum locking implies that processes $g_{4,\perp}, g_{1,\perp}$ (and $g_{1,\parallel}, g_{2,\parallel}$) are absent. In particular g_1-like interactions are suppressed, since it is impossible to change the chiral branch and keep the same spin. Therefore, the only remaining interaction term is proportional to $g_{2,\perp} = g_2$,

$$H^{\text{helical}}_{\text{int}} = H_2 = g_2 \sum_r \int \mathrm{d}x\ \psi^\dagger_{r,\sigma_r}(x)\psi^\dagger_{-r,\sigma_{-r}}(x)\psi_{-r,\sigma_{-r}}(x)\psi_{r,\sigma_r}(x). \tag{2.45}$$

If interactions are not contact but finite range, there will be as well interactions of the type $g_{4,\parallel} = g_4$. By inspection of Eqs. (2.44) and (2.45), we see that, importantly, the helical liquid is only formally spinless, but there is a crucial difference when it comes to electron interactions.

2.3. Commutators and correlation functions

2.3.1. Commutators

We here give some important commutation relations, using in general time-dependent fields in the coordinates of Eq. (2.11), so $z_r = -i(rx - vt) = -irx + v\tau$. The most

fundamental commutation relation is derived from Eqs. (2.9) and (2.10), and reads

$$\begin{aligned}\left[\varphi_r(z_r),\varphi^\dagger_{r'}(z'_{r'})\right] &= \delta_{rr'}\sum_{q>0}\frac{1}{n_q}e^{-q(z_r-z'_{r'}+a)} = -\delta_{rr'}\log\left[1-e^{-\frac{2\pi}{L}(z_r-z'_{r'}+a)}\right]\\ &\overset{L\to\infty}{=} -\delta_{rr'}\log\left[\frac{2\pi}{L}(z_r-z'_{r'}+a)-\left(\frac{2\pi}{L}\right)^2(z_r-z'_{r'}+a)^2+\mathcal{O}(1/L^3)\right].\end{aligned} \tag{2.46}$$

Here, the identity $\sum_{n=1}^{\infty} y^n/n = -\log(1-y)$ was used. Whenever it is safely possible, we take the limits $L\to\infty$ and $a\to 0$ for simplicity. The following two expansions of Eq. (2.46) are frequently used,

$$e^{\left[\varphi_r(z_r),\varphi^\dagger_r(z_r)\right]} = \frac{L}{2\pi a}+\frac{1}{2}+\frac{a\pi}{6L}+\mathcal{O}((a/L)^2), \tag{2.47}$$

$$e^{-\left[\varphi_r(z_r),\varphi^\dagger_r(z_r)\right]} = \frac{2\pi a}{L}+\mathcal{O}((a/L)^2). \tag{2.48}$$

With that, one can derive the essential normal-ordering relation for exponentials of bosonic fields, so-called vertex-operators. In lowest order, we find

$$e^{ir\varphi^\dagger_r(z_r)}e^{ir\varphi_r(z_r)} = e^{ir(\varphi^\dagger_r(z_r)+\varphi_r(z_r))}e^{r^2[i\varphi^\dagger_r(z_r),i\varphi_r(z_r)]/2} \approx e^{ir\phi_r(z_r)}\left(\frac{L}{2\pi a}\right)^{1/2}. \tag{2.49}$$

Since above the left hand side is boson normal-ordered, while the right hand side is not, this equation defines a normal-ordering relation. With general coefficients λ,λ', it is

$${}^*_*e^{i\lambda\phi_r(z_r)}{}^*_* = e^{i\lambda\varphi^\dagger_r(z_r)}e^{i\lambda\varphi_r(z_r)} = e^{i\lambda\phi_r(z_r)}\left(\frac{L}{2\pi a}\right)^{\lambda^2/2}, \tag{2.50}$$

$${}^*_*e^{i\lambda\phi_r(z_r)}{}^*_*{}^*_*e^{i\lambda'\phi_r(z'_r)}{}^*_* = {}^*_*e^{i\lambda\phi_r(z_r)}e^{i\lambda'\phi_r(z'_r)}{}^*_*\left(\frac{2\pi}{L}(z_r-z'_r+a)\right)^{\lambda\lambda'}. \tag{2.51}$$

Obviously, normal-ordering for vertex operators works in a way different from the one for simple operators (compare to Eq. (2.14)). Analogously, we find normal-ordering relations for the non-chiral fields defined in Eq. (2.31)

$${}^*_*e^{i\lambda\phi(x,t)}{}^*_* = e^{i\lambda\phi(x,t)}\left(\frac{L}{2\pi a}\right)^{\lambda^2/4}, \tag{2.52}$$

$$\begin{aligned}{}^*_*e^{i\lambda\phi(x,t)}{}^*_*{}^*_*e^{i\lambda'\phi(x',t')}{}^*_* &= {}^*_*e^{i\lambda\phi(x,t)}e^{i\lambda'\phi(x',t')}{}^*_*\left(\frac{2\pi}{L}\sqrt{(z_+-z'_++a)(z_--z'_-+a)}\right)^{\lambda\lambda'/2}\\ &= {}^*_*e^{i\lambda\phi(x,t)}e^{i\lambda'\phi(x',t')}{}^*_*\left(\frac{2\pi}{L}\sqrt{x^2+(v\tau+a)^2}\right)^{\lambda\lambda'/2}.\end{aligned} \tag{2.53}$$

All the results are given in lowest order of a/L. The Eq. (2.53) can be understood as a operator product expansion of vertex operators (see below).

The bosonic fields in general do not commute,

$$[\phi_r(z_r),\phi_{r'}(z'_{r'})] \overset{L\to\infty}{=} \delta_{rr'}\log\left(\frac{z'_{r'}-z_r+a}{z_r-z'_{r'}+a}\right) = -2i\delta_{rr'}\arctan(i(z_r-z'_{r'})/a)$$
$$\overset{a\to 0}{=} -i\pi\delta_{rr'}\mathrm{sgn}(i(z_r-z'_{r'})), \tag{2.54}$$
$$[\phi(x,t),\phi(x',t')] = -i\frac{\pi}{4}\sum_r \mathrm{sgn}(i(z_r-z'_r)). \tag{2.55}$$

We used Eq. (A.5), and $\mathrm{sgn}(x)$ is the sign function with $\mathrm{sgn}(x)=\pm 1$ for $x \gtrless 0$, and $\mathrm{sgn}(0)=0$. Note that if both fields are at the same point in time, then

$$[\phi(x,t),\phi(x',t)] = 0. \tag{2.56}$$

Next, it is helpful to calculate the commutators

$$\left[\partial_x\varphi_r^\dagger(z_r),\varphi_{r'}(z'_{r'})\right] = \left[-ir\partial_{z_r}\varphi_r^\dagger(z_r),\varphi_{r'}(z'_{r'})\right] = ir\frac{2\pi}{L}\delta_{rr'}\frac{1}{e^{\frac{2\pi}{L}(z'_{r'}-z_r+a)}-1}$$
$$= ir\delta_{rr'}\left(\frac{1}{z'_{r'}-z_r+a}-\frac{\pi}{L}+\frac{\pi^2}{3L^2}(z'_{r'}-z_r+a)+\mathcal{O}(1/L^3)\right), \tag{2.57}$$
$$\left[\partial_x\varphi_r(z_r),\varphi_{r'}^\dagger(z'_{r'})\right] = ir\delta_{rr'}\left(\frac{1}{z_r-z'_{r'}+a}-\frac{\pi}{L}+\frac{\pi^2}{3L^2}(z_r-z'_{r'}+a)+\mathcal{O}(1/L^3)\right), \tag{2.58}$$

as well as

$$[\partial_x\phi_r(z_r),\phi_{r'}(z'_{r'})] = ir\delta_{rr'}\left(\frac{1}{z'_{r'}-z_r+a}+\frac{1}{z_r-z'_{r'}+a}-\frac{2\pi}{L}\right)$$
$$= ir\delta_{rr'}\left(\frac{2a}{a^2-(z_r-z'_{r'})^2}-\frac{2\pi}{L}\right) \overset{a\to 0}{=} 2ir\pi\delta_{rr'}\left(\delta(z_r-z'_{r'})-\frac{1}{L}\right). \tag{2.59}$$

With that, we arrive at the important relation

$$\begin{aligned}[\phi(x,t),\partial_{x'}\theta(x',t')] &= i\frac{\pi}{2}\sum_r\delta(z_r-z'_r)-\frac{i\pi}{L},\\ [\phi(x,t),\partial_{x'}\theta(x',t)] &= i\pi\delta(x-x')+\mathcal{O}(L^{-1}).\end{aligned} \tag{2.60}$$

In the first line, the term of order $1/L$ was kept, as it can be important. The two fields have the form of canonical conjugates. If both fields are at the same point in time, and sending $L\to\infty$, we recover the well-known identity in the second line of Eq. (2.60). Using the Heisenberg equation of motion and the above commutators, we can derive the characteristic relation of the Luttinger liquid,

$$\partial_t\phi(x,t) = i[H_{\mathrm{LL}},\phi(x,t)] = i\int \mathrm{d}x'\,\frac{1}{2\pi}vK[(\partial_{x'}\theta(x',t))^2,\phi(x,t)] = vK\partial_x\theta(x,t), \tag{2.61}$$

with H_{LL} given in Eq. (2.23). It can be interpreted as the continuity equation of the system, see Eq. (2.26).
It is easy to see that moreover,

$$[\partial_x \phi_r(z_r), \partial_{x'} \phi_{r'}(z'_{r'})] = \partial_{x'} \left[\partial_x \phi_r(z_r), \phi_{r'}(z'_{r'})\right] \overset{a\to 0}{=} 2ir\pi\delta_{rr'}\partial_{x'}\delta(z_r - z'_{r'}), \tag{2.62}$$

Using the definition of $\rho_r(x,t)$ in Eq. (2.30), the above equation is identified as the bosonic version of the anomalous density-density commutator in real space (compare with Eq. (2.15)). For the non-chiral fields of Eq. (2.31), this leads to the characteristic commutation properties at equal times,

$$\begin{aligned} &[\partial_x \phi(x,t), \partial_{x'}\phi(x',t)] = [\partial_x \theta(x,t), \partial_{x'}\theta(x',t)] = 0, \\ &[\partial_x \phi(x,t), \partial_{x'}\theta(x',t)] = i\pi\partial_x \delta(x-x'). \end{aligned} \tag{2.63}$$

2.3.2. Correlators

The correlation functions of the Luttinger liquid describe the decay of its elementary excitations with space (and time). They typically display a power-law behaviour, depending on the interaction strength K. There is an interesting connection to the Mermin-Wagner theorem [AS10], which states that continuous symmetries cannot be spontaneously broken in dimensions $D \leq 2$. This can be reformulated in the way that for such low dimensions "correlation functions of order parameters that transform under a continuous global symmetry cannot decay more slowly than as a power-law function of distance (or time)" ([Fra13], p.155). In that sense, one can say that the 1D system is at a quantum critical point.
For simplicity, we give the correlation functions in the limit $L \to \infty$, and use imaginary time $\tau = it \in (-\beta, \beta]$, where $\beta = 1/T$ is the inverse temperature. Of interest are the time-ordered fermionic and bosonic Green functions with $\mathcal{T}$ being the time-ordering operator. The latter is defined (for both real or imaginary time) by [BF04]

$$\mathcal{T}(A(t)B(t')) = A(t)B(t')Y(t-t') \pm B(t')A(t)Y(t'-t), \tag{2.64}$$

where the $\pm$ sign applies to a bosonic/fermionic character of the operators A and B. Furthermore, $Y(x)$ is the step function with $Y(x) = 1$ for $x > 0$, and $Y(x) = 0$ for $x < 0$. As the average is taken with respect to the kinetic energy (no interactions yet) given by H_0 in Eq. (2.17), the basic fermionic and bosonic correlations read $\langle c^\dagger_{r,k} c_{r',k'}\rangle = \frac{\delta_{rr'}\delta_{kk'}}{e^{\beta v k}+1}$ and $\langle b^\dagger_{r,k} b_{r',k'}\rangle = \frac{\delta_{rr'}\delta_{kk'}}{e^{\beta v k}-1}$. We then find with Ref. [vS98] the chiral fermionic Green functions, [7]

$$\begin{aligned} G^F_r(x,\tau) &= \langle \mathcal{T}\psi_r(x,\tau)\psi^\dagger_{r'}(0,0)\rangle = Y(\tau)\langle \psi_r(x,\tau)\psi^\dagger_{r'}(0,0)\rangle - Y(-\tau)\langle \psi^\dagger_{r'}(0,0)\psi_r(x,\tau)\rangle \\ &= \frac{\delta_{rr'}}{\frac{v\beta}{\pi}\sin(\pi(z_r+\sigma a)/(v\beta))} \overset{T\to 0}{=} \frac{\delta_{rr'}}{z_r+\sigma a}. \end{aligned} \tag{2.65}$$

In the process, a cutoff factor $e^{-k\sigma a}$ with $\sigma = \mathrm{sgn}(\tau)$ was introduced for the fermion fields to regularize the divergence at $z_r = 0$. This is equivalent to introducing a respective

[7] We denote here the time-ordered Green function in a slightly different way compared to Ref. [vS98], such that our $G^{F/B}_r(x,\tau)$ equals $-G_{rr'}(x,\tau)$ of this reference.

cutoff already in the definition of the fermionic field in Eq. (2.4). Such a regularization is not unique, and accordingly, alternative choices might slightly modify the form of the correlations.
For the bosonic Green function, we obtain

$$\begin{aligned} G_r^B(x,\tau) &= \langle \mathcal{T}\phi_r(x,\tau)\phi_{r'}(0,0)\rangle = Y(\tau)\langle\phi_r(x,\tau)\phi_{r'}(0,0)\rangle + Y(-\tau)\langle\phi_{r'}(0,0)\phi_r(x,\tau)\rangle \\ &= -\delta_{rr'}\log\left(\frac{2v\beta}{L}\sin(\pi(\sigma z_r + a)/(v\beta))\right) \overset{T\to 0}{=} -\delta_{rr'}\log\left(\frac{2\pi}{L}(\sigma z_r + a)\right). \end{aligned} \tag{2.66}$$

In particular, it is $G_r^B(0,0) = -\delta_{rr'}\log\left(\frac{2v\beta}{L}\sin(\pi a/(v\beta))\right) \approx -\delta_{rr'}\log\left(\frac{2\pi a}{L}\right)$ in the limit of small a. We may also write $G_r^{F/B}(x,\tau) = G_r^{F/B}(z_r)$. The fact that the fermionic Green function is proportional to the exponential of the bosonic Green function reflects the connection between the two representations, as given in the bosonization identity. Note that the sign σ is an artefact of the time-ordering of the correlation, so we can find the bosonic greater (lesser) Green function $G^{>,B}$ ($G^{<,B}$) from the time-ordered function G^B by simply taking $\sigma = +1$ (or $\sigma = -1$). This is because the bosonic greater and lesser Green functions are related by $G_r^{>,B}(x,\tau) = G_r^{<,B}(-x,-\tau)$, and thus, unlike their fermionic counterparts, are not independent of each other. [8] The above correlation was calculated making use of the Bose-Einstein statistics, which is possible in the non-interacting case of separate single-particle energy levels. Another approach, which has to be taken in the case of finite electron interactions, is to use Gaussian integrals, as explained for example in Refs. [AS10, Gia03].
For the non-chiral fields of Eq. (2.31), we have

$$\begin{aligned} G^{\phi\phi}(x,\tau) &= \langle \mathcal{T}\phi(x,\tau)\phi(0,0)\rangle = \frac{1}{4}(G_+^B(z_+) + G_-^B(z_-)) \\ &= -\frac{1}{4}\log\left(\left(\frac{2v\beta}{L}\right)^2 \sin(\frac{\pi}{v\beta}(\sigma z_+ + a))\sin(\frac{\pi}{v\beta}(\sigma z_- + a))\right) \\ &= -\frac{1}{4}\log\left(\left(\frac{2v\beta}{L}\right)^2 [\sin^2(\frac{\pi}{v\beta}(v|\tau| + a)) + \sinh^2(\pi x/(v\beta))]\right), \end{aligned} \tag{2.67}$$

$$G^{\theta\theta}(x,\tau) = \langle \mathcal{T}\theta(x,\tau)\theta(0,0)\rangle = G^{\phi\phi}(x,\tau), \tag{2.68}$$

$$\begin{aligned} G^{\phi\theta}(x,\tau) &= \langle \mathcal{T}\phi(x,\tau)\theta(0,0)\rangle = \frac{1}{4}(-G_+^B(z_+) + G_-^B(z_-)) = \frac{1}{4}\log\left(\frac{\sin(\frac{\pi}{v\beta}(\sigma z_+ + a))}{\sin(\frac{\pi}{v\beta}(\sigma z_- + a))}\right) \\ &= -\frac{i}{2}\arctan\left(\frac{\tanh(\frac{\pi}{v\beta}\sigma x)}{\tan(\frac{\pi}{v\beta}(\sigma v\tau + a))}\right) = G^{\theta\phi}(x,\tau). \end{aligned} \tag{2.69}$$

Here we used Eqs. (A.4) and (A.7) to simplify the expressions, and wrote $\sigma\tau = |\tau|$, but one should keep in mind that we employ imaginary time here. As the fields ϕ and θ only differ

[8] When comparing $\langle[\phi_r(z_r^{(1)}),\phi_r(z_r^{(2)})]\rangle \overset{?}{=} G_r^{>,B}(z_r^{(1)} - z_r^{(2)}) - G_r^{<,B}(z_r^{(1)} - z_r^{(2)})$ from Eqs. (2.54) and (2.66), one realizes that the two are equivalent only in the limits $T \to 0, L \to \infty$ or $a \to 0, L \to \infty$. This is because for the correlations we have previously made some assumptions, in the form of $L \to \infty$ and finite temperature. When taking the limit of both infinite length and zero temperature, the actual order of limits matters, an issue that is discussed in App. H of Ref. [vS98].

by signs, they have the same correlation with respect to the non-interacting Hamiltonian. Note that the above correlations coincide with the one of Ref. [Gia03], taking into account subtle differences in the notation (see App. B).
We are now able to evaluate correlations of vertex operators, which is the most important part. First of all, it can be shown that for any operator linear in boson operators, $\tilde{B} = \sum_{q>0}(a_q b_q^\dagger + a_q^* b_q)$, with c-number coefficients a_q, the average with respect to the free Hamiltonian in Eq. (2.17) obeys the relation [vS98]

$$\langle e^{\tilde{B}} \rangle = e^{\frac{1}{2}\langle \tilde{B}^2 \rangle}. \tag{2.70}$$

Evidently, our fields ϕ_r, ϕ are exactly of the form of $\tilde{B}$. For instance, we find with Eq. (2.66), that

$$\langle e^{i\lambda\phi_r(z_r)} \rangle = e^{-\frac{\lambda^2}{2}\langle \phi_r(z_r)\phi_r(z_r)\rangle} = \left(\frac{2\pi a}{L}\right)^{\lambda^2/2}. \tag{2.71}$$

With this and Eqs. (2.50) and (2.52) above, we see that normal-ordering of vertex-operators can be defined by its average value,

$${}^*_*e^{i\lambda\phi_r(z_r)}{}^*_* = e^{i\lambda\phi_r(z_r)}\left(\frac{L}{2\pi a}\right)^{\lambda^2/2} = \frac{e^{i\lambda\phi_r(z_r)}}{\langle e^{i\lambda\phi_r(z_r)}\rangle}, \tag{2.72}$$

$${}^*_*e^{i\lambda\phi(x,t)}{}^*_* = e^{i\lambda\phi(x,t)}\left(\frac{L}{2\pi a}\right)^{\lambda^2/4} = \frac{e^{i\lambda\phi(x,t)}}{\langle e^{i\lambda\phi(x,t)}\rangle}. \tag{2.73}$$

One can immediately observe that $\langle {}^*_*e^{i\lambda\phi_r(z_r)}{}^*_* \rangle = 1$, as it should be.
As $[\tilde{B}_i, \tilde{B}_j]$ is a c-number, the product of several vertex operators can be phrased with the help of Eqs. (A.3) and (2.70),

$$e^{\tilde{B}_1}e^{\tilde{B}_2}\dots e^{\tilde{B}_n} = e^{\sum_{j=1}^n \tilde{B}_j} e^{\frac{1}{2}\sum_{i<j}[\tilde{B}_i,\tilde{B}_j]}, \tag{2.74}$$

$$\langle e^{\tilde{B}_1}e^{\tilde{B}_2}\dots e^{\tilde{B}_n}\rangle = e^{\frac{1}{2}\langle(\sum_{j=1}^n \tilde{B}_j)^2\rangle} e^{\frac{1}{2}\sum_{i<j}[\tilde{B}_i,\tilde{B}_j]} \tag{2.75}$$

$$= e^{\frac{1}{2}\sum_{j=1}^n \langle \tilde{B}_j^2\rangle} e^{\sum_{i<j}\langle \tilde{B}_i\tilde{B}_j\rangle}. \tag{2.76}$$

In the last line we used that $(\sum_i \tilde{B}_i)^2 = \sum_i \tilde{B}_i^2 + \sum_{i\neq j}\tilde{B}_i\tilde{B}_j$, and further $\sum_{i<j}[\tilde{B}_i,\tilde{B}_j] = \sum_{i<j}\tilde{B}_i\tilde{B}_j - \sum_{i>j}\tilde{B}_i\tilde{B}_j$. Since the commutator is just a *c*-number, we can safely take its average at any time. Eq. (2.76) is one of the most important formulas in this field, known as the Debye-Waller relation, and has many parallels to Wick's theorem. The above formulas still hold for time-ordered products [Gia03, vS98], and the time-ordering will translate into all averages in the exponentials according to the rules for ordered exponentials. [9] Note that depending on the application, the form of Eq. (2.75) or Eq. (2.76) can be more convenient.

[9] In particular, no commutators appear from the addition of exponentials, since such an arrangement is already taken care of by time-ordering [Col15]. One can also understand this by the fact that $\mathcal{T}[\phi(\tau_1),\phi(\tau_2)] = 0$ by construction of bosonic time-ordering. Keep in mind that the operation of time-ordering is defined only for operators, so comparing $\mathcal{T}[\phi(\tau_1),\phi(\tau_2)]$ to Eq. (2.54) does not make a lot of sense.

We are interested in operators of the form $\tilde{B}_i = i\lambda_i \phi_r(z_r^{(i)})$, with $z_r^{(i)} = -irx_i + v\tau_i$. Therefore, we evaluate with Eq. (2.66) and $\sigma_{ij} = \mathrm{sgn}(\tau_i - \tau_j)$,

$$\begin{aligned}
&\langle \mathcal{T} e^{i\lambda_1 \phi_r(z_r^{(1)})} \dots e^{i\lambda_n \phi_r(z_r^{(n)})} \rangle = e^{-\frac{1}{2}\sum_{j=1}^n \lambda_j^2 G_r^B(0)} e^{-\sum_{i<j} \lambda_i \lambda_j G_r^B(z_r^{(i)} - z_r^{(j)})} \\
&= \left(\frac{2\pi a}{L}\right)^{\frac{1}{2}\sum_{j=1}^n \lambda_j^2} e^{\sum_{i<j} \lambda_i \lambda_j \log[\frac{2v\beta}{L} \sin(\frac{\pi}{v\beta}(\sigma_{ij}(z_r^{(i)} - z_r^{(j)}) + a))]} \\
&= a^{\frac{1}{2}\sum_{j=1}^n \lambda_j^2} \left(\frac{2\pi}{L}\right)^{\frac{1}{2}(\sum_{j=1}^n \lambda_j)^2} \prod_{i<j} \left[\frac{v\beta}{\pi} \sin(\frac{\pi}{v\beta}(\sigma_{ij}(z_r^{(i)} - z_r^{(j)}) + a))\right]^{\lambda_i \lambda_j} .
\end{aligned} \tag{2.77}$$

In the limit $L \to \infty$, the expectation value of a product of two or more operators is finite only if $\sum_j \lambda_j = 0$. This important observation is also known as "neutrality rule". It is physically motivated by the fact that the correlator, just as the kinetic energy Hamiltonian, should be invariant under a shift of $\phi_r \to \phi_r + \text{const.}$, which is the bosonic manifestation of continuous chiral symmetry [vS98, Fra13]. What is frequently needed is the two-vertex correlation,

$$\begin{aligned}
&\langle \mathcal{T} e^{i\lambda\phi(x_1,\tau_1)} e^{-i\lambda\phi(x_2,\tau_2)} \rangle = e^{-\frac{1}{2}2\lambda^2 G^{\phi\phi}(0)} e^{\lambda^2 G^{\phi\phi}(x_1 - x_2, \tau_1 - \tau_2)} \\
&= \left(\frac{\pi a}{v\beta}\right)^{\lambda^2/2} \left(\sin^2(\frac{\pi}{v\beta}(v|\tau_1 - \tau_2| + a)) + \sinh^2(\frac{\pi}{v\beta}(x_1 - x_2))\right)^{-\lambda^2/4} .
\end{aligned} \tag{2.78}$$

In the limit of zero temperature (and normal-ordering), we recover Eq. (2.53), which demonstrates the analogy of normal-ordering and averaging in this limit.

So far we have discussed averages taken with respect to the free Hamiltonian. The interesting question now is what happens if we include interactions, so taking the average with respect to the Luttinger liquid Hamiltonian in Eq. (2.23) instead of the non-interacting one of Eq. (2.17). Using Gaussian integration, it is found that in this case the bosonic averages become [Gia03]

$$\begin{aligned}
G^{\phi\phi}(x,\tau) &\to K G^{\phi\phi}(x,\tau), \\
G^{\theta\theta}(x,\tau) &\to K^{-1} G^{\theta\theta}(x,\tau), \\
G^{\phi\theta}(x,\tau) &\to G^{\phi\theta}(x,\tau).
\end{aligned} \tag{2.79}$$

Also, inside the correlations the velocity is renormalized by $v_F \to v$. Alternatively, to find the interacting averages, one could rescale the two fields $\phi \to \phi\sqrt{K}$ and $\theta \to \theta(\sqrt{K})^{-1}$, a transformation that importantly preserves the commutation relation of the two fields (see Eq. (2.60)). In this rescaled fields, the interacting kinetic energy Hamiltonian now looks exactly like the non-interacting one, such that correlations are readily computed. Quite generally, it can be helpful to realize that the interacting Hamiltonian exhibits the symmetry of a simultaneous interchange of $\phi \leftrightarrow \theta$ and $K \leftrightarrow K^{-1}$.

Via the correlation functions, the inclusion of electron interactions has important consequences on the scaling dimensions and the normal-ordering of operators. The scaling dimension Δ of an operator is introduced in the next section by the long-distance scaling of the two-point correlation functions (see Eq. (2.82)). This discussion anticipating, we

point out here, that while in the non-interacting case the scaling dimension of a fermionic operator of either chirality is $\Delta_{\psi_r(x)} = \Delta_{\psi_r^\dagger(x)} = 1/2$, in the presence of interactions we find $\Delta_{\psi_r(x)} = \Delta_{\psi_r^\dagger(x)} = (K + K^{-1})/4$. The former we infer from the correlation in Eq. (2.65), where $\langle \psi_r^\dagger(z_r)\psi_r(0)\rangle \propto |z_r|^{-1}$. For the latter, we observe using Eq. (2.32) and Eqs. (2.67)–(2.69), that in the presence of interactions the long-distance scaling of the Green function takes the form

$$\begin{aligned}\langle \psi_r^\dagger(z_r)\psi_r(0)\rangle &\propto \langle e^{i(r\phi(x,\tau)-\theta(x,\tau))} e^{-i(r\phi(0)-\theta(0))}\rangle \\ &\propto e^{KG^{\phi\phi}(x,\tau)+K^{-1}G^{\theta\theta}(x,\tau)-2rG^{\phi\theta}(x,\tau)} \propto |z_r|^{-(K+K^{-1})/2}. \end{aligned} \tag{2.80}$$

Here, we use that $\langle \phi(x,\tau)\phi(x,\tau)\rangle = \langle \phi(0)\phi(0)\rangle$ and similar correlations are only numbers, and do not contribute to the scaling. Furthermore, the mixed correlations are restricted by $|G^{\phi\theta}| \leq \pi/2$ and therefore do not matter for the long-distance behaviour. The scaling of a vertex operator $e^{\pm i\lambda\phi(x,\tau)}$ changes with interactions from $\Delta_{\exp(\pm i\lambda\phi(x,\tau))} = \lambda^2/4$ (compare Eq. (2.78)) to $\Delta_{\exp(\pm i\lambda\phi(x,\tau))} = K\lambda^2/4$. Since the normal-ordering of a vertex operator can be defined by its average, as given in Eq. (2.73), switching on interactions will as well affect the normal-ordering relations. Explicitly, Eq. (2.73) is then altered to

$$ {}_*^* e^{i\lambda\phi(x,t)} {}_*^* = e^{i\lambda\phi(x,t)} \left(\frac{L}{2\pi a}\right)^{K\lambda^2/4}. \tag{2.81}$$

As we see later, this has interesting implications, related to the fact that normal-ordering in the presence of finite interactions, $K \neq 1$, does no longer succeed in making the cutoff a disappear.

2.4. Normal-ordering and point-splitting, OPE

Above, we have introduced the concept of normal-ordering, in order to regularize potentially diverging expressions. The same can (in most cases) be achieved by a so-called point-splitting procedure. To illustrate this, we first have to introduce the concept of operator product expansion (OPE), as first described by Wilson and Zimmermann [WZ72]. The problem is, that products of quantum field operators at the same point will diverge in a way that is uncontrolled. Simply speaking, an OPE is a rule that tells us what happens if we bring two quantum field operators close together.

Let us first define a general quantum field operator. Suppose the system provides a complete set of (local) quantum field operators in real space, $\{\phi_n(x,t)\}$, with labels $n \in \{1,\ldots,N\}$, that can be of bosonic or fermionic nature. Such a complete set comprises the operators necessary to go from any possible state $|n\rangle$ of the Fock space to another (with possibly a different number of particles), for instance by fermionic creation and annihilation operators and powers thereof, and importantly includes the unity operator. In general, the fields ϕ_n can also have multiple components, for example in the case of Dirac fermions with spin, we have the two-component field $\vec{\psi}(x,t) = (\psi_\uparrow(x,t), \psi_\downarrow(x,t))^T$. For brevity let us write now $\phi_n(x,t) = \phi_n(z)$ (for the other chirality one can simply replace z by $\overline{z}$). From such fields we can compose arbitrary local field operators $O_i(z) = O_i(\phi_1(z),\ldots,\phi_N(z))$

with another label i. Adopting partly the notation of Ref. [WZ72], we include the hermitian conjugates such that with O_i also the $O_i^\dagger$ are listed. For many applications [AS10], such composed quantum field operators can be conceived of as arbitrary (normal-ordered) polynomials in the fields and their space-time derivatives. With this in mind, we restrict ourselves here only to such operators whose two-point correlations have a power-law decay for large distances, $|z - z'| \to \infty$, in the form of [Car96, Fra13]

$$\langle O_i(z) O_i(z') \rangle_0 \propto |z - z'|^{-2\Delta_i} \quad \forall i \in \{1, \ldots, N\}. \tag{2.82}$$

Such a power-law behaviour applies for instance to fermionic annihilation/creation operators in $1 + 1$ dimensions (see Eq. (2.65)). Above, we have defined the so-called scaling dimension Δ_i of the operator O_i. This number characterizes the respective field operator, and will be important in the context of renormalization group theory (see Sec. 2.5). Fermionic operators in the absence of interactions exhibit a scaling dimension $\Delta_{\psi(x)} = \Delta_{\psi^\dagger(x)} = 1/2$, since $\langle \psi^\dagger(z)\psi(z') \rangle \propto |z - z'|^{-1}$. Importantly, the scaling dimension defined this way is not necessarily the same as the "physical" (also called naive) scaling dimension Δ_i^{naive}, that we obtain by a dimensional analysis of the respective Hamiltonian. For instance, as given above, the vertex operator has scaling dimension $\Delta_{\exp(\pm i\lambda\phi(x,\tau))} = \lambda^2/4$ (in the absence of interactions), though at the same time $\Delta^{\text{naive}}_{\exp(\pm i\lambda\phi(x,\tau))} = 0$. The origin of this potential discrepancy is related to the fact, that the cutoff itself is a dimensionful quantity [AS10].
As we state below, in Eq. (2.91), a power-law decay of the correlation function in Eq. (2.82) follows naturally for many operators in the context of scaling theory, given that H_0 is a fixed point of the system and the O_i are scaling operators close to this fixed point. If the distance of two fields $O_i(z)$ and $O_j(z')$ is short, such that remote fields only have a small influence, the following approximation is valid [Car96, vS98],

$$O_i(z) O_j(z') \overset{z \to z'}{\simeq} \sum_k \frac{c_{ijk} O_k(z)}{|z - z'|^{\Delta_i + \Delta_j - \Delta_k}}. \tag{2.83}$$

Here, the c_{ijk} are c-numbers determined by normalization. The above equation is called OPE. This operation has a fundamental connection to normal-ordering: The expansion of two operators around the same center can be safely performed if the full product is normal-ordered. Now suppose that both operators O_i and O_j of Eq. (2.83) are already normal-ordered. To be able to perform the limit $z \to z'$ we have to normal-order the operator product, the terms emerging in the process will appear among the O_k in the OPE. Therefore, in order to determine the unknown right hand side of Eq. (2.83), the OPE practically means normal-ordering an operator product explicitly and subsequently expanding around $z \approx z'$. Let us assume that in the OPE the two coordinates are separated by a very small number a, so $|z - z'| = a$, that plays the role of a short-distance cutoff. Taking the average of Eq. (2.83), we recognize that the right hand side is nonzero only if the normal-ordered operator $O_k(z)$ is the unity operator (that we label with index one), given that O_k is a normal-ordered non-vertex operator. Then, $\langle O_k(z) \rangle = \delta_{k,1}$ and $O_1(z) = \mathbb{1}$ with $\Delta_1 = 0$. We can immediately see that the average diverges characteristically as a

power of a, since we get

$$O_i(z+a)O_j(z) = \sum_k \frac{c_{ijk}O_k(z)}{a^{\Delta_i+\Delta_j-\Delta_k}}, \tag{2.84}$$

$$\langle O_i(z+a)O_j(z)\rangle_0 = \frac{c_{ij1}}{a^{\Delta_i+\Delta_j}}. \tag{2.85}$$

To handle the diverging expectation value, we have before used the concept of normal-ordering, where the divergence was subtracted explicitly. Letting two operators approach the same point, was safely possible in a normal-ordered product. Similarly, another approach to regularization is the so-called point-splitting, denoted by colons $:(\ldots):$, where a finite distance between two operators of the product is kept and the divergence in Eq. (2.85) is subtracted. We define for a product of two operators [vS98] (compare definition of normal-ordering in Eq. (2.14))

$$:O_i(z)O_j(z): = O_i(z+a)O_j(z) - \langle O_i(z+a)O_j(z)\rangle_0. \tag{2.86}$$

On the right hand side, we see that point-splitting involves examples of OPEs. Note that the short-distance cutoff a here is not necessarily the same as the momentum cutoff of bosonic operators used before, however, the two should be identified with each other if one tries to make a connection between point-splitting and normal-ordering. Doing so, it appears that point-splitting and normal-ordering are equivalent strategies of regularization, for both fermionic or bosonic theories. This holds, however, only if the diverging part in Eq. (2.83) is simply a c-number, such that the divergence can be subtracted properly. As this is usually the case [vS98], we shall use in the following the notations $:(\ldots): = {}^*_*(\ldots){}^*_*$ as synonyms.
We illustrate this analogy for the density operator. From Eq. (2.16), we already know the normal-ordered version $\rho_r = {}^*_*\psi_r^\dagger(z_r)\psi_r(z_r){}^*_* = i\partial_{z_r}\phi_r(z_r) + \frac{2\pi}{L}N_r$, with $\partial_{z_r} = -ir\partial_x$. Now,

$$\begin{aligned}\psi_r^\dagger(z_r+a)\psi_r(z_r) &= \frac{1}{\Omega}\sum_{k,q} e^{(k-q)(z_r+a)}e^{-kz_r}c^\dagger_{r,k-q}c_{r,k} = \frac{1}{\Omega}\sum_{k,q\neq 0} e^{(k-q)(z_r+a)}e^{-kz_r}c^\dagger_{r,k-q}c_{r,k} \\ &\quad + \frac{1}{\Omega}\sum_{k>0} e^{ka}c^\dagger_{r,k}c_{r,k} + \frac{1}{\Omega}\sum_{k\leq 0} e^{ka}(1-c_{r,k}c^\dagger_{r,k}) \\ &= {}^*_*\psi_r^\dagger(z_r+a)\psi_r(z_r){}^*_* + \frac{1}{\Omega}\sum_{k\leq 0} e^{ka} = {}^*_*\psi_r^\dagger(z_r+a)\psi_r(z_r){}^*_* + \frac{1}{a}. \end{aligned} \tag{2.87}$$

First, because of $\langle 0|c^\dagger_{r,k-q}c_{r,k}|0\rangle = 0$ for $q \neq 0$, such products are already normal-ordered. If $q = 0$, normal-ordering (in the present notation) corresponds to bringing the annihilators to the right hand side for $k > 0$, and to the left hand side for $k \leq 0$. The only term that is not normal-ordered, is the last one, that diverges as $1/a$. From Eq. (2.87), we infer that $\langle\psi_r^\dagger(z_r+a)\psi_r(z_r)\rangle_0 = 1/a$, in agreement with Eq. (2.85). Note that point-splitting makes the divergence apparent and tractable. Once a product is regularized (normal-ordered), we can safely send a to zero, so

$$:\psi_r^\dagger(z_r)\psi_r(z_r): = {}^*_*\psi_r^\dagger(z_r+a)\psi_r(z_r){}^*_* \simeq {}^*_*\psi_r^\dagger(z_r)\psi_r(z_r){}^*_* = \rho_r. \tag{2.88}$$

2.5. (Perturbative) Renormalization group theory

Renormalization group (RG) theory is a fundamental and comprehensive method that can not be explained exhaustively in the scope of this Thesis. Instead, with an eye towards subsequent applications, we give here a short excerpt of the general theory of perturbative renormalization group around a fixed point, following Refs. [Car96, AS10, Fra13]. For more details, it is worthwhile to study for example Ref. [Sha94]. The general idea of the RG is to gain physical insight from rescaling the operators of the model, while at the same time integrating out high energy degrees of freedom. This way, one can learn how operators behave when going to an effective low-energy theory. If a perturbation grows upon RG, it is called relevant perturbation, and can have crucial impact on the ground state of the system, such as transitions to localized phases and the breakdown of transport. On the other hand, operators that shrink upon RG are called irrelevant, and indicate weak perturbations. Terms that do not change upon rescaling, and therefore possess the symmetry of scale-invariance, are called fixed points.
The physical properties of a system under consideration are represented by the partition function Z. Oftentimes, one employs a path integral formulation to write Z in the form of functional integrals. For this concept, we refer the reader to Refs. [AS10, Sha94, Fra13], and, as far as the RG is concerned, focus on an operator-based real space approach, following mostly Ref. [Car96].

2.5.1. Operator-based approach

We assume that the system is described by a Hamiltonian $H = H^* + H'$, where H^* is a fixed point of the theory, and H' is a small perturbation to the fixed point. In our model, the fixed point will be given by the interacting Luttinger liquid Hamiltonian $H^* = H_{\mathrm{LL}}$. The perturbation can in general be time-dependent, $H'(\tau)$ in imaginary time τ, with the time-dependence governed by the Heisenberg equation of motion. The canonical partition function then takes the form [Fra13]

$$Z = \mathrm{Tr}(\mathcal{T} e^{-\int_0^\beta \mathrm{d}\tau\ H(\tau)}) = \mathrm{Tr}(e^{-\beta H^*} \mathcal{T} e^{-\int_0^\beta \mathrm{d}\tau\ H'(\tau)}). \tag{2.89}$$

Here, $\mathcal{T}$ is the imaginary time-ordering operator. In the case of a time-independent perturbation, we recover the simple form $Z = \mathrm{Tr}(e^{-\beta H})$. The tracing operation has to be understood as $\mathrm{Tr}(\ldots) = \sum_n \langle n|(\ldots)|n\rangle$, where we sum over a complete set of Fock space states $\{|n\rangle\}$.
A complete set of (local) quantum field operators of the system H^* at the fixed point shall be given by $\{\phi_n(\vec{r})\}$, where now we write the vector $\vec{r} = (x, v\tau)$ in 2D space-time, using imaginary time $\tau = it$. Importantly, we consider the operators ϕ_n to be scaling operators (fields), which means that they transform homogeneously (or irreducibly) under rescaling,

$$\phi_n(b^{-1}\vec{r}) = b^{\Delta_n} \phi_n(\vec{r}). \tag{2.90}$$

Here, $b \neq 1$ rescales both components of $\vec{r}$ (isotropically), and Δ_n is the scaling dimension of ϕ_n. In other words, scaling operators do not mix under rescaling. Treating scale invariance as a symmetry of the fixed point, one can always choose a set of operators such that

the ϕ_n transform irreducibly [Fra13]. It can be shown from general symmetry arguments [Car96, Fra13], that at the fixed point the two-point correlations of scaling operators have a pure power-law behaviour, and are even orthogonal in the scaling dimensions,

$$\begin{aligned}\langle\phi_n(\vec{r})\phi_n(\vec{r}')\rangle_* &= |\vec{r}-\vec{r}'|^{-2\Delta_n},\\ \langle\phi_n(\vec{r})\phi_m(\vec{r}')\rangle_* &= \delta_{\Delta_n,\Delta_m}|\vec{r}-\vec{r}'|^{-2\Delta_n}.\end{aligned} \tag{2.91}$$

Now, let us again introduce more general operators $\{O_i(\vec{r})\}$, labeled by the index i, that are composed of the fields $\{\phi_n(\vec{r})\}$. We insist though, that the O_i are as well scaling operators, and decay as a power law for large distances, so

$$\begin{aligned}O_i(b^{-1}\vec{r}) &= b^{\Delta_i}O_i(\vec{r}),\\ \langle O_i(\vec{r})O_i(\vec{r}')\rangle_* &\propto |\vec{r}-\vec{r}'|^{-2\Delta_i}.\end{aligned} \tag{2.92}$$

Even though the above conditions seem quite restrictive, they will be fulfilled for most of the important physical operators we consider. We now study the rescaling of a quite general perturbation of the form [Fra13]

$$\int \mathrm{d}\tau\ H'(\tau) = \int \mathrm{d}^D r\ \sum_i a^{\Delta_i^{\mathrm{naive}}-D}\lambda_i O_i(\vec{r}), \tag{2.93}$$

where λ_i are coupling constants. Here, we have written an integral of general dimensionality D, which will be useful in the following. In the case of one spatial and one temporal dimension each, we have $D=2$ and $\mathrm{d}^2 r = v\mathrm{d}x\ \mathrm{d}\tau$. The power of a is introduced in order to make the couplings dimensionless. In this introductory part, we shall for simplicity assume that $\Delta_i^{\mathrm{naive}} = \Delta_i$, meaning that the physical scaling dimension equals the long-distance scaling dimension. For applications where this is not the case, the power of a can be readily adapted, for instance by writing powers of a/L, as emerging in the process of normal-ordering. Expanding Eq. (2.89) for small λ_i yields

$$\begin{aligned}Z = Z^*[1 &- \int \mathrm{d}^D r\ \sum_i \lambda_i a^{\Delta_i - D}\langle\mathcal{T}O_i(\vec{r})\rangle_*\\ &+ \frac{1}{2}\int \mathrm{d}^D r\ \mathrm{d}^D r'\ \sum_{i,j}\lambda_i\lambda_j a^{\Delta_i+\Delta_j-2D}\langle\mathcal{T}O_i(\vec{r})O_j(\vec{r}')\rangle_* + \mathcal{O}(\lambda^3)].\end{aligned} \tag{2.94}$$

Here, it is $Z^* = \mathrm{Tr}(e^{-\beta H^*})$. The perturbative RG is now supposed to tell us, how the couplings λ_i evolve, when going to an effective low-energy theory. A RG transformation always contains the three following steps: (i) integrating out high energy modes, (ii) rescaling and (iii) normalization of the operatorsO_i.
We use a real space formulation and consider the integral $\int_{r>a}\mathrm{d}^D r$, where $r=|\vec{r}|$. Here, we have introduced the short-distance cutoff (minimum length scale) a, since correlations potentially diverge for short separations in real space. In doing so, we by hand exclude some degrees of freedom in the form of short distances from the full integral. Integrating out further high-energy modes corresponds to increasing a, so $a \to ba$ with $b>1$. In a momentum space formulation, a high energy cutoff was instead given by excluding large momenta, so in the integrals $\int_{-\Lambda}^{\Lambda}\mathrm{d}^D k$, we can associate the momentum cutoff $\Lambda \approx 1/a$

with the short-distance cutoff. Λ then has to be reduced to integrate out high energy degrees of freedom. Note, that now we have imposed an isotropic cutoff on both space and time. In the second step, we rescale $\vec{r} \to b\vec{r}$ in order to restore the original range of the integral. In the third step, we normalize the operators O_i using the scaling properties of Eq. (2.92). Studying the first-order term in Eq. (2.94), the three steps are

$$\int_{r>a} \mathrm{d}^D r \sum_i a^{\Delta_i - D} \lambda_i \langle \mathcal{T} O_i(\vec{r}) \rangle_* \overset{\text{(i)}}{\to} \int_{r>ba} \mathrm{d}^D r \sum_i a^{\Delta_i - D} \lambda_i \langle \mathcal{T} O_i(\vec{r}) \rangle_* \\ \overset{\text{(ii)}}{\to} \int_{r>a} \mathrm{d}^D r \, b^D \sum_i a^{\Delta_i - D} \lambda_i \langle \mathcal{T} O_i(b\vec{r}) \rangle_* \overset{\text{(iii)}}{\to} \int_{r>a} \mathrm{d}^D r \sum_i a^{\Delta_i - D} b^{D-\Delta_i} \lambda_i \langle \mathcal{T} O_i(\vec{r}) \rangle_*. \quad (2.95)$$

After re-exponentiation of the expansion of Eq. (2.94), the effect of the (so far only first order) rescaling can be attributed to a change of the coupling constant $\lambda_i = \lambda_i(b)$, where $\lambda_i(b) = \lambda_i b^{D-\Delta_i}$ in Eq. (2.95). We use a new running parameter ℓ (instead of a), where $b > 1$ means a small change in ℓ by $d\ell$, as $b = e^{d\ell} \approx 1 + d\ell$ with $d\ell \ll 1$. For any power we get $b^x \approx 1 + x d\ell$. Note that effectively, we then have $a = a_0 e^{\ell}$, with a bare cutoff a_0, and rescale $a \to ba \approx a(1 + d\ell)$. In parameters ℓ only, this rescaling can be written as $\lambda_i(\ell) \overset{\ell \to \ell + d\ell}{\to} \lambda_i(\ell + d\ell) = \lambda_i(\ell) e^{(\Delta_i - D) d\ell} \approx \lambda_i(\ell)(1 + (\Delta_i - D) d\ell)$. Using that $\lambda_i(\ell + d\ell) \simeq \lambda_i(\ell) + \frac{d}{d\ell}\lambda_i(\ell) d\ell$, we find in first order

$$\frac{d}{d\ell}\lambda_i(\ell) = (D - \Delta_i)\lambda_i(\ell). \quad (2.96)$$

The right hand side of Eq. (2.96) (sometimes referred to as Gell-Mann-Low equation) is called β-function. This order of approximation (first order), is usually called "tree-level" [Fra13]. We see, that as long as the physical dimension and the scaling dimension are equivalent, the first-order RG of Eq. (2.95) can as well be achieved by rescaling the prefactor that compensates for the dimensions by $a \to a(1 - d\ell)$ (because the power exponent has the opposite sign). In this case, the tree level RG can often be read off by a simple inspection of the dimensions of the operator of interest.

It is readily checked that the Luttinger liquid Hamiltonian, given in Eq. (2.23), is indeed a fixed point: From the correlators given in Eqs. (2.67)–(2.69) (e.g. at zero temperature), we infer that $\langle \partial_x \phi(x) \partial_x \phi(0) \rangle \sim 1/x^2$, therefore $\Delta_{\partial_x \phi} = 1$, and analogously $\Delta_{\partial_x \theta} = 1$. The respective squared operators, making a appearance in H_{LL}, thus have a scaling dimension of two. Considering the Luttinger parameters, the coupling constants of the problem, Eq. (2.96) tells us that they will not change under renormalization, as $d/d\ell(vK)(\ell) = 0$ and $d/d\ell(v/K)(\ell) = 0$, which is the definition of a fixed point.

As pointed out in Ref. [Car96], the cutoff a enters in the RG in several ways. Most importantly, it appears explicitly in the form of prefactors $a^{\Delta_i - D}$, but also implicitly in the form of potential short-distance divergences of the two-point correlation functions. Moreover, the cutoff enters through dimensionless factors of a/L. Up to first order in the coupling constant, renormalization effects can be studied simply by power-counting of a (see Eq. (2.96)). Starting from second order in the couplings, however, cutoff-dependent correlations need to be accounted for in the perturbative RG, as we shall see in the following. With the OPE of Eq. (2.83), we can simplify the second-order term of Eq. (2.94)

to

$$\begin{aligned}
&\frac{1}{2}\int_{|\vec{r}-\vec{r}'|>a} \mathrm{d}^D r\ \mathrm{d}^D r'\ \sum_{i,j} \lambda_i\lambda_j a^{\Delta_i+\Delta_j-2D}\langle \mathcal{T}O_i(\vec{r})O_j(\vec{r}')\rangle_* \\
&\simeq \frac{1}{2}\int_{|\vec{r}-\vec{r}'|>a} \mathrm{d}^D r\ \mathrm{d}^D r'\ \sum_{i,j,k} \lambda_i\lambda_j c_{ijk} a^{\Delta_k-2D}\langle \mathcal{T}O_k(\vec{r})\rangle_* \\
&\overset{\text{(i)}}{\to} \frac{1}{2}\int_{|\vec{r}-\vec{r}'|>ba} \mathrm{d}^D r\ \mathrm{d}^D r'\ \sum_{i,j,k} \lambda_i\lambda_j a^{\Delta_k-2D} c_{ijk}\langle \mathcal{T}O_k(\vec{r})\rangle_* \\
&= \frac{1}{2}\left(\int_{|\vec{r}-\vec{r}'|>a} - \int_{ab>|\vec{r}-\vec{r}'|>a}\right) \mathrm{d}^D r\ \mathrm{d}^D r'\ \sum_{i,j,k} \lambda_i\lambda_j a^{\Delta_k-2D} c_{ijk}\langle \mathcal{T}O_k(\vec{r})\rangle_*. \qquad (2.97)
\end{aligned}$$

Anticipating divergences of the two-point correlation function, we restrict the distance of coordinates by a short-distance cutoff. While the first term simply gives back the second-order term in Eq. (2.94), the last term takes the form of the first-order contribution, and thus renormalizes λ. We approximate the integral by putting [GS88, Fra13, Car96] $|\vec{r}-\vec{r}'| = a$ on a shell of $ad\ell$. The integral over r' then yields a factor $S_D a^D d\ell$, where $S_D = 2\pi^{D/2}/\Gamma(D/2)$ is the surface of a D-dimensional hypersphere, with $\Gamma(x)$ being the Euler gamma function.

$$\begin{aligned}
&-\frac{1}{2}\int_{ab>|\vec{r}-\vec{r}'|>a} \mathrm{d}^D r\ \mathrm{d}^D r'\ \sum_{i,j,k} \lambda_i\lambda_j a^{\Delta_k-2D} c_{ijk}\langle \mathcal{T}O_k(\vec{r})\rangle_* \\
&\simeq -\frac{1}{2} S_D d\ell \int \mathrm{d}^D r\ \sum_{i,j,k} \lambda_i\lambda_j a^{\Delta_k-D} c_{ijk}\langle \mathcal{T}O_k(\vec{r})\rangle_*. \qquad (2.98)
\end{aligned}$$

Comparing to the first-order term in Eq. (2.94), we have found a correction in second order of λ. Note, that this contribution has a different physical origin (regularization of the correlation functions) than the first-order contribution. With this, the RG equation for the coupling λ now reads ("one-loop" β-function)

$$\frac{d}{d\ell}\lambda_i(\ell) = (D-\Delta_i)\lambda_i(\ell) - \frac{1}{2} S_D \sum_{n,m} \lambda_n(\ell)\lambda_m(\ell) c_{nmi}. \qquad (2.99)$$

We emphasize again, that above we have used an isotropic cutoff of the full space-time vector $\vec{r}$, as it is commonly done [Car96, Gia03]. Explicitly, in $D = 1+1$ dimensions, this means that we postulate the full space-time vector to be bounded by $r = |\vec{r}| = \sqrt{x^2 + (v\tau)^2} > a$. On the other hand, one might imagine an anisotropic cutoff to be imposed only on either of space or time. The choice of a cutoff can be important for the resulting scaling, as we demonstrate later. It therefore remains to be clarified what kind of cutoff should be imposed.

2.5.2. Meaning of the cutoff

According to Ref. [GNT04] (p.16), the cutoff a should be considered the "smallest possible interval between two points in (τ, x)-space", which applies to both isotropic and

anisotropic choices. Whether or not the cutoff is chosen to be isotropic, also depends on the physical meaning we assign to the cutoff, and the symmetries of the system.
First, Lorentz invariance of the system, which means invariance under space-time rotations, implies isotropy of the cutoff. For instance, in the context of RG, we find ([Fra13], p.65): "For simplicity, in what follows we assume that the rescaling is isotropic both in space and in space-time. Thus, we are assuming that there will be an effective Lorentz invariance in the system of interest." Indeed, Lorentz invariance is present in the Luttinger liquid model we study here. However, we like to point out, that introducing a cutoff itself breaks the translational, and therefore Lorentz invariance of the system. The same appears, if any kind of impurity or disorder potential is introduced. In a suchlike realistic system, we therefore do not expect global Lorentz symmetry.
In a discretized theory, the cutoff seems to have a natural physical meaning in the sense of the minimal distance between two sites, while in a continuum field theory this is less obvious. This point is, for instance, made in Ref. [Car96], in the context of potential short-distance divergences of the integrals ([Car96], p. 88): "On the lattice, this would be regulated by the lattice itself. In the continuum approach, it is more practical to introduce a rotationally invariant cut-off, and to insist that all integrals should be restricted to $|r_i - r_j| > a$. In the interacting gas picture, this corresponds to introducing a hard core repulsion of radius a between the particles. This cut-off, although crude, is quite sufficient for the first-order calculation of the renormalization group functions." These arguments make a case for a spatially homogeneous cutoff, but except for practical purposes, there would be no reason to use a cutoff that is isotropic in space and time. On the other hand, Haldane states that the regularization of momentum sums is more of a technical requirement, and should not be associated with a lattice spacing [Hal81b]. Nevertheless, it makes sense to relate the cutoff to the effective energy bandwidth of the system [vS98, ZvD00].
We conclude, that any realistic system should provide a momentum cutoff, that we understand as the effective bandwidth of the (linear) energy spectrum. The isotropic choice of a cutoff seems to be more a matter of convenience than a physical requirement. Based on the original, regularizing purpose of the cutoff, it can be as well sufficient to impose a cutoff only on one variable (space or time), depending on the application, as long as no fundamental symmetries of the system are violated.

3. Conductance of the helical liquid

Having set the stage in the previous chapter, we now turn to the actual transport signatures of the helical liquid. Most importantly, the conductance of a system reflects the hindrances for the electron flow. For a helical liquid with a single channel, the bare conductance has a precise, universal value. This leads to the typical quantization of the total conductance, that is a hallmark of the quantum spin Hall state. Obstacles such as interspersed impurities, generally induce backscattering processes, and thus reduce the conductance in the form of characteristic power-law corrections, that depend on the temperature and the applied bias voltage. At the helical edge, a peculiar protection mechanism (due to time-reversal symmetry) prevents the particles from backscattering elastically. Therefore, electron transport is robust up to corrections arising from inelastic backscattering processes, which renders helical states particularly interesting for the analysis of correlated electron effects. The goal of this Thesis is to examine such backscattering mechanisms, the corresponding microscopic sources, and the explicit transport signature, that one can expect in a realistic system. Hereby we study only backscattering within a single transport channel (no inter-channel or inter-edge scattering).
In this chapter, we briefly review the general methods of calculating the conductance in both equilibrium and non-equilibrium situations. The latter is typically given, if, of the two usual energy scales, the bias voltage is greater than the temperature. Furthermore, the influence of non-interacting leads, attached to the interacting LL, is discussed. Subsequently, we study the generic backscattering operators of the helical liquid. Generic here means, that the explicit form of the operators is derived by a general symmetry analysis, and not from microscopic processes. They can, or cannot, be present in a realistic material, depending on the specific properties of the system. Corresponding physical sources of backscattering, with a special emphasis on Rashba spin-orbit coupling, will be discussed in the subsequent Chap. 4 and Chap. 5.

3.1. Equilibrium theory

3.1.1. Conductivity and conductance

Following standard methods [KF92a, Mas95, MS95, Mas05, Gia03], we compute the (first position-dependent) conductivity σ of the system in equilibrium, at finite temperature. The result holds approximately in a regime, where the bias voltage is small compared to the temperature. Using the Kubo formula, we have

$$\sigma_\omega(x,x') = \frac{ie^2\omega_n^2}{\pi^2\omega} G_{\omega_n}(x,x')|_{\omega_n\to i\omega-\epsilon}, \tag{3.1}$$

$$G_{\omega_n}(x,x') = G_{\omega_n}(x-x') = \int_0^\beta \mathrm{d}\tau\ \langle \mathcal{T}\phi(x,\tau)\phi(x',0)\rangle e^{-i\omega_n\tau}. \tag{3.2}$$

Here, G_{ω_n} is called the Matsubara Green function, whereas ω_n are the Matsubara frequencies (that generally depend on the temperature). The above correlator can as well be related to the current-current correlation, using $j = \partial_t\phi/\pi = -i\partial_\tau\phi/\pi$. Eventually, we perform the analytical continuation $\omega_n \to i\omega - \epsilon$, with some positive infinitesimal ϵ, in order to find the conductivity in terms of real frequencies.
In the absence of perturbations, we can find the free propagator $G^0_{\omega_n}$ from the correlation functions given in Sec. 2.3. In the limit of small spatial distances, and low temperatures, the relevant dc-contribution to Eq. (3.1) can be given by [MS95, Mas95]

$$G^0_{\omega_n}(x,x') = \int_0^\beta \mathrm{d}\tau\ \langle \mathcal{T}\phi(x,\tau)\phi(x',0)\rangle_0 e^{-i\omega_n\tau} \simeq \frac{K\pi}{2|\omega_n|}. \tag{3.3}$$

From the inspection of the Matsubara and the retarded Green function (in the real frequency domain), one finds [Mas95], that the analytical continuation in the limit of $\omega \to 0$ results in $G^0_{\omega_n}(x,x')|_{\omega_n\to i\omega-\epsilon} = \frac{iK\pi}{2\omega}$, such that the conductivity is real, as it should be. As we are interested in the dc-transport properties, we eventually study the (position-independent) conductance G, which is the quantity of physical interest, [1]

$$G = \lim_{\omega\to 0}\frac{1}{L}\int \mathrm{d}x'\ \sigma_\omega(x-x'). \tag{3.4}$$

For instance, with Eq. (3.3), we obtain the free conductance $G_0 = e^2K/(2\pi)$ per edge channel. This leads to the well-known quantization of the total conductance in a 2D topological insulating system. In the presence of sources of backscattering, we expect corrections to the total conductance, such that (in the weak-coupling limit)

$$G = G_0 - \delta G. \tag{3.5}$$

Such corrections δG will be the subject to upcoming sections.
The above method relies on the assumption that the strength of the backscattering impurities is small, which means that we are in the so-called "weak-coupling limit". In order to determine the corresponding corrections to the conductance, the operator average in Eq. (3.2) can then be calculated perturbatively. On the other hand, if the impurity potential is very large at the energy scale under consideration, for instance because it is relevant in an RG sense, we face the "strong-coupling limit". In this case, a slightly different approach has to be employed (see more below).

3.1.2. LL with attached leads

As we have seen in the previous section, using an equilibrium framework, the free conductance per edge channel in the wire is found to be (see Eqs. (3.3) and (3.4))

$$G_0 = e^2\frac{K}{2\pi}, \tag{3.6}$$

[1] We defined here the position-dependent conductivity $\sigma_\omega(x-x')$, while the position-independent quantity simply reads $\sigma = \int \mathrm{d}x\ \sigma_\omega(x-x')$. Therefore, the relation $G = \sigma/L$ holds, as it should be for 1D systems (see e.g. [Gia03], Chap. 7).

and thus depends on the interaction strength K. The technical reason is that the propagator $G^0_{\omega_n} \propto \langle\phi\phi\rangle_0 \propto K$ in Eq. (3.3) is affected by the interactions in the channel [KF92a]. This result was shown to be in contrast to experiments, where the free conductance of long, high-mobility GaAs wires did not exhibit any interaction-dependence [THS95]. The experimental finding can be reproduced in the above model, when the conductance of a system is computed, where the wire is attached to non-interacting leads, that play the role of electron reservoirs [MS95, SS95, Pon95]. Such reservoirs are assumed to be higher-dimensional, metallic objects of great extent. As screening can work more efficiently there, than in the actual edge channel, it seems reasonable to consider the contacts as effectively non-interacting. Making use of the boundary conditions at the wire-lead interface, the free propagator $G^0_{\omega_n}$ is dominated by the lead properties, and K should be replaced by the effective $K_{\text{Lead}} \approx 1$ in Eq. (3.3), such that $G_0 = e^2/(2\pi)$.
If a finite bias voltage is applied, creating different chemical potentials for the right- and left-moving particles, the system is not expected to be in equilibrium anymore. In this case, non-equilibrium techniques such as the Keldysh framework have to be employed [Kel64] (see [Ram07] for a good review). We next discuss, how non-interacting leads that change the initial distribution of right- and left-movers can be included into the Keldysh model, following closely Ref. [PBW03], and later use this technique to calculate the non-equilibrium conductance in the presence of such contacts, and a single SOC impurity.

3.2. Non-equilibrium theory

3.2.1. Keldysh operator average

A non-equilibrium approach is required, for instance, when dealing with a finite bias voltage, that is expected to drive the system out of its thermal equilibrium. Let us first review the idea of a quantum mechanical operator expectation value in conventional equilibrium theory [BF04]. [2] Consider an operator $O(t)$, that might have an explicit time-dependence, in a system modeled by the Hamiltonian $H(t) = H_0 + H'(t)$, where $H'(t)$ is a small time-dependent perturbation. We define a general time evolution operator U_X, which describes the time-dependence governed by the Hamiltonian X, by

$$U_X(t, t_0) = \mathcal{T} e^{-i \int_{t_0}^{t} \mathrm{d}t' \, X(t')}, \tag{3.7}$$

where $\mathcal{T}$ is again the time-ordering operator defined in Eq. (2.64). Explicitly, it is $U_{H_0}(t, t_0) = e^{-iH_0(t-t_0)}$. Furthermore, we abbreviate an operator, whose time-dependence is governed by the Hamiltonian X, by

$$O_X(t) = U_X^\dagger(t, t_0) O(t) U_X(t, t_0). \tag{3.8}$$

Following a widely-used convention, the time evolution of an observable with respect to the free system shall as well be denoted by $O_{H_0}(t) = O_I(t)$.
In the Heisenberg picture, the initial states $|n\rangle = |n(t_0)\rangle$ gain a time-dependence [BF04]

$$|n(t)\rangle = U_{H_0}(t, t_0) U_{H'_I}(t, t_0) |n\rangle = U_H(t, t_0) |n\rangle. \tag{3.9}$$

[2] Note that in contrast to above, in the following we use a real-time formalism.

In the last line we used the Dyson formula [Ram07] $U_{H'_I}(t,t_0) = U^\dagger_{H_0}(t,t_0)U_H(t,t_0)$. Similarly, the density matrix of the free system, $\rho_0 = e^{-\beta H_0} = \sum_n |n\rangle\langle n|e^{-\beta E_n}$, evolves as $\rho(t) = \sum_n |n(t)\rangle\langle n(t)|e^{-\beta E_n} = U_H(t,t_0)\rho_0 U^\dagger_H(t,t_0)$. In the presence of the perturbation, the time-dependent expectation value of the operator $O(t)$ takes the form

$$\begin{aligned}\langle O(t)\rangle &= \frac{1}{Z_0}\mathrm{Tr}(\rho(t)O(t)) = \frac{1}{Z_0}\mathrm{Tr}(U_H(t,t_0)\rho_0 U^\dagger_H(t,t_0)O(t)) \\ &= \frac{1}{Z_0}\mathrm{Tr}(\rho_0 U^\dagger_H(t,t_0)O(t)U_H(t,t_0)) = \langle O_H(t)\rangle_0, \end{aligned} \tag{3.10}$$

where we used the cyclic permutation properties of the trace. $Z_0 = \mathrm{Tr}(\rho_0)$ is the partition function of the free system. To make a connection to the later Eq. (3.22), we note that this can be rewritten again in the form of

$$\langle O(t)\rangle = \frac{1}{Z_0}\mathrm{Tr}(\rho_0 U^\dagger_{H'_I} O_I(t) U_{H'_I}). \tag{3.11}$$

The concept of equilibrium perturbation theory is based on the assumption, that the system is unperturbed at an initial point in time, t_0, and subsequently, the perturbation is switched on adiabatically. The presence of the perturbation drives the system out of equilibrium, however, if it is switched on in a sufficiently slow way, the system remains approximately in its instantaneous eigenstate. This assumption is known as the "adiabatic theorem". It allows for particular simplifications, most importantly, the eigenstates of the system at times $t = \pm\infty$ can only differ by a phase, $|n(\infty)\rangle = e^{i\phi}|n(-\infty)\rangle$, with some scalar ϕ [Mac07, Ram07]. The process of turning on the perturbation can for instance be modeled by $H(t) = H_0 + e^{-\epsilon|t|}H'$, with a small positive number ϵ. Note that the term "equilibrium" should not be confused with the notion of "steady state", which simply means that the system does not change with time.
In a non-equilibrium theory, such as the Keldysh-Schwinger framework [Sch61, KB62, Kel64], adiabaticity is not expected to hold anymore. Instead, perturbations drive the system out of equilibrium immediately after being switched on. The eigenstates of the system at $t = \pm\infty$ then are not related in a simple way, however, one can avoid reference to the generally unknown state at $t = \infty$ by winding it back to $t = -\infty$, using Eq. (3.9), so $|n(\infty)\rangle = U_H(\infty,-\infty)|n(-\infty)\rangle$. This gives rise to a more refined time-ordering structure, called the Keldysh contour, including a forward (+), and backward (−) time branch. A more detailed description of the general theory can be found in the literature, e.g. Ref. [Ram07]. Here, we mainly use the finding that the non-equilibrium operator expectation value is given by [Mar05]

$$\langle O(t)\rangle = \frac{1}{2}\sum_{\eta=\pm}\left\langle \mathcal{T}_K\left[O^\eta_I(t)e^{-i\int_K \mathrm{d}t'\ H'_I(t')}\right]\right\rangle_0 . \tag{3.12}$$

Here, $\eta = \pm$ is the Keldysh index representing the position of the respective operator O^η on one of the two time branches of the Keldysh contour, and we used that $\int_K \mathrm{d}t\ X(t) = \sum_{\eta'}\int_{-\infty}^{\infty}\mathrm{d}t\ \eta' X^{\eta'}(t)$. The Keldysh contour is a closed time path, with the (+)-branch going from $t = -\infty$ to $t = \infty$, and the (−)-branch going all the way back from $t = \infty$ to $t = -\infty$. $\mathcal{T}_K$ denotes the Keldysh time-ordering operator, which sorts operators according

to their position along the contour. Importantly, the (−)-branch is always "later" on the contour than the (+)-branch and thus operators O^- will be contour-ordered to the left of all operators O^+. Explicitly, the contour ordering of two operators $A(t)$ and $B(t')$ corresponds to [Ram07]

$$\mathcal{T}_K A^\eta(t) B^{\eta'}(t') = \begin{cases} \mathcal{T} A(t)B(t') & \text{if } \eta = \eta' = +, \\ \pm B(t')A(t) & \text{if } \eta = +, \eta' = -, \\ A(t)B(t') & \text{if } \eta = -, \eta' = +, \\ \bar{\mathcal{T}} A(t)B(t') & \text{if } \eta = \eta' = -. \end{cases} \tag{3.13}$$

The regular time-ordering $\mathcal{T}$ holds on the (+)-branch, while anti time-ordering $\bar{\mathcal{T}}$ takes place on the (−)-branch. The upper (lower) sign in the second line of Eq. (3.13) applies to bosonic (fermionic) operators A and B.
In general, the equilibrium and non-equilibrium expectation values in Eqs. (3.10) and (3.12) are clearly different. However, in the lowest-order expansion of the perturbation H', the linear response regime, the two expectation values coincide and one recovers the well known Kubo formula [BF04]. To illustrate this, we compute Eq. (3.12) up to linear order. For bosonic operators, it is

$$\begin{aligned} \langle O(t)\rangle &\simeq \langle O_I(t)\rangle_0 - \frac{1}{2}i \sum_{\eta,\eta'=\pm} \int_{-\infty}^{\infty} \mathrm{d}t'\ \eta' \left\langle \mathcal{T}_K O_I^\eta(t) (H_I')^{\eta'}(t') \right\rangle_0 \\ &= \langle O_I(t)\rangle_0 - \frac{1}{2}i \int_{-\infty}^{\infty} \mathrm{d}t'\ \langle \mathcal{T} O_I(t) H_I'(t') + O_I(t) H_I'(t') \\ &\quad - H_I'(t') O_I(t) - \bar{\mathcal{T}} O_I(t) H_I'(t') \rangle_0 \\ &= \langle O_I(t)\rangle_0 - \frac{1}{2}i \int_{-\infty}^{\infty} \mathrm{d}t'\ 2\langle [O_I(t), H_I'(t')] \rangle_0 \theta(t-t') \\ &= \langle O_I(t)\rangle_0 - i \int_{-\infty}^{t} \mathrm{d}t'\ \langle [O_I(t), H_I'(t')] \rangle_0. \end{aligned} \tag{3.14}$$

This is exactly the Kubo expression, which can be obtained as well from a lowest-order expansion of the equilibrium expectation value, taking $t_0 \to -\infty$. For fermionic operators, the commutator in Eq. (3.14) is replaced by the anticommutator.

3.2.2. Implementation of a voltage bias

Let us consider a system governed by $H = H_0 + H'$, with a perturbation H'. Additionally, we take into account, that the system is brought out of equilibrium by the application of a bias voltage

$$H_V = -\frac{1}{\pi} \int \mathrm{d}x\ \left(\mu_+ \psi_+^\dagger(x)\psi_+(x) + \mu_- \psi_-^\dagger(x)\psi_-(x) \right) = \frac{eV}{2}(N_+ - N_-). \tag{3.15}$$

The bias represents a shift of the chemical potentials, $\mu_\pm = \pm eV/2$. We see that it only alters the zero modes, changing the ratio of right- and left-movers in the system. Defining

$H'_V = H_0 - H_V$, as well as $\rho_V = e^{-\beta H'_V}$, and $Z_V = \mathrm{Tr}(\rho_V)$, we assume that the operator average takes the form

$$\langle O(t)\rangle = \frac{1}{Z_V}\mathrm{Tr}\left(\rho_V(t)O\right) = \frac{1}{Z_V}\mathrm{Tr}\left(\rho_V U_H^\dagger O U_H\right) = \frac{1}{Z_V}\mathrm{Tr}\left(\rho_V O_H(t)\right), \tag{3.16}$$

where compared to Eq. (3.10), we have replaced ρ_0 by ρ_V. The physical assumption behind this approach is the following: Already in the initial, unperturbed state (time $t \to -\infty$), the bias voltage changes the energy of right- and left-moving particles relative to each other, such that the system is driven out of equilibrium. On the other hand, the contact bias is a static constraint, which does not affect the time-evolution of the states. Using that, $[H_0, H_V] = 0$, we can absorb the bias voltage in a unitary transformation U of the form

$$\begin{aligned} U\rho_0 U^\dagger = U e^{-\beta H_0} U^\dagger = e^{-\beta(H_0 - H_V)} e^C = \rho_V e^C, \\ U = \exp\left(i\frac{eVL}{4v_F\pi}(f_+ - f_-)\right) = (F_+^\dagger F_-)^{eVL/(4v_F\pi)}. \end{aligned} \tag{3.17}$$

Here, we use an exponential notation of the Klein factors of the form $F_\pm^\dagger = e^{if_\pm}$ and $F_\pm = e^{-if_\pm}$. The $f_\pm$ still have the characteristic commutation properties with the zero modes, as $[N_\eta, f_{\eta'}] = -i\delta_{\eta\eta'}$, and $[f_\eta, f_{\eta'}] = [N_\eta, N_{\eta'}] = 0$, with $\eta = \pm$ [PBW03]. By rewriting U in terms of the former $F_\pm$, we see that such a transformation can be interpreted as a change of the chiral particle numbers, proportional to the bias. Importantly, we assumed in the definition of the shifting operator U in Eq. (3.17), that the zero modes in H_0 are proportional to the bare velocity v_F, which corresponds to the assumption of non-interacting leads (see below). Using $U^\dagger$ on the particle number operators from the left hand side, is equivalent to a voltage-dependent shift of $N_\pm \to N_\pm \pm \frac{eVL}{4\pi v_F}$. An unimportant constant $C = \beta(eV)^2 L/(4\pi v_F)$ arises as well, that will cancel later on. With that, Eq. (3.16) can be rewritten as (we now drop the explicit time-dependence for brevity)

$$\begin{aligned} \langle O\rangle &= \frac{1}{Z_0}\mathrm{Tr}\left(U\rho_0 U^\dagger U_H^\dagger O U_H\right) = \frac{1}{Z_0}\mathrm{Tr}\left(\rho_0 (U^\dagger U_H^\dagger U)(U^\dagger O U)(U^\dagger U_H U)\right) \\ &= \frac{1}{Z_0}\mathrm{Tr}\left(\rho_0 \tilde{U}_H^\dagger \tilde{O} \tilde{U}_H\right). \end{aligned} \tag{3.18}$$

We defined the operation of U on a general operator O by

$$\tilde{O} = (U^\dagger O U). \tag{3.19}$$

We thus have to evaluate the modified time evolution $\tilde{U}_H$. Using again Dyson's equation, we obtain

$$\tilde{U}_H = U^\dagger U_H U = (U^\dagger U_{H_0} U)(U^\dagger U_{H'_I} U) = U_{H_0+H_V} e^C U_{(\tilde{H}')_{H_0+H_V}}. \tag{3.20}$$

Note, that while (by definition) $U U_{H_0} U^\dagger = U_{H_0 - H_V} e^C$, one finds $U^\dagger U_{H_0} U = \tilde{U}_{H_0} = U_{H_0+H_V} e^C$. The simplifications in the second factor of Eq. (3.20) can readily be checked [PBW03, GCT15]. Considering the bias a constituent of the free system, one might shorten the notation by labeling again $O_{H_0+H_V}$ as O_I, however, we shall refrain from doing so here

in order to not confuse the notation. Explicitly, the perturbation-dependent part of the time-evolution reads

$$U_{(\tilde{H}')_{H_0+H_V}} = \mathcal{T} \exp\left[-i \int_0^t \mathrm{d}t' \, (\tilde{H}')_{H_0+H_V}(t')\right]. \tag{3.21}$$

Eventually, we get from Eq. (3.18)

$$\langle O \rangle = \frac{1}{Z_0} \mathrm{Tr}\left(\rho_0 U^\dagger_{(\tilde{H}')_{H_0+H_V}} \tilde{O}_{H_0+H_V}(t) U_{(\tilde{H}')_{H_0+H_V}}\right). \tag{3.22}$$

When comparing this finding to Eq. (3.11), we observe, that the implementation of the bias corresponds to the effective substitution $O_I \to \tilde{O}_{H_0+H_V}$ and $H'_I \to (\tilde{H}')_{H_0+H_V}$. Because H_0 and H_V commute, and are both time-independent, such a replacement takes the simpler form

$$\begin{aligned} O &\to \tilde{O}_{H_V} = \tilde{O}_V, \\ H' &\to (\tilde{H}')_{H_V} = (\tilde{H}')_V. \end{aligned} \tag{3.23}$$

3.2.3. Free conductance with leads

To give an example, we use this approach to calculate the free conductance of the system. The free current, in the absence of perturbations, reads (putting back the elementary charge e, [GCT15])

$$j_0 = \frac{e v_F}{L}(N_+ - N_-). \tag{3.24}$$

This can be compared to the integrated current density, defined in Eq. (2.29),

$$\begin{aligned} j_0^{\text{no contacts}} &= \frac{e}{L}\int_{-L/2}^{L/2} \mathrm{d}x \; j(x) = \frac{e}{L}\int_{-L/2}^{L/2} \mathrm{d}x \; \left[\frac{vK}{2\pi}\partial_x(\phi_+(x) - \phi_-(x)) + \frac{vK}{L}(N_+ - N_-)\right] \\ &= \frac{evK}{L}(N_+ - N_-). \end{aligned} \tag{3.25}$$

The particle-hole excitations, ϕ_r, do not contribute to the integrated current due to the periodic boundary conditions of the bosonic fields, $\phi_r(L/2) = \phi_r(-L/2)$. In Eq. (3.24), only the bare Fermi velocity v_F enters, instead of vK in the free current of Eq. (3.25). This distinction is based on the following reasoning: In the former, we identify the zero modes with the non-interacting contacts attached to the LL wire, while in the latter, we did not assume any such leads. As mentioned above, in a composed system of leads connected to the 1D edge channel (see Fig. 3.1), the contacts can be viewed as reservoirs providing a large amount of electrons. Therefore, the particle numbers (zero modes) of the full system will be dominated by the number of particles of the contacts, and thus, the influence of the non-interacting leads can be incorporated in the decoupled zero-modes. This assumption has been used implicitly already in the definition of U in Eq. (3.17). [3]

[3] Implementing the bias was as well possible with interacting zero modes (no leads). Then, the transformation U only affects the combination $(N_+ - N_-)^2$ in H_0, and we have to replace v_F by vK in Eq. (3.17). The free conductance remains independent of K, if, consistently, we use the definition of j in Eq. (3.25).

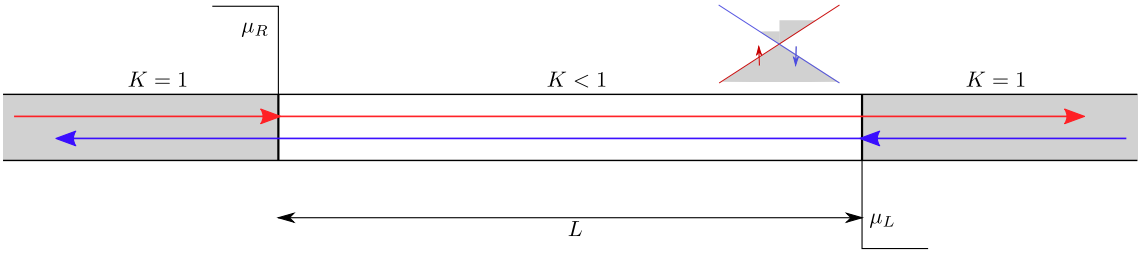

Figure 3.1.: Sketch of an interacting Luttinger liquid attached to non-interacting leads. The contacts represent electron reservoirs, that provide electrons for the counterpropagating transport channels. The energy of the particles depends on the applied bias voltage, which is proportional to the difference of the chemical potentials.

The respective interaction-independence will directly translate into the free conductance of the system. Alternatively to the definition of Eq. (3.4), the conductance can be given by the dI/dV-characteristics,

$$G = \frac{d\langle j\rangle}{dV}. \tag{3.26}$$

In the absence of a bias, the free current vanishes at thermal equilibrium, since right- and left-movers are then equally numerous. Adding a bias voltage the way we described above, we obtain with Eq. (3.23),

$$(\tilde{j_0})_V = j_0 + \frac{e^2 V}{2\pi}, \tag{3.27}$$

$$G_0 = \frac{d}{dV}\langle(\tilde{j_0})_V\rangle_0 = \frac{e^2}{2\pi}. \tag{3.28}$$

G_0 is the free conductance of the system, which does not depend on interactions here, in agreement with the discussion in Sec. 3.1.2. We see that in this model, a voltage bias can be conveniently introduced, resulting in a shift of operators as given in Eq. (3.23). This approach turns out to be especially useful in bosonic language. Furthermore, it allows to account for (non-interacting) contacts of the system by a simple modification of the effective velocity of the zero modes.

3.2.4. Galilean invariance

Whether the conductance of the free system, with or without leads, depends on the electron interaction strength, is fundamentally related to the distinction of the two velocities vK and v_F in the setup. Interestingly, these two parameters can be related by the symmetry of Galilean invariance, in systems with an underlying parabolic energy dispersion, which manifests itself in the requirement $vK = v_F$. This was first pointed out in an article by Haldane [Hal81a]. Let us briefly review the reasoning of this reference, applied to the case of a helical liquid (instead of a spinless LL considered there).
The usual Luttinger Hamiltonian models a 1D system with a linear energy spectrum of fermions. As we discussed before, it applies to both the scenarios of a truly linear

energy dispersion relation (such as the edge states of a 2D QSH sample), and a parabolic dispersion that is linearized around certain points of interest. In the latter case, the information about the underlying parabolic spectrum is seemingly lost, however, as we explain in the following, it remains incorporated in the form of additional constraints.
With zero modes written explicitly, and in the presence of interactions, we have (compare with Eq. (2.23)),

$$\begin{aligned} H_{\mathrm{LL}} = \frac{1}{(4\pi)^2}\int_{-L/2}^{L/2} \mathrm{d}x \, \left[vK(\partial_x\phi_+(x) - \partial_x\phi_-(x))^2 + \frac{v}{K}(\partial_x\phi_+(x) + \partial_x\phi_-(x))^2 \right] \\ + \frac{1}{4L}\left[vKJ^2 + \frac{v}{K}N^2 \right]. \end{aligned} \tag{3.29}$$

Here, we temporarily defined the relative and total particle numbers

$$\begin{aligned} J &= (N_+ - N_-), \\ N &= (N_+ + N_-), \end{aligned} \tag{3.30}$$

that are related to the density and the current in the form of $\rho_0 = N/L$ and $j_0 = vKJ/L$ (see Eq. (2.29)). In lowest order (or zero temperature), bosonic particle-hole excitations associated with the fields ϕ and θ are expected to be absent. We can then calculate the total momentum operator of the helical liquid to be approximately

$$P = \sum_r \int_{-L/2}^{L/2} \mathrm{d}x \; {}^*_*\psi_r^\dagger(x)(-i\partial_x)\psi_r(x)^*_* \simeq \frac{\pi}{L}(N_+^2 - N_-^2) = \frac{\pi}{L}NJ = \pi\rho_0 J. \tag{3.31}$$

Above, the same bosonization scheme as in Eq. (2.17) was used (note the immediate parallels between the momentum operator, $(-i\partial_x)$, and the kinetic energy operator, $(-ir\partial_x)$ of the linearized spectrum). Importantly, the momentum operator here does not know about the interactions in the system, as it simply sums up the momenta of the individual particles.
We now study the term proportional to J^2 in Eq. (3.29), which we can interpret as a net (or current) energy of the system. With Eq. (3.31), we obtain

$$E_{\mathrm{net}} = \frac{1}{4L}vKJ^2 = \frac{vK}{4\pi^2\rho_0}\frac{P^2}{N}. \tag{3.32}$$

This quadratic energy-momentum dependence is not in contrast with the fact that each single particle has a linear dispersion in the Luttinger liquid model, since E_{net} comprises the totality of all particles. It next seems intuitive to associate E_{net} with the net kinetic energy of the system, which in the classical, non-relativistic case is given by the relation $E_{\mathrm{kin}} = P^2/(2Nm)$. Here, m is the mass of a single particle, and thus Nm the total mass. This allows for the identification

$$vK = 2\pi^2\frac{\rho_0}{m} = v_F, \tag{3.33}$$

meaning that the product vK is not affected by the electron interaction strength in the Luttinger liquid (unlike v/K).

With interactions present in the system, it is not a priori clear that the above identification of $E_{\text{net}} = E_{\text{kin}}$ is valid, so that E_{net} can be considered purely kinetic. As we demonstrate in the following, this is only the case if the system features Galilean invariance. A Galilean boost changes the momentum $P \to P'$, and therefore the difference of right- and left-movers, $J \to J'$ (see Eq. (3.31)). We assume hereby that the bare density ρ_0 remains fixed. In the process, the kinetic energy of the system changes to $E_{\text{kin}} = P'^2/(2Nm)$. For illustration, consider a particle moving to the right with a small momentum (deep in the Fermi sea). If we change the coordinate system by a Galilean transformation in the same direction, and with a boost velocity that is greater than the one of the particle, the particle effectively becomes a left-mover in the moving frame. Given that Galilean invariance is present, such boosts can not change the model description of the system, and any two states parametrized by J and J' can possibly be mapped onto each other by means of a corresponding Galilean boost. In particular, any state characterized by a specific value of J, can be conceived of emerging from a reference ground state with $J = 0$ in Eq. (3.29). As a Galilean transformation does not induce interactions (alter the prefactor vK), but only changes J, the energy E_{net} has to be purely kinetic, and vK a constant of the model. Crucially, the above conclusion is based on the assumption of a constant electron mass m. For electrons moving in a solid state system, the bare mass should generally be replaced by the effective band mass m^*, which can be deduced from the single-particle energy dispersion $\varepsilon(k)$ by [AM76] $m^* = (d^2\varepsilon(k)/dk^2)^{-1}$. Therefore, in a LL system with an underlying parabolic energy dispersion, m^* is indeed a constant, while in a truly linear spectrum, one finds a diverging band mass, and the above argumentation breaks down.

We conclude, that in 1D systems with an underlying parabolic spectrum, Galilean symmetry provides an additional constraint in the form of $vK = v_F$. It is a well-known problem, that this point is not automatically accounted for in Luttinger liquid theory, since this model uses linearization of the energy spectrum as an indispensable prerequisite for bosonization [SMHG99]. Therefore, when studying linearized models in an underlying parabolic system, one faces the problem of artificially broken Galilean invariance. To overcome this problem, different routes were suggested. For instance, it is possible to redefine the Luttinger parameters v and K such as to fulfill $vK = v_F$ [SMHG99]. Alternatively, higher-order harmonics of the density functions can be included into the model [CPG00, Mas05, IG09a, IG09b, ISG12].
On the other hand, for 1D systems with a truly linear energy dispersion, no such modifications are necessary, and the Luttinger liquid relation $vK = v_F[1 + (g_4 - g_2)/(2\pi v_F)] \neq v_F$ remains in general valid. This is, for instance, expected to be the case for the edge states of a 2D topological insulator. Except for the influence of remote bulk bands, the energy dispersion of both chiral branches within the gap is shown to be almost linear in momentum. In such quasi-relativistic systems, Galilean invariance is replaced by an emergent Lorentzian invariance. Note further that the parameter vK can as well be renormalized by additional perturbative terms, such that ([Gia03], p. 221) "the effective v and K to put in a low-energy theory can (and in general will) be different from $vK = v_F$".

3.3. Generic backscattering

3.3.1. Protection against elastic backscattering

One of the most important and genuine properties of the 1D helical liquid is the absence of elastic backscattering. This is a consequence of the topological protection of the helical state by time-reversal symmetry (TRS). Here, we denote time reversal by the anti-unitary operator T, and since we deal with spinful particles, it is $T^2 = -1$. The general mechanism can simplest be understood with the help of the following symmetry argument [XM06, WBZ06].
Let $|\psi\rangle$ and $|\phi\rangle$ be two single-particle states of fermions with opposite chirality, that are time-reversal partners, $|\psi\rangle = T|\phi\rangle$. According to Kramer's theorem, the two states are then degenerate in energy. Next, we make use of the general relation

$$\langle T\alpha|T\beta\rangle = \langle\beta|\alpha\rangle, \tag{3.34}$$

which holds for any anti-unitary T and arbitrary states $|\alpha\rangle$ and $|\beta\rangle$. With this, we show that the backscattering matrix element of any time-reversal invariant perturbation H' vanishes,

$$\begin{aligned}\langle\psi|H'|\phi\rangle = \langle\psi|H'\phi\rangle &\overset{\text{Eq. (3.34)}}{=} \langle TH'\phi|T\psi\rangle \overset{[H',T]=0,|\psi\rangle=T|\phi\rangle}{=} \langle H'T\phi|TT\phi\rangle \\ &\overset{T^2=-1}{=} -\langle H'\psi|\phi\rangle = -\langle\psi|H'|\phi\rangle = 0.\end{aligned} \tag{3.35}$$

Therefore, the perturbation H' can not induce elastic single-particle backscattering at the helical edge. As a consequence, electronic transport in such a system is very robust compared to regular spinless or spinful 1D systems, where such a protection mechanism is absent. [4]
Importantly, the above argument involves wave functions that describe a single fermionic particle. We can generalize this idea to multiple-particle states of n fermions, assuming that the many-body wave functions $|\psi\rangle$ and $|\phi\rangle$ remain time-reversal partners. States containing an even number of particles have an integer total spin, and therefore $T^2 = 1$ in this case, while for an odd number of particles it is $T^2 = -1$. We then obtain similar to Eq. (3.35),

$$\langle\psi|H'|\phi\rangle = (-1)^n\langle\psi|H'|\phi\rangle. \tag{3.36}$$

The above Eq. (3.36) states that backscattering of an even number of particles, such as two-particle backscattering, is not forbidden by symmetry. Note that the latter requires an inelastic exchange of momentum between the individual particles of the many-body state, to be of nonzero rate. Otherwise, if no interactions are present, the diagram of the corresponding (elastic) backscattering process is disconnected, and can be split into n single-particle processes, that vanish by virtue of Eq. (3.35).

[4] There, two states of opposite chirality are not necessarily time-reversal partners (for example because right-moving particles can have any spin-orientation).

Despite the protection mechanism described above, backscattering in a truly one-dimensional helical channel can occur for various reasons. In essence, those are: (i) time-reversal symmetry might be broken, for instance due to an applied magnetic field, and elastic backscattering is no longer suppressed, (ii) in the presence of spinful perturbations (magnetic moments) coupling to the electron spins, the time-reversal constraints change such that elastic backscattering is again possible, (iii) there can be inelastic processes. In this case, kinetic energy is transferred between the individual particles of the many-body state, which can be mediated, for instance, by electron interactions or phonons. Also the inelastic backscattering of a single electron is compatible with TRS, since then the initial and final states of the process are not Kramer's partners, different from what was assumed in Eq. (3.35). The corresponding correlated backscattering operators are studied in the next section.

3.3.2. Generic backscattering operators

The generic, lowest-order backscattering operators of the helical Luttinger liquid [LOB12] take the form of elastic and inelastic single-particle backscattering (SPB), as well as two-particle backscattering (TPB). The latter is also called "umklapp"-scattering if being uniform. When time-reversal symmetry is broken, this allows for an elastic term of the form

$$\begin{aligned} H_{\mathrm{m}} &= \int \mathrm{d}x\; g_m(x)\psi_L^\dagger(x)\psi_R(x) + \mathrm{h.c.} \\ &= F_R^\dagger F_L \frac{v}{a^2}\left(\frac{2\pi a}{L}\right)^K \int \mathrm{d}x\; \tilde{g}_m(x){:}e^{2i\phi(x)}{:} + \mathrm{h.c.}. \end{aligned} \tag{3.37}$$

We refer to such a term as to a magnetic perturbation, since TRS could most naturally be broken by a magnetic field. This mechanism is found to be structurally similar to the backscattering off a simple electron-density impurity (or disorder) in the spinless LL, as studied e.g. in the Refs. [KF92a, KF92b, FG96, AR82, GS88].
If time-reversal symmetry is present, only inelastic backscattering processes are possible. The lowest-order terms then read [LOB12, WBZ06]

$$\begin{aligned} H_{1p}^{\mathrm{generic}} &= \int \mathrm{d}x\; \gamma_{1p}(x)\left(\partial_x\psi_L^\dagger(x)\psi_L(x) - \psi_R^\dagger(x)\partial_x\psi_R(x)\right)\psi_L^\dagger(x)\psi_R(x) + \mathrm{h.c.} \\ &= F_R^\dagger F_L v\left(\frac{2\pi a}{L}\right)^K \int \mathrm{d}x\; \tilde{\gamma}_{1p}(x){:}(\partial_x^2\theta(x))e^{2i\phi(x)}{:} + \mathrm{h.c.}, \end{aligned} \tag{3.38}$$

$$\begin{aligned} H_{2p}^{\mathrm{generic}} &= \int \mathrm{d}x\; \gamma_{2p}(x)\psi_R^\dagger(x)\partial_x\psi_R^\dagger(x)\psi_L(x)\partial_x\psi_L(x) + \mathrm{h.c.} \\ &= F_R^\dagger F_R^\dagger F_L F_L \frac{v}{a^2}\left(\frac{2\pi a}{L}\right)^{4K} \int \mathrm{d}x\; \tilde{\gamma}_{2p}(x){:}e^{4i\phi(x)}{:} + \mathrm{h.c.}. \end{aligned} \tag{3.39}$$

These three types of backscattering processes are illustrated in Fig. 3.2. In contrast to the simple (elastic) SPB, inelastic SPB involves backscattering of a single particle accompanied by another particle-hole excitation in one of the branches. TPB represents the event of two-particles being backscattered across the Fermi surface simultaneously. As we explain in detail later, Rashba spin-orbit coupling in combination with electron interactions, for

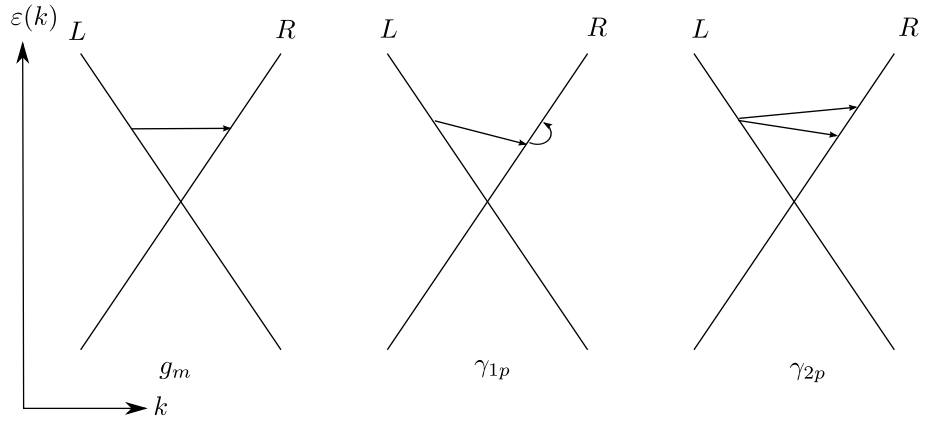

Figure 3.2.: The lowest-order generic backscattering processes in the helical liquid are (from left to right) elastic SPB, inelastic SPB, and (inelastic) TPB. Note that elastic SPB requires broken time-reversal symmetry. Adapted with permission from Ref. [LOB12]. Copyrighted by the American Physical Society.

instance, gives rise to both inelastic SPB [SRvG12, KGCM14, GKT17] and TPB [SJJ10, CBD$^+$12, KGCM14, GCT14, GKT17]. TPB was as well shown to emerge from SOC and phonon coupling [BDR11], or quenched disorder of anisotropic, Kondo-like spin-spin interactions [WBZ06]. If the coupling potential is uniform, $\tilde{\gamma}_{2p}(x) = \tilde{\gamma}_{2p}e^{-4ik_F x}$, umklapp scattering is sometimes associated with the parameter g_3 in the g-ology. As the oscillating factors tend to zero the integral, such terms are expected to be present only at half filling, $k_F = 0$, or in the the presence of an underlying lattice and commensurate filling (where $4k_F = 2\pi/a$, with a being some lattice spacing) [Gia91, XM06, WBZ06].
In order to examine the effect of a localized perturbation (single impurity), inducing a certain type of backscattering, let us for the moment define the couplings $\tilde{g}_m(x) = \tilde{g}_m a\delta(x)$, $\tilde{\gamma}_{1p}(x) = \tilde{\gamma}_{1p}a\delta(x)$, and $\tilde{\gamma}_{2p}(x) = \tilde{\gamma}_{2p}a\delta(x)$. This allows us to infer the scaling dimensions of the respective operators in the interacting case, $\Delta_m = K$, $\Delta_{1p} = K + 2$ and $\Delta_{2p} = 4K$. With effectively one, temporal dimension left, we find the tree-level RG equations

$$\begin{aligned}
\frac{d\tilde{g}_m}{d\ell}(\ell) &= (1 - K(\ell))\,\tilde{g}_m(\ell), \\
\frac{d\tilde{\gamma}_{1p}}{d\ell}(\ell) &= (-1 - K(\ell))\,\tilde{\gamma}_{1p}(\ell), \\
\frac{d\tilde{\gamma}_{2p}}{d\ell}(\ell) &= (1 - 4K(\ell))\,\tilde{\gamma}_{2p}(\ell).
\end{aligned} \tag{3.40}$$

As we can see, the magnetic impurity is a relevant perturbation for all, repulsive interaction strengths, and therefore, transport is expected to be blocked by even the weakest barrier at low energies [KF92a, KF92b]. On the other hand, while the localized SPB impurity is always irrelevant, its TPB counterpart becomes relevant at very strong interactions, $K < 1/4$.
In the weak-coupling limit, when all the mentioned coupling constants are irrelevant, and thus small, the correction to the conductance can be readily evaluated from the above operators. Quite generally, it scales with the greater of the energy scales of the system,

temperature and voltage bias, in a way that depends on the respective scaling dimensions Δ of the generic operators. Defining the dominant energy scale by

$$E = \max(T, eV), \tag{3.41}$$

the correction to the conductance (in the case of a localized impurity) is shown to take the form of the power law [LOB12]

$$\delta G \sim E^{2\Delta-2}. \tag{3.42}$$

In the limit of weak interactions, $K \to 1$, this suggests a lowest-order correction of $\delta G \sim$ const. for the magnetic impurity, $\delta G \sim E^4$ for SPB, as well as $\delta G \sim E^6$ for TPB. However, this is only the scaling of the generic, single impurity operators – if the generic expressions are renormalized by a specific, microscopic source of backscattering, which has its own scaling dynamics, this scaling can change accordingly, as we show below for the example of a localized Rashba SOC impurity.
Note that such scaling predictions depend on the actual form of the perturbation profile. Above, we have studied the case of a Dirac-like single impurity. In the case of uniform TPB umklapp scattering (where $\tilde{\gamma}_{2p}(x) = \tilde{\gamma}_{2p} e^{-4ik_F x}$), for instance, one obtains from Eq. (3.39) the operator

$$H_{2p}^{\text{umklapp}} = F_R^\dagger F_R^\dagger F_L F_L \frac{v}{a^2} \left(\frac{2\pi a}{L}\right)^{4K} \tilde{\gamma}_{2p} \int \mathrm{d}x \; e^{-4ik_F x} {:}e^{4i\phi(x)}{:} + \text{h.c.}. \tag{3.43}$$

Because of the additional spatial derivative in this case, and $\Delta_{um} = \Delta_{2p} = 4K$, we find the RG flow

$$\frac{d\tilde{\gamma}_{2p}}{d\ell}(\ell) = (2 - 4K(\ell))\, \tilde{\gamma}_{2p}(\ell), \tag{3.44}$$

meaning that umklapp scattering is a relevant perturbation already for moderate repulsive interactions $K < 1/2$, different from the single impurity case (compare with Eq. (3.40). The expected correction to the conductance then takes the form $\delta G \sim E^{2\Delta_{um}-4} = E^{8K-4}$.

3.3.3. Strong-coupling limit

If the impurity strength is large compared to the other length scales of the system, and thus can not be treated perturbatively, we face the strong-coupling regime. This occurs for coupling parameters that are relevant in a RG sense, such that they grow under renormalization towards low energies. For a truly one-dimensional system, at zero energy, transport is then expected to be fully blocked, and the conductance vanishes. Effectively, the system undergoes a transition from a metallic to a (Mott) insulating phase, which is equivalent to opening up a gap in the energy spectrum. In the process, time-reversal symmetry is said to be spontaneously broken in the helical liquid [WBZ06]. This concept describes the following effect: Even though all the constituents of the system might be invariant under time-reversal, the system can possibly choose a configuration of its ground state, that is not invariant under time-reversal anymore (for instance by opening a gap). Given that suchlike relevant perturbations affect the system to its full extent, as it is assumed for

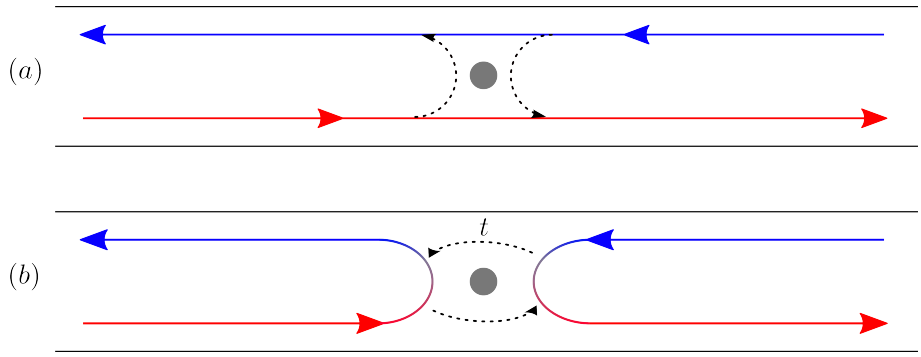

Figure 3.3.: Illustration of the (a) weak- and (b) strong-coupling limit. In the former, the conductance at zero energy is $G_0 > 0$, and backscattering off the impurity yields corrections δG at finite energy. In the latter, transport is blocked at zero energy – corrections δG are then provided by tunneling processes at finite energy.

instance for strong disorder (see Sec. 4.6.3), the electrons in the wire become immobile, and the physical state of the system can be described in terms of many-body localization (or Anderson localization [And58] in the non-interacting case). Peculiar phases are as well found at finite, but ultra-low energies. For instance, in the presence of strong electron interactions and relevant TPB, the particles form a Wigner crystal in the ground state of the helical LL [ZCT15], where the potential energy exceeds the kinetic energy of each electron. For higher energies, a finite value of the conductance is generally restored.

In the 2D QSH sample, it is important to note that we consider one-dimensional edge states embedded in a two-dimensional (bulk) system. The system then has two options of how to react to a relevant perturbation, and the spontaneous breaking of TRS. First, there can be a transition to a Mott insulating state, and the conductance vanishes, as explained above. This is the case for a non-topological one-dimensional model. Second, due to the peculiar nature of the topological QSH channel, the edge state can simply adapt to the new boundary of the system, and penetrate into the bulk in order to bypass the barrier. In this case, the spontaneous breaking of TRS is cured, and the remaining helical edge channel provides a nonzero conductance of $G_0 = e^2/h$. Which of the two scenarios occurs, depends on the form of the perturbation. For a spinless magnetic impurity in the strong-coupling limit, the conductance vanishes, because TRS is then broken explicitly. In the case of a relevant TPB perturbation, the situation is not fully clear, and both scenarios could in principle apply. The Refs. [XM06, WBZ06] suggest that the QSH state is eliminated by relevant TPB. Moreover, in the presence of a relevant Kondo impurity, the topological edge state is expected to be restored in the strong-coupling limit, as the perturbation gets screened by the formation of a singlet state with another edge electron (see discussion in Chap. 5).

Let us study the transport signature of elastic SPB and TPB processes in the strong-coupling limit, under the assumption that no topological bypass mechanism takes place,

and the edge conductance breaks down at zero energy. To model the situation of a single impurity, we consider a helical edge that is cut into two disconnected pieces at the position of the impurity (see Fig. 3.3). At finite energy, transport across the impurity is achieved by particles tunneling between the two disconnected ends. Assuming that $t(T, eV)$ is the tunneling (hopping) strength in the strong-coupling limit, with some energy dependence, the conductance is proportional to [MLO$^+$09]

$$G \propto t^2(T, eV). \tag{3.45}$$

We now examine the corresponding corrections for relevant magnetic and TPB backscattering (inelastic SPB can never be relevant). Let us therefore define the tunneling amplitudes t_m and t_{2p}, respectively. An RG analysis shows, that those parameters scale as [KF92a, KF92b, MLO$^+$09, Gia03]

$$\begin{aligned} \frac{d}{d\ell} t_m(\ell) &= (1 - 1/K) t_m(\ell), \\ \frac{d}{d\ell} t_{2p}(\ell) &= (1 - 1/(4K)) t_{2p}(\ell). \end{aligned} \tag{3.46}$$

At the order of the temperature, $\ell = \log(v\beta/a_0)$, and zero bias for simplicity, this leads to a conductance correction of $G \sim t_m^2(0) E^{2/K-2}$ and $G \sim t_{2p}^2(0) E^{2/(4K)-2}$. A summary of the most important power laws related to the generic processes described in this section, is given in Tab. 3.1.

Generally, the conductance provides the following transport signatures in the low-energy limit: In the strong-coupling regime, we expect interaction-dependent power-law corrections from $G = 0$, while in the weak-coupling regime, there are corrections from G_0, which exhibit a different power exponent. This behaviour is illustrated in Fig. 3.4. In the limit of high energies, the conductance approaches its bare value, since such highly energetic particles will be hardly affected by the perturbation. Typically, corrections to G_0 in that regime then are of logarithmic form (e.g. [MLO$^+$09, CBD$^+$12]). The distinct transport mechanisms, in the weak and strong-coupling limit, is as well reflected in the transferred effective charge, e^*, that can be estimated from the ratio of the average backscattering current and the shot noise (see definition in Sec. 4.5.2). For TPB, the value of e^* in the strong-coupling regime can be derived as follows. In this phase, the bosonic field ϕ gets pinned such as to adjust to the minima of energy. Using $H_{2\mathrm{p}} \propto \cos(4\phi)$, those are given by $\phi = (2n+1)\pi/4$, with $n = (0, \pm 1, \ldots)$, and the difference in phase between two neighbouring minima is consequently $\Delta\phi = \pi/2$. At finite energy, a nonzero conductance is restored from tunneling processes of particles across the allowed configurations of the ground state. Tunneling between two adjacent minima hereby corresponds to a change of the charge by $\Delta Q = e \int \mathrm{d}x\, \rho(x) = e\Delta\phi/\pi = e/2$, and therefore, we identify an effective charge of $e^* = e/2$ per tunneling event [MLO$^+$09]. On the other hand, the effective (backscattered) charge in the weak-coupling regime is $e^* = 2e$. For the magnetic perturbation studied above, due to the different periodicity of the cosine compared to the TPB impurity, the effective charge in both the weak and strong-coupling regime reads $e^* = e$.

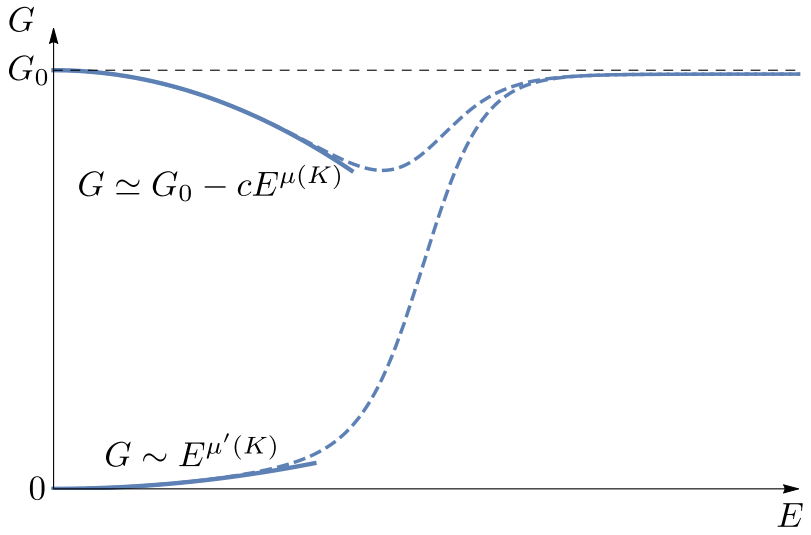

Figure 3.4.: Schematics of the low-energy behaviour of the conductance (using $E = \max(T, eV)$ as an energy scale). In the weak-coupling regime (upper curve), one expects power-law corrections from the bare value G_0 with a characteristic exponent $\mu(K)$, depending on the respective backscattering mechanism (c is some constant). In the strong-coupling regime (lower curve), we find a nonzero conductance at finite energies due to tunneling processes (see text). They generally come with a different power-law exponent $\mu'(K)$. For high energies, the bare value of the conductance is restored.

	weak coupling $[\mu(K)]$	strong coupling $[\mu'(K)]$
elastic SPB	$2K-2$ if $K>1$	$2/K-2$ if $K<1$
inelastic SPB	$2K+2$	–
TPB	$8K-2$ if $K>1/4$	$2/(4K)-2$ if $K<1/4$

Table 3.1.: Power-law exponents of the correction to the conductance at low energies, that is generated by a single, localized perturbation inducing various types of (generic) backscattering processes (cf. Fig. 3.2 and Eq. (3.42)). The exponents compare to the parameters $\mu(K)$ and $\mu'(K)$ in Fig. 3.4. In the tabular cells, we also list the strength of the interaction parameter K, that is required to reach the weak- or strong-coupling regime, respectively.

3.4. Many (dilute) impurities in the weak-coupling limit

Above, we have studied the case of a single, localized perturbation in the weak-coupling limit. The effect of several of those perturbations (of the same type) can be accounted for by summing up the single contributions, given that correlations between the impurities are negligible. This is justified, if the distribution of impurities along the edge is sufficiently dilute. Otherwise, interference effects resulting from coherent backscattering lead to additional corrections of the form of weak (anti-)localization [AS87, GMP05, GMP07]. Importantly, the conductance of the system in the case of only a few impurities or many of them takes a different form, respectively. For more than one perturbation, the resistance quanta δR add up. In lowest order of δG, those can be expressed as $\delta R = \delta G/G_0^2$ (e.g.

[VGGG14]), where the weak-coupling limit implies that $\delta G/G_0 \ll 1$, or $\delta R \ll G_0^{-1} = R_0$. Adding the contributions of a number of N uniform impurities leads us to a total resistance of $R = R_0 + N\delta R$. The total conductance is obtained by $G = R^{-1}$, so

$$G = \left(G_0^{-1} + N\frac{\delta G}{G_0^2}\right)^{-1} = G_0\left(1 + N\frac{\delta G}{G_0}\right)^{-1}. \tag{3.47}$$

In the following, we can distinguish two scenarios. First, we refer to the case of only a few impurities for $N\delta G/G_0 \ll 1$. We then can approximate Eq. (3.47) by

$$G \simeq G_0 - N\delta G. \tag{3.48}$$

For a single impurity, $N = 1$, we obviously recover Eq. (3.5). On the other hand, the 1D-system can contain so many impurities, that the mere amount compensates for the weak contributions of every individual perturbation. In this limit, we have $N\delta G/G_0 \gg 1$, and obtain

$$G \simeq \frac{G_0^2}{N\delta G}. \tag{3.49}$$

As the impurities are distributed along the edge in a dilute way, this limit implies that the system size L is large. This proportionality is as well expected to be observable in the conductance, $G \propto N^{-1} \propto L^{-1}$.
Note that the correction $\delta G(E)$ generally depends on the energy E of the system. Hereby, the weak-coupling regime is met for irrelevant impurities at low energies, and in particular then $\delta G(E \to 0) = 0$, and for relevant impurities at high energies, where then $\delta G(E \to \infty) = 0$. We readily observe, that in the two limits mentioned above, the condition $N\delta G(E)/G_0 \gg 1$ can not be fulfilled, and therefore, Eq. (3.49) does not hold for very weak coupling strengths. Instead, in the case of many impurities, we expect a crossover energy defined by $N\delta G(E)/G_0 \approx 1$, where the weak-coupling behaviour of the conductance changes from the dependence given in Eq. (3.48) to the one of Eq. (3.49). This point, for instance, becomes apparent in the Kondo impurity problem we discuss in Chap. 5.

4. Rashba spin-orbit coupling

4.1. Microscopic origin of SOC

Spin-orbit coupling emerges in quantum mechanics from a non-relativistic approximation to the relativistic Dirac equation, in the presence of an electromagnetic potential [Sak67]. More precisely, one uses the assumptions of $E \approx mc^2$ for the electron energy E, as well as $|eV| \ll mc^2$, where m is the electron mass, V an (time-independent) electric potential, c the speed of light and v the particle velocity, in order to perform an expansion in terms of small $(v/c)^2$. In lowest (zeroth) order, one simply recovers the non-relativistic Schrödinger equation. In first order of $(v/c)^2$, additional relativistic corrections to the non-relativistic Hamiltonian are obtained, among which there is an effective operator coupling the electrons spin to its momentum,

$$H_{\mathrm{R}} = -a\vec{\sigma} \cdot (\vec{p} \times \vec{\nabla} V) = -a\vec{\nabla} V \cdot (\vec{\sigma} \times \vec{p}). \tag{4.1}$$

Here, a is some constant and $\vec{\sigma} = (\sigma_x, \sigma_y, \sigma_z)$ the vector of Pauli matrices. The physical origin of this SOC operator can be understood the following way: The electron, moving with a velocity v in an electric field, feels an effective magnetic field that couples to its spin. For a single atom, the electromagnetic force is for instance provided by the central Coulomb force of the atomic core, and $\vec{\sigma} \cdot (\vec{p} \times \vec{\nabla} V) \propto \vec{\sigma} \cdot (\vec{p} \times \vec{r}) \propto \vec{\sigma} \cdot \vec{L}$, with $\vec{L}$ being the orbital angular momentum. Therefore, in the single atom, the electron energy is shifted due to the coupling of its spin to an orbital degree of freedom (this is called fine structure). In a crystalline solid state system, we have a large number of atoms, that are arranged periodically in a lattice. The electrons motion and energy is now affected by the total ensemble of atomic cores, and just like the kinetic energies transform from discrete levels to energy bands, also the spin-orbit term feels the effect of all atoms, and transforms into a "crystalline" spin-orbit coupling, that one might imagine as stemming from a "crystalline orbit". Clearly, the symmetries of the lattice structure play an important role, and determine the lowest-order coupling terms. For example, in a three-dimensional zinc blende structure without inversion symmetry, this leads to the presence of a so-called "Dresselhaus" spin-orbit coupling, while the term "Rashba" SOC is for historical reasons used more for systems with uniaxial symmetry (one crystal axis different from the other ones), like wurtzite crystals. Later, it was pointed out that the k-linear Rashba SOC in such crystals is very similar to the spin-orbit splitting found in quasi 2D heterostructures [BR84, Win03, BRW15]. Importantly, the potential V in Eq. (4.1) can not only originate from the "intrinsic" atomic potentials of the crystal bulk, but also from external sources. In a 2D heterostructure, those include: (i) a gate on top of the sample, that evokes an electric field perpendicular to the system plane, (ii) effective fields arising at the interfaces of two different materials, on the top or bottom surface of the sample (also called structure

inversion asymmetry), or (iii) impurities merged into the system.
Here, we are concerned with one-dimensional states at the topological edges of quasi 2D systems. In one dimension, the momentum vector is restricted to a specific direction, say x, such that the above SOC operator becomes $H_\mathrm{R} = -a[(\vec{\nabla}V)_y\sigma_z - (\vec{\nabla}V)_z\sigma_y]p_x$. The interesting term, that couples different spin species, is proportional to the electric field in z-direction, which we define to be out of plane relative to the 2D system. As the SOC coupling parameter can vary along the edge, we may write the general profile $\alpha(x) = a(\vec{\nabla}V)_z(x)$. The Hamiltonian reads in the helical basis, $\vec{\psi}(x) = (\psi_R(x), \psi_L(x))^T$,

$$\begin{aligned} H_\mathrm{R} &= \int \mathrm{d}x\ \vec{\psi}^\dagger(x) H_\mathrm{R} \vec{\psi}(x) + \mathrm{h.c.} = \int \mathrm{d}x\ \alpha(x)\vec{\psi}^\dagger(x)\sigma_y p_x \vec{\psi}(x) + \mathrm{h.c.} \\ &= \int \mathrm{d}x\ \alpha(x)[(\partial_x\psi_R^\dagger(x))\psi_L(x) - \psi_R^\dagger(x)(\partial_x\psi_L(x))] + \mathrm{h.c.}, \end{aligned} \tag{4.2}$$

with $p_x = -i\partial_x$.
This "Rashba Hamiltonian" H_R, as given in Eq. (4.2), is the lowest-order perturbation (meaning that it entails the least fermionic operators), that corresponds to a backscattering process and, at the same time, is invariant under time-reversal. However, it is crucial to note that due to its elastic character, this term alone is not able to induce an effective backscattering current in the helical system. Only in combination with another inelastic component, such as Coulomb electron interactions, Rashba SOC can generate one of the generic backscattering processes presented in Sec. 3.3, and alter the transport properties of the system.

4.2. Bosonization

Let us take a look at the bosonized version of Eq. (4.2). Explicitly, with Eq. (2.32), one finds [Dol12, CBD+12, BDR11]

$$\begin{aligned} &(\partial_x\psi_R^\dagger(x))\psi_L(x) - \psi_R^\dagger(x)(\partial_x\psi_L(x)) = -i(\partial_{\overline{z}}\psi_R^\dagger(\overline{z}))\psi_L(x) - i\psi_R^\dagger(x)(\partial_z\psi_L(z)) \\ &= \frac{-i}{L}F_R^\dagger F_L(\partial_{\overline{z}} + \partial_z)e^{n_R\overline{z}}e^{-i\varphi_R^\dagger(\overline{z})}e^{-i\varphi_R(\overline{z})}e^{-n_L z}e^{-i\varphi_L^\dagger(z)}e^{-i\varphi_L(z)} \\ &= \frac{-i}{2\pi a}F_R^\dagger F_L e^{n_R\overline{z}}e^{-n_L z}((n_R - n_L)e^{-i\phi_R(\overline{z})}e^{-i\phi_L(z)} \\ &\quad + (-i){:}\partial_{\overline{z}}\phi_R(\overline{z})e^{-i\phi_R(\overline{z})}{:}e^{-i\phi_L(z)} + e^{-i\phi_R(\overline{z})}(-i){:}\partial_z\phi_L(z)e^{-i\phi_L(z)}{:}) \\ &= \frac{-i}{2\pi a}F_R^\dagger F_L e^{-2ix(k_F - \frac{\pi}{L})}{:}2\partial_x\theta(x,t)e^{i2\phi(x,t)}{:}. \end{aligned} \tag{4.3}$$

Here, $\partial_x = -ir\partial_{z_r}$, where we use $z_+ = \overline{z}$ and $z_- = z$ (see Eq. 2.11), as well as $n_r = (k_F - \frac{\pi}{L} + \frac{2\pi}{L}N_r)$. Point-splitting is not necessary here, since the two fermionic field operators have opposite chirality. When taking the derivative of the exponential operators above, factors of the form of $\partial_z\varphi^\dagger$ or $\partial_z\varphi$ are positioned right behind the corresponding exponents, such that for this operation, normal-ordering of the full expression with respect to the fields $\varphi, \varphi^\dagger$ is preserved. Right- and left-moving operators can then safely be combined, since the respective fields commute. The outer normal-ordering signs indicate here, that the field $\partial_x\theta$ is normal-ordered with respect to the exponential factors. For a

complete normal-ordering, however, we also have to order the factor $e^{2i\phi}$, which gives rise to another factor of $(2\pi a/L)^K$, according to Eq. (2.81). We eventually obtain

$$H_{\mathrm{R}} = -iF_R^\dagger F_L \left(\frac{2\pi a}{L}\right)^K \int \mathrm{d}x \, \frac{\alpha(x)}{\pi a} {:}\partial_x\theta(x,t){:}e^{i2\phi(x,t)}{::}e^{-2ik_F x} + \mathrm{h.c.}. \tag{4.4}$$

In the limit of large system sizes, the term $e^{2ix\pi/L}$ can be neglected. We see that even though normal-ordering was performed carefully, the cutoff-dependence does not fully disappear at finite electron interaction strength. To lighten the notation, one sometimes drops the inner colons, which leaves the notation slightly ambiguous though. In the following, we use the convention that even if inner colons are absent, we refer to the form of H_{R} as given here, in Eq. (4.4), unless explicitly stated otherwise. [1]

4.3. SOC as a rotation of basis states

Before we continue with a perturbative analysis of the interacting Rashba problem, it is worth emphasizing that Rashba SOC can as well be introduced in a different way, as discussed below. The consequences, in terms of power-law corrections to the conductance, are found to be qualitatively the same.

4.3.1. Basis transformation

In the Refs. [SRvG12, KGCM14], another approach was taken to implement SOC into the helical LL model. Instead of using the perturbation operator of Eq. (4.2), spin-orbit coupling is considered a rotation of the spin basis of the helical states. While the s_z-component of the wave functions is clearly conserved (and thus a good quantum number) in the free helical liquid, this does not hold anymore in the presence of Rashba SOC, since states of opposite chirality get mixed then. [2] This observation gives a motivation to define SOC by a momentum-dependent, rotational matrix B_k, where

$$\begin{aligned} \begin{pmatrix} \psi_{\uparrow,k} \\ \psi_{\downarrow,k} \end{pmatrix} &= B_k \begin{pmatrix} \psi_{+,k} \\ \psi_{-,k} \end{pmatrix}, \\ B_k &\approx \begin{pmatrix} 1 & -(k/k_0)^2 \\ (k/k_0)^2 & 1 \end{pmatrix}. \end{aligned} \tag{4.5}$$

Here, the states $\psi_{\pm,k}$ are eigenstates of the system in the presence of SOC (where the s_z-component is not conserved), and form a new basis of the helical liquid. Importantly, those states are still orthogonal and time-reversal partners. The parameter k_0 quantifies the strength of Rashba SOC. Note that the explicit form of the rotation matrix in Eq. (4.5) is determined by the two constraints of TRS, implying $B_k = B_{-k}$, and unitarity. Applying this rotation to a system governed by $H = H_0 + H_{\mathrm{imp}} + H_{\mathrm{int}}$ (see definitions

[1] Sometimes the bosonized Rashba Hamiltonian of Eq. (4.4) is written in terms of a cosine of ϕ. This, however, is only possible in a notation where the Klein factors are either dropped, or chosen in a way such that $F^\dagger \simeq F$, while in general the conjugate term is proportional to $F_L^\dagger F_R = -F_R F_L^\dagger$.

[2] Formally, Rashba SOC is proportional to $H_{\mathrm{R}} \propto k\sigma_y$, which does not commute with σ_z.

below in Eqs. (4.9)–(4.11)), including electron interactions, H_{int}, and an electron density perturbation, H_{imp}, will naturally induce inelastic single-particle backscattering.
To match the notation of Refs. [SRvG12, GKT17], we shall use for all fermionic calculations in this chapter a notation, that is slightly different from the one introduced in Sec. 2.1.1 (compare also with App. B). We define

$$\psi_r(x) = \frac{1}{\sqrt{L}} \sum_k e^{ikx} c_{r,k}, \tag{4.6}$$

where $r = \uparrow, \downarrow = \pm$, as well as the energy dispersion relation of right- and left-movers,

$$\varepsilon_r(k) = r v_F k. \tag{4.7}$$

The fields obey the usual anticommutation rules

$$\{c_{r,k}, c^\dagger_{r',k'}\} = \delta_{kk'}\delta_{rr'}. \tag{4.8}$$

Performing the SOC rotation introduced in Eq. (4.5), one finds in the new basis [SRvG12],

$$H_0 = \sum_{k,r} \varepsilon_r(k) c^\dagger_{r,k} c_{r,k} = \sum_k v_F k (c^\dagger_{+,k} c_{+,k} - c^\dagger_{-,k} c_{-,k}), \tag{4.9}$$

$$\begin{aligned} H_{\text{int}} &= \int \mathrm{d}x\, \mathrm{d}x'\, U(x-x')\rho(x)\rho(x') \\ &= \frac{1}{L} \sum_{k,k',q} \sum_{\alpha,\beta,\alpha',\beta'=\pm} U(q) [B^\dagger_k B_{k-q}]^{\alpha\beta} [B^\dagger_{k'} B_{k'+q}]^{\alpha'\beta'} c^\dagger_{\alpha,k} c_{\beta,k-q} c^\dagger_{\alpha',k'} c_{\beta',k'+q} \\ &\simeq \frac{U_0}{L} \sum_{k,k',q} \Big[\frac{(k^2 - k'^2)}{k_0^2} c^\dagger_{+,k+q} c^\dagger_{-,k'-q} c_{+,k'} c_{+,k} - \{+ \leftrightarrow -\} + \text{h.c.} \\ &\quad + (c^\dagger_{+,k+q} c^\dagger_{-,k'-q} c_{-,k'} c_{+,k} - c^\dagger_{+,k+q} c^\dagger_{+,k'-q} c_{+,k} c_{+,k'}) + \{+ \leftrightarrow -\} \Big], \end{aligned} \tag{4.10}$$

$$\begin{aligned} H_{\text{imp}} &= \int \mathrm{d}x\, V(x)\rho(x) = \frac{1}{L} \sum_{k_1,k_2} \sum_{\alpha,\beta=\pm} V(k_1 - k_2) [B^\dagger_{k_1} B_{k_2}]^{\alpha\beta} c^\dagger_{\alpha,k_1} c_{\beta,k_2} \\ &\simeq \frac{V_0}{L} \sum_{k_1,k_2} \left(\frac{1}{2} c^\dagger_{+,k_1} c_{+,k_2} + \{+ \leftrightarrow -\} + \frac{(k_1^2 - k_2^2)}{k_0^2} c^\dagger_{+,k_1} c_{-,k_2} \right) + \text{h.c.}. \end{aligned} \tag{4.11}$$

Here, $\rho(x) = \rho_\uparrow(x) + \rho_\downarrow(x)$ is the total electron density. The sign $\{+ \leftrightarrow -\}$ denotes the preceding term with reversed chirality. For simplicity, the respective potentials were assumed to be localized in real space, so $U(x-x') = U_0\delta(x-x')$ and $V(x) = V_0\delta(x)$. Furthermore, only the terms of lowest order in momentum are presented. We observe, that while the kinetic energy is not affected by the unitary rotation, both the electron interactions and the impurity perturbation generate additional backscattering terms. Here, those are of second order in momentum, in contrast to the linear dependence of the generic inelastic SPB term given in Eq. (3.38). At finite k_F, however, the effective operators in Eqs. (4.10) and (4.11) can be linearized to match the generic expression. As we see later, the lowest-order momentum expansion of a backscattering operator quite generally determines its leading-order transport signature.

4.3.2. Correction to the conductance – Fermi golden rule

Deviations from the perfect conductance, due to the effective operators given above, are calculated perturbatively with the help of the generalized Fermi golden rule (FGR). Note that this implies weak electron interactions, in contrast to a bosonic analysis. The average backscattering current in this framework is given by [BF04]

$$\begin{aligned} \langle \delta I \rangle &= \sum_{if} \Gamma_{f \leftarrow i} \Delta N_{f \leftarrow i}, \\ \Gamma_{f \leftarrow i} &= 2\pi |\langle f|T|i\rangle|^2 w_i \delta(E_f - E_i). \end{aligned} \tag{4.12}$$

Here, w_i represents the probability to find the (multi-particle) state $|i\rangle$ in the set of all states, while $\Delta N_{f \leftarrow i}$ is the backscattered charge per backscattering event. E_i and E_f are the energies of the initial and final states $|i\rangle$ and $|f\rangle$, respectively, which are (unperturbed) eigenstates of the free Hamiltonian H_0. In this formalism, the transfer operator T takes the form

$$T = H' + H' G_0 T, \tag{4.13}$$

and a perturbative solution can be found self-consistently. Energies of intermediate states are measured relative to the initial or final state by the free Green function $G_0 = \left(E_{i/f} - H_0\right)^{-1}$. In our model, we consider the perturbation $H' = H_{\text{int}} + H_{\text{imp}}$. At finite bias voltage, we simply infer the correction to the conductance from the backscattering current by $\delta G = d\langle \delta I \rangle / dV$.

Let us briefly review the main results of the perturbative analysis of Ref. [SRvG12]. Because of the way SOC is introduced, even in the absence of impurities there is a joint, inelastic backscattering effect of interactions and SOC. Therefore, in the first order of $T = H_{\text{int}}$, one finds a contribution (using temperature as an energy scale)

$$\delta G \sim L \frac{U_0^2}{k_0^4 v_F^7} T^5. \tag{4.14}$$

This correction is of a higher power than the one expected from a generic inelastic SPB operator, as H_{int} is quadratic in momentum. Implicitly, we used $k_F = 0$ here. Since there are no localized perturbations that break the translational invariance at the edge, the total momentum is conserved, which translates into a linear dependence of the current on the system size L.

To next order, the cross terms $T = H_{\text{int}} G_0 H_{\text{imp}} + H_{\text{imp}} G_0 H_{\text{int}}$ generate translationally non-invariant single-particle backscattering (see more about the corresponding diagrams in the subsequent section). Importantly, the authors of Ref. [SRvG12] now consider a finite chemical potential, and use the fact that all momenta can be expanded around $k_F \neq 0$, to obtain an effective backscattering operator linear in momentum. This results in a correction of lower power in the temperature,

$$\delta G \sim L n_{\text{imp}} \left(\frac{V_0 U_0}{k_0^6}\right)^2 \left(\frac{k_F}{v_F}\right)^8 T^4, \tag{4.15}$$

if $v_F|k_F| \gg T$. The average density of impurities in the system is given by n_{imp}, such that Ln_{imp} is independent of the system size. The contributions of each individual impurity can simply be added up, if interference terms are small, and multiple impurity scattering can be neglected. This holds approximately for $T \gg v_F/L$ [AS87]. The correction to the conductance presented in Eq. (4.15) exhibits the same power-law exponent, that one would expect from generic SPB, in the limit of $K \to 1$ (compare with Tab. 3.1).

4.4. Fermionic perturbative analysis

4.4.1. Model description

In order to explore the combined effect of Rashba SOC and electron interactions in the weak interaction limit, a perturbative analysis in terms of fermionic operators is performed. This allows us to identify, under which circumstances single- and two-particle backscattering processes generally arise, and to study the expected power-law corrections to the conductance. Importantly, we find that the latter depend on the microscopic details of the system, such as the presence, and the form of a momentum cutoff. The respective results are as well presented in Ref. [GKT17].
Using the definitions in Eqs. (4.6)–(4.8), we consider a system modeled by the Hamiltonian $H = H_0 + H_{\mathrm{R}} + H_2 + H_4$, where

$$H_0 = v_F \sum_{r=\pm} \int \mathrm{d}x\ \psi_r^\dagger(x)(-ir\partial_x)\psi_r(x) = \sum_{k,r=\pm} \varepsilon_r(k) c_{r,k}^\dagger c_{r,k}, \tag{4.16}$$

$$\begin{aligned} H_{\mathrm{R}} &= \int \mathrm{d}x\ \mathrm{d}x'\ \alpha(x,x') \left[\left(\partial_x \psi_+^\dagger(x)\right) \psi_-(x') - \psi_+^\dagger(x) \left(\partial_{x'}\psi_-(x')\right) \right] + \mathrm{h.c.} \\ &= -\frac{i}{L} \sum_{k,k'} \alpha_{k,k'}(k+k') c_{+,k}^\dagger c_{-,k'} + \mathrm{h.c.}, \end{aligned} \tag{4.17}$$

$$\begin{aligned} H_2 &= \frac{1}{2} \int \mathrm{d}x_1\ \mathrm{d}x_2\ g_2(x_1,x_2) \psi_+^\dagger(x_1)\psi_-^\dagger(x_2)\psi_-(x_2)\psi_+(x_1) + \{+ \leftrightarrow -\} \\ &= \frac{1}{L^2} \sum_{k_1,k_2,q,q'} g_{q,q'}^{(2)} c_{+,k_1-q}^\dagger c_{-,k_2+q'}^\dagger c_{-,k_2} c_{+,k_1}, \end{aligned} \tag{4.18}$$

$$\begin{aligned} H_4 &= \frac{1}{2} \int \mathrm{d}x_1\ \mathrm{d}x_2\ g_4(x_1,x_2) \psi_+^\dagger(x_1)\psi_+^\dagger(x_2)\psi_+(x_2)\psi_+(x_1) + \{+ \leftrightarrow -\} \\ &= \frac{1}{2L^2} \sum_{k_1,k_2,q,q'} g_{q,q'}^{(4)} c_{+,k_1-q}^\dagger c_{+,k_2+q'}^\dagger c_{+,k_2} c_{+,k_1} + \{+ \leftrightarrow -\}. \end{aligned} \tag{4.19}$$

Above, we introduce SOC (H_{R}) and interaction terms (H_2 and H_4) that are generally of non-local character. The respective potentials therefore depend on two spatial coordinates. Non-localities in the SOC term are associated with higher-order derivatives, as can be seen, for instance, from a symmetric expansion of the spatial coordinates around a common center. Non-local electron interactions simply refer to the possibility of two interacting electrons being separated in space. Going to momentum space, we define the

two-dimensional Fourier transforms of the SOC potential and the interaction profiles

$$\begin{aligned} \alpha_{k,k'} &= \int \mathrm{d}x\ \mathrm{d}x'\ \alpha(x,x')e^{-i(xk-x'k')}, \\ g^{(n)}_{q,q'} &= \int \mathrm{d}x_1\ \mathrm{d}x_2\ g_n(x_1,x_2)e^{i(x_1q-x_2q')}, \end{aligned} \tag{4.20}$$

with $n \in \{2,4\}$. Making use of the fact that the interaction potential is symmetric under an exchange of particles, $g_n(x_1,x_2) = g_n(x_2,x_1)$, we realize that $g^{(n)}_{q,q'} = g^{(n)}_{-q',-q}$. Importantly, time-reversal symmetry in combination with hermicity manifests itself in imposing the following restriction on the SOC potential,

$$\begin{aligned} \alpha(x,x') &= \alpha(x',x), \\ \alpha_{k,k'} &= \alpha_{-k',-k}. \end{aligned} \tag{4.21}$$

The physical character of an operator is recognized from the form of the respective potentials. This translates from real space to momentum space in the following way: If a potential $f(x,x')$, with f being either α or g_n here, is local in the sense of $f(x,x') = f(x)\delta(x-x')$, its Fourier transform only depends on the difference of the two momenta, $f_{k,k'} = f_{k-k'}$. Likewise, a translationally invariant potential, $f(x,x') = f(x-x')$, translates into $f_{k,k'} = f_k\delta(k-k')$. A profile that is local, and at the same time translationally invariant, maintains its form upon Fourier transformation, so $f(x,x') = c\delta(x-x')$ leads to $f_{k,k'} = c\delta(k-k')$, where c is some constant.

4.4.2. Effective operators of SPB and TPB

We study a one-dimensional helical transport channel in the presence of spin-orbit coupling and electron interactions, that are both weak and can therefore be treated perturbatively, so $H' = H_\mathrm{R} + H_2 + H_4$ in the T-matrix in Eq. (4.13). The average backscattering current is calculated using the Fermi golden rule, as given by Eq. (4.12). For single- and two-particle backscattering terms, we hereby expand the matrix T up to first and second order in H_R, respectively.
First, we realize that in the absence of interactions no backscattering is possible. In the above FGR formalism, this can be observed from the lowest-order terms (see Eq. (4.17))

$$\begin{aligned} H_\mathrm{R} &= -\frac{i}{L}\sum_{k,k'} \alpha_{k,k'}(k+k')c^\dagger_{+,k}c_{-,k'} + \mathrm{h.c.}, \\ H_\mathrm{R}G_0H_\mathrm{R} &= -\frac{1}{2v_FL^2}\sum_{k_1\ldots k_4} \alpha_{k_1,k_2'}\alpha_{k_2,k_1'}(k_1+k_2+k_2'+k_1')c^\dagger_{+,k_1}c^\dagger_{+,k_2}c_{-,k_2'}c_{-,k_1'} \\ &\quad + \mathrm{h.c.} + \ldots \end{aligned} \tag{4.22}$$

Once energy conservation is applied, the factors linear in k become zero in both expressions, and there will be no contribution to the backscattering current. In the last line, the dots indicate that there are more terms arising from the combination of $H_\mathrm{R}G_0H_\mathrm{R}$, however, they do not correspond to backscattering and are therefore not explicitly stated here.

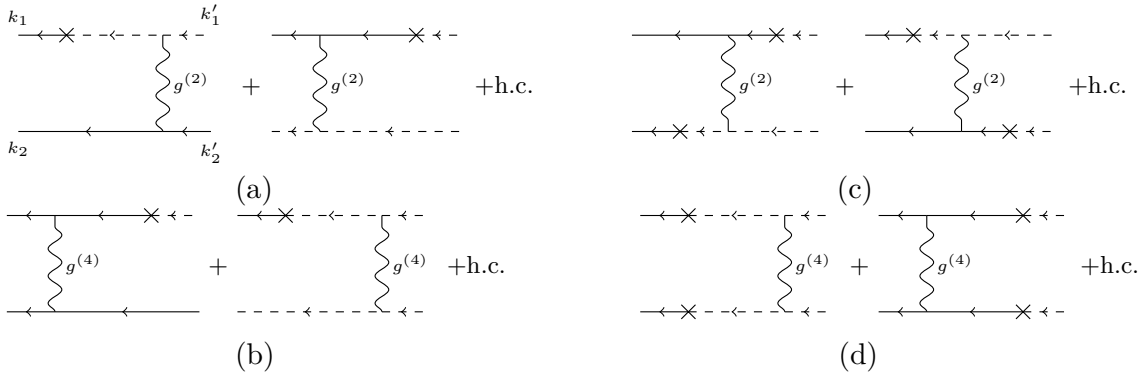

Figure 4.1.: Single- (a,b) and two-particle (c,d) backscattering processes of lowest order involving interactions of the type g_2 (upper row) and g_4 (lower row). Backscattering of a single particle is accompanied by a particle-hole excitation, mediated by interactions. Dashed (full) lines indicate left-moving (right-moving) particles. Rashba SOC and Coulomb interactions are represented by crosses and wiggly lines, respectively. The two diagrams in (c) can be shown to be equivalent, but are both given here for illustrating purposes.

Analyzing the transfer operator in Eq. (4.13), we next explore the possibility of correlated single- and two-particle backscattering at nonzero electron interaction strength. Throughout, we ignore diagrams that do not represent backscattering but merely renormalize interactions, or the Fermi velocity. Moreover, operators involving more than four fermionic operators are generally not considered here, in order to identify the lowest-order processes.

We find that SPB arises from the cross terms (see corresponding diagrams in Fig. 4.1a,b)

$$\begin{aligned} H_2G_0H_{\mathrm{R}}+H_{\mathrm{R}}G_0H_2 \propto & -\frac{i}{v_FL^3}\sum_{k_1,k_2,k_1',k_2',q} g^{(2)}_{q,k_2-k_2'} \\ & \times c^\dagger_{+,k_1}(\alpha_{k_1,k_1'-q}c^\dagger_{+,k_2}c_{+,k_2'}-\alpha_{k_1+q,k_1'}c^\dagger_{-,k_2}c_{-,k_2'})c_{-,k_1'}+\mathrm{h.c.}, \qquad (4.23) \\ H_4G_0H_{\mathrm{R}}+H_{\mathrm{R}}G_0H_4 \propto & \frac{i}{v_FL^3}\sum_{k_1,k_2,k_1',k_2',q} g^{(4)}_{q,k_2-k_2'} \\ & \times c^\dagger_{+,k_1}(\alpha_{k_1+q,k_1'}c^\dagger_{+,k_2}c_{+,k_2'}-\alpha_{k_1,k_1'-q}c^\dagger_{-,k_2}c_{-,k_2'})c_{-,k_1'}+\mathrm{h.c.}. \qquad (4.24) \end{aligned}$$

Note that the linear momentum-dependence of the Rashba potential is exactly compensated by the k-linear energy dispersion in the denominator of G_0, allowing for a fairly simple presentation of the terms in Eqs. (4.23) and (4.24). Combining the two expressions, we conclude that Rashba SOC and interactions give rise to the effective inelastic

SPB operator

$$H_{1p}^{\text{eff}} = \sum_{k_1,k_2,k_1',k_2'} P_{k_2k_2'}^{k_1k_1'} c_{+,k_1}^\dagger c_{+,k_2}^\dagger c_{+,k_2'} c_{-,k_1'} - (P')_{k_2k_2'}^{k_1k_1'} c_{+,k_1}^\dagger c_{-,k_2}^\dagger c_{-,k_2'} c_{-,k_1'} + \text{h.c.},$$

$$P_{k_2k_2'}^{k_1k_1'} = -\frac{i}{v_F L^3} \sum_q \left(g_{q,k_2-k_2'}^{(2)} \alpha_{k_1,k_1'-q} - g_{q,k_2-k_2'}^{(4)} \alpha_{k_1+q,k_1'} \right), \tag{4.25}$$

$$(P')_{k_2k_2'}^{k_1k_1'} = -\frac{i}{v_F L^3} \sum_q \left(g_{q,k_2-k_2'}^{(2)} \alpha_{k_1+q,k_1'} - g_{q,k_2-k_2'}^{(4)} \alpha_{k_1,k_1'-q} \right).$$

All these processes represent the backscattering of a single particle, accompanied by a particle-hole excitation on the right- or left-moving branch. This mechanism has been identified before [LOB12, SRvG12, KGCM14], and was found to generate a power-law correction to the backscattering current.

Furthermore, TPB was proposed in Ref. [CBD+12] to emerge in lowest order in the form of the third-order diagrams illustrated in Fig. 4.1c,d. These processes are contained in the following T-matrix terms [3]

$$H_{\text{R}} G_0 H_2 G_0 H_{\text{R}} \propto -\frac{1}{v_F^2 L^4} \sum_{k_1,k_2,k_1',k_2',q,q'} g_{q,q'}^{(2)} \alpha_{k_2+q,k_1'} \alpha_{k_1,k_2'+q'} \times c_{+,k_1}^\dagger c_{+,k_2}^\dagger c_{-,k_2'} c_{-,k_1'} + \text{h.c.}, \tag{4.26}$$

$$H_4 G_0 H_{\text{R}} G_0 H_{\text{R}} + H_{\text{R}} G_0 H_{\text{R}} G_0 H_4 \propto \frac{1}{2v_F^2 L^4} \sum_{k_1,k_2,k_1',k_2',q,q'} g_{q,q'}^{(4)} \times (\alpha_{k_2-q',k_1'} \alpha_{k_1+q,k_2'} + \alpha_{k_2,k_1'+q'} \alpha_{k_1,k_2'-q}) c_{+,k_1}^\dagger c_{+,k_2}^\dagger c_{-,k_2'} c_{-,k_1'} + \text{h.c.}. \tag{4.27}$$

As a consequence, the effective operator of two-particle backscattering can be written as

$$H_{2p}^{\text{eff}} = \sum_{k_1,k_2,k_1',k_2'} Q_{k_2k_2'}^{k_1k_1'} c_{+,k_1}^\dagger c_{+,k_2}^\dagger c_{-,k_2'} c_{-,k_1'} + \text{h.c.},$$

$$Q_{k_2k_2'}^{k_1k_1'} = -\frac{1}{v_F^2 L^4} \sum_{q,q'} (g_{q,q'}^{(2)} \alpha_{k_2+q,k_1'} \alpha_{k_1,k_2'+q'} - \frac{1}{2} g_{q,q'}^{(4)} [\alpha_{k_2-q',k_1'} \alpha_{k_1+q,k_2'} + \alpha_{k_2,k_1'+q'} \alpha_{k_1,k_2'-q}]). \tag{4.28}$$

Both the operators in Eqs. (4.25) and (4.28) are expected to induce characteristic power-law corrections to the conductance. Before studying the corresponding low-energy scaling, we first demonstrate, that no backscattering is possible in the special case of only local potentials, and no momentum cutoff. This property was pointed out in Ref. [XLCF16].

4.4.3. Suppression of terms with all-local potentials

From Eqs. (4.25) and (4.28), we find that there is zero backscattering if both the SOC and the electron interactions potentials are local, and the momentum spectrum is not

[3] Note that due to energy conservation, G_0 can be applied to the left or to the right in order to keep track of the cancellation of the k-linear terms of the Rashba SOC, and the energy denominator.

restricted. Formally, this is observed from the fact that we can then use shifts and relabelings of the internal momenta q and q', such that the effective operators become asymmetric with respect to the anticommutation of two fermionic fields. For instance, the g_2-part of the TPB operator in Eq. (4.28) reads, with local potentials,

$$\begin{aligned} H_{2p}^{\text{eff}} &\propto \sum_{k_1,k_2,k_1',k_2',q,q'} g^{(2)}_{q-q'} \alpha_{k_2+q-k_1'} \alpha_{k_1-k_2'-q'} c^\dagger_{+,k_1} c^\dagger_{+,k_2} c_{-,k_2'} c_{-,k_1'} + \text{h.c.} \\ &\overset{\substack{q\to q+k_1-k_2 \\ q'\to q'+k_1-k_2}}{=} \sum_{k_1,k_2,k_1',k_2',q,q'} g^{(2)}_{q-q'} \alpha_{k_1+q-k_1'} \alpha_{k_2-k_2'-q'} c^\dagger_{+,k_1} c^\dagger_{+,k_2} c_{-,k_2'} c_{-,k_1'} + \text{h.c.} \\ &\overset{k_1\leftrightarrow k_2}{=} \sum_{k_1,k_2,k_1',k_2',q,q'} g^{(2)}_{q-q'} \alpha_{k_2+q-k_1'} \alpha_{k_1-k_2'-q'} c^\dagger_{+,k_2} c^\dagger_{+,k_1} c_{-,k_2'} c_{-,k_1'} + \text{h.c.} \\ &= - \sum_{k_1,k_2,k_1',k_2',q,q'} g^{(2)}_{q-q'} \alpha_{k_2+q-k_1'} \alpha_{k_1-k_2'-q'} c^\dagger_{+,k_1} c^\dagger_{+,k_2} c_{-,k_2'} c_{-,k_1'} + \text{h.c.} = 0. \end{aligned} \tag{4.29}$$

Similar shifts are found individually for all the terms in Eqs. (4.25) and (4.28). The same mechanism of momentum shifts can be used as well to illustrate, that terms involving interactions of the type g_4 generally vanish for local interaction potentials and arbitrary SOC potential, as it should be, by virtue of the Pauli exclusion principle.

Importantly, if at least one of the two potentials is slightly non-local (for local SOC and non-local electron interactions there is the additional constraint that interactions are not $SU(2)$-invariant, see below), such an asymmetry is not provided anymore, and we expect in general a nonzero contribution to the backscattering current. This point can as well be understood in the following way. The generic operators of inelastic SPB and TPB – for instance given in Sec. 3.3 – involve spatial derivatives associated with products of field operators of the same kind. Such terms can be considered an OPE of the form $\lim_{x'\to x} \psi_r^\dagger(x)\psi_r^\dagger(x') = \psi_r^\dagger(x)\psi_r^\dagger(x+ia) \simeq ia\psi_r^\dagger(x)\partial_x\psi_r^\dagger(x)$, with a minimal distance a that can be interpreted as a short-distance cutoff. Due to the Pauli exclusion principle, the operator product vanishes if a goes to zero. Operators that contain suchlike products can therefore be viewed as non-local in nature. Thus, they are present only if the underlying model provides a certain type of non-locality. It is then clear that a contribution to these generic backscattering processes emerges only from microscopic sources of the same, non-local character. Note that Rashba SOC itself (as defined in Eq. (4.17)) is not intrinsically non-local in this sense, even though it contains a spatial derivative, since there the derivative connects two operators of opposite chirality, and the corresponding product can not be associated with a proper OPE.

Non-local effects in real space are as well induced by imposing a momentum cutoff, which reflects the analogy of blurring in real space and confinement in momentum space. Such a cutoff often appears naturally in realistic systems, in the form of a high-energy cutoff. For instance, for 1D edge states of a 2D topological insulator, a momentum cutoff is enforced by the presence of a finite bulk band gap. Generally, any restriction of the energy spectrum conceptually allows for non-local operators in real space, and consequently for backscattering induced by the combination of Rashba SOC and interactions (for an explicit calculation, see Sec. 4.4.8). A suppression of this effect is expected only in the

hypothetical case of an unbounded spectrum, and a specific choice of potentials.

The observation that an all-local combination of interactions and SOC does not induce backscattering in the helical liquid, is in agreement with the findings of Ref. [XLCF16, Dol17]. There, it was shown on general grounds that such a system can be mapped onto a free bosonic model by the use of a suitable basis transformation. Let us briefly review the line of reasoning of Ref. [Dol17]. The helical LL – in the presence of electron interactions and a local Rashba SOC perturbation – is described by $H = H_0 + H_\mathrm{R}$, with the expressions given in Eqs. (2.20), (2.38) and (4.2), respectively. The Hamiltonian can be phrased as [Dol17] [4]

$$\begin{aligned} H_0 &= v_F \int \mathrm{d}x\ \vec{\psi}^\dagger(x)\sigma_z p_x \vec{\psi}(x) + \int \mathrm{d}x_1\ \mathrm{d}x_2\ g_2(|x_1 - x_2|) n_\uparrow(x_1) n_\downarrow(x_2) \\ &\quad + \frac{1}{2}\int \mathrm{d}x_1\ \mathrm{d}x_2\ g_4(|x_1 - x_2|)\left[n_\uparrow(x_1)n_\uparrow(x_2) + n_\downarrow(x_1)n_\downarrow(x_2)\right], \\ H_\mathrm{R} &= \int \mathrm{d}x\ \alpha(x)\vec{\psi}^\dagger(x)\sigma_y p_x \vec{\psi}(x) + \mathrm{h.c.}, \end{aligned} \tag{4.30}$$

where we use the notation $\vec{\psi}(x) = (\psi_\uparrow(x), \psi_\downarrow(x))^T$, and $p_x = -i\partial_x$ like in Chap. 2, as well as the electron densities $n_r(x) = \psi_r^\dagger(x)\psi_r(x)$ with $r = \uparrow, \downarrow$. If the electron interactions are fully local in the sense of $g_{2/4}(|x_1 - x_2|) = g_{2/4}\delta(x_1 - x_2)$, terms of the type g_4 are suppressed by the Pauli principle, which is incorporated in the anticommutation relations of the fermionic fields. Effectively, the parameter g_4 can then be chosen in an arbitrary way, for instance such as to render the interaction potentials $SU(2)$-invariant by $g_4 = g_2 = g$. With this choice, the full expression reads

$$H = v_F \int \mathrm{d}x\ \vec{\psi}^\dagger(x)\sigma_z p_x \vec{\psi}(x) + \frac{1}{2} g \int \mathrm{d}x\ n^2(x) + \int \mathrm{d}x\ \alpha(x)\vec{\psi}^\dagger(x)\sigma_y p_x \vec{\psi}(x) + \mathrm{h.c.}. \tag{4.31}$$

Here, the total density is denoted by $n(x) = \vec{\psi}^\dagger(x)\vec{\psi}(x) = n_\uparrow(x) + n_\downarrow(x)$. In order to absorb the Rashba perturbation, a basis transformation to new fields $\vec{\chi}(x) = (\chi_+(x), \chi_-(x))^T$ can be found, that takes the form [Dol17]

$$\begin{aligned} \vec{\psi}(x) &= \exp(i\sigma_x \theta_R(x)/2)\vec{\chi}(x), \\ \theta_R(x) &= \arctan(\alpha(x)/v_F). \end{aligned} \tag{4.32}$$

The matrix exponential can be rephrased explicitly as

$$\begin{pmatrix} \psi_\uparrow(x) \\ \psi_\downarrow(x) \end{pmatrix} = \begin{pmatrix} \cos(\theta_R/2) & i\sin(\theta_R/2) \\ i\sin(\theta_R/2) & \cos(\theta_R/2) \end{pmatrix} \begin{pmatrix} \chi_+(x) \\ \chi_-(x) \end{pmatrix}. \tag{4.33}$$

Eventually, the Hamiltonian in the new basis is simply of the form of the free helical liquid, but with a modified, position-dependent velocity,

$$\begin{aligned} H &= \int \mathrm{d}x\ v(x)\vec{\chi}^\dagger(x)\sigma_z p_x \vec{\chi}(x) + \frac{1}{2} g \int \mathrm{d}x\ n^2(x), \\ v(x) &= v_F \sqrt{1 + \left(\frac{\alpha(x)}{v_F}\right)^2}. \end{aligned} \tag{4.34}$$

[4] Note that interactions are not presented in a normal-ordered way here.

Importantly, the $SU(2)$-invariant electron interactions are not affected by this unitary basis transformation, as $n(x) = \vec{\psi}^\dagger(x)\sigma_0\vec{\psi}(x) = \vec{\chi}^\dagger(x)\sigma_0\vec{\chi}(x)$, where σ_0 is the unity operator. The Hamiltonian in Eq. (4.34) can be mapped onto a system of free bosons by the standard bosonization scheme, and as a consequence, no backscattering is expected to arise from Rashba SOC, even in the presence of an electromagnetic field [Dol17]. Note that this mapping procedure is well-defined only if $\alpha(x)$ varies smoothly in space. After bosonization, one faces the helical Luttinger liquid with altered, inhomogeneous Luttinger parameters. In particular, the effective interaction strength is then given by (compare with Eq. (2.22))

$$K(x) = \left(1 + \frac{g}{\pi v(x)}\right)^{-1/2}. \tag{4.35}$$

4.4.4. Backscattering current

Given that the involved potentials are of non-local character, a finite backscattering current can be generated from the effective operators in Eqs. (4.25) and (4.28). The contributions are calculated with Eq. (4.12), choosing suitable initial and final states in the transition matrix element.
The SPB current, induced by the operator in Eq. (4.25), entails the four terms

$$\langle \delta I\rangle_{1p} = \langle \delta I\rangle_{1p}^{P,L\to R} + \langle \delta I\rangle_{1p}^{P',L\to R} - \langle \delta I\rangle_{1p}^{P,R\to L} - \langle \delta I\rangle_{1p}^{P',R\to L}. \tag{4.36}$$

Hereby, the separate contributions are of the form

$$\begin{aligned}
\langle \delta I\rangle_{1p}^{P,R\to L} &= 2\pi e/v_F \sum_{k_1,k_2,k_1',k_2'} \left| P_{k_2k_2'}^{k_1k_1'} - P_{k_1k_2'}^{k_2k_1'}\right|^2 \\
&\quad \times \delta(-k_1' + k_2' - k_2 - k_1) f_+(k_1) f_+(k_2)(1 - f_+(k_2'))(1 - f_-(k_1')), \qquad (4.37)\\
\langle \delta I\rangle_{1p}^{P,L\to R} &= 2\pi e/v_F \sum_{k_1,k_2,k_1',k_2'} \left| (P^*)_{k_2'k_2}^{k_1'k_1} - (P^*)_{k_1'k_2}^{k_2'k_1}\right|^2 \\
&\quad \times \delta(k_1' + k_2' - k_2 + k_1) f_-(k_1) f_+(k_2)(1 - f_+(k_2'))(1 - f_+(k_1')), \qquad (4.38)\\
\langle \delta I\rangle_{1p}^{P',R\to L} &= 2\pi e/v_F \sum_{k_1,k_2,k_1',k_2'} \left| (P')_{k_2k_2'}^{k_1k_1'} - (P')_{k_2k_1'}^{k_1k_2'}\right|^2 \\
&\quad \times \delta(-k_1' - k_2' + k_2 - k_1) f_+(k_1) f_-(k_2)(1 - f_-(k_2'))(1 - f_-(k_1')), \qquad (4.39)\\
\langle \delta I\rangle_{1p}^{P',L\to R} &= 2\pi e/v_F \sum_{k_1,k_2,k_1',k_2'} \left| (P'^*)_{k_2'k_2}^{k_1'k_1} - (P'^*)_{k_2'k_1}^{k_1'k_2}\right|^2 \\
&\quad \times \delta(k_1' - k_2' + k_2 + k_1) f_-(k_1) f_-(k_2)(1 - f_-(k_2'))(1 - f_+(k_1')). \qquad (4.40)
\end{aligned}$$

The functions $f_\pm(p) = (e^{(\varepsilon_\pm(p)\pm eV/2)/T} + 1)^{-1}$ represent the Fermi-Dirac distributions including a bias voltage eV.
On the other hand, the TPB current from the operator in Eq. (4.28) reads

$$\langle \delta I\rangle_{2p} = \langle \delta I\rangle_{2p}^{L\to R} - \langle \delta I\rangle_{2p}^{R\to L}, \tag{4.41}$$

where

$$\langle \delta I \rangle_{2p}^{R\to L} = 4\pi e/v_F \sum_{k_1,k_2,k_1',k_2'} \left| Q_{k_2k_2'}^{k_1k_1'} - Q_{k_2k_1'}^{k_1k_2'} - Q_{k_1k_2'}^{k_2k_1'} + Q_{k_1k_1'}^{k_2k_2'} \right|^2 \times \delta(k_1+k_2+k_2'+k_1') f_+(k_1) f_+(k_2)(1-f_-(k_2'))(1-f_-(k_1')), \tag{4.42}$$

$$\langle \delta I \rangle_{2p}^{L\to R} = 4\pi e/v_F \sum_{k_1,k_2,k_1',k_2'} \left| (Q^*)_{k_2'k_2}^{k_1'k_1} - (Q^*)_{k_2'k_1}^{k_1'k_2} - (Q^*)_{k_1'k_2}^{k_2'k_1} + (Q^*)_{k_1'k_1}^{k_2'k_2} \right|^2 \times \delta(k_1+k_2+k_2'+k_1') f_-(k_1) f_-(k_2)(1-f_+(k_2'))(1-f_+(k_1')). \tag{4.43}$$

As we can see from the explicit expressions of the average current above, the prefactors P, P', Q in Eqs. (4.25) and (4.28), and likewise their low-energy expansions, have to exhibit a certain symmetry under permutation of momentum indices, in order to give a nonzero contribution to the backscattering current. Taking this point into account, we define the relevant antisymmetrized combinations by $\mathcal{P}, \mathcal{P}'$ and $\mathcal{Q}$, with

$$\begin{aligned} \mathcal{P}_{k_2k_2'}^{k_1k_1'} &= \frac{1}{2}\left(P_{k_2k_2'}^{k_1k_1'} - P_{k_1k_2'}^{k_2k_1'} \right), \\ (\mathcal{P}')_{k_2k_2'}^{k_1k_1'} &= \frac{1}{2}\left((P')_{k_2k_2'}^{k_1k_1'} - (P')_{k_2k_1'}^{k_1k_2'} \right), \\ \mathcal{Q}_{k_2k_2'}^{k_1k_1'} &= \frac{1}{4}\left(Q_{k_2k_2'}^{k_1k_1'} - Q_{k_1k_2'}^{k_2k_1'} - Q_{k_2k_1'}^{k_1k_2'} + Q_{k_1k_1'}^{k_2k_2'} \right). \end{aligned} \tag{4.44}$$

To identify the low-energy scaling of the SPB and TPB operators, we have to estimate the momentum dependence of the antisymmetrized prefactors in Eq. (4.44). The Fermi functions in Eqs. (4.37) – (4.43) confine the external momenta to a (small) energy window of the range of the bias. For simplicity, we hereby take the limit of zero temperature. The lowest-order scaling of the backscattering current will therefore be determined by the lowest-order expansion of interaction and SOC potentials, that are contained in the prefactors in Eq. (4.44), in those momenta.

4.4.5. General factorization

In the following, we aim not only at deriving the lowest-order scaling of the conductance with energy, but also at analyzing the dependence of the current on the important length scales of the system. One way to make them appear, is to assume a factorization of the non-local SOC potential, defined in Eq. (4.17), into two separate functions of the form of $\alpha(x,x') = \delta_l((x+x')/2)\tilde{\alpha}(x-x')$. Here, δ_l describes the (generally inhomogeneous) profile of the Rashba SOC potential along the helical edge, while $\tilde{\alpha}$ reflects its non-local character. Under the assumption that the SOC perturbation features a certain localization in real space, as it applies for instance to the case of a single impurity, the typical decay length of the modulating function δ_l is represented by the parameter l. For a translationally invariant system, the edge profile becomes homogeneous in the limit $l \to L$. On the other hand, the non-local character of the SOC potential here is supposed to be only weakly pronounced, such that $\tilde{\alpha}$ is a peaked function with a typical width of a (where a is a small parameter, $a \leq l$). With the above assumptions, we have introduced the additional energy scales $V_l = v_F/l$ and v_F/a into the model. Eventually, the physical properties of

the system will depend on the competition of the energies eV and V_l, at zero temperature. In momentum space, the factorized version of the SOC potential in Eq. (4.20) reads

$$\alpha_{k,k'} = \delta_l(k - k')\tilde{\alpha}_{(k+k')/2}. \tag{4.45}$$

Evidently, δ_l takes the form of a delta function in Fourier space, if the edge profile is translationally invariant (constant) in real space. Quite generally, we take $\delta_l(k)$ to be a peaked function of height l and decay width $1/l$ (note that in momentum space δ_l is of dimension length). Moreover, $\tilde{\alpha}$ typically decays at a large scale of $1/a$, and becomes a constant if the SOC potential is local. On this part, according to Eq. (4.21), TRS imposes the constraint

$$\tilde{\alpha}_k = \tilde{\alpha}_{-k}. \tag{4.46}$$

Using the notation $\tilde{\alpha}'_k = d\tilde{\alpha}_k/dk$, we have $\tilde{\alpha}'_k = -\tilde{\alpha}'_{-k}$, and in particular $\tilde{\alpha}'_0 = 0$. Implicitly, we hereby make the assumption that the full Rashba SOC potential is an analytic function, such that a Taylor expansion is well-defined at all points in momentum space.
Moreover, the nature of Coulomb interactions suggests to adopt a translationally invariant form of the electron interaction potential, such that $g^{(n)}_{q,q'} = g^{(n)}_q \delta(q - q')$. A regular behaviour of the (analytic) function $g_n(x_1, x_2)$ at short distances, results in a small-momentum expansion of

$$g^{(n)}_q = c^{(n)}_0 + c^{(n)}_2 (aq)^2 + \mathcal{O}(q^4), \tag{4.47}$$

with coefficients $c^{(n)}_i$ and a regularizing parameter a, which can be associated with a short-distance cutoff (importantly, it is not a general cutoff on all distances here, but only related to the interaction potential). This cutoff is not necessarily the same as the decay width of the non-local part of the SOC potential given above, however, the two parameters shall be identified here for simplicity. The expansion in Eq. (4.47) implies that the electron interaction potential, that we associate with screened Coulomb interactions, decays sufficiently fast for large separations in real space. Such an assumption prevents diverging integrands in the later analysis, see for instance Eq. (4.53).
Eventually, using the factorization in Eq. (4.45), the effective prefactors of SPB and TPB from Eqs. (4.25) and (4.28) can be rephrased as

$$\begin{aligned} P^{k_1 k'_1}_{k_2 k'_2} &= -\frac{i}{v_F L^2}\delta_l(2\Delta K)\left(g^{(2)}_{k_2-k'_2}\tilde{\alpha}_{(k_1+k'_1-k_2+k'_2)/2} - g^{(4)}_{k_2-k'_2}\tilde{\alpha}_{(k_1+k_2-k'_2+k'_1)/2}\right), \\ (P')^{k_1 k'_1}_{k_2 k'_2} &= -\frac{i}{v_F L^2}\delta_l(2\Delta K)\left(g^{(2)}_{k_2-k'_2}\tilde{\alpha}_{(k_1+k_2-k'_2+k'_1)/2} - g^{(4)}_{k_2-k'_2}\tilde{\alpha}_{(k_1+k'_1-k_2+k'_2)/2}\right), \end{aligned} \tag{4.48}$$

and

$$\begin{aligned} Q^{k_1 k'_1}_{k_2 k'_2} = -\frac{1}{v_F^2 L^2}\int \mathrm{d}q\ \delta_l(\Delta K + q)\delta_l(\Delta K - q)\Big(&g^{(2)}_{q+K/2}\tilde{\alpha}_{(k_2+q+k'_1)/2+K/4}\tilde{\alpha}_{(k_1+k'_2+q)/2+K/4} \\ &- \frac{1}{2}g^{(4)}_{q-K/2}\left[\tilde{\alpha}_{(k_2-q+k'_1)/2+K/4}\tilde{\alpha}_{(k_1+q+k'_2)/2-K/4} + \tilde{\alpha}_{(k_2+k'_1+q)/2-K/4}\tilde{\alpha}_{(k_1+k'_2-q)/2+K/4}\right]\Big). \end{aligned} \tag{4.49}$$

In Eq. (4.49), we performed the shifts $q \to q \pm K/2$, respectively, and made use of the shortcuts

$$\begin{aligned} \Delta K &= (k_1 + k_2 - k_2' - k_1')/2, \\ K &= k_1 - k_2 + k_1' - k_2'. \end{aligned} \tag{4.50}$$

Note that the combination ΔK is proportional to the total momentum of both the operators in Eqs. (4.25) and (4.28). It further remains invariant under any of the permutations of momenta, that are involved in the antisymmetrization of the prefactors in Eq. (4.44).

4.4.6. Low-energy expansion

To explore the low-energy transport properties of the system, we distinguish the two scenarios of effectively translational invariant, and non-invariant SOC perturbations.
First, if $V \ll V_l$, the external momenta remain small compared to $1/l$, and the full potential $\alpha_{k,k'}$ can be expanded accordingly. In this case, the SOC profile changes considerably at the energy scale of the bias, and we refer to this case as to a translationally non-invariant Rashba potential. The antisymmetrized lowest-order contributions then take the form (from Eqs. (4.48) and (4.49))

$$\begin{aligned} \mathcal{P}^{k_1 k_1'}_{k_2 k_2'} &\simeq -\frac{i}{v_F L^2}\delta_l(0)\Big[\frac{1}{4}c_0^{(2)}(k_1-k_2)(k_1'+k_2')\tilde{\alpha}_0'' \\ &\quad + \frac{1}{2}a^2(c_2^{(2)} - c_2^{(4)})(k_1-k_2)(2k_2' - (k_1+k_2))\tilde{\alpha}_0\Big], \end{aligned} \tag{4.51}$$

$$\begin{aligned} (\mathcal{P}')^{k_1 k_1'}_{k_2 k_2'} &\simeq -\frac{i}{v_F L^2}\delta_l(0)\Big[\frac{1}{4}c_0^{(2)}(k_1'-k_2')(k_1+k_2)\tilde{\alpha}_0'' \\ &\quad + \frac{1}{2}a^2(c_2^{(2)} - c_2^{(4)})(k_1'-k_2')(2k_2 - (k_1'+k_2'))\tilde{\alpha}_0\Big], \end{aligned} \tag{4.52}$$

$$\begin{aligned} \mathcal{Q}^{k_1 k_1'}_{k_2 k_2'} &\simeq -\frac{1}{4v_F^2 L^2}(k_1-k_2)(k_1'-k_2')\int \mathrm{d}q\ \delta_l(q)\delta_l(-q) \\ &\quad \times \Big[g_q^{(2)}(\tilde{\alpha}'_{q/2})^2 + 2\partial_q(g_q^{(2)} - g_q^{(4)})\tilde{\alpha}'_{q/2}\tilde{\alpha}_{q/2} + \partial_q^2(g_q^{(2)} - g_q^{(4)})\tilde{\alpha}^2_{q/2}\Big]. \end{aligned} \tag{4.53}$$

In the case of SPB, we find that the lowest-order expansion starts from second order in momentum. For such processes, permutation symmetry generically allows also for terms linear in momentum [LOB12], as one can see from

$$\begin{aligned} H_{1p}^{\text{generic}} &= \int \mathrm{d}x\ g_{1p}(x)\left(\psi_+^\dagger(x)\partial_x\psi_+^\dagger(x)\psi_+(x)\psi_-(x) + \psi_+^\dagger(x)\psi_-^\dagger(x)\psi_-(x)\partial_x\psi_-(x)\right) + \text{h.c.} \\ &= -\frac{i}{2L^2}\sum_{k_1,k_1',k_2,k_2'} g_{1p}(2\Delta K)\Big[(k_2-k_1)c^\dagger_{+,k_1}c^\dagger_{+,k_2}c_{+,k_2'}c_{-,k_1'} \\ &\quad - (k_1'-k_2')c^\dagger_{+,k_1}c^\dagger_{-,k_2}c_{-,k_2'}c_{-,k_1'}\Big] + \text{h.c.} \\ &\simeq -\frac{i}{2L^2}g_{1p}(0)\sum_{k_1,k_1',k_2,k_2'}\Big[(k_2-k_1)c^\dagger_{+,k_1}c^\dagger_{+,k_2}c_{+,k_2'}c_{-,k_1'} \\ &\quad - (k_1'-k_2')c^\dagger_{+,k_1}c^\dagger_{-,k_2}c_{-,k_2'}c_{-,k_1'}\Big] + \text{h.c.}. \end{aligned} \tag{4.54}$$

Here, we use the Fourier transform $g_{1p}(k) = \int \mathrm{d}x\, g_{1p}(x)e^{-ixk}$ (and analogous for g_{2p} below). In the presence of a small bias voltages (or a very local perturbation), we can expand $g_{1p}(k) \approx g_{1p}(0)$. Contributions linear in momentum such as in Eq. (4.54) arise as well in our perturbative analysis, for instance in the form of $P \propto c_0^{(2)}(k_1 - k_2)\tilde{\alpha}_0'\delta_l(0)$. However, they are suppressed by TRS, which enforces $\tilde{\alpha}_0' = 0$. We therefore conclude, that under the given assumptions, a generic SPB term as presented in Eq. (4.54) can not be induced by Rashba SOC, at least to lowest order.
In the case of TPB, the lowest-order expansion with the correct permutation symmetry is of second order in momentum as well. This is what we expect from a generic TPB perturbation (after antisymmetrization, see also Sec. 3.3) [WBZ06, XM06],

$$\begin{aligned} H_{2p}^{\text{generic}} &= \int \mathrm{d}x\, g_{2p}(x)\psi_+^\dagger(x)\partial_x\psi_+^\dagger(x)\psi_-(x)\partial_x\psi_-(x) + \text{h.c.} \\ &= -\frac{1}{4L^2}\sum_{k_1,k_1',k_2,k_2'} g_{2p}(2\Delta K)(k_1 - k_2)(k_1' - k_2')c_{+,k_1}^\dagger c_{+,k_2}^\dagger c_{-,k_2'}c_{-,k_1'} + \text{h.c.} \\ &\simeq -\frac{1}{4L^2}g_{2p}(0)\sum_{k_1,k_1',k_2,k_2'} (k_1 - k_2)(k_1' - k_2')c_{+,k_1}^\dagger c_{+,k_2}^\dagger c_{-,k_2'}c_{-,k_1'} + \text{h.c.}. \end{aligned} \tag{4.55}$$

Using that $\delta_l(0) = l$ and $\tilde{\alpha}_0'' \approx a^2\tilde{\alpha}_0$ in Eqs. (4.51)–(4.53), we can estimate the scaling of the backscattering current at zero temperature,

$$\begin{aligned} \langle \delta I\rangle_{1p} &\simeq \frac{22\pi}{315} e v_F^{-3} a^4 l^2 \tilde{\alpha}_0^2 c^2 (eV/v_F)^7, \\ \langle \delta I\rangle_{2p} &\simeq \frac{128\pi}{315} e v_F a^4 l^2 n_1 (eV/v_F)^7. \end{aligned} \tag{4.56}$$

Above, we defined $c^2 = \left(c_0^{(2)}\right)^2 + \left(c_2^{(2)} - c_2^{(4)}\right)^2 + c_0^{(2)}\left(c_2^{(2)} - c_2^{(4)}\right)$, and the dimensionless factor of n_1 stems from the integration of q, given a general Rashba profile along the edge. Note that by a dimensional analysis, integration of q generally yields a factor of $1/l$. From the backscattering current, we simply infer the correction to the conductance by $\delta G = d\langle \delta I\rangle/dV$. Using Eq. (4.56), we find that both single- and two-particle backscattering processes, induced by Rashba SOC in the translationally non-invariant regime, lead to a correction to the conductance that scales as

$$\delta G \sim a^4 l^2 \left(eV/v_F\right)^6 . \tag{4.57}$$

This is the power-law behaviour we expect from a generic TPB perturbation in the non-interacting limit, $K \to 1$ (compare with Sec. 3.3).

On the other hand, if $V \gg V_l$, the SOC profile appears to be effectively homogeneous at the energy scale of the bias, and can therefore be considered as effectively translational invariant (see Fig. 4.2). As the impurity decay length l now is very large compared to the respective length scale of the bias, the edge profile is a sharply peaked function in Fourier space. The expansion of the function δ_l in the external momenta then is not justified anymore, whereas we can safely expand the slowly varying, non-local part $\tilde{\alpha}$. The SOC profile function characteristically depends on the total momentum ΔK, which is therefore

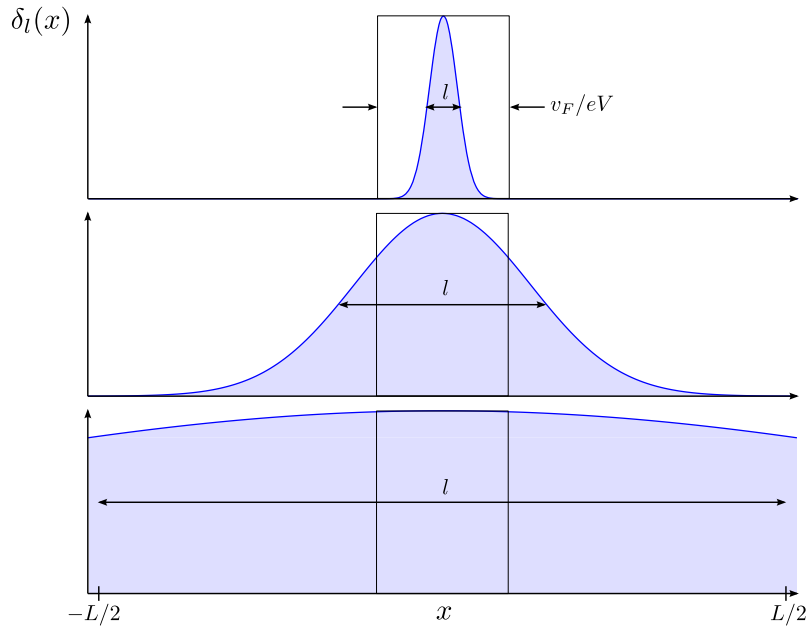

Figure 4.2.: Competition of the length scales associated with bias voltage (v_F/eV), impurity localization length (l), and system size (L). From top to bottom: the translationally non-invariant ($l \ll v_F/eV$), effectively invariant ($v_F/eV < l < L$), and invariant ($l \to L$) regime. The SOC profile along the edge is given by the function $\delta_l(x)$.

restricted to a small value of $1/l$, in the same way as q. This observation manifests itself in replacing one factor of eV by V_l, when integrating out the external momenta. While the difference in the prefactors $\mathcal{P}$ and $\mathcal{P}'$ in this regime is captured by the simple replacement $\delta_l(0) \to \delta_l(2\Delta K)$ in Eqs. (4.51) and (4.52), we find a slightly different expression for the TPB low-energy expansion, from Eq. (4.49),

$$\begin{aligned}\mathcal{Q}^{k_1 k_1'}_{k_2 k_2'} \simeq -\frac{1}{16 v_F^2 L^2}(k_1 - k_2)(k_1' - k_2') \int \mathrm{d}q\, \delta_l(\Delta K + q)\delta_l(\Delta K - q) \\ \times \left(c_0^{(2)} q^2 (\tilde{\alpha}_0'')^2 + 8(c_2^{(2)} - c_2^{(4)})\tilde{\alpha}_0^2 a^2 \right).\end{aligned} \tag{4.58}$$

As a consequence, the resulting backscattering current takes the form

$$\begin{aligned}\langle \delta I \rangle_{1p} &\simeq e v_F^{-3} a^4 l \tilde{\alpha}_0^2 c^2 n_2 \mathrm{sgn}(eV)(eV/v_F)^6, \\ \langle \delta I \rangle_{2p} &\simeq e v_F^{-5} a^4 l \tilde{\alpha}_0^4 (c')^2 \mathrm{sgn}(eV)(eV/v_F)^6.\end{aligned} \tag{4.59}$$

The factor c^2 was defined below Eq. (4.56), while in the TPB term here, we find a term of the similar structure $(c')^2 = n_3 (c_0^{(2)})^2 (a/l)^4 + n_4 (c_2^{(2)} - c_2^{(4)})^2 + n_5 c_0^{(2)} (c_2^{(2)} - c_2^{(4)})(a/l)^2$, and different numerical factors n_2 to n_5. The correction to the conductance arising from the effectively translationally invariant SOC perturbation, therefore displays the scaling

$$\delta G \sim a^4 l \left(|eV|/v_F\right)^5, \tag{4.60}$$

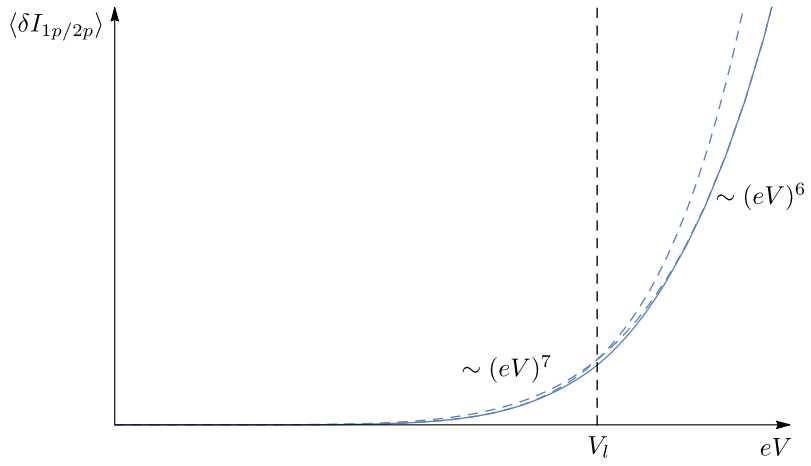

Figure 4.3.: The typical decay length l of the SOC impurity defines an energy scale V_l. For $eV \ll V_l$ (or $eV \gg V_l$), the perturbation appears translationally non-invariant (invariant), at the energy scale of the bias voltage (compare with Fig. 4.2). With increasing energy, we expect a crossover between the two regimes, which manifests itself in a change of the scaling of the backscattering current (both SPB and TPB) from seventh to sixth power (see Eqs. 4.56 and 4.59). Note that these characteristic power exponents can change in the presence of a non-analytic cutoff function (see Sec. 4.4.8).

which is in agreement with the SPB scaling predicted in Ref. [SRvG12], for translational invariance and $k_F = 0$ (see Eq. (4.14)). By comparison with Eq. (4.57), we can directly verify a crossover of scales at $eV \approx V_l$, which represents the transition from the effectively translational invariant to the non-invariant regime.
If the SOC impurity profile does not vary significantly over the entire size of system, $l \to L \to \infty$, we reach the limit of true translational invariance (see Fig. 4.2). The correction to the conductance in Eq. (4.60) then becomes proportional to the system size, reflecting its dependence on the effective region of backscattering. Consistently, the edge profile part δ_l then takes the form of momentum conservation. Note that in the truly translationally invariant system, a TPB contribution arising from contact interactions is generally suppressed.
The results of the above analysis can be summarized the following way: Assuming that either the SOC perturbation or the electron interactions are non-local, and given that the potential functions are analytic, the scaling of the backscattering current is found to be either of seventh or sixth power, depending on the competition of eV and V_l. Correspondingly, the correction to the conductance is of sixth or fifth power in the bias voltage, respectively. With increasing energy, we predict a crossover of scales, originating from the transition of a translationally non-invariant to an effectively invariant edge profile (see Fig. 4.3).

4.4.7. $SU(2)$ symmetry

Some important aspects concerning the underlying symmetries of the system should be noted. First, we realize that electron interactions of finite range, that exhibit $SU(2)$ sym-

metry, can not induce backscattering in combination with a local Rashba SOC potential (at least to this order of perturbation theory, compare also with Sec. 4.4.3 or Ref. [Dol17]). This point can already be observed from the general prefactors in Eqs. (4.25) and (4.28), choosing a local potential $\alpha_{k,k'} = \alpha_{k-k'}$. We then obtain

$$\begin{aligned} P^{k_1 k_1'}_{k_2 k_2'} &= (P')^{k_1 k_1'}_{k_2 k_2'} = -\frac{i}{v_F L^3} \sum_q \left(g^{(2)}_{q,k_2-k_2'} - g^{(4)}_{q,k_2-k_2'} \right) \alpha_{k_1-k_1'+q}, \\ Q^{k_1 k_1'}_{k_2 k_2'} &= -\frac{1}{v_F^2 L^4} \sum_{q,q'} \left(g^{(2)}_{q,q'} - g^{(4)}_{q,q'} \right) \alpha_{k_2+q-k_1'} \alpha_{k_1-k_2'-q'}. \end{aligned} \tag{4.61}$$

If electron interactions are $SU(2)$-invariant, meaning that they do not distinguish particles of different chirality, the two potentials of the type g_2 and g_4 have the same momentum dependence. After a cancellation of terms, effectively, we recover the situation of contact interactions. As argued in the previous Sec. 4.4.3, such an all-local model does not generate backscattering. A compensation of the respective coefficients can as well be observed in the low-energy expansions of Eqs. (4.51)–(4.53) and Eq. (4.58). However, a finite contribution to the backscattering current can arise from $SU(2)$-invariant interactions, in combination with a non-local SOC potential. The latter can be associated with a breaking of "local $SU(2)$ gauge symmetry" of the SOC, as explained in the following. At the helical edge, due to the conservation of the electrons s_z-component, $SU(2)$ symmetry is reduced to an effective $U(1)$ symmetry. When spin-orbit coupling is introduced, the conservation of the s_z-component is in general broken. Nevertheless, if the Rashba term contains a single spatial derivative (which according to our definition in Eq. (4.17) means locality in real space), it can be absorbed in the kinetic term by a local $SU(2)$ transformation of the spin basis (see Sec. 4.4.3). This is not possible anymore, if the SOC potential includes higher-order derivatives (i.e. if it is non-local in real space). Therefore, the requirement for nonzero backscattering off the Rashba impurity can as well be phrased in the way that either the $SU(2)$ symmetry of the interactions, or the local $SU(2)$ gauge symmetry of the SOC potential, must be broken. The table in Tab. 4.1 provides a summary of the above findings.

4.4.8. Backscattering at finite cutoff

In the previous sections, we have demonstrated that a nonzero backscattering current is generated by SOC perturbations involving non-local potentials in real space. Here, we explicitly explore the possibility of backscattering off originally local potentials, but in the presence of a momentum cutoff. As discussed above, this can be viewed as an alternative way of inducing non-local effects in real space. Interestingly, the lowest-order scaling of the correction to the conductance then depends on the form of the chosen cutoff.
A momentum cutoff can be imposed in various ways. In a systematic approach, we may introduce a general cutoff function F_k already in the definition of fermionic creation and annihilation operators, in the form of a general scaling factor [GKT17]

$$c_{r,k} \to c_{r,k} \sqrt{F_k}. \tag{4.62}$$

	SOC local	SOC non-local
interactions local	×	✓
interactions non-local and $SU(2)$-symmetric	×	✓
interactions non-local and $SU(2)$-asymmetric	✓	✓

Table 4.1.: Occurrence (✓) and absence (×) of inelastic backscattering according to the analysis of this section: In the absence of a momentum cutoff, we expect a finite contribution to the backscattering current, given that the model includes non-local potentials (except for non-local but $SU(2)$-invariant interactions and local SOC). Importantly, if a momentum cutoff is present, we generally find nonzero backscattering for all the cases above (see also discussion in Sec. 4.4.8).

This will alter the anticommutation relation of Eq. (4.8) to

$$\{c_{r,k}, c^\dagger_{r',k'}\} = \delta_{kk'}\delta_{rr'}F_k, \tag{4.63}$$

and in the real-space version of Eq. (4.63), the delta function is smeared out. The cutoff function enters into the effective prefactors of SPB and TPB, in Eqs. (4.25) and (4.28), respectively, in the form of

$$P^{k_1k_1'}_{k_2k_2'} \to -\frac{i}{v_F L^3}\tilde{F}\sum_q \left(g^{(2)}_{q,k_2-k_2'}\alpha_{k_1,k_1'-q}F_{k_1'-q} - g^{(4)}_{q,k_2-k_2'}\alpha_{k_1+q,k_1'}F_{k_1+q}\right), \tag{4.64}$$

$$(P')^{k_1k_1'}_{k_2k_2'} \to -\frac{i}{v_F L^3}\tilde{F}\sum_q \left(g^{(2)}_{q,k_2-k_2'}\alpha_{k_1+q,k_1'}F_{k_1+q} - g^{(4)}_{q,k_2-k_2'}\alpha_{k_1,k_1'-q}F_{k_1'-q}\right), \tag{4.65}$$

$$\begin{aligned} Q^{k_1k_1'}_{k_2k_2'} \to -\frac{1}{v_F^2 L^4}\tilde{F}\sum_{q,q'} \big(&g^{(2)}_{q,q'}\alpha_{k_2+q,k_1'}\alpha_{k_1,k_2'+q'}F_{k_2+q}F_{k_2'+q'} \\ &- \frac{1}{2}g^{(4)}_{q,q'}[\alpha_{k_2-q',k_1'}\alpha_{k_1+q,k_2'}F_{k_2-q'}F_{k_1+q} + \alpha_{k_2,k_1'+q'}\alpha_{k_1,k_2'-q}F_{k_1'+q'}F_{k_2'-q}]\big), \end{aligned} \tag{4.66}$$

where

$$\tilde{F} = \left(F_{k_1}F_{k_2}F_{k_2'}F_{k_1'}\right)^{1/2}. \tag{4.67}$$

We observe that, in particular, the electron momenta that represent the internal lines in the diagrams of Fig. 4.1, are restricted by the cutoff. In the following, we assume translationally invariant and local interactions, $g^{(2,4)}_{q,q'} = c_0^{(2,4)}\delta(q-q')$, as well as local Rashba SOC, to evaluate the low-energy scaling of the backscattering current at finite

cutoff. This means we face simplified prefactors, where the antisymmetrized versions read

$$\mathcal{P}^{k_1k_1'}_{k_2k_2'} = -\frac{i}{2v_F L^2}\tilde{F}c_0^{(2)}\tilde{\alpha}_0\delta_l(2\Delta K)(F_{k_1'+k_2'-k_2} - F_{k_1'+k_2'-k_1}), \tag{4.68}$$

$$(\mathcal{P}')^{k_1k_1'}_{k_2k_2'} = -\frac{i}{2v_F L^2}\tilde{F}c_0^{(2)}\tilde{\alpha}_0\delta_l(2\Delta K)(F_{k_1+k_2-k_2'} - F_{k_1+k_2-k_1'}), \tag{4.69}$$

$$\begin{aligned}\mathcal{Q}^{k_1k_1'}_{k_2k_2'} &= -\frac{1}{4v_F^2L^2}\tilde{F}c_0^{(2)}\tilde{\alpha}_0^2\int \mathrm{d}q\ \delta_l(k_2+q-k_1')\delta_l(k_1-k_2'-q)\\ &\quad\times\left(F_{k_2+q} - F_{k_2+q+k_2'-k_1'}\right)\left(F_{k_2'+q} - F_{k_2'+q+k_2-k_1}\right)\\ &\overset{q\to q+K/2}{=} -\frac{1}{4v_F^2L^2}\tilde{F}c_0^{(2)}\tilde{\alpha}_0^2\int \mathrm{d}q\ \delta_l(q+\Delta K)\delta_l(-q+\Delta K)\\ &\quad\times\left(F_{q+\Delta K+k_1'} - F_{q+\Delta K+k_2'}\right)\left(F_{q-\Delta K+k_1} - F_{q-\Delta K+k_2}\right).\end{aligned} \tag{4.70}$$

We naturally expect, that the cutoff function F_k decays at a large typical scale of $1/a \gg \max(eV/v_F, 1/l)$. Associating $1/a$ with the effective bandwidth of the system, this suggests that the influence of remote bulk states can be neglected.

First, we consider the scenario of a smooth, analytic cutoff function. In this case, F_k can be expanded safely in all the external momenta. We note that $F_0' = [dF_k/dk]_{k=0} = 0$, since F_k has its global maximum at $k = 0$. This constraint suppresses terms linear in momentum in the low-energy expansions of Eqs. (4.71) and (4.72) below. We find

$$\mathcal{P}^{k_1k_1'}_{k_2k_2'} \simeq -\frac{i}{2v_F L^2}F_0^2c_0^{(2)}\tilde{\alpha}_0\delta_l(2\Delta K)F_0''(k_1-k_2)(k_1'+k_2'), \tag{4.71}$$

$$(\mathcal{P}')^{k_1k_1'}_{k_2k_2'} \simeq -\frac{i}{2v_F L^2}F_0^2c_0^{(2)}\tilde{\alpha}_0\delta_l(2\Delta K)F_0''(k_1'-k_2')(k_1+k_2), \tag{4.72}$$

$$\mathcal{Q}^{k_1k_1'}_{k_2k_2'} \simeq -\frac{1}{4v_F^2L^2}F_0^2c_0^{(2)}\tilde{\alpha}_0^2(k_1-k_2)(k_1'-k_2')\int \mathrm{d}q\ \delta_l(q+\Delta K)\delta_l(-q+\Delta K)(F_q')^2. \tag{4.73}$$

Both the SPB and TPB contributions are of second order in momentum. The lowest-order terms exhibit the same structure as the expressions we found before, employing non-local potentials in the absence of a cutoff (compare with Eqs. (4.51)–(4.53)). Therefore, the scaling of the backscattering current will be the same as in Eqs. (4.56) and (4.59), resulting in corrections to the conductance of $\delta G \sim V^6$ or $\delta G \sim V^5$, for a translational non-invariant or invariant perturbation, respectively.

The nature of a momentum cutoff implies, that the cutoff function is not necessarily analytic in a realistic system. For instance, a simple way to model the cutoff is to truncate the energy spectrum at a finite threshold $1/a$. Such an approach reflects the general idea of a RG analysis, where high energy degrees of freedom are excluded. Let us study the effects of this type of hard cutoff on the transport properties of the system. From

Eqs. (4.64)–(4.66), we derive

$$P^{k_1k_1'}_{k_2k_2'} = -\frac{i}{v_F L^2} c_0^{(2)} \tilde{F}\tilde{\alpha}_0 [\delta_l(2\Delta K)]_{-\frac{1}{a}\le k_1' - (k_2 - k_2')\le \frac{1}{a}} = -\frac{i}{v_F L^2} c_0^{(2)} \tilde{\alpha}_0 \delta_l(2\Delta K), \quad (4.74)$$

$$(P')^{k_1k_1'}_{k_2k_2'} = -\frac{i}{v_F L^2} c_0^{(2)} \tilde{F}\tilde{\alpha}_0 [\delta_l(2\Delta K)]_{-\frac{1}{a}\le k_1 + (k_2 - k_2')\le \frac{1}{a}} = -\frac{i}{v_F L^2} c_0^{(2)} \tilde{\alpha}_0 \delta_l(2\Delta K), \quad (4.75)$$

$$\begin{aligned} Q^{k_1k_1'}_{k_2k_2'} &= -\frac{1}{v_F^2 L^2} c_0^{(2)} \tilde{F}\tilde{\alpha}_0^2 \int_{\substack{-\frac{1}{a}\le k_2+q\le \frac{1}{a} \\ -\frac{1}{a}\le k_2'+q\le \frac{1}{a}}} \mathrm{d}q\ \delta_l(k_2 + q - k_1')\delta_l(k_1 - k_2' - q) \\ &= -\frac{1}{v_F^2 L^2} c_0^{(2)} \tilde{\alpha}_0^2 \int_{-\frac{1}{a} - \min(k_2, k_2')}^{\frac{1}{a} - \max(k_2, k_2')} \mathrm{d}q\ \delta_l(k_2 + q - k_1')\delta_l(k_1 - k_2' - q). \end{aligned} \quad (4.76)$$

It is important to note that any combination of external momenta remains unaffected by the cutoff constraints, given that $1/a \gg eV/v_F$ (so e.g. $\tilde{F} = 1$). As a consequence, the SPB contribution vanishes,

$$\mathcal{P}^{k_1k_1'}_{k_2k_2'} = (\mathcal{P}')^{k_1k_1'}_{k_2k_2'} = 0, \quad (4.77)$$

$$\begin{aligned} \mathcal{Q}^{k_1k_1'}_{k_2k_2'} &\simeq -\frac{1}{4v_F^2 L^2} c_0^{(2)} \tilde{\alpha}_0^2 \delta_l\left(\frac{1}{a}\right) \delta_l\left(-\frac{1}{a}\right) [\, -\max(k_2, k_2') + \max(k_1, k_2') + \max(k_2, k_1') \\ &\quad - \max(k_1, k_1') + \min(k_2, k_2') - \min(k_1, k_2') - \min(k_2, k_1') + \min(k_1, k_1')] \\ &= -\frac{1}{4v_F^2 L^2} c_0^{(2)} \tilde{\alpha}_0^2 \delta_l\left(\frac{1}{a}\right) \delta_l\left(-\frac{1}{a}\right) \left(-|k_2 - k_2'| + |k_1 - k_2'| + |k_2 - k_1'| - |k_1 - k_1'|\right). \end{aligned} \quad (4.78)$$

To estimate the integral of finite range, we used the approximation given in Eq. (A.8). With this, we arrive at the backscattering current [GKT17]

$$\begin{aligned} &\langle \delta I_{1p} \rangle = 0, \\ &\langle \delta I_{2p} \rangle \simeq 1.4\pi e v_F^{-5} \tilde{\alpha}_0^4 \delta_l^2\, (1/a)\, \delta_l^2\, (-1/a) \left(c_0^{(2)}\right)^2 (eV/v_F)^5. \end{aligned} \quad (4.79)$$

A numerical factor of $3240116/2278125 \approx 1.4$ is obtained from the integration of the external momenta. As before, we assume that the function $\delta_l(q)$, which is of dimension length, is proportional to the SOC profile width l, such that correction to the conductance scales as

$$\delta G \sim l^4 (eV/v_F)^4. \quad (4.80)$$

Next, we study another example of a non-analytic cutoff function, in the form of an exponential damping $F_k = e^{-a|k|}$. This type of cutoff is for instance widely used in the bosonization scheme, in order to define bosonic fields with non-diverging two-point

correlations (see Eq. (2.10)). Starting from Eqs. (4.68)–(4.70), we obtain [5]

$$\begin{aligned}\mathcal{P}^{k_1k_1'}_{k_2k_2'} &= -\frac{i}{2v_FL^2}c_0^{(2)}\tilde{\alpha}_0\delta_l(2\Delta K)\left(e^{-a|k_1'+k_2'-k_2|}-e^{-a|k_1'+k_2'-k_1|}\right)\\ &\simeq \frac{i}{2v_FL^2}c_0^{(2)}\tilde{\alpha}_0\delta_l(2\Delta K)a\left(|k_1'+k_2'-k_2|-|k_1'+k_2'-k_1|\right), \qquad (4.81)\\ (\mathcal{P}')^{k_1k_1'}_{k_2k_2'} &\simeq \frac{i}{2v_FL^2}c_0^{(2)}\tilde{\alpha}_0\delta_l(2\Delta K)a\left(|k_1+k_2-k_2'|-|k_1+k_2-k_1'|\right), \qquad (4.82)\\ \mathcal{Q}^{k_1k_1'}_{k_2k_2'} &= -\frac{1}{4v_F^2L^2}c_0^{(2)}\tilde{\alpha}_0^2\int \mathrm{d}q\ \delta_l(q+\Delta K)\delta_l(-q+\Delta K)\\ &\quad\times\left(e^{-a|q+\Delta K+k_1'|}-e^{-a|q+\Delta K+k_2'|}\right)\left(e^{-a|q-\Delta K+k_1|}-e^{-a|q-\Delta K+k_2|}\right). \qquad (4.83)\end{aligned}$$

Since the cutoff function is non-analytic at zero momentum, its first derivative is ill-defined. However, we can still expand Eqs. (4.81) and (4.82) for small values of a, while in Eq. (4.83) this depends on the convergence properties of the integral.
For translationally non-invariant profiles, in order to deal with the integral in Eq. (4.83), we argue that the dominant contribution stems from the large momenta of $|q| \geq |eV/v_F|$ [GKT17], in which case we can simplify

$$\mathcal{Q}^{k_1k_1'}_{k_2k_2'} \simeq -\frac{1}{4v_F^2L^2}c_0^{(2)}a^2(k_1'-k_2')(k_1-k_2)\tilde{\alpha}_0^2\int \mathrm{d}q\ \delta_l(q)\delta_l(-q)e^{-2a|q|}. \qquad (4.84)$$

With that, we find the backscattering currents

$$\begin{aligned}\langle\delta I_{1p}\rangle &= \frac{191\pi}{2880}ev_F^{-3}a^2l^2\tilde{\alpha}_0^2\left(c_0^{(2)}\right)^2(eV/v_F)^5,\\ \langle\delta I_{2p}\rangle &= \frac{128\pi}{315}ev_F^{-5}a^4l^2\tilde{\alpha}_0^4\left(c_0^{(2)}\right)^2 n_6(eV/v_F)^7.\end{aligned} \qquad (4.85)$$

Here, n_6 is numerical factor that depends on the particular form of δ_l. The leading-order correction to the conductance at small bias voltages thus originates from SPB terms, and exhibits the scaling

$$\delta G \sim a^2l^2\left(eV/v_F\right)^4, \qquad (4.86)$$

while the correction due to TPB processes is proportional to $\delta G \sim a^4l^2\left(eV/v_F\right)^6$.
For effectively translational invariant perturbations, the profile function can not be expanded in the external momenta. As we have seen before, one power of eV is eventually replaced by V_l in the average current. The integral in Eq. (4.83) can be evaluated approximately by taking the integrand at $q=0$, on a range of $1/l$. We then obtain

$$\mathcal{Q}^{k_1k_1'}_{k_2k_2'} \simeq -\frac{1}{4v_F^2L^2}c_0^{(2)}l^{-1}\tilde{\alpha}_0\delta_l^2(\Delta K)a^2\left(|k_1'|-|k_2'|\right)\left(|k_1|-|k_2|\right), \qquad (4.87)$$

and the resulting currents

$$\begin{aligned}\langle\delta I_{1p}\rangle &= 4\pi ev_F^{-3}a^2l\tilde{\alpha}_0^2\left(c_0^{(2)}\right)^2 n_7(eV/v_F)^4\mathrm{sgn}(eV),\\ \langle\delta I_{2p}\rangle &= 4\pi ev_F^{-5}a^4l\tilde{\alpha}_0^4\left(c_0^{(2)}\right)^2 n_8(eV/v_F)^6\mathrm{sgn}(eV),\end{aligned} \qquad (4.88)$$

[5] In lowest order, we have again $\tilde{F}\approx 1$.

with numerical factors n_7 and n_8. The TPB terms induce a correction of the form $\delta G \sim a^4 l \left(|eV|/v_F\right)^5$, whereas the dominant transport signature is given by the SPB processes,

$$\delta G \sim a^2 l \left(|eV|/v_F\right)^3 . \tag{4.89}$$

We observe that these scalings, derived from two different examples of non-analytic cutoff functions, are in general different from the ones arising in the context of non-local potentials in real space, see Eqs. (4.57) and (4.60). This is due to the fact that the low-energy expansion here allows for terms linear in momentum, that come with an absolute value, which prevents immediate cancellations upon antisymmetrization. In contrast, the assumption of an analytic form of the SOC potentials suppressed the appearance of such terms in the previous analysis, and the lowest-order contributions were found to be of second order in momentum. By comparison of Eq. (4.85) and Eq. (4.88), we further state that the specific choice of the cutoff generally affects the power-law scaling of the backscattering current.

So far, we have analyzed the possibility of inelastic backscattering induced by Rashba SOC in a fermionic scheme, where electron interactions were treated perturbatively. In the next sections we turn to a bosonic approach, which bears the great advantage that interactions can be included into the model exactly. This is of particular interest when studying phase transitions between the regimes of weak and strong coupling, since those transitions usually occur at intermediate or strong interactions. Note that in such a bosonic framework, the presence of a finite momentum cutoff is in general essential to avoid divergences. We shall explore two fundamental scenarios: the setup of a single, localized SOC perturbation, possibly attached to external reservoirs, and the case of many, randomly disordered SOC impurities.

4.5. Single Rashba impurity

Approaching actual realizations of a Rashba potential along the edge, the simplest idea was to assume a single, localized perturbation, that we refer to as a "Rashba impurity" (see Fig. 4.4). In an experiment, such a single barrier could be accomplished by placing a local gate on top of the QSH edge. If the system contains many impurities of the same kind, the single impurity contributions can be added up, given that interference effects and multiple-scattering can be neglected (see discussion in Sec. 3.4).

We first review the single-impurity setup studied in Ref. [CBD$^+$12], under the assumption of finite temperature, without attached leads. Going beyond that analysis, we subsequently consider a system composed of an interacting helical LL attached to non-interacting contacts (and applied bias). As we see below, such a specification allows for an additional single-particle contribution, that can be associated with broken Galilean invariance. This result was published in Ref. [GCT15].

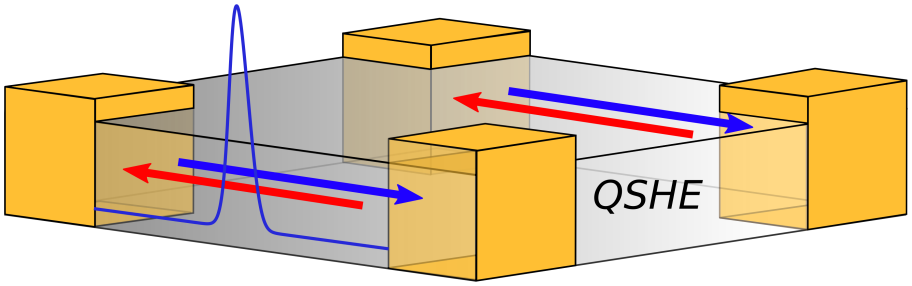

Figure 4.4.: Sketch of a 2D QSH system with one-dimensional, helical edge states. The Rashba SOC potential (blue curve) is here modeled in the form of a localized perturbation.

4.5.1. System without leads

Modeling the local potential by $\alpha(x) = \alpha(av_F)\delta(x)$, with the dimensionless coupling constant α, we find from Eq. (4.4),

$$H_{\mathrm{R}} = iF_+^\dagger F_- \frac{\alpha v_F}{\pi}\left(\frac{2\pi a}{L}\right)^K :\partial_x\theta(0)e^{2i\phi(0)}: + \text{h.c.}. \tag{4.90}$$

A scaling analysis reveals, that α is always an irrelevant perturbation: As the spatial derivative increases the scaling dimension by one, we find $\Delta_\alpha = K + 1$. Effectively, there is only one temporal dimension in the problem, such that

$$\frac{d}{d\ell}\alpha(\ell) = -K\alpha(\ell). \tag{4.91}$$

The transport signature of the above perturbation depends on the induced backscattering mechanism. Using an OPE very similar to the one given in App. C, one finds that the single Rashba impurity contributes in fourth order to a (local) TPB process, as defined in Eq. (3.39). Explicitly, using $\tilde{\gamma}_{2p}(x) = \tilde{\gamma}_{2p}a\delta(x)$, with a dimensionless coupling constant $\tilde{\gamma}_{2p}$, the local version of the TPB operator is proportional to $H_{2p} \propto \tilde{\gamma}_{2p}e^{4i\phi(0)}/a$. As explained in more detail in Sec. 4.8, one accounts for the so-called missing piece in the course of the RG by defining the (truly) inelastic contribution $\tilde{\gamma}_{2p}(\ell) = \tilde{\gamma}_{2p}^{\mathrm{in}}(\ell) - \alpha^2(\ell)(1-2K)/2K$. This leads to a renormalization of the form [CBD+12]

$$\frac{d}{d\ell}\tilde{\gamma}_{2p}^{\mathrm{in}}(\ell) = (1-4K)\tilde{\gamma}_{2p}^{\mathrm{in}}(\ell) + \left(1-\frac{1}{K}\right)(1-2K)\alpha^2(\ell). \tag{4.92}$$

At zero electron interactions, $K = 1$, there is no Rashba-induced backscattering, as it should be. The above renormalization can as well be derived in fermionic language [CBD+12], where importantly, a momentum cutoff needs to be introduced in order to recover the non-interacting limit of Eq. (4.92).
Integrating Eqs. (4.91) and (4.92) yields the solution

$$\tilde{\gamma}_{2p}^{\mathrm{in}}(\ell) = \tilde{\gamma}_{2p}^{\mathrm{in}}(0)e^{(1-4K)\ell} + \alpha(0)^2\left(1-\frac{1}{K}\right)\left(e^{(1-4K)\ell} - e^{-2K\ell}\right). \tag{4.93}$$

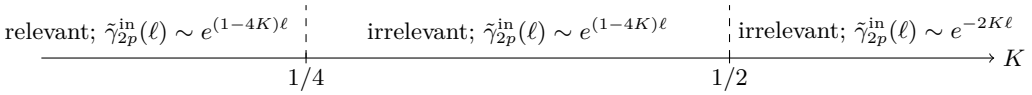

Figure 4.5.: Relevance and dominant scalings of the local TPB coupling $\tilde{\gamma}^{\rm in}_{2p}(\ell)$ in the presence of a single Rashba impurity (compare with Eq. (4.93)).

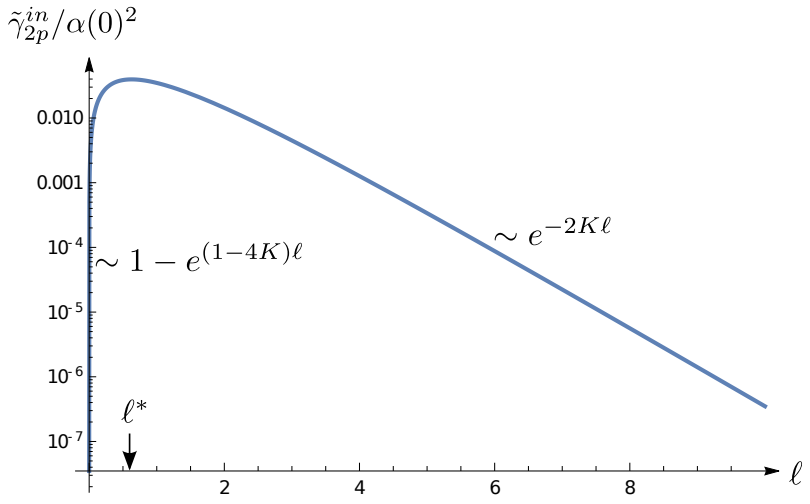

Figure 4.6.: Log-Plot of the function $\tilde{\gamma}^{\rm in}_{2p}(\ell)$, cf. Eq. (4.93), using parameters $\tilde{\gamma}^{\rm in}_{2p}(0) = 0$ and moderately weak interactions, $K = 0.7$. We observe a crossover of scales at the threshold ℓ^*, transitioning from a scaling of $\tilde{\gamma}^{\rm in}_{2p}(\ell) \sim e^{(1-4K)\ell}$ to $\tilde{\gamma}^{\rm in}_{2p}(\ell) \sim e^{-2K\ell}$. The limit of $\ell \to \infty$ corresponds to low energies.

Importantly, the TPB operator becomes relevant for strong interactions $K < 1/4$. The interesting limit of low energies is studied by sending the RG running scale, ℓ, to infinity. Depending on the interaction strength K, two different scalings of the TPB coupling strength can dominate in this limit, and we identify a crossover of scalings from $\tilde{\gamma}^{\rm in}_{2p}(\ell) \sim e^{(1-4K)\ell}$ for $K < 1/2$, to $\tilde{\gamma}^{\rm in}_{2p}(\ell) \sim e^{-2K\ell}$ for $K > 1/2$, which will translate into corresponding corrections to the conductance. The Fig. 4.5 illustrates the scalings of the TPB coupling parameter at low energies. For increasing temperatures (so decreasing ℓ), we observe yet another crossover between the two respective scalings (see Fig. 4.6). This occurs at the critical value $\ell^* = 1/(2K-1)\log[(4K-1)/2K]$, which we can associate with the temperature $T^* = (v/a_0)e^{-\ell^*}$.

The correction to the conductance can be calculated at finite temperature with a generating functional approach [BF04]. Essentially, we use Eqs. (3.2) and (3.3), as well as the correlation functions given in Sec. 2.3, to obtain the contribution of lowest order in the perturbation $\tilde{\gamma}^{\rm in}_{2p}$. More details of the explicit calculation can be found in the Sec. 4.7.1 below. Here, we anticipate this discussion to state that the correction to the conductance

is proportional to

$$\delta G \propto e^2 \frac{\beta^2}{a^2} \left(\frac{\pi a}{v\beta}\right)^{8K} \left(\tilde{\gamma}_{2p}^{\mathrm{in}}(\ell)\right)^2 . \tag{4.94}$$

Importantly, we can make use of the results of the RG analysis, assuming that $\tilde{\gamma}_{2p}^{\mathrm{in}}(\ell)$ and $a(\ell)$ are running parameters, and thus change upon rescaling. Note that compared to Eq. (4.167) of the next section, the TPB operator employed here is roughly speaking only half of the (double) TPB operator used in Eq. (4.142), which is why the conductance is of second order in the perturbation $(\tilde{\gamma}_{2p}^{\mathrm{in}}(\ell))^2$, while we have a first-order contribution proportional to $\gamma_{2p}^{\mathrm{loc}}(\ell)$ in Eq. (4.167).
Scaling the cutoff up to the order of the temperature, $\ell \to \log(v/(Ta_0))$, we find that the correction the conductance is simply given by the square of the renormalized TPB parameter. Therefore, in the regime of irrelevant TPB, the Rashba impurity affects transport in the following way,

$$\delta G \sim \begin{cases} (Ta_0/v)^{4K} & \text{if } 1/2 < K < 1, \\ (Ta_0/v)^{8K-2} & \text{if } 1/4 < K < 1/2. \end{cases} \tag{4.95}$$

In the limit of weak electron interactions, we find a power-law correction in fourth order of the temperature. This is different from the expected correction (of sixth power) due to a generic TPB perturbation (see Sec. 3.3), because here we consider TPB generated by a Rashba impurity. The specific dynamics of the SOC perturbation have altered the resulting scaling. In a transport experiment, this approach could be used to identify distinct microscopic sources of backscattering, that induce the same (generic) backscattering mechanism.

4.5.2. Attached leads and shifted operators

In the following, we extend our model such as to include physical contacts, which are assumed to be of non-interacting character (see discussion in Sec. 3.1.2). The energy scale of interest is now the bias voltage, while temperature is set to zero for simplicity. To understand better the physical implications, we compare the calculation to the analogous scenario of a localized magnetic impurity (that breaks TRS). Its general form is given in Eq. (3.37), where we use $g_m(x) = m v_F \delta(x)$, with the dimensionless parameter m, to obtain

$$H_{\mathrm{m}} = F_+^\dagger F_- \frac{m v_F}{2\pi a} \left(\frac{2\pi a}{L}\right)^K :e^{2i\phi(0)}: + \mathrm{h.c.}, \tag{4.96}$$

$$\frac{d}{d\ell} m(\ell) = (1-K) m(\ell). \tag{4.97}$$

In the last line, we repeated the tree-level RG equation already given in Eq. (3.40), using that the scaling dimension of the perturbation operator is $\Delta_m = K$. Clearly, the scaling behaviour of the two coupling constants α and m, as given in Eq. (4.91) and Eq. (4.97), is quite different: With repulsive interactions, $0 < K \leq 1$, the single Rashba impurity is always irrelevant in a low-energy theory. On the opposite, the magnetic impurity always

grows upon renormalization, except for the non-interacting case, where it is marginal. The backscattered current operator, resulting from the presence of such perturbations, can be represented as [LOB12, GCT15]

$$j_{\mathrm{bs}}^{\mathrm{R/m}}(t) = -\frac{i}{2v_F}\int \mathrm{d}x\ \left[H_{\mathrm{R/m}}(t), j_0\right]. \tag{4.98}$$

The assumption of non-interacting leads, where $j_0 = \frac{ev_F}{L}(N_+ - N_-)$, was previously discussed in Sec. 3.1.2. As we are interested in the transport properties of this setup, we calculate the correction to the conductance, which is directly related to the above current. This approach becomes more clear, if we first define the current transmitted through the system as the difference of the free, and the backscattered current, $j_{\mathrm{tr}} = j_0 - j_{\mathrm{bs}}$. The correction to the conductance (see Eq. (3.26)), is then determined by

$$\delta G = \frac{d\langle \delta j_{\mathrm{tr}}\rangle}{dV} = -\frac{d\langle j_{\mathrm{bs}}\rangle}{dV}, \tag{4.99}$$

where we used the notation $\delta j_{\mathrm{tr}} = j_{\mathrm{tr}} - \langle j_{\mathrm{tr}}\rangle_0 = -j_{\mathrm{bs}}$.
To discriminate between single- and two-particle backscattering, another useful quantity besides the current is the shot noise at zero frequency. It is given by the symmetrized current-current correlation function [Mar05],

$$S(\omega \to 0) = \sum_\eta \int \mathrm{d}t_2\ \langle \mathcal{T}_K \delta {j_{\mathrm{tr}}}^{\eta}(t)\delta {j_{\mathrm{tr}}}^{-\eta}(t_2)\rangle = \sum_\eta \int \mathrm{d}t_2\ \langle \mathcal{T}_K {j_{\mathrm{bs}}}^{\eta}(t){j_{\mathrm{bs}}}^{-\eta}(t_2)\rangle. \tag{4.100}$$

In the weak backscattering limit, it can be related to the effective backscattered charge e^*, or to the Fano factor e^*/e, by the Schottky formula [Sch18, BB00]

$$e^* = \frac{S}{2|\langle j_{\mathrm{bs}}\rangle|}. \tag{4.101}$$

Next, we implement a nonzero bias voltage, applied to the non-interacting leads, as explained in Sec. 3.2.2. In this formalism, the bias acts on the Klein factors and on the zero modes of an operator, where the latter have so far been included in the fields ϕ, θ. For the Rashba Hamiltonian in Eq. (4.90), for instance, the corresponding bias-induced shift (see Eq. (3.23)) can be rephrased as a shift of the fields $\phi(x) \to \phi(x) + \frac{eV}{2}t$ and $\partial_x\theta(x) \to \partial_x\theta(x) + \frac{eV}{2v_F}$. With that, we arrive at

$$\begin{aligned}
\left(\tilde{H}_R\right)_V(t) &= i\frac{\alpha v_F}{\pi}\left(\frac{2\pi a}{L}\right)^K \left[:\left(\partial_x\theta(0,t) + \frac{eV}{2v_F}\right)e^{2i(\phi(0,t)+\frac{eV}{2}t)}: + \mathrm{h.c.}\right] \\
&= \frac{\alpha v_F}{2\pi}\left(\frac{2\pi a}{L}\right)^K \left[\frac{1}{vK}:\left(\partial_t e^{2i\phi(0,t)}\right):e^{ieVt} + \frac{1}{v_F}:e^{2i\phi(0,t)}:\left(\partial_t e^{ieVt}\right) + \mathrm{h.c.}\right], \\
\left(\tilde{H}_{\mathrm{m}}\right)_V &= F_+^\dagger F_- \frac{mv_F}{2\pi a}\left(\frac{2\pi a}{L}\right)^K :e^{2i\phi(0)}e^{ieVt}: + \mathrm{h.c.}.
\end{aligned} \tag{4.102}$$

Above, we made use of the identity $\partial_t\phi(x,t) = vK\partial_x\theta(x,t)$ (see Eq. (2.61)), to transform one field into a time derivative. The structure of the backscattering current operator is

similar to the perturbation itself, but note the opposite sign of the conjugate terms,

$$\begin{aligned}\left(\tilde{j}^{\mathrm{R}}_{\mathrm{bs}}\right)_V(t) &= -e\frac{\alpha v_F}{\pi}\left(\frac{2\pi a}{L}\right)^K\left[:\left(\partial_x\theta(0,t)+\frac{eV}{2v_F}\right)e^{2i(\phi(0,t)+\frac{eV}{2}t)}: - \text{h.c.}\right]\\ &= ie\frac{\alpha v_F}{2\pi}\left(\frac{2\pi a}{L}\right)^K\left[\frac{1}{vK}:\left(\partial_t e^{2i\phi(0,t)}\right):e^{ieVt}+\frac{1}{v_F}:e^{2i\phi(0,t)}:\left(\partial_t e^{ieVt}\right) - \text{h.c.}\right],\end{aligned} \tag{4.103}$$

and one finds an analogous expression for the magnetic perturbation.
A few comments about Eqs. (4.102) and (4.103) are in order. First, we observe that both $\left(\tilde{H}_R\right)_V$ and $\left(\tilde{j}^{\mathrm{R}}_{\mathrm{bs}}\right)_V$ will be of the form of a total time derivative in the case of vanishing interactions ($v \to v_F$ and $K \to 1$), Galilean invariance ($vK = v_F$), or a model with interacting leads. As we see in more detail below, any of these conditions leads to a zero average backscattering current, in lowest order. Generally, the neutrality rule ensures that there is no such average current in any odd order of the impurity strength. Second, we emphasize, that the Klein factors are essential to obtain the correct voltage bias shift. Only after the bias is implemented, in Eqs. (4.102) and (4.103), the limit $L \to \infty$ can be taken safely, and as a consequence, the zero modes disappear. Then, the Klein factors commute with all remaining field operators, and can be dropped, since they will eventually compensate in the averaged expression.

4.5.3. Backscattering current in second order

Using the Keldysh framework, we calculate the expectation value of the backscattering current perturbatively in the impurity strength (weak-coupling limit). In lowest (second) order, we find from Eq. (3.12) the expression (for details see Ref. [GCT15] and App. C thereof),

$$\begin{aligned}\langle j^{\mathrm{R}}_{\mathrm{bs}}\rangle &= \frac{1}{2}\sum_{\eta=\pm}\left\langle T_K\left[\left(\tilde{j}^{\mathrm{R}}_{\mathrm{bs}}\right)^{\eta}_V(t)(-i)\int_K \mathrm{d}t_2\,\left(\tilde{H}_R\right)^{\eta'}_V(t_2)\right]\right\rangle_0\\ &= 2i\frac{ev_F^2\alpha^2}{(2\pi)^2}\left(\frac{2\pi a}{L}\right)^{2K}\frac{(Kv-v_F)^2}{(Kvv_F)^2}(eV)^2\int \mathrm{d}\tau\; h(\tau)\sin(eV\tau)\\ &= \frac{e\alpha^2v_F^2}{2\pi\Gamma(2K)}\left(\frac{a}{v}\right)^{2K}\frac{(Kv-v_F)^2}{(Kvv_F)^2}(eV)^{2K+1}.\end{aligned} \tag{4.104}$$

Here, we denoted $\tau = t - t_2$, and further wrote (cf. Eq. (2.53))

$$h(\tau) = \langle :e^{2i\phi(\tau)}::e^{-2i\phi(0)}:\rangle_0 = \left(\frac{2\pi}{L}(iv\tau + a)\right)^{-2K}, \tag{4.105}$$

using that $\langle :e^{2i\phi(t)}e^{-2i\phi(t_2)}:\rangle_0 = 1$. Note that the assumption of zero temperature allows us to restrict ourselves to ground state expectation values of vertex operators only. The correction to the conductance can again be given by the dI/dV-characteristics,

$$\delta G = -(2K+1)\frac{e^2\alpha^2v_F^2}{2\pi\Gamma(2K)}\left(\frac{a}{v}\right)^{2K}\frac{(vK-v_F)^2}{(vKv_F)^2}(eV)^{2K}. \tag{4.106}$$

In the non-interacting limit, there is no correction due to elastic backscattering, as it should be. More interestingly, also in the case of Galilean invariance, when $vK = v_F$ (see Sec. 3.2.4), the above contribution to the current is absent. The calculated shot noise takes a form directly proportional to the average current, resulting in $e^* = e$. This indicates, that the physical mechanism captured above is indeed a single-particle process. Notably, this setup (featuring non-interacting leads) generates a SPB backscattering correction of a lower power – $\delta G \sim V^2$ for weak interactions – than all the inelastic SPB processes (without leads) analyzed before [SRvG12, LOB12, KGCM14], which predict a correction of fourth or fifth power in the bias voltage. The mechanism described here, is therefore expected to be of high relevance in a realistic scenario.
The current in Eq. (4.104) can as well be verified in a fermionic, perturbative approach (see model description in Sec. 4.4). Assuming weak interactions, the lowest-order diagrams that contribute to SPB arise from the cross terms $T = H_{\mathrm{R}} G_0 H_{\mathrm{int}} + H_{\mathrm{int}} G_0 H_{\mathrm{R}}$. In Ref. [GCT15], the average backscattering current is evaluated numerically, using finite system size. The findings are fully consistent with the above result: If processes featuring any possible exchange of momenta, within the range of the bias voltage, are taken into account, the average current is zero due to a systematic cancellation of terms. On the other hand, if all the elastic processes ($q = 0$ in Ref. [GCT15]) are excluded by hand, we obtain a finite backscattering current, $\langle j_{\mathrm{bs}}^{\mathrm{R}} \rangle \sim e\alpha^2 g_2^2 (eV)^3$. Such processes are proportional to the zero modes of the system. Given that those zero modes are non-interacting, they should not contribute to the current. Excluding the corresponding terms is therefore equivalent to the implementation of non-interacting leads. The scaling of the current matches the one of Eq. (4.104) in the limit of weak interactions, $K \to 1$. We further realize that $Kv - v_F = g_2/2\pi$ for contact interactions.

In comparison, for the magnetic impurity, we obtain in an identical fashion

$$\langle j_{\mathrm{bs}}^{\mathrm{m}} \rangle = \frac{e m^2 v_F^2}{2\pi a^2 \Gamma(2K)} \left(\frac{a}{v}\right)^{2K} (eV)^{2K-1}, \tag{4.107}$$

$$\delta G = -(2K-1) \frac{e^2 m^2 v_F^2}{2\pi a^2 \Gamma(2K)} \left(\frac{a}{v}\right)^{2K} (eV)^{2K-2}, \tag{4.108}$$

and the same effective charge $e^* = e$. Note that we assumed weak backscattering off the magnetic impurity, which, according to Eq. (4.97), applies only to high energies (or $K > 1$), as m is relevant in the RG sense for $K < 1$. Therefore, the result in Eq. (4.108) only holds for large values of eV (or attractive interactions). For small eV and repulsive interactions, when m is large, the system is in the strong-coupling regime. As explained in Sec. 3.1.1, the current effectively corresponds to the one in the weak-coupling limit after the replacement $K \to 1/K$. We then obtain $\delta G \sim m^2 (eV)^{2/K-2}$, which recovers the main result of the seminal articles by Kane and Fisher [KF92a, KF92b]. For the Rashba impurity, as α is always irrelevant, we never reach the strong-coupling regime.

4.5.4. Backscattering current in fourth order

In order to study TPB, we have to examine the backscattering current to fourth order in the impurity strength. After contour time-ordering, the resulting expression exhibits

multi-dimensional, coupled integrals, that in general defy an analytical evaluation. The expectation value has to be understood as a mixture of diverse processes involving two particles, coupled by interactions. The variety of arising terms does not allow to give an exact result in this order, however, we can account for the physically most interesting limits of (strongly coupled) two-particle backscattering, and single-particle backscattering of two (weakly coupled) particles. Further details of the calculation are given in the App. E of Ref. [GCT15].
Terms of fourth order in α arise in a third-order expansion of Eq. (3.12) in the impurity Hamiltonian,

$$\begin{aligned}
&\langle j_{\mathrm{bs}}^{\mathrm{R}}(t_2)\rangle \\
&= \frac{1}{2}\sum_{\eta_2=\pm}\left\langle \mathcal{T}_K\left[\left(\tilde{j}_{\mathrm{bs}}^{\mathrm{R}}\right)_V^{\eta_2}(t_2)\frac{i}{6}\int_K \mathrm{d}t_3\ \mathrm{d}t_4\ \mathrm{d}t_5\ \left(\tilde{H}_R\right)_V^{\eta_3}(t_3)\left(\tilde{H}_R\right)_V^{\eta_4}(t_4)\left(\tilde{H}_R\right)_V^{\eta_5}(t_5)\right]\right\rangle_0 \\
&= -\frac{e v_F^4 \alpha^4}{4(2\pi)^4}\left(\frac{2\pi a}{L}\right)^{4K}\sum_{\eta_2,\eta_3,\eta_4,\eta_5=\pm}\int_{-\infty}^{\infty}\mathrm{d}t_3\ \mathrm{d}t_4\ \mathrm{d}t_5\ C_0^{\eta_2,\eta_3,\eta_4,\eta_5}(t_2,t_3,t_4,t_5) \\
&\quad\times\left(C_1^{+}(t_2,t_3,t_4,t_5)-C_1^{-}(t_2,t_3,t_4,t_5)\right).
\end{aligned} \tag{4.109}$$

The Keldysh contour ordering is performed according to Eq. (3.13). Here, we have factorized the correlation function into two parts, C_0 and $C_1^{\pm}$. In this shorthand notation, C_0 captures the explicit time-ordering of the operators, and can be simplified with Wick's theorem,

$$\begin{aligned}
C_0^{\eta_2,\eta_3,\eta_4,\eta_5}(t_2,t_3,t_4,t_5) &= \eta_3\eta_4\eta_5\left\langle T_K{:}e^{i2\phi^{\eta_2}(t_2)}{::}e^{i2\phi^{\eta_3}(t_3)}{::}e^{-i2\phi^{\eta_4}(t_4)}{::}e^{-i2\phi^{\eta_5}(t_5)}{:}\right\rangle_0 \\
&= \eta_3\eta_4\eta_5\prod_{\substack{i<j\\(i,j)\in\{2,3,4,5\}}}\left\langle T_K{:}e^{2i\phi^{\eta_i}(t_i)}{::}e^{-2i\phi^{\eta_j}(t_j)}{:}\right\rangle_0 .
\end{aligned} \tag{4.110}$$

The second function $C_1^{\pm}$ is a voltage-dependent scalar,

$$\begin{aligned}
C_1^{\pm}(t_2,t_3,t_4,t_5) &= \nu^{-1}(\partial_{t_2})\nu^{-1}(\partial_{t_3})\nu^{-1}(\partial_{t_4})\nu^{-1}(\partial_{t_5}) \\
&\times\left(\frac{\left(\partial_{t_2}\partial_{t_3}\partial_{t_4}\partial_{t_5}\right)\left[\left(h(2,3)h(2,4)h(2,5)h(3,4)h(3,5)h(4,5)\right)e^{\pm ieV(t_2+t_3-t_4-t_5)}\right]}{\left(h(2,3)h(2,4)h(2,5)h(3,4)h(3,5)h(4,5)\right)}\right)\Bigg|_{\mathrm{ord}}.
\end{aligned} \tag{4.111}$$

For brevity, we used $h(i,j)=h(t_i,t_j)=h(t_i-t_j)$, as given in Eq. (4.105), and $i,j\in\{2,3,4,5\}$. In order to keep the notation compact, we further introduced the scalar $\nu^{-1}(\partial_t)$, postulating that $\nu^{-1}(\partial_t)\partial_t{:}e^{2i\phi(0,t)}{:}=(vK)^{-1}\partial_t{:}e^{2i\phi(0,t)}{:}$, if the derivative acts on the bosonic part, and $\nu^{-1}(\partial_t)\partial_t e^{ieVt}=(v_F)^{-1}\partial_t e^{ieVt}$, if on the other hand the temporal derivative acts on the voltage part. As before, we argue that those contributions where the temporal derivatives act on the vertex operators, vanish when taking the ground state average at zero temperature. The index $(\ldots)|_{\mathrm{ord}}$ indicates, that $C_1^{\pm}$ is still implicitly affected by time-ordering in the following sense: If the four time variables are ordered as $t_2>t_3>t_4>t_5$ on the contour, this label can be dropped in Eq. (4.111), while otherwise,

the dependence of the functions h needs to be adapted accordingly.

We next study the limit of strongly correlated two-particle backscattering, which is a subset of all terms included in Eq. (4.109). In this limit, we assume that the two particles involved in the correlated backscattering process couple strongly together, and are thus scattered to the branch of opposite chirality at almost the same time. In our model, such contributions are dominated by the terms decaying the fastest in the differences $y = t_2 - t_3$ and $y' = t_4 - t_5$ (see for instance Eq. (4.110)). Those are the ones where the derivatives in Eq. (4.111) only act on the functions $h(2,3)$ and $h(4,5)$. Integrating out short time differences up to the order of the next higher energy scale, $1/eV$, we encounter the integrals [GCT15]

$$\int_0^{1/eV} \mathrm{d}y\, (\pm ivy + a)^{2K-2} \simeq \mp \frac{ia^{2K-1}}{(1-2K)v} + \frac{e^{\pm i\pi K}(v/eV)^{2K-1}}{(1-2K)v}, \tag{4.112}$$

and the same for y'. Given that $a \ll v/eV$, the first term is more relevant for $K < 1/2$, while the second one dominates if $K > 1/2$, leading again to a crossover of scalings. The remaining third time integral, on the other hand, contributes with a scaling of $(eV/v)^{8K-1}$. With this, we find the resulting backscattering current

$$\langle j_{\mathrm{bs}}^{\mathrm{R}} \rangle \simeq \frac{2^{8K-1}}{K^2\Gamma(8K)} \frac{e\alpha^4}{\pi^3} \left(\frac{v_F}{v}\right)^4 \times \begin{cases} (a/v)^{8K-2}\,(eV)^{8K-1} & \text{if } K < 1/2, \\ (a/v)^{4K}\,(eV)^{4K+1}(1-\cot^2(K\pi))^{-1} & \text{if } K > 1/2. \end{cases} \tag{4.113}$$

The interaction-dependent factor of $(1-\cot^2(K\pi))^{-1}$ in the last line of Eq. (4.113) is a relict of the approximations performed in the process of time contractions. It can be interpreted though as to suppress the backscattering current in the elastic, non-interacting limit.
The characteristic scaling of the correction to the conductance, in this TPB limit, takes the form (we here fix the cutoff to $a \to a_0$)

$$\delta G \sim \alpha^4 \times \begin{cases} (eVa_0/v)^{8K-2} & \text{if } K < 1/2, \\ (eVa_0/v)^{4K} & \text{if } K > 1/2. \end{cases} \tag{4.114}$$

It is therefore consistent with the finding of Ref. [CBD+12], presented in the previous section. Strictly speaking, we have to restrict our analysis to interaction strengths $K < 1/4$, since even stronger interactions allow for relevant TPB terms. Then, α is not necessarily a small parameter anymore, and the present perturbation theory becomes invalid.
Moreover, the shot noise takes the form

$$S(\omega \to 0) = 4e\langle j_{\mathrm{bs}}^{\mathrm{R}} \rangle, \tag{4.115}$$

and hence we find an effective charge of $e^* = 2e$. In addition to the expected scaling with the bias, this verifies, that the contractions in time performed above have sorted out pure TPB processes. In contrast to the SPB contribution, derived in Eq. (4.106), the TPB current survives in the limit of $vK \to v_F$, and no particular consequences arise from the fact that we implemented non-interacting leads. For systems featuring an underlying

Galilean invariance, a transport experiment should therefore observe a correction to the conductance only due to TPB (see Eq. (4.114)), and a Fano factor of two. In the absence of this symmetry, the leading-order correction is provided by SPB if $K > 1/3$, and the Fano factor takes a value of one (for very strong interactions $K < 1/3$, TPB dominates again over SPB). Thus, apart from the distinct power scaling, we identify the Fano factor as a direct evidence for the presence of Galilean invariance in the regime of weak and moderate interactions.
Note that in the case of a magnetic impurity, time contractions associated with the strongly coupled TPB limit, such as performed above, are not justified, since the respective correlation functions do not decay at all for large temporal distances. In other words, due to the lack of derivatives in the Hamiltonian, this type of perturbation can not contribute to TPB in second order.

The opposite physical limit is represented by two weakly coupled SPB events. To study the respective terms, we contract time variables in pairs of two, that come with opposite signs in the exponent of the vertex operators. This procedure requires to account for several cases. Defining for instance relative and center of mass coordinates $y = t_2 - t_4$, $y' = t_3 - t_5$, $Y = (t_2 + t_4)/2$ and $Y' = (t_3 + t_5)/2$, the subsequent approximation $y, y' \ll Y, Y'$ models the situation of two separated, decoupled SPB events. We find [GCT15]

$$\langle j_{\mathrm{bs}}^{\mathrm{R}} \rangle \simeq \frac{(vK - v_F)^4}{(vK)^4} \frac{\alpha^4 e}{16\pi^2 \Gamma(2K)^2} \left(\frac{a}{v}\right)^{4K+1} (eV)^{4K+2}, \tag{4.116}$$

$$\langle j_{\mathrm{bs}}^{\mathrm{m}} \rangle \simeq \frac{m^4 e}{16\pi^2 \Gamma(2K)^2} \left(\frac{a}{v}\right)^{4K-3} \left(\frac{v_F}{v}\right)^4 (eV)^{4K-2}. \tag{4.117}$$

The scaling of these contributions is exactly the square of the SPB currents in Eqs. (4.104) and (4.107), indicating that we have selected terms that represent two individual single-particle events. Clearly, this mechanism always has a higher scaling than the single SPB. By comparison of Eqs. (4.116) and (4.113), we furthermore note that also the scaling of the TPB contribution is lower for any interaction strength. Therefore, the above double SPB process is expected to be of little relevance at low energies. An analysis of the shot noise reveals in both cases $e^* = 2e$, corresponding to the double backscattering of a single charge. Therefore, on the level of the shot noise, we are not able to tell apart the two physically distinct cases of correlated TPB, and uncorrelated double SPB processes.
Another way of sorting out SPB processes in the above integrals was to contract three times altogether, which, by a scaling analysis, yields a contribution proportional to $\alpha^4 V^{2K+1}$. Such terms represent corrections to the single SPB processes, in fourth order of the impurity strength.

4.6. Random disorder – RG

Following Ref. [GCT14], we next study a setup of randomly disordered Rashba SOC (see Fig. 4.7). Such a scenario is motivated by the edge states of 2D topological insulator in the presence of a fluctuating electric field along the edge, as it might occur naturally for

instance due to free charge accumulations at the interfaces etc. In order to handle the randomness of the potential functions, additional techniques such as the "replica trick" need to be employed.

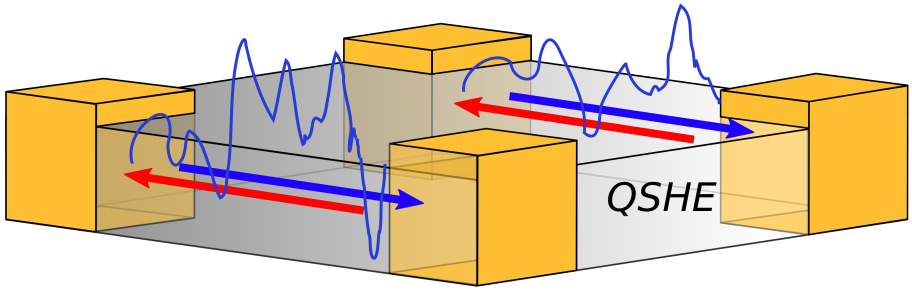

Figure 4.7.: Sketch of a 2D QSH system with one-dimensional, helical edge states. The Rashba SOC potential (blue curve) is assumed to be randomly fluctuating along the edge to model disorder. Reprinted figure with permission from Ref. [GCT14]. Copyright 2014 by the American Physical Society.

4.6.1. Replica trick

Let us assume that Rashba SOC is the only perturbation to the Luttinger liquid system, so $H = H_0 + H_\mathrm{R}$. As given in Eq. (2.89), the partition function then takes the form

$$Z = \mathrm{Tr}\left[\mathcal{T} e^{-\int_0^\beta \mathrm{d}\tau\ H(\tau)}\right] = \mathrm{Tr}\left[e^{-\beta H_0} U(\beta, 0)\right], \tag{4.118}$$

where $U(\beta,0) = \mathcal{T}\exp\left(-\int_0^\beta \mathrm{d}\tau\ H_\mathrm{R}(\tau)\right)$ is the imaginary time evolution operator.
We now consider the Rashba profile $\alpha(x)$ to be a random function along the sample edge. First, we explore the physical constraints on the form of the potential. If both $\alpha(x)$ and the fields $\phi(x)$, $\theta(x)$ typically vary only on length scales much larger than the Fermi wavelength, the integrand of Eq. (4.4) will average out upon integration, and we will miss the interesting physics. In a helical Luttinger liquid, $\phi(x)$ and $\theta(x)$ are not necessarily slowly varying functions compared to the oscillating factors $e^{\pm i2k_F x}$, since the chemical potential may very well be close to the Dirac point, $k_F = 0$. Directly at half filling, we may think of a conceptionally interesting, though rather specific case of disorder-induced two-particle backscattering of order α^2. Away from half filling, one can compensate the factors of $e^{\pm i2k_F x}$ with the Rashba potential $\alpha(x)$, assuming that the combinations appearing in Eq. (4.4),

$$\eta(x) = \alpha(x) e^{-i2k_F x}, \tag{4.119}$$

and $\eta^*(x) = \alpha(x) e^{i2k_F x}$, are slowly varying. This is the situation we will address in the following. Instead of α, we thus shall use the complex random functions η and η^*.

Dealing with disorder is a notoriously difficult task, and only a handful of analytical methods are available. The one we chose here is based on the replica trick, and has

proven to be efficient for the study of 1D interacting electron gases in disordered potentials [Gia03, AS10]. The (thermal) average of an arbitrary observable $O = O(x, \tau)$ is given by

$$\langle O \rangle = \frac{1}{Z} \mathrm{Tr} \left[e^{-\beta H_0} U(\beta, 0) O \right]. \tag{4.120}$$

Here, we have to take the average value with respect to a Hamiltonian, that depends on a random variable. In the end we are interested in the average over both the thermal, and the random disorder configurations. The latter average we denote by $\overline{O}$, and phrase it in the form of the functional integral

$$\overline{\langle O \rangle} = \frac{1}{P} \int \mathcal{D}\eta \mathcal{D}\eta^* \; p(\eta, \eta^*) \langle O \rangle, \tag{4.121}$$

where the probability distribution of the random potential is given by $p(\eta, \eta^*)$, while $P = \int \mathcal{D}\eta \mathcal{D}\eta^* \; p(\eta, \eta^*)$ is a normalization constant. The functional $\mathcal{D}\eta$ indicates that we sum over all possible configurations of the functions $\eta(x)$. In this model, we consider a Gaussian probability distribution of the form $p(\eta, \eta^*) = e^{-D_\eta^{-1} \int \mathrm{d}x \; \eta^*(x)\eta(x)}$, where now a parameter D_η, that we associate with the disorder strength, enters as the weight of the Gaussian statistics. We assume the random potentials to be short-ranged,

$$\overline{\eta^*(x_1)\eta(x_2)} = D_\eta \delta(x_1 - x_2), \tag{4.122}$$

and with zero mean value, i.e. $\overline{\eta(x)} = \overline{\eta^*(x)} = 0$. With that assumption and Eq. (4.120), we express Eq. (4.121) once more explicitly (using Eq. (4.120)),

$$\overline{\langle O \rangle} = \frac{1}{P} \int \mathcal{D}\eta \mathcal{D}\eta^* e^{-D_\eta^{-1} \int \mathrm{d}x \; \eta^*(x)\eta(x)} \frac{1}{Z} \mathrm{Tr} \left[e^{-\beta H_0} \mathcal{T} e^{-\int_0^\beta \mathrm{d}\tau \; H_\mathrm{R}(\tau)} O \right]. \tag{4.123}$$

Since H_R depends linearly on the random variable η, we realize that if it was not for the denominator $1/Z$, we could perform a Gaussian integration [Gia03] to average out η. However, the partition function in the denominator makes the average in Eq. (4.123) intractable. The replica trick now builds on the observation that $Z^{-1} = Z^{N-1}$ in the limit $N \to 0$. We then express the denominator using $N - 1$ identical (replicated) copies of the system. In a similar way, we can introduce N copies of the average $\langle O \rangle$, that are trivially the same. Merging the two replicated expressions, we obtain from Eqs. (4.118) and (4.120),

$$\begin{aligned} \langle O \rangle &= \lim_{N \to 0} \frac{1}{N} \sum_{a=1}^{N} \langle O \rangle^{(a)} = \lim_{N \to 0} \frac{1}{N} \sum_{a=1}^{N} \mathrm{Tr} \left[Z^{N-1} e^{-\beta H_0} U(\beta, 0) O^{(a)} \right] \\ &= \lim_{N \to 0} \frac{1}{N} \sum_{a=1}^{N} \mathrm{Tr} \left[e^{-\beta H_{0,\mathrm{rep}}} U_\mathrm{rep}(\beta, 0) O^{(a)} \right], \end{aligned} \tag{4.124}$$

where $H_{0,\mathrm{rep}} = \sum_{a=1}^{N} H_0^{(a)}$ and $U_\mathrm{rep}(\beta, 0) = \mathcal{T} \exp \left[- \sum_{a=1}^{N} \int_0^\beta \mathrm{d}\tau \; H_\mathrm{R}^{(a)}(\tau) \right]$. The replica index labels copies of the same operator, and can as well be shifted to the operator argument, e.g. $O^{(a)}(\phi) = O(\phi_a)$. Since it is not necessarily clear that the limit $N \to 0$ is always well-defined, this method is only called the replica "trick". Using Eq. (4.124)

in Eq. (4.123), and subsequently interchanging replica sum and disorder average, we are eventually free to perform Gaussian integration,

$$\overline{\langle O\rangle} = \lim_{N\to 0}\frac{1}{N}\sum_{a=1}^{N}\mathrm{Tr}\left[e^{-\beta H_{0,\mathrm{rep}}}\overline{U}_{\mathrm{rep}}(\beta,0)O^{(a)}\right]. \tag{4.125}$$

Now, the random SOC is absorbed in the disorder-averaged, effective evolution operator

$$\overline{U}_{\mathrm{rep}}(\beta,0) = \mathcal{T}\exp\left[\int_0^\beta \mathrm{d}\tau_1\,\mathrm{d}\tau_2\; H_{\mathrm{dis}}(\tau_1,\tau_2)\right], \tag{4.126}$$

where

$$\begin{aligned} H_{\mathrm{dis}}(\tau_1,\tau_2) = \frac{D_\eta}{2}\frac{1}{\pi^2 a^2}\left(\frac{2\pi a}{L}\right)^{2K}\sum_{a,b=1}^{N}\int_0^L \mathrm{d}x\; &:\partial_x\theta_a(x,\tau_1)e^{i2\phi_a(x,\tau_1)}: \\ &\times :\partial_x\theta_b(x,\tau_2)e^{-i2\phi_b(x,\tau_2)}: + \text{h.c.}. \end{aligned} \tag{4.127}$$

Note that the Klein factors compensate in the effective disorder term. Importantly, due to the assumption of short-range correlations in Eq. (4.122), one spatial integral disappears, and the fields in H_{dis} are local in position, though in general, non-local in time. For future reference, we also define the replicated version of the partition function $Z_{\mathrm{rep}} = \mathrm{Tr}\left[e^{-\beta H_{0,\mathrm{rep}}}\overline{U}_{\mathrm{rep}}(\beta,0)\right]$. At small disorder strengths D_η, operator averages can be calculated perturbatively in this effective action.
It remains to be clarified what happens to the replica indices, once the limit $N\to 0$ is performed. As it turns out, this limit corresponds to canceling disconnected diagrams [Gia03, KGCM14], as we shall demonstrate in the following. Let us define for brevity $\overline{U}_{\mathrm{rep}}(\beta,0) = \mathcal{T}\exp(\sum_{a,b}S_{\mathrm{dis}}^{(a,b)})$ with the effective disorder-averaged action $\sum_{a,b}S_{\mathrm{dis}}^{(a,b)} = \int_0^\beta \mathrm{d}\tau_1\,\mathrm{d}\tau_2\; H_{\mathrm{dis}}(\tau_1,\tau_2)$, where we write the replica labels explicitly. As an example, we consider the time-ordered two-point correlation in the presence of disorder, up to first order in D_η. It reads with the help of Eq. (4.125),

$$\begin{aligned} \langle\mathcal{T}O(\tau_1)O(\tau_2)\rangle &= \lim_{N\to 0}\frac{1}{N}\sum_{a=1}^{N}\mathrm{Tr}\left[e^{-\beta H_{0,\mathrm{rep}}}\mathcal{T}e^{\sum_{b,c}S_{\mathrm{dis}}^{(b,c)}}O^{(a)}(\tau_1)O^{(a)}(\tau_2)\right] \\ &\simeq \lim_{N\to 0}\frac{1}{N}\left(\sum_{a=1}^{N}\langle\mathcal{T}O^{(a)}(\tau_1)O^{(a)}(\tau_2)\rangle_0 + \sum_{a,b,c=1}^{N}\langle\mathcal{T}S_{\mathrm{dis}}^{(b,c)}O^{(a)}(\tau_1)O^{(a)}(\tau_2)\rangle_0\right) \\ &= \langle\mathcal{T}O(\tau_1)O(\tau_2)\rangle_0 + \langle\mathcal{T}S_{\mathrm{dis}}O(\tau_1)O(\tau_2)\rangle_0 - \langle\mathcal{T}S_{\mathrm{dis}}\rangle_0\langle\mathcal{T}O(\tau_1)O(\tau_2)\rangle_0. \end{aligned} \tag{4.128}$$

Hereby, the replica sums in the term of first order in D_η were evaluated by

$$\begin{aligned}
&\sum_{a,b,c=1}^{N} \langle \mathcal{T} S_{\text{dis}}^{(b,c)} O^{(a)}(\tau_1) O^{(a)}(\tau_2)\rangle_0 \\
&= \lim_{N\to 0} \frac{1}{N} \sum_{\substack{a;\\ b=c=a}}^{N} \langle \mathcal{T} S_{\text{dis}}^{(a,a)} O^{(a)}(\tau_1) O^{(a)}(\tau_2)\rangle_0 + \lim_{N\to 0} \frac{1}{N} \sum_{\substack{a,b;\\ b=c\neq a}}^{N} \langle \mathcal{T} S_{\text{dis}}^{(b,b)} O^{(a)}(\tau_1) O^{(a)}(\tau_2)\rangle_0 \\
&= \langle \mathcal{T} S_{\text{dis}} O(\tau_1) O(\tau_2)\rangle_0 + \lim_{N\to 0} \frac{1}{N} \sum_{a}^{N} (N-1) \langle \mathcal{T} S_{\text{dis}}\rangle_0 \langle \mathcal{T} O^{(a)}(\tau_1) O^{(a)}(\tau_2)\rangle_0 \\
&= \langle \mathcal{T} S_{\text{dis}} O(\tau_1) O(\tau_2)\rangle_0 - \langle \mathcal{T} S_{\text{dis}}\rangle_0 \langle \mathcal{T} O(\tau_1) O(\tau_2)\rangle_0 .
\end{aligned} \tag{4.129}$$

The average in the absence of disorder here was denoted by $\langle(\ldots)\rangle_0 = \text{Tr}\left[e^{-\beta H_{0,\text{rep}}}(\ldots)\right]$. Once there is only one replica index per average left, it can be dropped, and the replica sum simply yields a factor of N. A few comments are in order about Eq. (4.129): As we might think of operators with different replica indices as of physically distinct objects, it is important to note, that only averages of operator products with the same replica index are nonzero. It follows, that in the second line of Eq. (4.129), the labels b and c have to be equal, and can be again equal or not to a. If $b \neq a$, the two averages factorize, and there are $N-1$ possible copies for b. The term proportional to N^2 will vanish in the limit of $N \to 0$, and we are left with a combination of terms that is usually associated with a connected diagram [Gia03].
When dealing with physical observables, we are interested in operator averages, and thus the replica labels will eventually be eliminated. In a RG approach, however, where we study only the scaling of operators, the replica indices remain. The perturbative expansion will then be performed for the replicated partition function Z_{rep}, which is the quantity of interest. Even though the limit of $N \to 0$ in general can not be performed in this case, the RG still succeeds in capturing the important physics.

4.6.2. RG in first order of D_η

A disorder average always needs to be taken into account before the RG analysis, a fact that renders the replica method especially useful. The reversed order of deriving flow equations before self-averaging over disorder, will lead to unphysical results, as a special configuration of disorder may break symmetries of the system. Simply speaking, this would correspond to studying only a small piece of the full system, and assuming, that its behaviour is representative for the full system [Gia03].
We next analyze the RG flow of the disorder parameter, defining the dimensionless coupling constant $\tilde{D}_\eta = D_\eta/(av^2)$. For clarity, let us repeat the disorder term of Eq. (4.127) in this notation,

$$\begin{aligned}
H_{\text{dis}}(\tau_1,\tau_2) = \tilde{D}_\eta \frac{v^2}{2\pi^2 a} \left(\frac{2\pi a}{L}\right)^{2K} \sum_{a,b=1}^{N} \int_0^L \mathrm{d}x \; &:\partial_x \theta_a(x,\tau_1) e^{i2\phi_a(x,\tau_1)}: \\
&\times :\partial_x \theta_b(x,\tau_2) e^{-i2\phi_b(x,\tau_2)}: + \text{h.c.}.
\end{aligned} \tag{4.130}$$

As discussed before, the Rashba operator $\partial_x\theta\exp(2i\phi)$ has the scaling dimension $K+1$, and therefore the disorder-averaged operator in Eq. (4.130) exhibits two times this scaling dimension, $\Delta_{\rm dis} = 2K+2$ (note that the physical scaling dimension is only $\Delta_{\rm dis}^{\rm naive} = 2$). From the RG analysis of Sec. 2.5, Eq. (2.96), we infer directly that the first-order RG for $\tilde{D}_\eta$ takes the form

$$\frac{d\tilde{D}_\eta}{d\ell}(\ell) = (1-2K(\ell))\,\tilde{D}_\eta(\ell). \tag{4.131}$$

Here, the effective dimension of the problem is $D=3$, because of two temporal and one spatial integration, so $D-\Delta_{\rm dis} = 3-(2K+2) = 1-2K$. Vice versa, disorder also renormalizes interactions, as the first-order expansion of the action contains the contribution (see App. C)

$$\mathcal{T}\exp\left[\int d\tau_1 d\tau_2 H_{\rm dis}(\tau_1,\tau_2)\right] \simeq \left(\frac{2\tilde{D}_\eta v}{\pi^2 K}\right)(1-K)(1-2K)d\ell\int {\rm d}x\ {\rm d}\tau\ :(\partial_x\theta(x,\tau))^2:. \tag{4.132}$$

This leads to the flow equations

$$\begin{aligned}\frac{dK}{d\ell}(\ell) &= -\frac{2\tilde{D}_\eta(\ell)}{\pi}\,(1-K(\ell))\,(1-2K(\ell))\,,\\ \frac{dv}{d\ell}(\ell) &= -\frac{2\tilde{D}_\eta(\ell)v(\ell)}{K(\ell)\pi}\,(1-K(\ell))\,(1-2K(\ell))\,.\end{aligned} \tag{4.133}$$

The renormalization is derived along the general lines of Sec. 2.5, and involves OPE and RG beyond tree-level. We give details of the calculation in App. C, following Ref. [GCT14].
The RG flow equations of Eqs. (4.131) and (4.133) are illustrated in Fig. 4.8a. In the absence of electron interactions, $K=1$, no effective interactions can be generated by Rashba disorder in the course of the RG, as it should be: In first order of $\tilde{D}_\eta$, disorder is formally not able to produce an interaction term of the type g_2 or g_4, because of the derivatives in the (fermionic) Rashba Hamiltonian.
From the above equations, we see that Rashba disorder is an irrelevant perturbation for $K>1/2$, and its effect on electronic transport is expected to be small in the low-energy limit. At $K=1/2$, we find a line of fixed points that separates the regimes of relevant and irrelevant disorder, such that interactions of this strength appear to represent a quite special case. For $K<1/2$, on the other hand, disorder is a relevant perturbation and the system flows towards strong coupling.

4.6.3. Question of localization in the strong-coupling regime

Let us briefly comment on the physics of this strong-coupling regime. In this case, our perturbative RG analysis, that considered $\tilde{D}_\eta$ a small parameter, is not valid anymore, since relevant disorder means that the disorder strength $\tilde{D}_\eta$ diverges in the low-energy limit. Above, we explained that Rashba SOC alone does not cause backscattering, so it is not clear yet whether $\tilde{D}_\eta$ can be associated with physical backscattering. In the next sections, however, we will find that $\tilde{D}_\eta$ contributes in second order to the operator

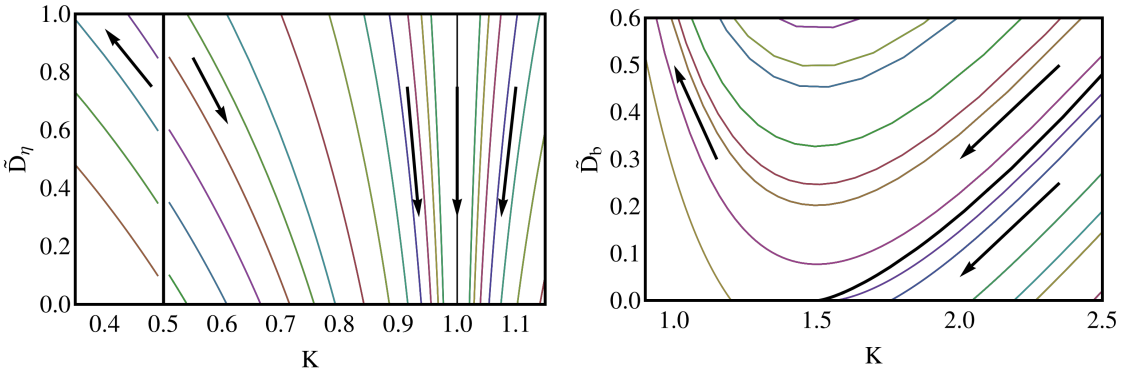

Figure 4.8.: (a) Phase diagram of the RG flow of Rashba disorder $\tilde{D}_\eta$, up to first order, versus interactions K, see Eqs. (4.131) and (4.133). For comparison we give in (b) the first-order RG flow of magnetic disorder $\tilde{D}_b$ in a helical liquid, according to Eq. (4.136). Note that we plot here $\tilde{D}_b$, not $\tilde{D}_b^{1/2}$, as it is sometimes seen in the literature (e.g. Ref. [Gia03]). Arrows indicate the variation of parameters upon increasing ℓ (going to lower energies). Thick lines represent separatrices of regimes of irrelevant and relevant perturbations. For Rashba disorder in (a), this separatrix is in addition a line of fixed points. The left hand side figure is adapted with permission from Ref. [GCT14]. Copyrighted by the American Physical Society.

of (physical) two-particle backscattering, and the strength of TPB will diverge as $\tilde{D}_\eta$ diverges. Therefore, via TPB, we can for now think of $\tilde{D}_\eta$ as of a parameter of physical backscattering. Usually, a diverging backscattering parameter, such as $\tilde{D}_\eta$ for $K < 1/2$, is an indication for a drastic change of the systems low-energy transport properties (see discussion in Sec. 3.3.3): With backscattering becoming very effective, electrons can not move freely anymore. Instead they localize, which leads to a breakdown of electronic transport and the opening of an energy gap in the system. The system is then expected to undergo a phase transition from a metallic to a (Mott) insulating state. This phase transition due to disorder effects is called Anderson localization in the non-interacting case [And58]. With electron interactions present, an analogous phase transition is usually denoted many-body localization. Suchlike localization was predicted for backscattering due to regular (scalar) disorder in a non-helical Luttinger liquid [GS88], even for arbitrary repulsive electron interactions, a finding that represents one of the landmarks of the field of interacting 1D systems. It can as well be adopted for magnetic disorder in a helical liquid.

The question arises naturally, whether a phase transition due to Rashba disorder occurs in the helical system. Indeed, the relevant disorder parameter in Eq. (4.131) for $K < 1/2$ suggests many-body localization in this regime. However, the situation is less clear than in the case of regular disorder, as we shall explicate in the following.

Let us revisit the effect of magnetic disorder in the helical LL (similar to Ref. [GS88]). As given in Eq. (3.37), a magnetic, time-reversal breaking impurity allows for a term

$$H_\mathrm{m} = \int \mathrm{d}x\, \xi(x)\psi_L^\dagger(x)\psi_R(x) + \xi^*(x)\psi_R^\dagger(x)\psi_L(x). \tag{4.134}$$

If ξ was a real function, the above operator could be rephrased as well as $\vec{\psi}^\dagger \xi(x)\sigma_x \vec{\psi}$. The same term emerges in a spinless 1D electron liquid from a simple perturbation $\psi^\dagger \xi(x)\psi$, in addition to a forward scattering part. [6] Therefore, the effect of magnetic disorder in a helical liquid can be derived in direct analogy to the latter case, see Refs. [GS88, Gia03]. Proceeding as before, we bosonize and perform Gaussian disorder average, assuming again short-range correlations $\overline{\xi(x)\xi^*(x')} = D_b\delta(x-x')$. With the replica trick, we find that magnetic disorder takes the form of the effective operator

$$H_{\mathrm{dis}}^{\mathrm{m}} = \tilde{D}_b \frac{v^2}{2^4\pi a^3}\left(\frac{2\pi a}{L}\right)^{2K} \sum_{a,b=1}^{N} \int \mathrm{d}x \, :e^{2i\phi_a(x,\tau_1)}::e^{-2i\phi_b(x,\tau_2)}: + \mathrm{h.c.}, \tag{4.135}$$

with the dimensionless parameter $\tilde{D}_b = 2D_b a/(\pi v^2)$. This leads to the RG equations in first order of $\tilde{D}_b$ [Gia03],

$$\begin{aligned} \frac{d\tilde{D}_b}{d\ell}(\ell) &= (3-2K(\ell))\,\tilde{D}_b(\ell), \\ \frac{dK}{d\ell}(\ell) &= -\frac{1}{2}K(\ell)^2\tilde{D}_b(\ell), \\ \frac{dv}{d\ell}(\ell) &= -\frac{1}{2}v(\ell)K(\ell)\tilde{D}_b(\ell). \end{aligned} \tag{4.136}$$

The RG flow in the K-$\tilde{D}_b$-plane is illustrated in Fig. 4.8b. We readily see, that the disorder strength $\tilde{D}_b$ is a relevant parameter for interactions $K < 3/2$, a point that corresponds to moderate, attractive interactions. Clearly, the non-interacting point, $K = 1$, lies within the regime of relevant disorder, and the emergence of Anderson localization in a 1D disordered system, in the absence of interactions, is well-established [GS88]. Therefore, the extended regime of relevant disorder (including the non-interacting point) can safely be associated with a localized phase. On the opposite, in the case of Rashba disorder, the non-interacting point is located in the regime of irrelevant disorder strength, and consequently, the appearance of many-body localization in the strongly interacting phase of $K < 1/2$ is not evident. Even though the relevance of the Rashba disorder operator is a clear hint at localization, the question of finding the strong-coupling fixed point, and whether it corresponds to many-body localization, remains open. This issue was discussed in Ref. [SJJ10], where the authors make a case for a localized phase in the strong-coupling regime, however, a conclusive proof is pending.

[6] The forward scattering term does not affect transport, and can be absorbed by a gauge transformation [Gia03].

4.6.4. Second order of D_η – definition of local and non-local TPB

In second order of $\tilde{D}_\eta$, we focus on the terms representing two-particle backscattering. As we show in App. C, the OPE yields a contribution

$$\mathcal{T}\exp\left[\int \mathrm{d}\tau_1\ \mathrm{d}\tau_2\ H_{\mathrm{dis}}(\tau_1,\tau_2)\right] \simeq \frac{1}{2a^4}\left(\frac{\tilde{D}_\eta}{\pi^2 K}\right)^2\left(\frac{2\pi a}{L}\right)^{8K}\sum_{a,b}\int \mathrm{d}x\ \mathrm{d}x'\ \mathrm{d}y_1\ \mathrm{d}y_2\ (1+2d\ell)$$
$$\times\, m\left(\frac{x-x'}{a}\right)\mathcal{T}{:}e^{2i\phi_a(x,y_1)}e^{2i\phi_a(x',y_1)}{::}e^{-2i\phi_b(x,y_2)}e^{-2i\phi_b(x',y_2)}{:}+\mathrm{h.c.}, \tag{4.137}$$

with a dimensionless factor

$$m\left(\frac{x-x'}{a}\right) = \left(\frac{(1-2K)-\left(\frac{x-x'}{a}\right)^2}{\left(1+\left(\frac{x-x'}{a}\right)^2\right)^{2-K}}\right)^2 . \tag{4.138}$$

Physically, the operator in Eq. (4.137) represents a double two-particle backscattering event, where two particles are backscattered from left to right at a time τ_1, but at slightly different positions, and another two particles are backscattered from right to left at the time τ_2 (see Fig. 4.9). Note that even though the electron interactions and the SOC Hamiltonian are defined in a local form, the disorder and RG procedures employed here allow for the above TPB processes at finite separation, given that the cutoff is nonzero. This non-local aspect could be suppressed by contracting the two spatial coordinates in the course of the RG (see Eq. (4.140)). In general, however, we face the form factor in Eq. (4.138), which incorporates the spatially non-local character of the two-particle backscattering event. Of particular interest are the short- and long-distance limits,

$$\begin{aligned}\lim_{x-x'\to 0} m\left(\frac{x-x'}{a}\right) &= (1-2K)^2,\\ \lim_{x-x'\to\infty} m\left(\frac{x-x'}{a}\right) &\sim \left(\frac{x-x'}{a}\right)^{4K-4},\end{aligned} \tag{4.139}$$

as well as the non-interacting limit $\lim_{K\to 1} m((x-x')/a) = 1$. With m, we therefore find a spatial modulation that is nontrivial only in the case of finite interactions, and decays for long distances if $K < 1$ (see also Fig. 4.10). The smaller the cutoff and the stronger the interactions, the sharper becomes the confinement around $x = x'$. This allows us to identify the interesting mechanism of non-local two-particle backscattering, induced by Rashba disorder [GCT14].

The limit of local TPB is readily obtained, assuming that we contract as well x and x'. This yields another factor of $2a(1+d\ell)$, and Eq. (4.137) then becomes

$$\mathcal{T}\exp\left[\int \mathrm{d}\tau_1\ \mathrm{d}\tau_2\ H_{\mathrm{dis}}(\tau_1,\tau_2)\right] \simeq \frac{1}{a^3}\left(\frac{\tilde{D}_\eta}{\pi^2 K}\right)^2\left(\frac{2\pi a}{L}\right)^{8K}(1-2K)^2$$
$$\times\,(1+3d\ell)\sum_{a,b}\int \mathrm{d}x\ \mathrm{d}y_1\ \mathrm{d}y_2\ \mathcal{T}{:}e^{4i\phi_a(x,y_1)}{::}e^{-4i\phi_b(x,y_2)}{:}+\mathrm{h.c.}. \tag{4.140}$$

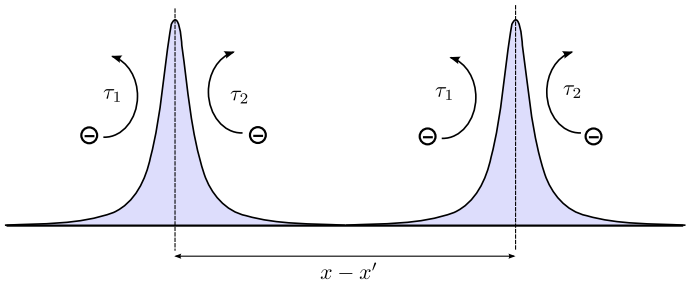

Figure 4.9.: Schematic of a non-local TPB process, as defined in Eqs. (4.137) and (4.141). Reprinted figure with permission from Ref. [GCT14]. Copyright 2014 by the American Physical Society.

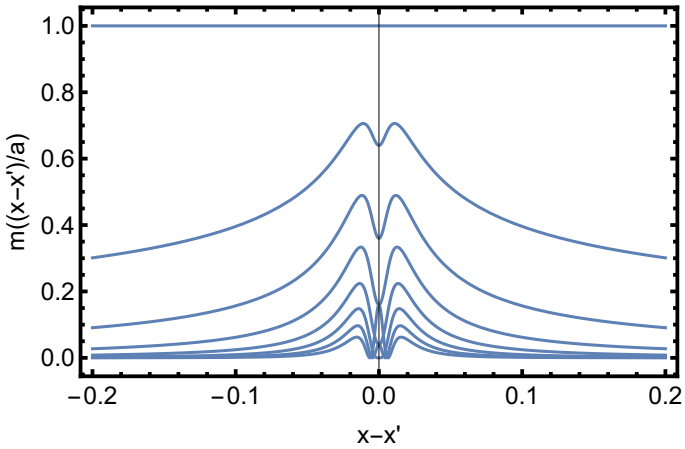

Figure 4.10.: Form factor m of the non-local TPB (see Eq. (4.138)). The different curves depict different interaction strengths, decreasing from $K = 1$ (top curve) in steps of 0.1, and the cutoff is fixed to $a = 0.01$ here. The local minima at $x = x'$ for $K > 1/2$, as well as the ones away from $x = x'$ for $K < 1/2$, result from the finite cutoff a of the model. Figure adapted with permission from Ref. [GCT14]. Copyrighted by the American Physical Society.

Such a term was analyzed in Refs. [SJJ10, XM06]. The question sometimes arises, whether a contraction procedure naturally results in such a local version of the TPB term. One may argue, that a contraction should be performed only for two complete points in $(1+1)$-dimensional space-time, and when contracting two times (see App. C) one should as well contract the respective spatial coordinates. The underlying assumption then is that the cutoff is isotropic, such that the modulus of the space-time vector as a whole is restricted by a minimal length, and spatial and temporal distances change equivalently upon rescaling. However, as we discussed in Sec. 2.5, the choice of such an isotropic cutoff does not seem compulsory. Therefore, we emphasize that a spatial contraction is not generally required, and Eq. (4.137) provides a more general manifestation of TPB. The issue of locality or non-locality of the TPB process will make a difference in the RG analysis, as we show in the following. For the physical TPB current though, this point is of less importance, since the respective separations will be integrated out. As we shall see, the TPB processes at

small distances then provide the dominant contribution.
Motivated by the above findings, and the generic operator in Eq. (3.39), let us define the local and non-local TPB operators,

$$H_{2p} = \gamma_{2p}\frac{v^2}{a^4}\left(\frac{2\pi a}{L}\right)^{8K}\sum_{a,b}\int \mathrm{d}\xi\ \mathrm{d}\Xi\ m\left(\frac{\xi}{a}\right) \times :e^{i2\phi_a(\Xi+\frac{\xi}{2},\tau_1)}e^{i2\phi_a(\Xi-\frac{\xi}{2},\tau_1)}::e^{-i2\phi_b(\Xi+\frac{\xi}{2},\tau_2)}e^{-i2\phi_b(\Xi-\frac{\xi}{2},\tau_2)}:, \tag{4.141}$$

$$H_{2p}^{\mathrm{loc}} = \gamma_{2p}^{\mathrm{loc}}\frac{v^2}{a^3}\left(\frac{2\pi a}{L}\right)^{8K}\sum_{a,b}\int \mathrm{d}x\ :e^{4i\phi_a(x,\tau_1)}::e^{-4i\phi_b(x,\tau_2)}:. \tag{4.142}$$

In the first line above, we introduced relative and center of mass coordinates $\xi = x - x'$ and $\Xi = (x + x')/2$. For the moment, we presume that both terms are generically present in the helical liquid. Both the dimensionless parameters γ_{2p} and $\gamma_{2p}^{\mathrm{loc}}$ can in principle be renormalized by Rashba disorder.

4.6.5. RG of local TPB

Next, a RG analysis is performed, using that the scaling dimension of both the above local and non-local (double) TPB operator is $\Delta_{2\mathrm{p}} = 2(2+2)^2K/4 = 8K$.
First, we analyze the simpler case of local TPB. We find with Eqs. (4.142) and (4.140),

$$\frac{d\gamma_{2p}^{\mathrm{loc}}}{d\ell}(\ell) = (3 - 8K(\ell))\,\gamma_{2p}^{\mathrm{loc}}(\ell) + 3\left(\frac{\tilde{D}_\eta(\ell)}{\pi^2 K(\ell)}\right)^2(1-2K(\ell))^2. \tag{4.143}$$

The above equation does not yet exhibit the correct non-interacting limit, as it seems that in the absence of interactions, $K = 1$, (inelastic) TPB can be generated by (elastic) Rashba disorder. To overcome this problem, we have to implement the missing piece, as explained in Sec. 4.8. With that, the strength of truly inelastic local TPB, say $\gamma_{2p}^{\mathrm{loc,\ in}}$, can be defined by

$$\gamma_{2p}^{\mathrm{loc}} = \gamma_{2p}^{\mathrm{loc,\ in}} + \left(\frac{\tilde{D}_\eta}{\pi^2 K}\right)^2(1-2K)^2. \tag{4.144}$$

Here, the missing piece was read off Eq. (4.140). Making use of the RG flow of $\tilde{D}_\eta$, given in Eq. (4.131), we find

$$\frac{d\gamma_{2p}^{\mathrm{loc,\ in}}}{d\ell}(\ell) = (3 - 8K(\ell))\,\gamma_{2p}^{\mathrm{loc,\ in}}(\ell) + 4\left(\frac{\tilde{D}_\eta(\ell)}{\pi^2 K(\ell)}\right)^2(1-2K(\ell))^2(1-K(\ell)), \tag{4.145}$$

which correctly preserves the non-interacting limit. To analyze the dominant scalings, the above differential equation can be solved exactly, and we find (up to second order in $\tilde{D}_\eta$),

$$\gamma_{2p}^{\mathrm{loc,\ in}}(\ell) = \gamma_{2p}^{\mathrm{loc,\ in}}(0)e^{(3-8K)\ell} + \frac{4(1-2K)^2(1-K)}{\pi^4K^2(4K-1)}\tilde{D}_\eta^2(0)\left(e^{(2-4K)\ell} - e^{(3-8K)\ell}\right). \tag{4.146}$$

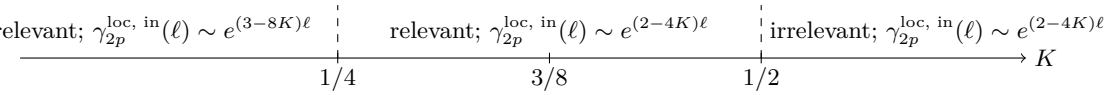

Figure 4.11.: Relevance and dominant scaling of the local TPB coupling $\gamma_{2p}^{\mathrm{loc,\ in}}(\ell)$ in the low-energy limit (large ℓ), see Eq. (4.146). If Rashba disorder was absent, $\tilde{D}_\eta(0) = 0$, the local TPB would be relevant only for $K < 3/8$.

In the presence of disorder, $\gamma_{2p}^{\mathrm{loc,\ in}}(\ell)$ is exponentially increasing with the running scale for $K < 1/2$, as illustrated in Fig. 4.11. This threshold originates from the RG flow of the Rashba disorder operator, that is itself relevant for $K < 1/2$, while the generic operator of local TPB is relevant only for $K < 3/8$. Random Rashba disorder therefore shifts the phase transition point towards weaker interactions. Moreover we find a crossover of scalings at the point $K = 1/4$.

4.6.6. RG of non-local TPB

The situation for non-local TPB is slightly more complicated. Let us first keep the spatial distance ξ as a parameter, and study the non-local coupling $\gamma_{2p}(l, \xi)$. As we focus on the true, inelastic part of the process, we add the missing piece in Eq. (4.137) to define

$$\gamma_{2p}(l, \xi) = \gamma_{2p}^{\mathrm{in}}(l, \xi) + \tilde{D}_\eta^2 / 2\pi^4 K^2. \tag{4.147}$$

After some algebra [GCT14], we arrive at the following flow equation

$$\begin{aligned} \frac{d}{d\ell}\gamma_{2p}^{\mathrm{in}}(\ell, \xi) = \gamma_{2p}^{\mathrm{in}}(\ell, \xi) \left[(4 - 8K) + \frac{\xi}{a(\ell)} \frac{m'\left(\frac{\xi}{a(\ell)}\right)}{m\left(\frac{\xi}{a(\ell)}\right)} \right] \\ + \frac{\tilde{D}_\eta(\ell)^2}{2\pi^4 K^2} \left[(4 - 4K) + \frac{\xi}{a(\ell)} \frac{m'\left(\frac{\xi}{a(\ell)}\right)}{m\left(\frac{\xi}{a(\ell)}\right)} \right]. \end{aligned} \tag{4.148}$$

Here, we used that $m\left((1 + d\ell)\frac{\xi}{a}\right) \simeq m\left(\frac{\xi}{a}\right) + m'\left(\frac{\xi}{a}\right)\frac{\xi}{a} d\ell$, where $m'\left(\frac{\xi}{a}\right) = dm\left(\frac{\xi}{a}\right)/d\left(\frac{\xi}{a}\right)$. From the definition of m in Eq. (4.138), we can specify

$$\left(\frac{\xi}{a}\right) \frac{m'\left(\frac{\xi}{a}\right)}{m\left(\frac{\xi}{a}\right)} = -4(1 - K)\left(\frac{\xi}{a}\right)^2 \frac{\left(-3 + 2K + \left(\frac{\xi}{a}\right)^2\right)}{\left(1 + \left(\frac{\xi}{a}\right)^2\right)\left(-1 + 2K + \left(\frac{\xi}{a}\right)^2\right)}. \tag{4.149}$$

This factor vanishes in the non-interacting limit, as it should be. Eq. (4.148) provides, in principle, a full solution for the evolution of $\gamma_{2p}^{\mathrm{in}}(l, \xi)$, depending on the ratio $\xi/a(\ell)$ with $a(\ell) = a_0 e^\ell$. We next consider the two limits of small, or large ratios of ξ/a. The cutoff a starts at the bare value a_0 and grows in the course of the RG, however, this flow should be terminated once a reaches a comparable energy scale of the system, such as $\xi, v\beta$ or L (where usually $L \to \infty$). In the following, we imply the following hierarchy, $a_0 \ll v\beta \leq L$. On the other hand, since we do not consider an isotropic cutoff here, ξ is not necessarily

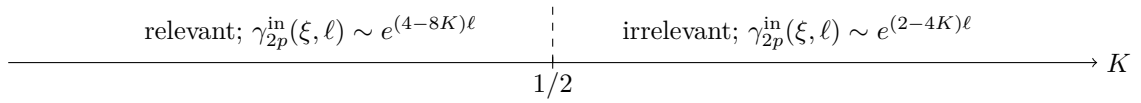

Figure 4.12.: Relevance and dominant scaling of the non-local TPB coupling $\gamma_{2p}^{\rm in}(\xi,\ell)$ in the low-energy limit (large ℓ), which is mainly governed by the contribution of short separations $\xi \ll a$, see Eq. (4.150).

restricted by the cutoff, and we have $0 \leq \xi \leq L$ (as long as no regularization is required). With this assumptions, the limit $\xi \ll a$ is possible, in contrast to a scenario with an isotropic cutoff. The rescaling of a is stopped by the lesser of ξ and $v\beta$.
If $\xi/a \to 0$, Eq. (4.148) and its solution become

$$\begin{aligned} \frac{d}{d\ell}\gamma_{2p}^{\rm in}(\ell,\xi \ll a) &\simeq \gamma_{2p}^{\rm in}(\ell)(4-8K) + \frac{\tilde{D}_\eta(\ell)^2}{2\pi^4 K^2}(4-4K), \\ \gamma_{2p}^{\rm in}(\ell,\xi \ll a) &= \gamma_{2p}^{\rm in}(0)e^{(4-8K)\ell} + \frac{\tilde{D}_\eta^2(0)}{\pi^4 K^2}\frac{(1-K)}{(1-2K)}\left(e^{(4-8K)\ell} - e^{(2-4K)\ell}\right). \end{aligned} \tag{4.150}$$

Again, $\gamma_{2p}^{\rm in}$ grows upon rescaling for $K < 1/2$ (see Fig. 4.12). Note that $\gamma_{2p}^{\rm in}(l,\xi \to 0)$ does not correspond to local TPB, as given in Eq. (4.145), since Eq. (4.150) then only describes the local limit of the coupling of a conceptually non-local TPB term. This difference is embodied in the factors of $(4-8K)$ versus $(3-8K)$ in Eq. (4.150) and Eq. (4.145), respectively. We do recover the local TPB term from Eq. (4.141), once the additional integration of spatial separations is taken care of, for instance, by a contraction of this variable (see previous section).
On the other hand, in the limit $\xi \gg a$, we find

$$\begin{aligned} \frac{d}{d\ell}\gamma_{2p}^{\rm in}(\ell,\xi \gg a) &\simeq -4K\gamma_{2p}^{\rm in}(\ell) + \frac{12\tilde{D}_\eta(\ell)^2}{2\pi^4 K^2}(1-K)\frac{a(\ell)^2}{\xi^2}. \\ \gamma_{2p}^{\rm in}(\ell,\xi \gg a) &= \gamma_{2p}^{\rm in}(0)e^{-4K\ell} + \frac{3\tilde{D}_\eta^2(0)}{2\pi^4 K^2}(1-K)\frac{a_0^2}{\xi^2}\left(e^{(4-4K)\ell} - e^{-4K\ell}\right) \\ &= \gamma_{2p}^{\rm in}(0)e^{-4K\ell} + \frac{3\tilde{D}_\eta^2(0)}{2\pi^4 K^2}(1-K)\frac{a(\ell)^2}{\xi^2}\left(e^{(2-4K)\ell} - e^{-2-4K\ell}\right). \end{aligned} \tag{4.151}$$

Since by assumption the ratio a/ξ is small, the last term can possibly be large only for $K < 1/2$. Due to the decay of the factor m with large ξ, the effect of Rashba disorder vanishes for $a/\xi \to 0$, and TPB can not be generated by disorder at all in this limit. We observe from Eqs. (4.150) and (4.151), that for all strengths of the electron interactions, the coupling for small spatial separations grows faster (and shrinks slower) upon rescaling, than the coupling for large separations. The dominant behaviour is therefore expected to arise from TPB processes at short spatial distances, $\gamma_{2p}^{\rm in}(\ell,\xi \ll a)$.

4.7. Random disorder – conductance

4.7.1. Position-dependent conductance

In order to study the effects of non-local TPB on the transport properties of the system, we here calculate the conductance in a perturbative equilibrium theory, as explained in Sec. 3.1.1. To do so, one expands the correlation G_{ω_n} in Eq. (3.3), and obtains the first-order correction,

$$\begin{aligned}\delta G_{\omega_n}(x,x') &= \int_0^\beta \mathrm{d}\tau \int \mathrm{d}\tau_1\, \mathrm{d}\tau_2\, e^{-i\omega_n\tau}\langle \mathcal{T}\phi(x,\tau)H_{2p}(\tau_1,\tau_2)\phi(x',0)\rangle_0 \\ &= \frac{\gamma_{2p}}{a^4}\sum_{a,b}\int_0^\beta \mathrm{d}\tau\, e^{-i\omega_n\tau}\int \mathrm{d}\Xi\, \mathrm{d}\xi\, \mathrm{d}\tau_1\, \mathrm{d}\tau_2\, \tilde{m}\left(\frac{\xi}{a}\right) \\ &\quad \times \langle \mathcal{T}\phi(x,\tau)e^{i2\phi_a(\Xi+\frac{\xi}{2},\tau_1)}e^{i2\phi_a(\Xi-\frac{\xi}{2},\tau_1)}e^{-i2\phi_b(\Xi+\frac{\xi}{2},\tau_2)}e^{-i2\phi_b(\Xi-\frac{\xi}{2},\tau_2)}\phi(x',0)\rangle_0.\end{aligned} \tag{4.152}$$

Undoing the normal-ordering brings another ξ-dependent factor, that we absorb in a new modulating function $\tilde{m}$, where

$$\tilde{m}\left(\frac{\xi}{a}\right) = m\left(\frac{\xi}{a}\right)\left(1+\left(\frac{\xi}{a}\right)^2\right)^{-2K} = \left(\frac{(1-2K)-\left(\frac{\xi}{a}\right)^2}{\left(1+\left(\frac{\xi}{a}\right)^2\right)^2}\right)^2. \tag{4.153}$$

The correlation in the last line of Eq. (4.152) can be calculated using the generating functions-approach [BF04], and upon averaging, the replica indices are taken care of. Making use of the bosonic single-particle propagator $G^0_{\omega_n}(x,x')$ in Eq. (3.3), the evaluation of $\delta G_{\omega_n}(x,x')$ comes down to the correlator (for more details of the calculation see Ref. [GCT14])

$$\begin{aligned}F(x_1,x_2,\tau_1,\tau_2) &= \langle e^{2i(\phi(x_1,\tau_1)+\phi(x_2,\tau_1)-\phi(x_1,\tau_2)-\phi(x_2,\tau_2))}\rangle_0 \\ &= \exp\big[-2K\big(\langle[\phi(x_1,\tau_1)-\phi(x_2,\tau_1)]^2\rangle_0 - \langle[\phi(x_1,\tau_1)-\phi(x_1,\tau_2)]^2\rangle_0 \\ &\quad - \langle[\phi(x_1,\tau_1)-\phi(x_2,\tau_2)]^2\rangle_0 - \langle[\phi(x_2,\tau_1)-\phi(x_1,\tau_2)]^2\rangle_0 \\ &\quad - \langle[\phi(x_2,\tau_1)-\phi(x_2,\tau_2)]^2\rangle_0 + \langle[\phi(x_1,\tau_2)-\phi(x_2,\tau_2)]^2\rangle_0)\big].\end{aligned} \tag{4.154}$$

Using variables $\xi = x_1 - x_2$ and $\tau = \tau_1 - \tau_2$, we have (see correlations in Sec. 2.3)

$$\begin{aligned}&\langle[\phi(x_1,\tau_1)-\phi(x_2,\tau_2)]^2\rangle_0 = \\ &\frac{1}{4}\log\left[\frac{\left(\sinh^2\left(\frac{\pi\xi}{v\beta}\right)+\sin^2\left(\frac{\pi}{v\beta}(v\tau-a)\right)\right)\left(\sinh^2\left(\frac{\pi\xi}{v\beta}\right)+\sin^2\left(\frac{\pi}{v\beta}(v\tau+a)\right)\right)}{\sin^4\left(\frac{\pi a}{v\beta}\right)}\right].\end{aligned} \tag{4.155}$$

With Eq. (4.155), we can find an exact expression for the function $F(x_1,x_2,\tau_1,\tau_2) = F(\xi,\tau)$. In general, the Fourier transform of the full, position-dependent correlation to frequency space will be difficult though. Nevertheless, we can again keep ξ as a fixed parameter, and consider the two limits of large and small separations, which are readily

solvable.
In the limit of short and large separations, respectively, we obtain

$$\begin{aligned} F(\xi \to 0, \tau) &= \left(\frac{\pi a}{v\beta}\right)^{8K} \left(\sin\left(\frac{\pi\tau}{\beta}\right)\right)^{-8K}, \\ F(\xi \to \infty, \tau) &= \left(\frac{\pi a}{v\beta}\right)^{4K} \left(\sin\left(\frac{\pi\tau}{\beta}\right)\right)^{-4K}. \end{aligned} \tag{4.156}$$

As far as the Fourier transforms are concerned, we are only interested in terms linear in frequency,

$$\begin{aligned} [F_{\omega_n=0}(\xi) - F_{\omega_n}(\xi)]_{\xi\to 0} &= C_0(K) \left(\frac{\pi a}{v\beta}\right)^{8K} \beta^2\omega_n + \mathcal{O}(\omega_n^2), \\ [F_{\omega_n=0}(\xi) - F_{\omega_n}(\xi)]_{\xi\to \infty} &= C_\infty(K) \left(\frac{\pi a}{v\beta}\right)^{4K} \beta^2\omega_n + \mathcal{O}(\omega_n^2). \end{aligned} \tag{4.157}$$

Here, $C_0(K)$ and $C_\infty(K)$ are factors generated in the process of Fourier transformation. Eventually, we arrive at the corrected two-point correlations [7]

$$\begin{aligned} \delta G_{\omega_n}(x - x', \xi \approx 0) &\simeq \gamma_{2p} \frac{(v\beta)^2}{a^4} L\omega_n C_0'(K) \left(\frac{K}{2|\omega_n|}\right)^2 (1-2K)^2 \left(\frac{v\beta}{\pi a}\right)^{-8K}, \\ \delta G_{\omega_n}(x - x', \xi \to \infty) &\simeq \gamma_{2p} \frac{(v\beta)^2}{a^4} L\omega_n C_\infty'(K) \left(\frac{K}{2|\omega_n|}\right)^2 \left(\frac{\xi}{a}\right)^{-4} \left(\frac{v\beta}{\pi a}\right)^{-4K}. \end{aligned} \tag{4.158}$$

Some constants were absorbed in the new prefactors $C_0'(K)$ and $C_\infty'(K)$. Due to the approximation in Eq. (3.3), the result will not depend on the initial positions x, x' anymore. We note that $\delta G_{\omega_n}(\xi) \sim \omega_n^{-1}$, and therefore the dc-limit of the conductivity is well defined. This results in a (still position-dependent) correction to the conductance of

$$\begin{aligned} \delta G(\xi \approx 0) &\simeq \gamma_{2p} e^2 C_0''(K) L \frac{(v\beta)^2}{a^4} \left(\frac{v\beta}{\pi a}\right)^{-8K}, \\ \delta G(\xi \to \infty) &\simeq \gamma_{2p} e^2 C_\infty''(K) L \frac{(v\beta)^2}{\xi^4} \left(\frac{v\beta}{\pi a}\right)^{-4K}. \end{aligned} \tag{4.159}$$

As a check, the above scaling of the conductance with the temperature can be reproduced with the results of the RG in Eqs. (4.150) and (4.151), assuming that $\gamma_{2p} \to \gamma_{2p}(\ell)$ becomes a running coupling in Eq. (4.159). When taking only the bare parameters (so $\tilde{D}_\eta(0) = 0$, $\gamma_{2p}^{\text{in}}(0) > 0$), and scaling up to $a(\ell) \to v\beta$, we recover the same power-law decay. Note that the conductance is suppressed as a power law for large separations ξ.

4.7.2. Position-independent conductance

Above, we have computed the backscattering current in the two limits of very small and very large separations. A general solution for arbitrary ξ, however, which is the quantity of physical interest, bears the problem of integrals that are too complicated to be solved analytically. Our goal is thus to first find an approximate expression for a general $\delta G(\xi)$,

[7] A factor of L appears simply from the integration of the center of mass coordinate Ξ.

such that subsequently the position-independent correction to the conductance can be evaluated by $\delta G = \int \mathrm{d}\xi\, \delta G(\xi)$.
We first present a simple approximation, in order to illustrate the procedure. Second, we give a slightly more refined estimate, that we assume to indicate the correct power-law scaling. Let us in the following assume a hierarchy of length scales $a_0 \ll \xi \ll v\beta$, where the lower limit is introduced again to regularize potential divergences.
The decay of the form factor m for large separations emphasizes the fact, that short-distance backscattering events provide the dominant contribution, and suggests, that we approximately ignore long-distance correlations in the current. In a first step, we therefore approximate $\xi \approx 0$ in the vertex operators, which leaves $m(\xi/a)$ as the only ξ-dependent factor. The non-local TPB operator in Eq. (4.141) (see also Eq. (4.152)) then factorizes to

$$H_{2p} = \gamma_{2p} \frac{v^2}{a^4} \sum_{a,b} \int \mathrm{d}\xi\; m\left(\frac{\xi}{a}\right) \int \mathrm{d}\Xi\; e^{i4\phi_a(\Xi,\tau_1)} e^{-i4\phi_b(\Xi,\tau_2)}. \tag{4.160}$$

Such an ansatz results in [GCT15] (also compare with Eq. (4.159))

$$\delta G(\xi) \simeq e^2 C L \beta^2 \left(\frac{v\beta}{\pi a_0}\right)^{-8K} \frac{\gamma_{2p}}{a_0^4} m\left(\frac{\xi}{a_0}\right), \tag{4.161}$$

where C is a constant, and we now fix the cutoff to the bare value a_0. Eventually, the integration of ξ yields (with some constants c_1 and c_2)

$$\int_{a_0}^{v\beta} \mathrm{d}\xi\; m\left(\frac{\xi}{a_0}\right) \simeq a_0^{4-4K} \left(c_1 a_0^{4K-3} + c_2 (v\beta)^{4K-3}\right), \tag{4.162}$$

and we have

$$\delta G^{(\mathrm{simple})} \sim \gamma_{2p} \frac{L}{a_0} \times \begin{cases} (v\beta/a_0)^{-1-4K} & \text{if } 3/4 < K < 1, \\ (v\beta/a_0)^{2-8K} & \text{if } K < 3/4. \end{cases} \tag{4.163}$$

As a consequence, in this simple approach, we find a crossover of scales at $K = 3/4$.

The approximation used here was based on the fact, that the modulation m carries all the information about the spatial separations. Revisiting the origin of m, it is found to emerge in the process of contracting two out of the four time variables (see App. C, Eq. (C.10)). It turns out, that such time integrals can be treated in a more refined way, which results in a lower (so more dominant) scaling of the conductance with the temperature. Rather than to set them to zero on a shell of finite range, we can perform the integration explicitly,

$$\begin{aligned} m_2\left(\frac{\xi}{a_0}, \frac{\beta}{a_0}\right) &= a_0^{-4K+2} \int_0^{v\beta} \mathrm{d}y\; \frac{(1-2K)(y+a_0)^2 - \xi^2}{((y+a_0)^2+\xi^2)^{2-K}} \int_0^{v\beta} \mathrm{d}y'\; \frac{(1-2K)(y'+a_0)^2 - \xi^2}{((y'+a_0)^2+\xi^2)^{2-K}} \\ &\simeq \left(\left(\frac{\xi}{a_0}\right)^{2K-2} - \left(\frac{v\beta}{a_0}\right)^{2K-1}\right)^2. \end{aligned} \tag{4.164}$$

Here, we used that $a_0 \ll \xi \ll v\beta$. The factor m_2 then replaces the previous modulation m in Eqs. (4.160) and (4.161). Note that we recover m from m_2 if we approximate the

integrals by putting both y and y' to zero on a shell of a_0. The two form factors m and m_2 have the same asymptotic behaviour for large separations, while in contrast to m, m_2 has an explicit dependence on temperature for small separations. After integration, we obtain the leading-order contributions

$$\int_{a_0}^{v\beta} \mathrm{d}\xi \; m_2\left(\frac{\xi}{a_0}, \frac{\beta}{a_0}\right) \simeq a_0^{2-4K}\left(c_3 a_0^{4K-1} + c_4 (v\beta)^{4K-1}\right). \tag{4.165}$$

The position-independent corrections to the dc-conductance now exhibit a crossover of scales at $K = 1/4$, and we find ($\beta = 1/T$)

$$\delta G \sim \gamma_{2p}\frac{L}{a_0} \times \begin{cases} (Ta_0/v)^{4K-1} & \text{if } 1/4 < K < 1, \\ (Ta_0/v)^{8K-2} & \text{if } K < 1/4. \end{cases} \tag{4.166}$$

As a main conclusion, the scaling of the conductance for weak interactions in the disordered system differs by one power from the one of the single impurity setup [CBD$^+$12] (compare with Eq. (4.95)). Furthermore, the scaling crossover point is shifted from $K = 1/2$ to $K = 1/4$. This crossing point must not be confused with the critical threshold, that separates regimes of relevant and irrelevant coupling parameters, which is still $K = 1/2$ (again in contrast to the case of a single impurity, where it is $K = 1/4$). It is a consequence of the fact that disorder itself can be a relevant operator, in contrast to the single Rashba impurity strength.

The observation of a crossover of scalings results from the two different microscopic sources of two-particle backscattering, that come with a distinct scaling. First, there is a generic (for instance intrinsically present) contribution, and second, we have TPB induced by the SOC potential. The latter naturally emerges in a form that depends on the spatial separation (see Eq. (4.137)), and therefore allows for non-local backscattering. Consequently, the fact, that the TPB process at hand can potentially be generated by Rashba SOC, is embodied in the presence of the factor $m(\xi/a)$. The resulting difference in scaling becomes apparent after spatial integration. If in the above approach, for instance, we drop this factor and use instead the local version of TPB, as given in Eq. (4.142), the scaling will simply read $\delta G \sim \gamma_{2p}^{\mathrm{loc}}(L/a_0)(Ta_0/v)^{8K-2}$, for a given cutoff and all $K < 1$. This is the same power-law behaviour we find, when starting from a generic TPB operator only. Clearly, no crossover of scalings is found then.

Another route to obtain the correct crossover, and one that is for instance chosen in Ref. [CBD$^+$12], is to combine the general expression for the conductance with the results of the RG (see also Eq. (4.94)). In this case, one replaces the coupling constant γ_{2p} above by the respective running parameter $\gamma_{2p}(\ell)$. This is in general difficult here, since we do not have an exact expression for $\gamma_{2p}(\ell, \xi)$ at hand (only for the limits of very small and large ξ). However, the above results are recovered by the following estimate: Using the local version of the TPB operator in Eq. (4.142), and the RG evolution of Eq. (4.146), we find an (position-independent) expression for the conductance, analogous to Eq. (4.161),

$$\delta G \simeq e^2 C' L \beta^2 \left(\frac{\pi a}{v\beta}\right)^{8K} \frac{\gamma_{2p}^{\mathrm{loc,\,in}}(\ell)}{a^3}. \tag{4.167}$$

To obtain the above result, the correlation function $F(\xi, \tau)$ was approximately taken at zero distance, as given in Eq. (4.157), and the spatial integral entailed in H_{2p}^{loc} simply results in a factor of L. Importantly, the cutoff $a = a(\ell)$ is as well a running parameter here, in contrast to the bare value a_0 in Eq. (4.161). Furthermore, C' represents another constant. The two microscopic sources of TPB now enter through the running coupling constant $\gamma_{2p}^{\mathrm{loc}}(\ell)$, where from Eq. (4.146) we understand that $\gamma_{2p}^{\mathrm{loc}}(\ell) \sim e^{(3-8K)\ell}$ for $K < 1/4$, and $\gamma_{2p}^{\mathrm{loc}}(\ell) \sim e^{(2-4K)\ell}$ for $K > 1/4$. Rescaling the cutoff as $a \to v\beta$, or $\ell \to \log(v\beta/a_0)$, we find in Eq. (4.167) the same crossover as given in Eq. (4.166). This argumentation reflects once more, that the spatial integration of $m(\xi/a)$ above, is dominated by the (local) terms with vanishing separations.

4.8. Contractions and the missing piece

In this section, we explore the more technical issue of contracting two variables, in space or time, in the context of a RG treatment. This process is closely related to the concept of the missing piece of the RG, both ideas were mostly developed and studied in Ref. [GS88] (see also Ref. [NH79]).

First, it is crucial to clarify that with "contraction" of two or more points, one means more than a short-distance expansion, but the analysis, what happens at small distances of the order of a when the cutoff is changed under rescaling. Here, we study the case of a one-dimensional contraction. Assume we have the double integral of a function $f(y_1, y_2)$, that potentially diverges at small separations of its arguments, $y_1 - y_2$. We can then regularize the integral by

$$\int \mathrm{d}y_1 \, \mathrm{d}y_2 \; f(y_1, y_2) = \int_{|y|>a} \mathrm{d}Y \, \mathrm{d}y \; f(Y, y), \tag{4.168}$$

where we employed relative and center of mass coordinates, $y = y_1 - y_2$ and $Y = (y_1 + y_2)/2$. [8] Anticipating divergences at zero distance, we restrict y to be at least of the order of the cutoff. As a consequence, the integral now depends on this cutoff, and will therefore change under rescaling. Possibly, the integration of short distances can be performed exactly, however, this is not necessary if we are interested only in what happens upon changing the cutoff. Similar to the analysis of the one-loop correction in Sec. 2.5, a contribution arises from the short distances $|y| \approx a$ upon rescaling, as

$$\int_{|y|>a} \mathrm{d}y \; f(Y, y) = \int_{|y|>a(1+d\ell)} \mathrm{d}y \; f(Y, y) + \int_{a<|y|<a(1+d\ell)} \mathrm{d}y \; f(Y, y). \tag{4.169}$$

The last term has the potential to renormalize another quantity of interest, and is the important one here. Therefore, the contraction selects this piece. With that, we are able to write the following operation as a preliminary definition of a one-dimensional contraction,

$$\int \mathrm{d}y_1 \, \mathrm{d}y_2 \; f(y_1, y_2) \to \int_{a<|y|<a(1+d\ell)} \mathrm{d}Y \, \mathrm{d}y \; f(Y, y) \simeq 2ad\ell \int \mathrm{d}Y \; f(Y, |y| \to a). \tag{4.170}$$

[8] For most situations we face here, time-ordering will ensure positive time-differences only, such that usually $f(Y, y) = f(Y, |y|)$.

Above, the integration was estimated by putting $|y| = a$ on the one-dimensional hypersphere shell, $S_1 a d\ell = 2a d\ell$. Hereby, the surface of a general, n-dimensional hypersphere is defined by $S_n = 2\pi^{n/2}/\Gamma(n/2)$, where Γ is the Euler Gamma function. Note that the contraction, given in Eq. (4.170), represents rather an operation (sign "$\to$") than an approximation, as it anticipates a contribution of the integral that will emerge upon rescaling. This is very clear from the presence of the factor $d\ell$. However, in the practice of an RG analysis, one often indicates a contraction by a simple approximation sign. For instance, in the first-order RG analysis in App. C, we used that (with time-ordering)

$$\int_{-\infty}^{\infty} \mathrm{d}y \, \left(\frac{2\pi}{L}||y| + a|\right)^{-2K} = 2\int_{y>a}^{\infty} \mathrm{d}y \, \left(\frac{2\pi}{L}y\right)^{-2K} \simeq 2a d\ell \left(\frac{2\pi a}{L}\right)^{-2K}. \tag{4.171}$$

Next, we discuss the concept of the "missing piece", as explored in Ref. [GS88]. Its implementation is in general needed when working with a real-space RG, in order to discriminate between elastic and inelastic scattering processes, and to obtain correct non-interacting limits.
In Eq. (4.168), we have intentionally excluded times $|y| < a$ for the purpose of regularization. The absence of this part, coined the "missing piece", can have important consequences for the RG procedure, since it alters the character of the whole expression in terms of elasticity. Due to the fundamental correspondence of time translation and energy conservation, a purely elastic process generally corresponds to an unlimited integral, while the introduction of a regularization, as given above, induces some artificial inelasticity [GS88]. In the model we consider here, the elastic and inelastic character is directly related to the absence and presence of electron interactions. Therefore, the implementation of the missing piece is crucial to obtain the correct non-interacting limit. In particular, we expect no backscattering in this limit due to TRS protection. This difficulty can be overcome by adding the extra piece P to the right hand side of Eq. (4.168), with

$$P = \int_{|y|<a} \mathrm{d}Y \, \mathrm{d}y \, f(Y, y) \simeq 2a \int \mathrm{d}Y \, f(Y, |y| \to a). \tag{4.172}$$

To avoid potential divergences at zero distance, the integral was approximated by putting $|y| \to a$ over the full range of $2a$. Including the missing piece P, the one-dimensional contraction in Eq. (4.170) now reads

$$\int \mathrm{d}y_1 \, \mathrm{d}y_2 \, f(y_1, y_2) \to 2a(1 + d\ell) \int \mathrm{d}Y \, f(Y, |y| \to a). \tag{4.173}$$

Simply speaking, the factor of $d\ell$ has been replaced by $1 + d\ell$.
When n one-dimensional contractions are performed separately (the same result up to prefactors is obtained for one n-dimensional contraction [9]), this generates a factor of $(1 + d\ell)^n = 1 + nd\ell + \mathcal{O}(d\ell^2)$. The missing piece thus modifies the original coupling constants upon rescaling. Eventually, to obtain the original (truly inelastic) constants,

[9] One then has to compare the surface area (times $a d\ell$) and the volume (the missing piece) of a n-dimensional hypersphere of radius a. This ratio is again n, so a factor proportional to $1 + nd\ell$ is obtained.

usually labeled with an index λ^{in}, from the modified ones, λ, one needs to add the missing piece

$$\lambda = \lambda^{\text{in}} \pm P, \tag{4.174}$$

where the sign depends on the RG flow of λ (see for example Sec. 4.6.4).

5. Magnetic moments

Apart from Rashba SOC, backscattering at the helical edge can emerge from various other microscopic sources. Because of their importance, let us briefly discuss charge puddles in this context. Due to imperfections of the band curvature or additional doping, electronic states ("puddles") might exist in the bulk of an insulating solid state system, at energies that are expected to be within the band gap. Edge electrons with a comparable energy, can then tunnel from the edge channel into, or out of, the puddle. Assuming that such puddles are typically of small spatial extent, it is reasonable to model them by quantum dots. An electron that tunnels from a helical edge state into a bulk puddle, and stays in there for a given time, in general loses its phase coherence with the other edge electrons, and the spin orientation relaxes from its quantized value. In addition, various interactions mechanisms with other particles in the puddle can possibly cause a spin relaxation, or a spin flip, of the electron. At the 2D QSH edge, an effective backscattering process can then occur as a series of the following, subsequent steps: Tunneling of a helical edge electron into the puddle, a spin flip (or relaxation of the spin) in the puddle, tunneling back into the edge channel of opposite chirality. Such processes were shown to lead to power-law corrections to the conductance with temperature [VGG13, VGGG14]. If the dwelling time of an electron in the puddle is long enough such that the information about its original spin orientation is fully lost, and if the tunneling mechanism is very effective, the conductance per edge channel is reduced to half its value. This is because an electron can end up in any of the two counterpropagating channels, with about equal probability, when tunneling from the puddle back into the edge states. Depending on whether there is an even or odd number of electrons in the puddle, it can be considered an effectively spinless or spinful perturbation, respectively. The latter resembles the case of a magnetic impurity with an internal spin, or magnetic moment.
On more general grounds, in this chapter, we attend to study magnetic moments of spin 1/2 as an essential microscopic source of backscattering at the helical edge. Given a coupling between the spin of the edge electrons and the impurity spin, elastic single-particle backscattering processes are generated, similar to the ones discussed in Sec. 3.3, while crucially, time reversal symmetry remains preserved. This mechanism was first explored by J. Kondo, and succeeded in explaining the so-far puzzling increase of the resistivity at low energies in dilute magnetic alloys [Kon64]. Usually, the general coupling term is therefore coined "Kondo coupling". At the helical edge, where transport is topologically protected against (regular) elastic backscattering, magnetic moments represent one of the fundamental sources of backscattering [WBZ06, MLO$^+$09, TFM11, ESSJ12, KRB16]. We here focus on the transport signature of a local, single magnetic moment in the presence of electron interactions. Note, that in contrast to the previous discussion of Rashba SOC, electron interactions are not necessarily required for the backscattering process to be nonzero, as the additional spin degree of freedom of the magnetic moment ensures com-

patibility with TRS. However, a finite strength of electron interactions alters the expected power-law exponent of the correction to the conductance. Our analysis will be extended to the case of many dilute moments, in order to demonstrate the agreement of the theoretical predictions with transport experiments in QSH samples, made of InAs/GaSb.

5.1. The diagonal Kondo model

The Kondo exchange coupling represents the spin-spin interaction between the electron spin density $\vec{s} = (s_x, s_y, s_z)$ at the edge, and another magnetic moment, $\vec{S} = (S_x, S_y, S_z)$. As mentioned above, this model is appropriate to describe both spinful perturbations at the helical edge, as well as bulk charge puddles with an odd number of electrons.
We now consider the Kondo model for a single magnetic moment of spin 1/2, that is localized at a certain position x_0 along the one-dimensional transport channel. The total Hamiltonian is then given by $H = H_0 + H_J$, with the Kondo interaction term, H_J. Assuming that the moment interacts only with electrons in immediate proximity, we use the electron spin density

$$\vec{s}(x_0) = \frac{1}{2} \sum_{\alpha\beta} \psi^\dagger_\alpha(x_0) \vec{\sigma}_{\alpha\beta} \psi_\beta(x_0), \tag{5.1}$$

to define the Kondo coupling by

$$H_J = \sum_{i,j=\{x,y,z\}} J_{ij} S_i s_j(x_0). \tag{5.2}$$

Here, the J_{ij} are the matrix elements of the Kondo coupling strength. Both types of spin operators (electron/impurity) obey the usual commutation relations, individually, while commuting with the other sort of spin,

$$\begin{aligned} [s_i(x), s_j(x')] &= i\epsilon_{ijk} s_k(x) \delta(x - x'), \\ [S_i, S_j] &= i\epsilon_{ijk} S_k, \\ [s_i(x), S_j] &= 0. \end{aligned} \tag{5.3}$$

For a general spin-spin exchange, all the elements J_{ij} in Eq. (5.2) are different. To tackle the Kondo problem, however, a first approximation is to assume that the coupling matrix only has diagonal elements. Such a simplified model is explored in the next section.

5.1.1. The *xxz*-model – RG

Defining the spin flip operators $s_\pm = s_x \pm i s_y$ and $S_\pm = S_x \pm i S_y$ (from now on, let us choose $x_0 = 0$ and drop the position label), we find that

$$\begin{aligned} J_{xx} S_x s_x + J_{yy} S_y s_y &= \frac{1}{2}[(J_{xx} - J_{yy})(S_x s_x - S_y s_y) + (J_{xx} + J_{yy})(S_x s_x + S_y s_y)] \\ &= \frac{1}{4}[(J_{xx} - J_{yy})(S_+ s_+ + S_- s_-) + (J_{xx} + J_{yy})(S_+ s_- + S_- s_+)]. \end{aligned} \tag{5.4}$$

The spin quantization axis of the helical liquid here is pointing in z-direction. The x- and y-axis span the 2D plane of the underlying physical system (e.g. the QSH sample), and the respective coupling constants are expected to be of similar strength, $J_{xx} \approx J_{yy} = J_\perp$. On the other hand, helicity of the system implies the general anisotropy $J_z \neq J_\perp$. Our coupling then takes the form $J_{ij} = \mathrm{diag}(J_\perp, J_\perp, J_z)_{ij}$. This model is called xxz-model [EK92]. We therefore define the Kondo Hamiltonian of the xxz-model, call it H_{ex} [VGG16], as a simplified version of the general Kondo exchange H_J in Eq. (5.2),

$$\begin{aligned} H_{\mathrm{ex}} &= J_z S_z s_z + \frac{1}{2} J_\perp (S_+ s_- + S_- s_+) \\ &= \frac{1}{L} \sum_{k,k'} J_z S_z \left(c^\dagger_{\uparrow,k} c_{\uparrow,k'} - c^\dagger_{\downarrow,k} c_{\downarrow,k'} \right) + \frac{1}{2} J_\perp (S_+ c^\dagger_{\downarrow,k} c_{\uparrow,k'} + S_- c^\dagger_{\uparrow,k} c_{\downarrow,k'}). \end{aligned} \tag{5.5}$$

The first term, proportional to J_z, can as well be absorbed by a unitary transformation of the basis [EK92, VO11, ESSJ12]. Going to a bosonic representation, we find $s_\pm = \pm i (2\pi a)^{-1} e^{\pm 2i\sqrt{K}\phi}$ and $s_z = \frac{1}{2\pi\sqrt{K}} \partial_x \theta$, such that the exchange coupling is expressed as [1]

$$H_{\mathrm{ex}} = J_\perp \frac{-i}{4\pi a} (S_+ e^{-2i\sqrt{K}\phi} - S_- e^{2i\sqrt{K}\phi}) + J_z \frac{1}{2\pi\sqrt{K}} S_z \partial_x \theta. \tag{5.6}$$

From the scaling dimension of the operators $s_\pm$ and s_z, we directly infer, that the scaling dimension of the Kondo couplings are $\Delta_\perp = K$ and $\Delta_z = 1$ (the impurity spin S does not contribute to the scaling dimension). This means, that even if we choose an isotropic coupling, $J_\perp = J_z$, at a given energy, the two operators will in general evolve differently upon rescaling, in the presence of interactions, and some anisotropy $J_\perp \neq J_z$ will be generated inevitably. Therefore, for the Kondo Hamiltonian in Eq. (5.5), $SU(2)$ symmetry is in general replaced by an effective $U(1)$ symmetry. In particular, to the order of tree level, there will be no renormalization of the s_z-component, as $1 - \Delta_z = 0$. Going to the next order of one-loop corrections, one can for instance use the poor man's scaling approach [And70, WBZ06, Nev15] to derive the RG equations [2]

$$\begin{aligned} \frac{d}{d\ell} J_\perp &= (1 - K) J_\perp + \rho J_\perp J_z, \\ \frac{d}{d\ell} J_z &= \rho J_\perp^2. \end{aligned} \tag{5.7}$$

Here, $\rho = 1/(2\pi v)$ represents the density of states per spin (branch) per unit length of the edge [VGG16]. [3] The RG flow is illustrated in Fig. 5.1. Assuming that $J_z(0) > 0$,

[1] Note that different bosonization schemes lead to different expressions, compare with Refs. [MLO+09, TFM11].

[2] What is the difference to the regular RG scheme? In essence ([Nev15], p.6), "the term *poor man* refers to the fact that the bandwidth is not rescaled to its original size after each progressive renormalization. This simplifies the matter as there is no need to rescale the Hamiltonian, eliminating the second step in the renormalization group procedure. Nevertheless, the results obtained via this simplified renormalization procedure are qualitatively accurate and correctly describe the low-energy behavior of the Kondo model."

[3] This is derived from the total density of states,

$$\rho^{\mathrm{tot}}(E) = \sum_{k,\sigma=\pm} \delta(E - v(\sigma k - k_F)) = \frac{L}{2\pi} \sum_\sigma \frac{1}{|v\sigma|} \int \mathrm{d}k \; \delta((E/v + k_F)/\sigma - k) = \frac{L}{\pi v}.$$

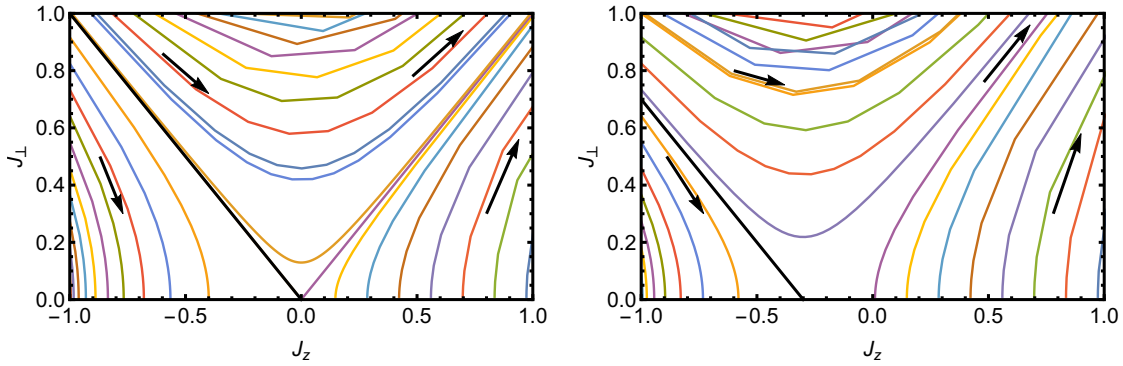

Figure 5.1.: RG flow of the two couplings $J_\perp$ and J_z of the xxz-Kondo model, see Eq. (5.7) (with $\rho = 1$), for the two different interaction strengths (a) $K = 1$ and (b) $K = 0.7$. Arrows indicate the evolution of parameters upon increasing ℓ (going to lower energies), while thick lines represent separatrices of regimes of irrelevant and relevant perturbations. Such a separatrix is here given by the two points $(-1, K)$ and $(K - 1, 0)$.

meaning that the coupling is antiferromagnetic, we find that both J_z and $J_\perp$ are relevant perturbations at all interaction strengths, such that the spin-impurity coupling diverges towards low energies ($J_z, J_\perp \to \infty$). In the limit of zero energy ($\ell \to \infty$), the Kondo coupling becomes as well isotropic, $J_z \approx J_\perp$.
Note, that we employed the perturbative RG only to second order, such that it is not yet clear, whether higher-order terms change the strong-coupling behaviour. In fact, one finds negative corrections to the β-function for instance in third order of the RG [Nev15]. It was eventually proved with the help of a numerical RG scheme, that higher-order corrections do not change the qualitative behaviour, and the strong-coupling fixed point is indeed given by ($J_z, J_\perp \to \infty$) [Noz74, Wil75]. The ground state in the strong-coupling regime is a singlet of the electron and the impurity spin.

5.1.2. Weak- and strong-coupling regime – definition of T_K

For an antiferromagnetic Kondo coupling, by inspection of Eq. (5.7), we therefore expect the system to be in the strong-coupling regime at low energies. According to the discussion in Sec. 3.3.3, this can usually be interpreted in the sense that the conductance approaches zero at zero energy. Indeed, in a 1D spinful liquid, the conductance vanishes for all $K < 1$, and the transport channel is effectively cut into two semi-infinite pieces (this holds even for both ferromagnetic and antiferromagnetic Kondo couplings)[FN94]. As the magnetic moment binds a spinful edge electron in a robust singlet state, the electron is pinned, and forms a barrier for the remaining particles in the transport channel. At the same time, the impurity spin is fully screened. At the helical QSH edge, however, due to the peculiar topological nature of the system, the edge state simply follows the new effective shape of the boundary. Therefore, electrons can bypass the local Kondo singlet, and the conductance at zero energy for a single channel is not zero, but $G_0 = e^2/h$ [MLO+09].

Note, that such a bypass mechanism does not occur for a relevant (spinless) magnetic perturbation, as was discussed in Sec. 3.3.3, because the latter explicitly breaks time-reversal symmetry, and a topological healing of the edge state becomes impossible.
A perturbative analysis in terms of the coupling constants is valid only in the weak-coupling limit, i.e. if the corresponding coupling strengths are small. So far, we have always discriminated between the strong- and weak-coupling regimes by studying the evolution of coupling constants towards low energies, depending on the strength of the electron interactions. As the Kondo coupling is relevant for all $K < 1$, we always are in the strong-coupling regime at low energies. On the other hand, irrespective of electron interactions, the Kondo coupling becomes smaller with increasing energy, such that at sufficiently high energies we find ourselves in the weak-coupling limit as well. The typical transition temperature between those two domains is called the Kondo temperature, T_K. Figuratively, it symbolizes the energy threshold, below which perturbation theory breaks down. We can define the Kondo temperature by the condition [Nev15, Gia03]

$$\rho J(E \to T_K) \approx 1, \tag{5.8}$$

where for simplicity we approximate the coupling to be isotropic for the moment, so $J(\ell) = J_z(\ell) \simeq J_\perp(\ell)$. To find an estimate for the Kondo temperature, we take $K = 1$ in Eq. (5.7), such that the RG flow is indeed fully isotropic. This yields the solution

$$J(\ell) = \frac{J(0)}{1 - J(0)\rho\ell}. \tag{5.9}$$

Expressing ℓ in terms of energy, we have $\ell = \log(a/a_0) = -\log(Ea_0/v)$, where $E = \max(eV, T)$ is the dominant energy scale, and a_0 the bare cutoff. As discussed before, $v/a_0 \approx E_g$ plays the role of the band gap E_g in the QSH system. With that, we find that the running coupling strength decreases logarithmically with increasing energies,

$$J(E) = \frac{J(E_g)}{1 + \rho J(E_g)\log(E/E_g)} \sim \log^{-1}(E/E_g). \tag{5.10}$$

Here, $J(E_g)$ is the bare coupling strength (at very high energies). Assuming that $\rho J(E_g) \ll 1$, we use Eqs. (5.8) and (5.10) to estimate the Kondo temperature by

$$T_K \simeq E_g e^{-1/(\rho J(E_g))}. \tag{5.11}$$

For $E \gg T_K$, the system is in the weak-coupling regime, while for $E \ll T_K$, we reach strong coupling.

5.1.3. Influence of interactions – definition of T^*

The anisotropic xxz-Kondo model, as given in Eq. (5.7), entails two important scenarios at finite electron interactions (throughout, we imply repulsive interactions, $K < 1$). A transition between the two can be associated with another critical temperature, say T^*.
First, if $\rho J_z \gg (1 - K)$, we can drop the first term in the first line of Eq. (5.7), and the RG flow is similar to the one of a non-interacting setup [VGGG14]. In this regime, both

the couplings J_z and $J_\perp$ evolve in a similar way, such that it seems reasonable to assume a nearly isotropic coupling, as given in Eq. (5.9), that decays logarithmically with increasing energies.
On the other hand, at energies where $\rho J_z \ll (1-K)$, we find ourselves in a qualitatively different regime, where the presence of interactions elicits new, interesting physics. In this case, we can drop the second term in the first line of Eq. (5.7), and the evolution of $J_\perp$ is mainly governed by the tree level contribution $\frac{d}{d\ell} J_\perp = (1-K) J_\perp$. Note that this approximation is possible even if interactions are weak (but finite), as long as ρJ_z is sufficiently small. The RG solutions then take the form

$$\begin{aligned} J_\perp(\ell) &\simeq J_\perp(0) e^{(1-K)\ell}, \\ J_z(\ell) &\simeq J_z(0) + \frac{\rho J_\perp(0)^2}{2(1-K)} e^{2(1-K)\ell}. \end{aligned} \tag{5.12}$$

In terms of energy, we observe a power-law decay for increasing energies, that scales as

$$\begin{aligned} J_\perp(E) &= J_\perp(E_g) \left(\frac{E}{E_g}\right)^{K-1}, \\ J_z(E) &= J_z(E_g) + \frac{\rho J_\perp(E_g)^2}{2(1-K)} \left(\frac{E}{E_g}\right)^{2(K-1)}. \end{aligned} \tag{5.13}$$

Similar to the definition of the Kondo temperature, we can identify the typical threshold temperature, T^*, by the condition [Gia03] $\rho J_z(E \to T^*) \approx (1-K)$. With the help of Eq. (5.13), we use this constraint to estimate

$$\begin{aligned} \left(\frac{a_0 T^*}{v}\right)^{-2(1-K)} &= 2\left(\frac{(1-K)^2}{(\rho J_\perp(E_g))^2} - \frac{J_z(E_g)(1-K)}{\rho J_\perp(E_g)^2} + \frac{1}{2}\right) \simeq 2\left(\frac{(1-K)}{\rho J_\perp(E_g)}\right)^2, \\ T^* &\simeq E_g \left(\frac{\rho J_\perp(E_g)}{\sqrt{2}(1-K)}\right)^{\frac{1}{1-K}}. \end{aligned} \tag{5.14}$$

Here, we exploited that the solution of Eq. (5.13) implies $\rho J_z(E_g) \ll (1-K)$. The isotropic regime mentioned above (see Eq. (5.9)) corresponds to energies $E \ll T^*$, while the solution derived in Eq. (5.12) holds for $E \gg T^*$.
In the following, we assume the hierarchy of energy scales $T^* \gg T_K$, and focus mainly on high energies $E \gg T^*$, which defines the energy range of the weak-coupling regime, where electron interactions can have interesting effects. In particular, at energies above T^*, electron interactions induce an anisotropy of the couplings $J_\perp$ and J_z, while below T^*, this anisotropy is erased in the course of the RG. One should keep in mind though, that the definition of T^* makes sense only in the presence of nonzero electron interaction strength. A schematics of the energy-dependent evolution of the running Kondo couplings of the xxz-model is illustrated in Fig. 5.2.

5.1.4. Backscattering current

In the free helical liquid, the spin component along the quantization axis, here s_z, is conserved. In the presence of the Kondo impurity, it is useful to introduce the total spin

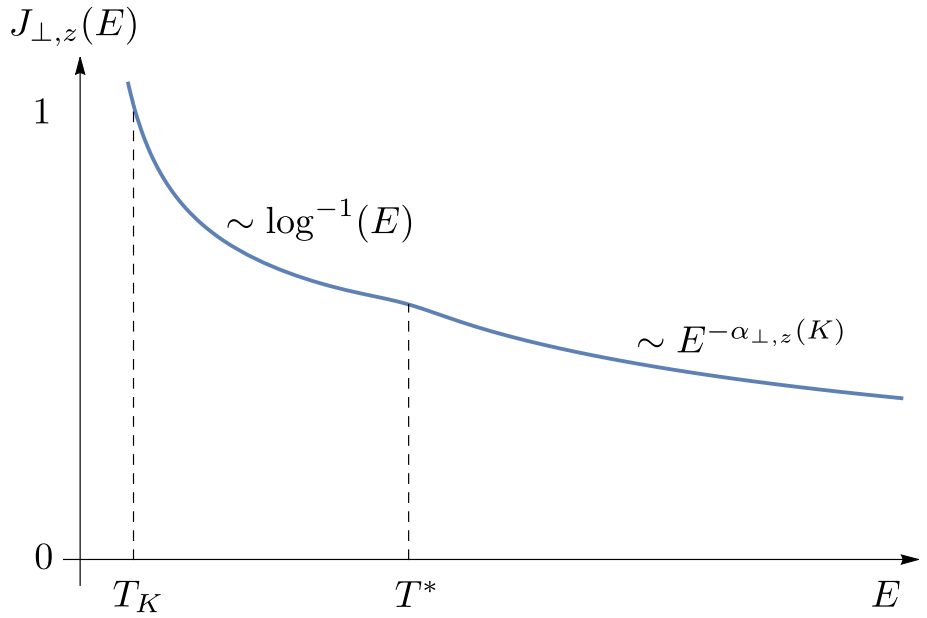

Figure 5.2.: RG flow of the anisotropic Kondo couplings $J_\perp$ and J_z, as given by Eqs. (5.10) and (5.13), in the presence of interactions. For $E < T_K$, we are in the strong-coupling regime, where perturbation theory breaks down. At energies $T_K < E < T^*$, we find a logarithmic decay of the (weak) coupling constants, that is nearly isotropic, so $J_z \simeq J_\perp$. Eventually, for $E > T^*$, the Kondo couplings exhibit a power-law dependence on the energy. Some anisotropy is generated, as $J_\perp$ and J_z evolve differently, with a power exponent $\alpha_\perp(K) = 1 - K$, and $\alpha_z(K) = 2(1 - K)$, respectively.

of the system along the same direction by

$$S_z^{\text{tot}} = S_z + \int \mathrm{d}x\; s_z(x) = S_z + \frac{1}{2}(N_R - N_L). \tag{5.15}$$

With that, the backscattering current at the edge can be defined by [VGG16]

$$\delta I(t) = -e\partial_t S_z^{\text{tot}}(t) = -ie[H_J(t), S_z^{\text{tot}}(t)]. \tag{5.16}$$

Note that we implied an additional contribution to the current from a potential flip of the magnetic moment, instead of simply using $\delta I(t) = -e\partial_t s_z(t)$. The reasoning is that in steady state, the spin of the impurity is bounded, and thus time-independent, such that $\partial_t S_z(t) = 0$. Therefore, the above definition of the backscattering current is well-justified in this case. Importantly, we realize with the help of Eq. (5.3), that the z-component of the total spin has the commutation properties $[S_z^{\text{tot}}, H_0] = 0$, as well as

$$[S_z^{\text{tot}}, H_{\text{ex}}] = 0. \tag{5.17}$$

In the presence of a perturbation of the type H_{ex}, S_z^{tot} is still conserved, since the spin flip of an electron is accompanied by the reversed spin flip of the impurity spin. As a consequence, such a diagonal coupling alone will not induce any steady-state backscattering current [TFM11].

Let us next give an example of a simple Kondo perturbation, beyond the xxz-model, that induces a nonzero backscattering current at the helical edge. First, we present a simple calculation using the Fermi golden rule, in order to illustrate the correct power-law scaling. In the subsequent sections, a refined approach is described, which can be used to derive a more accurate result for backscattering off a general Kondo impurity.
To drive a current through the system, we apply a dc bias voltage, such that the full system is given by $H = H_0 + H_V + H_J$, where

$$H_0 = \sum_{k,r} \varepsilon_r(k) c^\dagger_{r,k} c_{r,k}, \tag{5.18}$$

$$H_V = eV S^{\mathrm{tot}}_z, \tag{5.19}$$

with the single-particle energies $\varepsilon_r(k) = r v_F k$. As shown above, a xxz-like Kondo coupling is not sufficient to induce backscattering. Instead, we can for instance study a perturbation with diagonal couplings, that are all of different strength, $J_{xx} \neq J_{yy} \neq J_{zz}$. According to Eq. (5.4), this gives rise to an additional, perturbative term, H', of the form

$$\begin{aligned} H_J &= H_{\mathrm{ex}} + H', \\ H' &= \frac{1}{4}(J_{xx} - J_{yy})(S_+ s_+ + S_- s_-) = \delta J (S_+ s_+ + S_- s_-). \end{aligned} \tag{5.20}$$

The coupling H_{ex} is defined in Eq. (5.5), and we assume that $\delta J \ll J_\perp, J_z$. Realizing that $[H', S^{\mathrm{tot}}_z] \neq 0$, the backscattering current is expected to be finite, and can be calculated perturbatively in δJ. With the FGR approach described in Sec. 4.3.2, we find a lowest-order backscattering current of the form $\langle \delta I \rangle = \sum_{if} 2\pi |\langle i|H'|f\rangle_0|^2 w_i \delta(E_i - E_f) \Delta N_{f \leftarrow i}$, where the unperturbed average, $\langle (\ldots) \rangle_0$, is taken with respect to the free system at finite bias. The averages of the impurity spin and the electron spin density simply factorize, such that we obtain

$$\langle \delta I \rangle = e^2 V \pi (\rho \delta J)^2. \tag{5.21}$$

It furthermore needs to be taken into account, that the coupling strength δJ changes with energy as well. The corresponding RG flow of all the coupling constants of the Kondo model is discussed in more detail in Sec. 5.2.3 and the App. D.3, for the two different energy domains of the weak-coupling regime, respectively. Anticipating this analysis, we identify the RG flow of the anisotropic perturbation in the case of $E \gg T^* \gg T_K$ to be $\delta J(T, V) = \delta J(E_g)(E/E_g)^{K-1}$ (see Eq. (5.35)). This leads us to

$$\langle \delta I \rangle = e^2 V \pi (\rho \delta J(E_g))^2 \left(\frac{\max(T, eV)}{E_g} \right)^{2(K-1)} \quad \text{if } \max(T, eV) \gg T^*. \tag{5.22}$$

We have thus found a characteristic power-law correction to the current, caused by backscattering off the magnetic moment. The resulting correction to the conductance has the same exponent, $\delta G \sim E^{2K-2}$, that we expect from a single-particle backscattering off a (spinless) magnet impurity, as analyzed in Sec. 3.3. This is not a coincidence, since the Kondo

backscattering mechanism here is the very same elastic SPB process, however, accompanied by a simultaneous flip of the impurity spin. This modification renders the Kondo backscattering time-reversal invariant, in contrast to the SPB off a magnetic impurity. Note that in previous sections (e.g. Sec. 3.3), we have always considered the limit of low energies. The question of being in the weak- or strong-coupling regime then was related only to the electron interactions strength. With the Kondo coupling, we here discuss a perturbation that is relevant at low energies and repulsive interactions (the same holds for a TRS-breaking magnetic impurity). Nevertheless, by studying the system at high energies, $E \gg T_K$, we find ourselves in the weak-coupling regime for $K < 1$. As a consequence, the backscattering current can be calculated perturbatively in the impurity strength.
Finally, in the regime of $T_K \ll E \ll T^*$, the RG flow of the perturbation takes a different form. The scaling behaviour can be read off Eq. (D.15), and we obtain

$$\langle \delta I \rangle \propto e^2 V \pi (\rho^2 \delta J(T^*) J(T^*))^2 \log^2 \left(\frac{\max(T, eV)}{T^*} \right) \quad \text{if } T_K \ll \max(T, eV) \ll T^*. \tag{5.23}$$

Here, J is the isotropic coupling strength of this regime, $J(E) = J_\perp(E) \approx J_z(E)$. The above FGR analysis can as well be performed for off-diagonal perturbations, with the outcome remaining qualitatively the same as in Eqs. (5.22) and (5.23).

5.2. Kondo model with non-diagonal couplings

5.2.1. Backscattering current

Following the analysis of Ref. [VGG16], we next study the transport signature of a helical LL coupled to a general Kondo impurity, that features as well off-diagonal elements. Assuming that T^* is very small in a realistic setup, we here focus on the regime of $E \gg T^*$ (and $T^* \gg T_K$). Including a bias voltage, the full system is modeled by $H = H_0 - H_V + H_J$ (here, the sign of the bias voltage was chosen such that the spin-up configuration has the minimum energy at positive bias V). The first two terms are the same as in Eqs. (5.18) and (5.19), but the perturbative part of the Kondo coupling takes the more general form

$$\begin{aligned} H_J &= H_{\text{ex}} + H', \\ H' &= \sum_{i,j=\{x,y,z\}} \delta J_{ij} S_i s_j. \end{aligned} \tag{5.24}$$

Still, we assume that all the $\delta J_{ij} \ll J_z, J_\perp$. Using Eqs. (5.16) and (5.17), the backscattering current can be phrased as

$$\begin{aligned} \delta I(t) &= -ie[H'(t), S_z^{\text{tot}}(t)] = e \sum_{k,l,r,p=\{x,y,z\}} (\delta J_{kr} \epsilon_{rzl} + \delta J_{pl} \epsilon_{pzk}) S_k(t) s_l(t) \\ &= eS_x(t) \left[(\delta J_{xy} + \delta J_{yx}) s_x(t) + (\delta J_{yy} - \delta J_{xx}) s_y(t) + \delta J_{yz} s_z(t) \right] \\ &\quad + eS_y(t) \left[(\delta J_{yy} - \delta J_{xx}) s_x(t) - (\delta J_{xy} + \delta J_{yx}) s_y(t) - \delta J_{xz} s_z(t) \right] \\ &\quad + eS_z(t) (\delta J_{zy} s_x(t) + \delta J_{zx} s_y(t)). \end{aligned} \tag{5.25}$$

The time-dependence of an operator O in the interaction picture is hereby given as $O(t) = e^{iH_0 t} O e^{-iH_0 t}$, where the impurity spin does not evolve with time, $S_i(t) = S_i$, since trivially $[S_i, H_0] = 0$. We are interested in the thermal average of the backscattering current $\langle \delta I(t) \rangle$, taken with respect to the full Hamiltonian, so $\langle (\dots) \rangle = \mathrm{Tr}(\rho(\dots))/Z$, where $\rho = e^{-\beta(H_0 + H_J - H_V)}$ and $Z = \mathrm{Tr}(\rho)$. This average can be calculated perturbatively in the Kondo couplings, at sufficiently large energies. In the end, the unperturbed average, $\langle (\dots) \rangle_0$, is taken with respect to $\rho_0 = e^{-\beta(H_0 - H_V)}$.
Since H_{ex} itself does not cause any backscattering, it was desirable to evaluate the correlations exactly in $H_0 + H_{\mathrm{ex}}$, and to consider only H' a perturbation to the free system. However, unfortunately, the corresponding correlations are not feasible with standard techniques. In the course of the following perturbation theory, we shall instead try to find a way to take into account H_{ex} in a more exact way than H', in order to justify the assumption of $\delta J_{ij} \ll J_z, J_\perp$. This is achieved by expanding two of our intermediate results to lowest order in the couplings δJ (in the RG flow of the running couplings, and in the Bloch equations, see below).
Next, we use the normal-ordered expressions of the spin densities to write $:s_i(t): = s_i(t) - \langle s_i(t) \rangle_0$, where

$$\begin{aligned} \langle s_x(t) \rangle_0 &= \langle s_y(t) \rangle_0 = 0, \\ \langle s_z(t) \rangle_0 &= \frac{1}{2L} \sum_k \left(f_+(k) - f_-(k) \right) = \rho \frac{1}{2} eV. \end{aligned} \tag{5.26}$$

The thermal (and bias-dependent) energy distribution is given here by the Fermi functions $f_\pm(k) = (e^{\beta(vk \mp eV/2)} + 1)^{-1}$. In a similar way, we find the unperturbed impurity spin averages

$$\begin{aligned} \langle S_x \rangle_0 &= \langle S_y \rangle_0 = 0, \\ \langle S_z \rangle_0 &= \frac{\mathrm{Tr}(e^{\beta eV S_z} S_z)}{\mathrm{Tr}(e^{\beta eV S_z})} = \frac{\sinh(\beta eV/2)}{2\cosh(\beta eV/2)} = \frac{1}{2} \tanh(\beta eV/2). \end{aligned} \tag{5.27}$$

At a high bias voltage ($\beta |eV| \gg 1$), the z-component of the magnetic moment will be fully polarized, $\langle S_z \rangle_0 \to \pm 1/2$, while if temperature is the dominant energy scale ($\beta eV \to 0$), we have $\langle S_z \rangle_0 \to 0$.

The average backscattering current takes the form (see Eq. (5.25) with the explicit time-dependencies dropped for brevity)

$$\begin{aligned} \langle \delta I \rangle = {} & (\delta J_{yz} \langle S_x \rangle - \delta J_{xz} \langle S_y \rangle) \frac{1}{2} \rho e^2 V \\ & + e \left[(\delta J_{xy} + \delta J_{yx}) (\langle S_x : s_x : \rangle - \langle S_y : s_y : \rangle) \right] + e \left[(\delta J_{yy} - \delta J_{xx}) (\langle S_x : s_y : \rangle + \langle S_y : s_x : \rangle) \right] \\ & + e (\delta J_{yz} \langle S_x : s_z : \rangle + \delta J_{zy} \langle S_z : s_x : \rangle - \delta J_{xz} \langle S_y : s_z : \rangle - \delta J_{zx} \langle S_z : s_y : \rangle). \end{aligned} \tag{5.28}$$

The challenge is therefore all about the calculation of the spin correlations $\langle S_i : s_j : \rangle$ and the steady-state averages $\langle S_i \rangle$ in the above equation, given the presence of the Kondo impurity. In the next section, we present a way how to handle the mixed correlations $\langle S_i : s_j : \rangle$ perturbatively, using approximations concerning the dynamics of the two types of spin-spin correlations. Subsequently, building on this approximation, we are able to

calculate the steady-state averages of the impurity spin, $\langle S_i \rangle$, taking into account the xxz-like Kondo couplings exactly. Because of this procedure, our result will eventually be more than perturbative in $H_{\rm ex}$.

5.2.2. Spin-spin correlations

While the unperturbed product average $\langle S_k(t){:}s_l(t){:}\rangle_0$ factorizes and vanishes (because $\langle {:}s_l(t){:}\rangle_0 = 0$), the average $\langle S_k(t){:}s_l(t){:}\rangle$ in the presence of the Kondo coupling is in general finite. In App. D.1 we exploit the fact that the electron spin correlations decay faster than the impurity spin average, in order to derive the following approximation (let us abbreviate $J_{ij} = \mathrm{diag}(J_\perp, J_\perp, J_z)_{ij} + \delta J_{ij}$ for the moment),

$$\langle S_k(t){:}s_l(t){:}\rangle \simeq -\sum_{ij} J_{ij} \left(\sum_n \epsilon_{ikn} \langle S_n(t)\rangle \mathrm{Re}C_{jl} + \frac{1}{2}\delta_{ik}\mathrm{Im}C_{jl} \right), \tag{5.29}$$

with the electron spin density-density correlations $C_{jl} = \int_0^\infty \mathrm{d}t' \, \langle s_j(0){:}s_l(t'){:}\rangle_0$. The latter can be calculated in the presence of interactions and a finite bias voltage, using standard bosonization techniques and known integrals [Gia03, GR07]. Explicitly, the correlations needed for the present analysis are found to be of the form [VGG16, Väy16]

$$\begin{aligned}
\mathrm{Re}C_{xx} &= \left(\frac{1}{4\pi a}\right)^2 \left(\frac{2\pi a}{v\beta}\right)^{2K} \frac{\beta}{2\pi} B\left(K + i\frac{\beta eV}{2\pi}, K - i\frac{\beta eV}{2\pi}\right) \cosh\left(\frac{\beta eV}{2}\right), \\
\mathrm{Re}C_{zz} &= K\frac{\pi}{2}\rho^2\beta^{-1}, \\
\mathrm{Re}C_{xy} &= \left(\frac{1}{4\pi a}\right)^2 \left(\frac{2\pi a}{v\beta}\right)^{2K} \frac{\beta}{2\pi} B\left(K + i\frac{\beta eV}{2\pi}, K - i\frac{\beta eV}{2\pi}\right) \sinh\left(\frac{\beta eV}{2}\right) \cot(\pi K), \\
\mathrm{Im}C_{xy} &= \left(\frac{1}{4\pi a}\right)^2 \left(\frac{2\pi a}{v\beta}\right)^{2K} \frac{\beta}{2\pi} B\left(K + i\frac{\beta eV}{2\pi}, K - i\frac{\beta eV}{2\pi}\right) \sinh\left(\frac{\beta eV}{2}\right).
\end{aligned} \tag{5.30}$$

The remaining correlations can be obtained using the symmetries $C_{xx} = C_{yy}$, $C_{xy} = -C_{yx}$, and $C_{iz} = C_{zi} = \delta_{iz}C_{zz}$. Here, $B(x, y)$ is the Euler Beta function. In the limits of very large temperature or bias voltage, the correlations become pure power laws,

$$\begin{aligned}
&\beta^{1-2K} B\left(K + i\frac{\beta eV}{2\pi}, K - i\frac{\beta eV}{2\pi}\right) \sinh(\beta eV/2) \\
&\simeq \frac{\pi}{\Gamma(2K)} \times \begin{cases} (eV/2\pi)^{2K-1} & \text{if } \beta eV \gg 1, \\ \Gamma^2(K)\beta^{2-2K}(eV/2\pi) & \text{if } \beta eV \ll 1. \end{cases}
\end{aligned} \tag{5.31}$$

Above, $\Gamma(x)$ denotes the Euler Gamma function, and we have $B(K, K) = \Gamma^2(K)/\Gamma(2K)$. Likewise, when $\sinh(\beta eV/2)$ is replaced by $\cosh(\beta eV/2)$ in $\mathrm{Re}C_{xx}$, the lower limit in Eq. (5.31) becomes $\beta^{1-2K}\Gamma^2(K)/\Gamma(2K)$, whereas the upper limit stays the same. Using those two asymptotes, the following approximation can be found [VGG16], that holds particularly well for weak interactions, $K \approx 1$,

$$\beta^{1-2K} B\left(K + i\frac{\beta eV}{2\pi}, K - i\frac{\beta eV}{2\pi}\right) \sinh(\beta eV/2) \simeq \frac{eV}{2K}\beta^{2-2K} \frac{B(K, K)}{[1 + A(K)(\beta eV/2)^2]^{1-K}}, \tag{5.32}$$

where we defined

$$A(K) = \pi^{-2}\Gamma(K)^{2/(1-K)}. \tag{5.33}$$

With the help of Eq. (5.29), the average backscattering current of Eq. (5.28) can be phrased in terms of impurity averages $\langle S_n \rangle$ only,

$$\begin{aligned}\langle \delta I \rangle = &\left(\left[\delta J_{yz} + J_\perp \delta J_{zy} \frac{\mathrm{Re}C_{xy}}{\frac{1}{2}\rho e V} \right] \langle S_x \rangle - \left[\delta J_{xz} - J_\perp \delta J_{zx} \frac{\mathrm{Re}C_{xy}}{\frac{1}{2}\rho e V} \right] \langle S_y \rangle \right) \frac{1}{2}\rho e^2 V \\ &+ e \left((\delta J_{xx} - \delta J_{yy})^2 + (\delta J_{xy} + \delta J_{yx})^2 \right) \left(\frac{1}{2} \tanh \frac{\beta e V}{2} + \langle S_z \rangle \right) \mathrm{Re}C_{xx} \\ &+ e \left(\left[\delta J_{yz}^2 + \delta J_{xz}^2 \right] \langle S_z \rangle - J_z \left[\delta J_{yz} \langle S_y \rangle + \delta J_{xz} \langle S_x \rangle \right] \right) \mathrm{Re}C_{zz} \\ &+ e \sum_{i=x,y} \delta J_{zi} \left(\frac{1}{2} \delta J_{zi} \tanh \frac{\beta e V}{2} + J_\perp \langle S_i \rangle \right) \mathrm{Re}C_{xx}.\end{aligned} \tag{5.34}$$

5.2.3. Running couplings for $E \gg T^*$

The expression for the backscattering current in Eq. (5.34) can be simplified significantly, when using running couplings $J_{ij}(E)$, that have an implicit energy dependence. In the previous section (see Eq. (5.7)), we have already discussed the RG flow for the two couplings $J_\perp(E), J_z(E)$ of the diagonal xxz-Kondo model. The same RG analysis can be employed to derive the behaviour of a general coupling constant J_{ij} [ESSJ12, Eri13]. Assuming temperatures above T^*, we use that $J_{ij} = \mathrm{diag}(J_\perp, J_\perp, J_z)_{ij} + \delta J_{ij}$ to expand the RG equations to lowest order in the perturbations δJ. We then obtain [4]

$$\begin{aligned}\frac{d}{d\ell} X &= (1-K)X, \\ \frac{d}{d\ell} \delta J_{zz} &= \rho J_\perp (\delta J_{xx} + \delta J_{yy}), \\ \frac{d}{d\ell} \delta J_{xz} &= -\rho J_\perp \delta J_{zx}, \\ \frac{d}{d\ell} \delta J_{yz} &= -\rho J_\perp \delta J_{zy}.\end{aligned} \tag{5.35}$$

Here, X represents any of the couplings $\delta J_{xx}, \delta J_{yy}, \delta J_{xy}, \delta J_{yx}$ and δJ_{zi} with $i \in \{x, y\}$. These couplings evolve in the same way as $J_\perp$, and we can simply replace $J_\perp(E)$ by $X(E)$ in Eq. (5.13), so $X(E) = X(E_g)(E/E_g)^{K-1}$. The solutions for δJ_{iz} and δJ_{zz} are slightly different from the evolution of J_z, they read

$$\begin{aligned}\delta J_{iz}(E) &= \delta J_{iz}(E_g) - \frac{\rho}{2} \frac{1}{(1-K)} J_\perp(E_g) \delta J_{zi}(E_g) \left(\frac{E}{E_g} \right)^{2(K-1)}, \quad \text{if } i \in \{x, y\}, \\ \delta J_{zz}(E) &= \delta J_{zz}(E_g) + \frac{\rho}{2} \frac{1}{(1-K)} J_\perp(E_g) (\delta J_{xx}(E_g) + \delta J_{yy}(E_g)) \left(\frac{E}{E_g} \right)^{2(K-1)}.\end{aligned} \tag{5.36}$$

[4] Note that the coupling label is reversed compared to Ref. [Eri13], so we have $J_{ij} \to J_{ji}$. This is due to the different order of operators in the definition of the Kondo Hamiltonian.

The RG scheme, which is a qualitative analysis, only yields the scaling with the maximum energy $E = \max\{eV, T\}$, where $T^* < E < E_g = v/a_0$. In a realistic system, however, there will be a crossover dependence of bias and temperature, that is in general more complicated than the max-function. Inspecting the linearized versions of Eqs. (D.7)–(D.9), we infer that more precisely, in the RG equations above, there should be the replacement ($\beta = 1/T$, and use Eqs. (5.30) and (5.31))

$$\left(\frac{E}{E_g}\right)^{K-1} \to \left(\frac{\tanh\frac{eV}{2T}}{\frac{eV}{2T}}\frac{\mathrm{Re}C_{xx}}{\mathrm{Re}C_{zz}}\right)^{1/2} \sim \begin{cases} (eV/E_g)^{K-1} & \text{if } eV \gg T, \\ (T/E_g)^{K-1} & \text{if } eV \ll T. \end{cases} \tag{5.37}$$

This function provides the correct scaling, as predicted by the RG analysis. It therefore seems reasonable to assume that it models correctly the crossover between the two energy scales. The squared function can be written as $\left(\frac{\tanh\frac{eV}{2T}}{\frac{eV}{2T}}\frac{\mathrm{Re}C_{xx}}{\mathrm{Re}C_{zz}}\right) \approx -\frac{2}{\rho}(1-K)\frac{\mathrm{Re}C_{xy}(T,V)}{\frac{1}{2}\rho eV}$ for $1-K \ll 1$. Explicitly, we then obtain, for all running couplings up to second order in J (from Eqs. (5.13), and (5.35)– (5.37)),

$$\begin{aligned} X(T,V) &= X(E_g)\left(\frac{\tanh\frac{eV}{2T}}{\frac{eV}{2T}}\frac{\mathrm{Re}C_{xx}}{\mathrm{Re}C_{zz}}\right)^{1/2} \\ &\simeq X(E_g)\left(\frac{E_g}{2\pi T}\right)^{1-K}\left(\frac{B(K,K)}{[1+A(K)(eV/2T)^2]^{1-K}}\right)^{1/2}, \\ J_z(T,V) &= J_z(E_g) - J_\perp(E_g)^2\frac{\mathrm{Re}C_{xy}}{\frac{1}{2}\rho eV}, \\ \delta J_{iz}(T,V) &= \delta J_{iz}(E_g) + J_\perp(E_g)\delta J_{zi}(E_g)\frac{\mathrm{Re}C_{xy}}{\frac{1}{2}\rho eV} \quad \text{if } i \in \{x,y\}, \\ \delta J_{zz}(T,V) &= \delta J_{zz}(E_g) - J_\perp(E_g)(\delta J_{xx}(E_g) + \delta J_{yy}(E_g))\frac{\mathrm{Re}C_{xy}}{\frac{1}{2}\rho eV}. \end{aligned} \tag{5.38}$$

Here, X can be any of the couplings $J_\perp, \delta J_{xx}, \delta J_{yy}, \delta J_{xy}, \delta J_{yx}$ and δJ_{zi} with $i \in \{x,y\}$, and further we employed Eq. (5.32) to simplify. Note the difference between $J_{ij}(E)$ and $J_{ij}(T,V)$, where the latter includes a crossover function, that is more accurate than the max-function. Using the above results of the RG in lowest order, we can now write the current of Eq. (5.34) in terms of the running couplings $J_{ij}(T,V)$. For brevity, we do not write the label (T,V) explicitly, but all the coupling strengths J in the following should be thought of as running couplings, unless explicitly stated otherwise.

$$\begin{aligned} \langle \delta I\rangle = &\left(\delta J_{yz}\langle S_x\rangle - \delta J_{xz}\langle S_y\rangle\right)\frac{1}{2}\rho e^2 V \\ &+ \frac{e^2V}{2T}\left([\delta J_{xx} - \delta J_{yy}]^2 + [\delta J_{xy} + \delta J_{yx}]^2\right)\left(\frac{1}{2} + \frac{\langle S_z\rangle}{\tanh\frac{eV}{2T}}\right)\mathrm{Re}C_{zz} \\ &+ e\left(\left[\delta J_{yz}^2 + \delta J_{xz}^2\right]\langle S_z\rangle - J_z\left[\delta J_{yz}\langle S_y\rangle + \delta J_{xz}\langle S_x\rangle\right]\right)\mathrm{Re}C_{zz} \\ &+ \frac{e^2V}{2T}\sum_{i=x,y}\left(\frac{1}{2}\delta J_{zi}^2 + \delta J_{zi}J_\perp\frac{\langle S_i\rangle}{\tanh\frac{eV}{2T}}\right)\mathrm{Re}C_{zz}. \end{aligned} \tag{5.39}$$

Eventually, we have to find a solution for the impurity spin averages $\langle S_i(t)\rangle$. For a steady-state current, this can be achieved with the help of the Bloch equations.

5.2.4. Bloch equations for impurity spin average

Via the Kondo coupling, the magnetic moment interacts with the helical edge electrons. In the limit of large times, we expect the system to reach a steady state, such that the impurity spin is aligned in a certain direction. This assumption leads us to a set of equations ($i = \{x, y, z\}$),

$$\begin{aligned}\frac{d}{dt}\langle S_i(t)\rangle &= i\langle[H_J(t), S_i(t)]\rangle = -\sum_{jk} J_{kj}\epsilon_{kin}\langle S_n(t)s_j(t)\rangle \\ &= -\frac{1}{2}\rho eV\sum_{kn} J_{kz}\epsilon_{kin}\langle S_n(t)\rangle - \sum_{jkn} J_{kj}\epsilon_{kin}\langle S_n(t){:}s_j(t){:}\rangle = 0. \end{aligned} \tag{5.40}$$

Using Eq. (5.29), this can be cast in the form of Bloch equations, which describe the characteristic time evolution of a magnetic moment in a magnetic field,

$$\frac{d}{dt}\langle S_i(t)\rangle = (\vec{h}\times\langle\vec{S}(t)\rangle)_i - (\gamma\langle\vec{S}\rangle)_i + c_i = 0. \tag{5.41}$$

Here, $\vec{h}$ plays the role of an effective magnetic field, γ is a (3×3)-matrix that determines the relaxation of the impurity spin, and $\vec{c}$ is some offset. All those quantities depend on the Kondo coupling strengths, and the thermodynamics of the system. The explicit expressions, as well as the solutions for the $\langle S_i\rangle$, are somewhat lengthy, and can be found in the App. D.2. Importantly, $\langle S_z\rangle$ is finite already in the absence of perturbations δJ, as given in Eq. (5.27). In contrast, the in-plane components $\langle S_{x,y}\rangle$ start from linear order in δJ. The expressions for the impurity spin averages in Eq. (D.13) are obtained in lowest order of δJ, in order to justify the assumption of $\delta J_{ij} \ll J_\perp, J_z$. See also Fig. 5.3 for an illustration of the time evolution of the average impurity spin.
Because of the way we introduced the voltage bias, $H_V = eVS_z^{\mathrm{tot}}$, it plays the role of an effective magnetic field here. In particular, we can associate the latter with the component (see Eq. (D.10))

$$h_z = \frac{1}{2}\rho eV(J_z + \delta J_{zz}). \tag{5.42}$$

On the other hand, the magnetic moment has a tendency to relax towards a non-ordered configuration, associated with the matrix γ. We can use the diagonal in-plane component $\gamma_\perp^{(0)} = (J_\perp^2\frac{(eV/2T)}{\tanh(eV/2T)} + J_z^2)$, see definition in the App. D.2, to identify the typical relaxation rate, or Korringa rate [Kor50, VGG16],

$$\tau_K^{-1} = \gamma_\perp^{(0)}\mathrm{Re}C_{zz} \sim \begin{cases} eVJ_\perp^2 & \text{if } eV \gg T, \\ T(J_\perp^2 + J_z^2) & \text{if } eV \ll T. \end{cases} \tag{5.43}$$

A large relaxation rate corresponds to a fast relaxation out of the ordered configuration. Quite generally, there will be a competition between the two parameters h_z and τ_K. As we

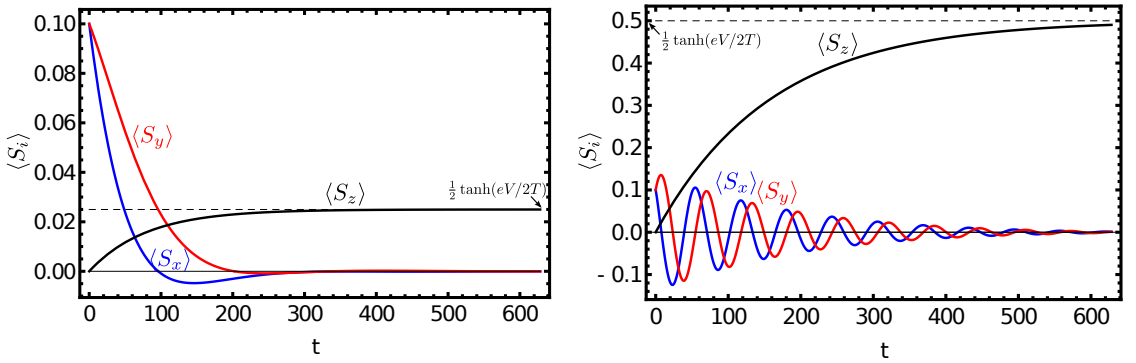

Figure 5.3.: Illustration of the time evolution of the impurity spin averages, $\langle S_i(t)\rangle$, with $i = \{x, y, z\}$, according to the left hand side of Eq. (5.41). The regimes of fast and slow relaxation are demonstrated: In (a), we use $eV = 1, T = 10$, such that $h_z/\tau_K \approx 0.05 \ll 1$, and observe a fast relaxation. On the other hand, in (b), a slow relaxation follows from $eV = 10, T = 1$, where $h_z/\tau_K \approx 17 \gg 1$. In the limit of large times, $t \to \infty$, we approach the steady-state solutions as given in Eq. (D.13). Here, we have chosen only the perturbative couplings δJ_{xx} and δJ_{yy} to be finite for simplicity. In this case, the respective steady-state averages of the in-plane components are zero. However, this does not hold for a general coupling. Further parameters for both plots are $\rho = 1$, $J_\perp \approx J_z = 0.02$, $\delta J_{xx} = 0.008$, $\delta J_{yy} = 0.001$, $\langle S_x(0)\rangle = \langle S_x(0)\rangle = 0.1$, and $\langle S_z(0)\rangle = 0$.

see below, this competition manifests itself in a (small) step of the backscattering current, from one constant to another. We here give the resulting expression for the backscattering current, using Eq. (D.13) in Eq. (5.39),

$$\begin{aligned}\langle \delta I\rangle = e\frac{\pi K}{4} eV\rho^2 \left([\delta J_{xx} - \delta J_{yy}]^2 + [\delta J_{xy} + \delta J_{yx}]^2\right) \\ + e\frac{\pi K}{4} eV \frac{1}{2} R(T,V) \sum_{i=x,y} \rho^2 [\delta J_{zi} + \frac{J_\perp}{J_z}\delta J_{iz}]^2.\end{aligned} \tag{5.44}$$

The term in the first line above arises from the nonzero $\langle S_z\rangle$, and a similar expression could be derived from a Fermi golden rule calculation (compare with Eq. (5.21)). In the second term, we have introduced a function that contains the information about the in-plane averages $\langle S_{x,y}\rangle$ (keep in mind that all the couplings are energy-dependent)

$$R(T,V) = \frac{\frac{J_z}{J_{\text{eff}}} + \left(\frac{eV}{2T}\frac{2}{\pi K\rho J_{\text{eff}}}\right)^2}{1 + \left(\frac{eV}{2T}\frac{2}{\pi K\rho J_{\text{eff}}}\right)^2} \approx \frac{\frac{J_z(T,0)}{J_{\text{eff}}(T,0)} + \left(\frac{eV}{2T}\frac{2}{\pi K\rho J_{\text{eff}}(T,0)}\right)^2}{1 + \left(\frac{eV}{2T}\frac{2}{\pi K\rho J_{\text{eff}}(T,0)}\right)^2}. \tag{5.45}$$

Here, we have defined yet another, effective coupling

$$J_{\text{eff}}(T,V) = \frac{\gamma_\perp^{(0)}}{J_z(T,V)} = \frac{J_\perp(T,V)^2 \frac{eV}{2T}}{\tanh\frac{eV}{2T}} + J_z(T,V)^2}{J_z(T,V)}. \tag{5.46}$$

The introduction of J_{eff} is motivated by the competition of the two quantities $h_z/\tau_K = eV/(\pi T\rho J_{\text{eff}})$. We can now distinguish the two cases of a fast and slow relaxation (see

Fig. 5.3). The former is given by $h_z/\tau_K \ll 1$, so $eV \ll T\rho J_{\text{eff}}$, and as a consequence, we find $R(T,V) \approx J_z/J_{\text{eff}}$ in this limit. On the other hand, for slow relaxations we have $h_z/\tau_K \gg 1$, i.e. $eV \gg T\rho J_{\text{eff}}$, and obtain $R(T,V) \approx 1$. As the bias-dependence only plays a minor role in both cases, we can approximately neglect it on the right hand side of Eq. (5.45). Note that at $eV \approx T\rho J_{\text{eff}}$, the function R, and therefore also the average backscattering current, changes from one constant to another. This crossover should as well be observable in a transport experiment, and could therefore be used to identify backscattering induced by Kondo impurities.

5.2.5. Conductance in terms of bare couplings

In general, Eq. (5.44) provides a full solution for the average backscattering current, in terms of the running couplings. Using the RG flow of Eq. (5.38), we can eventually transform the running couplings back into the bare ones, in order to make appear the explicit energy dependence. This brings us to the final result of our analysis,

$$\langle \delta I \rangle = e^2 V \rho^2 \frac{\pi K}{4} \delta J_{\text{tot}}^2(E_g) \left(\frac{E_g}{2\pi T}\right)^{2(1-K)} \frac{B(K,K)}{[1+A(K)(\frac{eV}{2T})^2]^{1-K}}\ f(T,V). \tag{5.47}$$

We have denoted here

$$\begin{aligned}
\delta J_{\text{tot}}^2(E_g) &= (\delta J_{xx}(E_g) - \delta J_{yy}(E_g))^2 + (\delta J_{xy}(E_g) + \delta J_{yx}(E_g))^2 \\
&\quad + \frac{1}{2}\sum_{i=x,y} [\delta J_{zi}(E_g) + \delta J_{iz}(E_g)]^2, \\
f(T,V) &= \frac{b(T) + \left(\frac{eV}{2T}\frac{2}{\pi\rho J_{\text{eff}}(T)}\right)^2}{1 + \left(\frac{eV}{2T}\frac{2}{\pi\rho J_{\text{eff}}(T)}\right)^2}, \\
b(T) &= 1 - \left(1 - \frac{J_z(T,0)}{J_{\text{eff}}(T)}\right) \frac{1}{2\delta J_{\text{tot}}^2(E_g)} \sum_{i=x,y} [\delta J_{zi}(E_g) + \delta J_{iz}(E_g)]^2.
\end{aligned} \tag{5.48}$$

The function $f(T,V)$ replaces $R(T,V)$ with the modification of $J_z(T)/J_{\text{eff}}(T) \to b(T)$, which has the following motivation. A more detailed analysis shows (see [VGG16] and supplement thereof), that the temperature-dependence of the factors $J_{\text{eff}}(T)$ and the ratio $J_z(T)/J_{\text{eff}}(T)$ only weakly influences the backscattering current in the regime of $T^* \ll T \ll E_g$, where our model is valid. For typical values of the bare exchange couplings, $b(T)$ is bounded by $2/3 \leq b(T) \leq 5/6$, and therefore, can effectively be replaced by a constant.

Comparing our result of the backscattering current in Eq. (5.47) to the initial estimate in Eq. (5.22), we note the following refinements. At a given temperature, the current in Eq. (5.47) exhibits two separated crossover scales for the applied bias. First, at $eV \approx T\rho J_{\text{eff}}(T)$ we find a crossover from one constant to another, that is associated with the impurity spin dynamics. This point is fully entailed in the function $f(T,V)$. Second, we find a crossover at $eV \approx T$, when the bias starts to become the dominant energy scale. Close to this point, one may set $f(T,V) \approx 1$ in Eq. (5.47), in which case we reproduce the scaling of Eq. (5.22), however, with an accurate crossover between the two

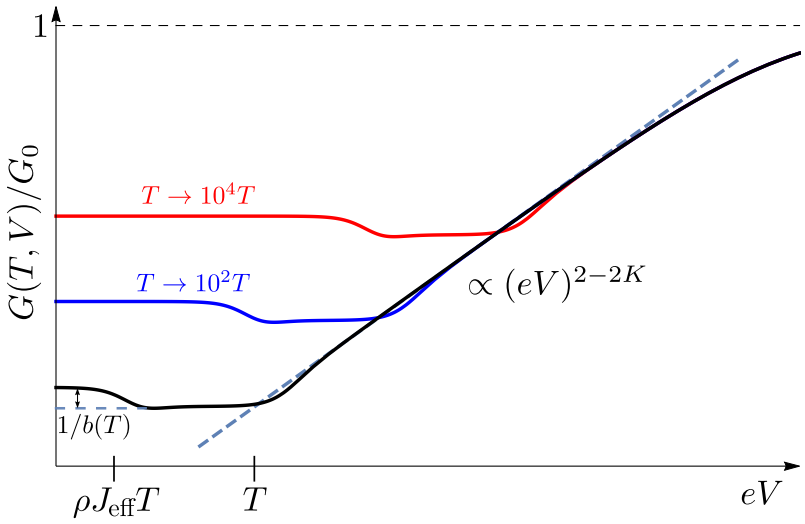

Figure 5.4.: Schematic of the conductance $G(T,V)$ in the presence of many, dilute Kondo impurities, using logarithmic scales. The energy dependence is given by Eq. (5.47) and $G \simeq G_0^2/(G_0 + N\delta G)$, where throughout $E \gg T^*$. Here, we fix T and vary eV. Note the following characteristics: First, there is a (small) step in the conductance of $1/b(T)$, at an energy where $eV/T \approx \rho J_{\rm eff}$. This point marks the approximate crossover from fast ($eV/T \ll \rho J_{\rm eff}$) to slow ($eV/T \gg \rho J_{\rm eff}$) relaxations of the impurity spin average (see text). Next, there is a crossover at $eV/T \approx 1$, when the bias voltage becomes the dominant energy scale. Beyond that point, we find a power-law increase of the form $G(V) \sim (\delta G(V))^{-1} \sim V^{2-2K}$ (with $K < 1$). When the temperature is raised, the conductance generally increases.

energies. Typically, the second crossover occurs at higher energies, as $\rho J_{\rm eff}(T) \ll 1$.
The correction to the conductance can easily be derived from the steady-state backscattering current in Eq. (5.47), using $\delta G = d\langle \delta I \rangle / dV$. Eventually, the energy-dependent conductance G of the full system depends on the Kondo impurity distribution at the helical edge. Here, we study the case of a large number of dilute impurities, $N \gg 1$, in order to make a connection to the experiment by Li et al. presented in Ref. [LWF+15]. Assuming that $N\delta G/G_0$ is not necessarily small, we calculate the conductance of the full system by (see Sec. 3.4, Eq. (3.47)) $G = G_0/(1 + N\delta G/G_0)$. Such an approach implies a long extent of the QSH edge, as $N \sim L$. A schematic plot of the conductance is shown in Fig. 5.4, where we fix the temperature and vary the bias voltage, making sure that throughout $\max(T, eV) \gg T^*$. From the energy dependence of $G(T,V)$, we observe the two crossovers at $eV/T \approx \rho J_{\rm eff}$ and $eV/T \approx 1$, as discussed above. In the typically quite wide range of intermediate energies where $eV/T \geq 1$, but $N\delta G(T,V) \gg G_0$, the conductance scales as a power law, $G \simeq G_0^2/(N\delta G) \sim (eV)^{2-2K}$. Note that the sign of the exponent is opposite to the one of Eq. (5.22), since here $G \sim \delta G^{-1}$. The conductance then grows with increasing energies, before saturating towards its bare value. [5]

[5] Note that in the case of a single Kondo impurity, where $G = G_0 - \delta G$, the conductance increases as well with (high and) increasing energies. This is because even though the correction δG decreases with energy (as a power law), the full conductance G increases, and approaches its bare value. However, this increase then does not follow the same characteristic power law as in Fig. 5.4.

5.3. Comparison with the experiment of Ref. [LWF$^+$15]

The authors of Ref. [LWF$^+$15] report on the observation of helical Luttinger liquid behaviour in two-dimensional InAs/GaSb quantum wells. Band inversion effects in these material systems were predicted to result in a QSH insulating phase [LHQ$^+$08]. Indeed, transport measurements have demonstrated a conductance, that is quantized in terms of e^2/h, pointing at a topologically non-trivial QSH state, and the existence of helical edge modes [KDS11, SND$^+$14, DKSD15]. We therefore expect those materials to be suitable candidate systems for the study of correlated backscattering effects in a helical liquid, that typically manifest themselves in energy-dependent power-law corrections to the quantized conductance. However, in the mentioned articles, edge transport was found to be independent of the applied temperature (at fixed bias). It turned out though [LWF$^+$15], that this was due to the fact that the bias voltage in the experiments was much larger than the temperature, even though the latter was varied in a wide range of $20mK < T < 30K$. In agreement with what we described in the previous chapters, the correction to the conductance scales with the dominant energy scale, $\max(T, eV)$, such that no temperature dependence could be observed.

In a follow-up measurement published in Ref. [LWF$^+$15], the fixed energy scale (temperature or bias voltage) was chosen to be sufficiently small. Interestingly, the authors then observed a power-law increase of the conductance with the complementary energy scale (bias voltage or temperature, respectively), where also the crossing point of the two energy scales can be clearly identified. The fitted power-law exponent hereby was fairly small, $\delta G \propto V^{0.37}$ (see inset of Fig. 4 in Ref. [LWF$^+$15], also reproduced in Fig. 5.5), and suggests an interpretation in the context of (strongly) correlated electron backscattering.

The authors of Ref. [LWF$^+$15] attribute the observed power-law behaviour to relevant two-particle backscattering at low energies. As discussed in previous sections (see for instance Tab. 3.1), this leads to a scaling of $G \sim \delta G \sim E^{2(1/(4K)-1)}$ in the strong-coupling regime, for electron interactions $K < 1/4$ [MLO$^+$09]. Even though this reasoning appears to be correct, we consider it problematic for the following reason. Matching the theoretically predicted power-law exponent with the one observed in the experiment, one finds $K \approx 0.21$. This estimated value of (very strong) interactions is in immediate proximity to the critical threshold of $K = 1/4$, which is required for the TPB, induced by a single or a few impurities, to be relevant. As the authors state themselves, the Luttinger parameter K is hereby related to the Fermi velocity of the system, and therefore controllable by fine-tuning of the gate voltage. This understood, it seems improbable that the gate voltage could be fine-tuned to such a stable value throughout the measurement, without crossing the critical value of $K = 1/4$, in which case a very different power-law is expected, and the above line of reasoning breaks down.

We here present an alternative interpretation of the observed power-law behaviour of the conductance, in the context of magnetic moments. In the previous section, we have shown that the transport signature of many dilute Kondo impurities at high energies, $E \gg T^*$, entails a power-law increase of the conductance, scaling as $G \sim E^{2-2K}$ over a wide energy range. Comparing to the experimental data, this yields $K \approx 0.82$, which corresponds to weak electron interactions in the system. Therefore, this explanation of the measured backscattering effects misses the difficulties mentioned above. Note, that

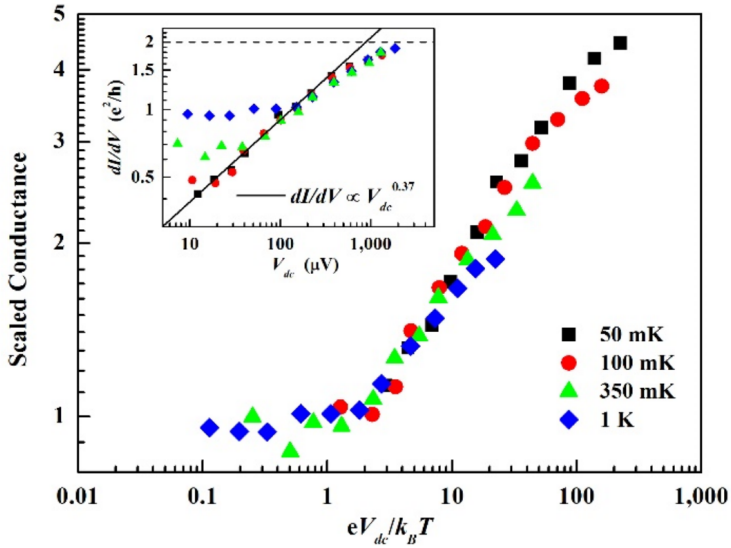

Figure 5.5.: Conductance versus applied bias voltage, as measured in a transport experiment in InAs/GaSb bilayers. For an intermediate regime of energies with $eV \geq T$, the conductance follows a power-law behaviour which hints at correlated backscattering effects in the interacting helical Luttinger liquid (see text). Reprinted figure with permission from Ref. [LWF+15]. Copyright 2015 by the American Physical Society.

also the full crossover function of the conductance, as sketched in Fig. 5.4, agrees very well with the experiment (compare to the inset of Fig. 5.5). Given the relatively large sample length of $L = 1.2\mu m$ used in the setup, the assumption of a great number of impurities seems justified. The origin of magnetic moments in the InAs/GaSb sample is not known, however, even in the absence of magnetic impurities, charge puddles with an odd number of electrons within the band gap (here $E_g \approx 40 - 60K$), can act as such [VGGG14, VGG16].

The two possible interpretations (TPB and strong interactions or magnetic moments and weak interactions) have different zero-energy limits. While for the former, the conductance should vanish at zero energy, we expect $G \to G_0 = 2e^2/h$ for the latter. In the experiment of Ref. [LWF+15], this limit can not be read off, as one of the two parameters T and eV is always fixed. Moreover, since the values of T_K and T^* are generally not known, it is not clear, how far the energy should be lowered in order to observe a significant increase of the conductance towards G_0. The two models could as well be distinguished in a shot-noise measurement, as we can expect distinct signatures from SPB and TPB, respectively. which are able to tell apart single-particle and two-particle backscattering processes. Furthermore, in the range of energies where a power-law behaviour is present, a set of experiments with varying sample sizes should demonstrate a dependence on L of the form of either $G \sim L$ (for a single or a few TPB impurities), $G \sim L^{-1}$ (for many magnetic moments), or even an interaction-dependent power-law scaling of the conductance in L (if v/L is the largest energy scale compared to temperature and bias voltage).

6. Conclusion and Outlook

6.1. Conclusion

In the present Thesis, we have studied electronic transport in one-dimensional helical states. First, the basic concepts of Luttinger liquid theory, and the employed analytic techniques were reviewed. A special emphasis was hereby put on the derivation of the bosonic field commutators and correlation functions, at nonzero electron interaction strength, which are essential for the subsequent analysis of transport properties. We discussed the question of introducing an isotropic or anisotropic cutoff, and illustrated, that this choice can have an impact on the RG flow of coupling constants. In particular, using a general anisotropic cutoff, we identified non-local TPB processes induced by randomly disordered Rashba SOC impurities. Next, we investigated the conductance of the helical liquid, which represents the most important transport signature observable in an experiment. We presented different approaches how to calculate this quantity in both an equilibrium, and a non-equilibrium scenario, and used a RG analysis to derive the corrections to the conductance, that are expected to arise from generic single- and two-particle backscattering processes. As TRS forbids regular elastic backscattering, the corresponding backscattering mechanisms are inelastic in nature. Hereby, an exchange of energy is mediated most commonly by nonzero electron interactions. The resulting corrections display a power-law scaling with the energy, and come with a characteristic exponent, that depends on the type of backscattering and the electron interaction strength. Importantly, the exponent related to a peculiar generic backscattering mechanism can change, if backscattering is induced by microscopic sources with a distinct scaling dynamics. This leads to crossovers of the scaling of the conductance, which could be used to identify specific perturbations in a given material. The above ideas were elaborated on for the combination of electron interactions and Rashba spin-orbit coupling, in the form of a single impurity or random disorder. An interesting contribution with a very low power-law exponent was found in the case of a single impurity, and broken Galilean invariance taken into account. Furthermore, the importance of a momentum cutoff was discussed. We find, that SOC and finite electron interactions induce backscattering only if the underlying model features non-locality, as the corresponding generic backscattering operators are as well of non-local character. Non-locality can be introduced explicitly, for instance by employing non-local potentials in a real-space description, or implicitly, by the implementation of a momentum cutoff (as it is typically done in the scheme of bosonization). A nonzero momentum cutoff renders real-space operators non-local, and is therefore of fundamental importance in this context. Besides, the concept of a missing piece appears to be essential in order to obtain the correct non-interacting limits of the inelastic backscattering corrections. Finally, we discussed magnetic moments as another important microscopic source of backscattering. Such perturbations generate elastic single-particle backscattering at the helical edge, even

at zero interaction strength, but do not break TRS, because the spin of the magnetic moment can flip as well. In the limit of very weak coupling, the equilibrium conductance as a function of the involved energy scales can be estimated by a careful treatment of the entailed spin dynamics. We find, that the result matches the behaviour of the conductance observed in Ref. [LWF$^+$15], and thus gives an alternative interpretation of the experiment in terms of magnetic moments and weak interactions.

6.2. Outlook – superconductor hybrid systems

Giving a prospect of future research, let us point out that topological insulators, and their peculiar surface states, have as well attracted a lot of attention in the context of exotic bound states with non-Abelian statistics, such as Majorana fermions or parafermions. Those could in principle be used to perform operations of fault-tolerant quantum computing [Kit03]. A key aspect hereby is the possibility to detect, and potentially manipulate the respective bound state.
It was first realized, that pairs of Majorana bound states (MBS) can exist at the boundaries of a spinless p-wave superconductor (SC), forming localized edge states in a 1D chain of atoms [Kit01]. A few years later, the discovery of new topological states of matter allowed to study similar bound states in a plethora of other candidate systems. For instance, MBS were predicted to appear in a 3D TI with proximity-induced s-wave superconductivity [FK08], or in 1D helical liquids with induced s-wave superconductivity, and in the presence of a Zeeman field [ORv10]. A simple structure of fundamental interest is given by the junction of a 1D helical liquid and an ordinary s-wave superconductor. When an additional magnetic impurity is positioned in close vicinity to the superconducting interface, a localized MBS emerges in between the magnetic and the superconducting domain [FK09b, CTD14]. Backscattering off the ferromagnetic impurity, and Andreev reflection at the superconductor boundary, then act as the two mirrors of a resonator, and confine the MBS wave function (see Fig. 6.1a). To detect Majorana bound states in an experiment, two general transport signatures are usually considered. First, tunnel current measurements in a normal-metal-superconductor (N-S) junction are expected to show a zero-bias peak, which reflects the existence of a MBS with zero energy at the interface [LLN09]. Second, in a S-N-S Josephson junction, a localized MBS leads to a 4π-periodicity of the Josephson current [Kit01, FK09a]. Suchlike characteristic fingerprints have been observed in recent transport experiments [MZF$^+$12, DRM$^+$12].
Non-Abelian fermions can in general be classified in terms of $\mathbb{Z}_n$ parafermions [AF16], where the $\mathbb{Z}_2$-case represents the Majorana fermion. Various parafermionic bound states were for instance predicted to form in an fractional quantum Hall system, at the interfaces of a Mott insulating (e.g. ferromagnetic) region and a s-wave superconductor [LBRS12, CAS13]. The authors of Ref. [OTMS15] analyze the setup of a 1D helical liquid, which is dominated by alternating sections of strong umklapp scattering and superconductivity. At the section interfaces, $\mathbb{Z}_4$ parafermionic bound states are identified, which could be detected by a 8π-periodicity of the Josephson current through the system.
Building on the above findings, an interesting setup is given by a N-S junction of a 1D helical liquid with a s-wave superconductor, in the presence of a Rashba SOC pertur-

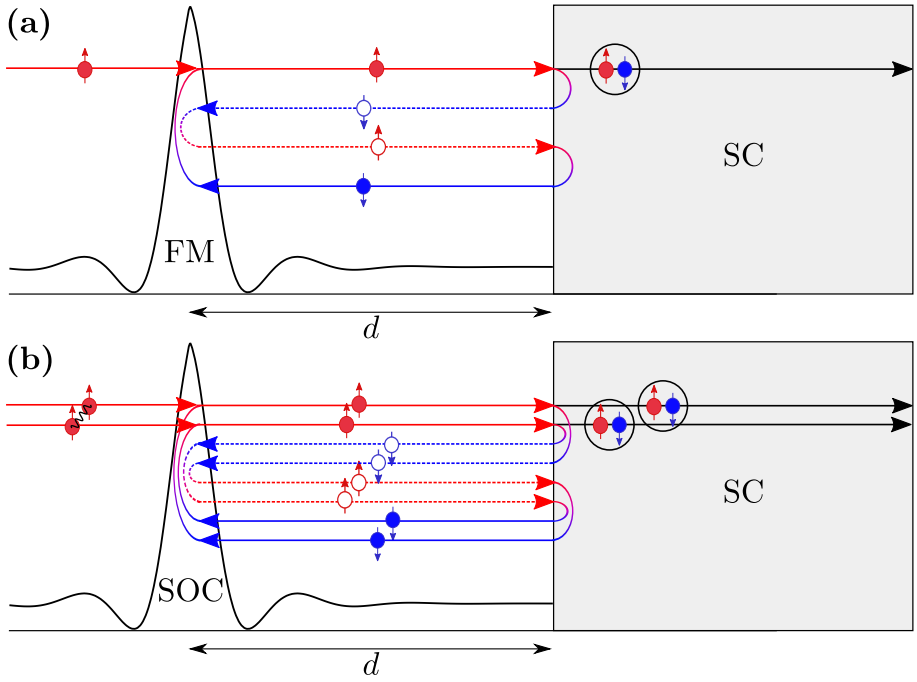

Figure 6.1.: Illustration of a helical liquid – superconductor junction, in the presence of a single, localized perturbation at a distance d from the SC surface. An incident particle is expected to be Andreev-reflected at the interface, and a Cooper pair enters the superconductor. Electrons here are denoted by full lines and full circles, while dashed lines and void circles represent holes. (a) In the case of a ferromagnetic (FM) impurity, sequential elastic single-particle backscattering leads to resonance (bound) states in the region between the impurity and the SC. Those can be shown to obey Majorana statistics [FK09b]. (b) If the ferromagnetic impurity is replaced by a Rashba spin-orbit coupling impurity, the mechanism of two-particle backscattering is induced. Importantly, the latter requires finite electron interactions (or another mediator of inelastic momentum exchange). We then expect the formation of a $\mathbb{Z}_4$-parafermionic bound state, similar to Ref. [OTMS15].

bation (see Fig. 6.1b). As the latter induces two-particle backscattering, we expect a $\mathbb{Z}_4$-parafermionic bound state at the interface, similar to the analysis of Ref. [OTMS15]. Here, however, such a bound state could emerge even in the presence of a weak, single Rashba impurity – a setup that seems more natural, and microscopically motivated. SOC perturbations could as well be created in a controlled way by an external gate on top of the QSH sample. Assuming that the superconducting gap is much larger than the energy of an incoming particle, Andreev reflection is the dominant backscattering mechanism at the SC interface. The presence of a superconducting domain then can simply be accounted for by the use of effective boundary conditions of the system [BTK82, MSGL96]. Calculating the current transmitted through the junction, in a bosonic framework, we find a characteristic modulation of its amplitude, depending on the distance between the impurity and the interface, and on the energy of the incident electron. The specific backscattering characteristics of the Rashba impurity, on the other hand, render the identification a parafermionic bound state more challenging. Since the Rashba SOC impurity can only induce inelastic backscattering, finite electron interactions need to be taken into account.

In a suchlike interacting system, properties of the single-particle wavefunctions can not be exploited easily, and the conclusive evidence of a parafermionic bound state remains difficult. A demonstration of the existence of a bound state with non-Abelian statistics at the interface, depending on the interaction strength, as well as its potential localization and electric control, could therefore be an interesting subject of further investigation.

A. Useful formulas

We here collect a few mathematical identities that are used occasionally. The Dirac delta function has the Fourier representation

$$\delta(x) = \int_{-\infty}^{\infty} \mathrm{d}k \; e^{-2\pi i k x}. \tag{A.1}$$

For exponentials of operators, the Baker-Campbell-Hausdorff formula states that, with $C = [A, B]$,

$$\exp(A)\exp(B) = \exp(A + B + \frac{1}{2}C + \frac{1}{12}[A, C] - \frac{1}{12}[B, C] + \ldots). \tag{A.2}$$

If $[A, C] = [B, C] = 0$, we find

$$\begin{aligned} e^A e^B &= e^{A+B} e^{C/2} = e^B e^A e^C, \\ [A, e^B] &= C e^B. \end{aligned} \tag{A.3}$$

In order to simplify some correlation functions, we use the identities

$$\sin(a + ib)\sin(a - ib) = \sin^2(a) + \sinh^2(b), \tag{A.4}$$

$$\arctan(x) = \frac{i}{2}\log\left(\frac{1 - ix}{1 + ix}\right). \tag{A.5}$$

With that, we can also simplify

$$\log\left(\frac{\sin(a + ib)}{\sin(a - ib)}\right) = \log\left(\frac{1 - i\tanh(b)(\tan(a))^{-1}}{1 + i\tanh(b)(\tan(a))^{-1}}\right), \tag{A.6}$$

$$-2i\arctan\left(\frac{\tanh(b)}{\tan(a)}\right) = -2i\arg\left(\tan(a) + i\tanh(b)\right). \tag{A.7}$$

Here, arg is the argument function.
In Sec. 4.4.8, we use the following approximation of an integral with finite boundaries,

$$\begin{aligned} \int_{-1/a+\epsilon'}^{1/a+\epsilon} \mathrm{d}q \; f(q) &= \left(\int_{-1/a+\epsilon'}^{-1/a} \mathrm{d}q \; + \int_{-1/a}^{1/a} \mathrm{d}q \; + \int_{1/a}^{1/a+\epsilon} \mathrm{d}q \; \right) f(q) \\ &\simeq -\epsilon' f(-1/a) + \int_{-1/a}^{1/a} \mathrm{d}q \; f(q) + \epsilon f(1/a), \end{aligned} \tag{A.8}$$

given that $\epsilon, \epsilon' \ll 1/a$.

B. Chiral fields – notation of Ref. [Gia03]

In this part, we make a connection to the notation of Ref. [Gia03], which can be considered a redefinition of bosonic operators, analogously to the one of Sec. 2.1.3. The main point is that in contrast to above, in Ref. [Gia03] the fermionic fields are defined from the start to have the same x-dependence, as $\psi_r(x) = \frac{1}{\sqrt{L}} \sum_k e^{ikx} c_{r,k}$. The density in Eq. (2.16) then reads for instance (in terms of the usual chiral fields of Eq. (2.10))

$$\rho_r(x) = (-{}^*_*\partial_x \phi_r(rx) {}^*_* + \frac{2\pi}{L} N_r)/2\pi. \tag{B.1}$$

However, since on the other hand the energy dispersion is defined in the form of $\varepsilon_r(k) = r v_F k$ (so $p = k + p_F$, compare to Eq. (2.2)), we have the time-dependence $c_{r,k}(t) = c_{r,k} e^{-irv_F kt}$, and the two chiral fields depend on $\psi_r(x,t) = \psi_r(x - rvt)$. Therefore, we also have right- and left-moving fields.
The non-chiral fields are given in terms of the chiral ones by (e.g. [Gia03], Eq. D.7)

$$\begin{aligned} \phi(x,t) &= \frac{1}{2}(\phi_R(z_+) + \phi_L(-z_-)) - \frac{\pi x}{L}(N_R + N_L), \\ \theta(x,t) &= \frac{1}{2}(-\phi_R(z_+) + \phi_L(-z_-)) + \frac{\pi x}{L}(N_R - N_L), \end{aligned} \tag{B.2}$$

where $z_r = -i(rx - vt)$, as before. In other words, $\phi_r(rz_r) = \phi(x,t) - r\theta(x,t) + \frac{2\pi x}{L} N_r$. We can thus relate the notation in Sec. 2.1.1 to the one of Ref. [Gia03] by the replacement

$$\begin{aligned} \phi_r(z_r) &\to r\phi_r(rz_r), \\ \psi_r &\to \psi_r/\sqrt{2\pi}. \end{aligned} \tag{B.3}$$

The bosonization identity reads in this language,

$$\begin{aligned} \psi_r(x) &= F_r \left(\frac{1}{2\pi a}\right)^{1/2} e^{ir(k_F - \frac{\pi}{L} + \frac{2\pi}{L} N_r)x} e^{-ir\phi_r(rx)} \\ &= F_r \left(\frac{1}{2\pi a}\right)^{1/2} e^{ir(k_F - \frac{\pi}{L})x} e^{-i(r\phi(x) - \theta(x))}. \end{aligned} \tag{B.4}$$

Note the analogy to the notation in Eq. (2.32) in a non-chiral representation. The total fermionic field is $\psi(x) = \sum_r \psi_r(x)$, since the factor of $e^{irk_F x}$ is included in Eq. (B.4).

C. OPE in lowest orders of the Rashba SOC disorder strength

C.1. OPE in first order of D_η

In this section, we explicitly present the OPE used to derive the first-order RG flow of Eqs. (4.131) and (4.133). Let us here introduce the time variables $y = v\tau$, and further abbreviate $\phi(x_1, y_1) = \phi(1)$ and $\theta(x_1, y_1) = \theta(1)$. Moreover, in H_{LL}, we rescale the fields as $\sqrt{K}\theta \to \theta$ and $\phi/\sqrt{K} \to \phi$. In order to make appear the renormalization of the Luttinger parameters K and v due to $\tilde{D}_\eta$, we expand the operator in Eq. (4.130) around a common center in time. Normal-ordering the full expression yields, with general coefficients λ, λ' (later we reinstate $\lambda = 2\sqrt{K}$),

$$
\begin{aligned}
&:\partial_x\theta_a(1)e^{i\lambda\phi_a(1)}: \times :\partial_x\theta_b(2)e^{i\lambda'\phi_b(2)}: + \text{h.c.} = h(1,2)\Big[:\partial_x\theta_a(1)\partial_x\theta_b(2)e^{i\lambda\phi_a(1)}e^{i\lambda'\phi_b(2)}: \\
&- \frac{1}{2}u(1,2):\left(\frac{\lambda}{2}\partial_x\theta_a(1) - \frac{\lambda'}{2}\partial_x\theta_b(2)\right)e^{i\lambda\phi_a(1)}e^{i\lambda'\phi_b(2)}: + \frac{1}{4}s_0(1,2):e^{i\lambda\phi_a(1)}e^{i\lambda'\phi_a(2)}:\Big] + \text{h.c.},
\end{aligned}
\tag{C.1}
$$

with some functions h, u and s_0 (see definition below), that are power-law functions in $x_1 - x_2$ and $y_1 - y_2$. To perform the OPE, we used Eq. (A.3) and the commutator in Eqs. (2.57) and (2.58). For instance, we calculate that

$$
\begin{aligned}
\left[\frac{1}{2}\left(\partial_x\varphi_R(1) - \partial_x\varphi_L(1)\right), e^{-i\frac{\lambda}{2}(\varphi_R^\dagger(2)+\varphi_L^\dagger(2))}\right] &= e^{-i\frac{\lambda}{2}(\varphi_R^\dagger(2)+\varphi_L^\dagger(2))} \\
&\times \frac{\lambda}{4}\left(\frac{1}{\overline{z}_1 - \overline{z}_2 + a} + \frac{1}{z_1 - z_2 + a}\right).
\end{aligned}
\tag{C.2}
$$

The explicit expressions in Eq. (C.1) read ([GCT14])

$$
\begin{aligned}
h(1,2) &= \left(\frac{2\pi}{L}|z_1 - z_2 + a|\right)^{\frac{\lambda\lambda'}{2}}, \\
u(1,2) &= \frac{1}{z_1 - z_2 + a} + \frac{1}{\overline{z}_1 - \overline{z}_2 + a} = \frac{2(y_1 - y_2 + a)}{|z_1 - z_2 + a|^2}, \\
u_2(1,2) &= \frac{1}{(z_1 - z_2 + a)^2} + \frac{1}{(\overline{z}_1 - \overline{z}_2 + a)^2} = \frac{2\left((y_1 - y_2 + a)^2 - (x_1 - x_2)^2\right)}{|z_1 - z_2 + a|^4}, \\
s_0(1,2) &= u_2(1,2) - \frac{\lambda\lambda'}{4}u(1,2)^2 = \frac{2\left((1 - \frac{\lambda\lambda'}{2})(y_1 - y_2 + a)^2 - (x_1 - x_2)^2\right)}{|z_1 - z_2 + a|^4}.
\end{aligned}
\tag{C.3}
$$

Away from half filling, only opposite signs $\lambda' = -\lambda$ are allowed due to the disorder-averaging procedure. Next, we contract the time variables in Eq. (C.1), which is safely possible in the normal-ordered expression. To do so, we go to relative and center of mass coordinates, $y = y_1 - y_2$ and $Y = (y_1 + y_2)/2$, and expand the exponentials in normal-ordering signs around small time distances $y \approx 0$. We can simplify these expressions even further, recalling that $x_1 = x_2 = x$. Given that suchlike time contractions can only be performed for fields diagonal in the replica indices, we drop the replica index in the process of the OPE. This short-time expansion reveals the following contributions,

$$\begin{aligned} :\partial_x\theta(1)e^{i\lambda\phi(1)}: \times :\partial_x\theta(2)e^{-i\lambda\phi(2)}: + \text{h.c.} \simeq h(y):(\partial_x\theta(x,Y))^2: \\ \times \left[1 - \frac{1}{2}u(y)\lambda^2(y+a) + \frac{1}{4}s_0(y)\frac{\lambda^2}{2}(y+a)^2\right]. \end{aligned} \tag{C.4}$$

With the help of the equation of motion, $\partial_Y\phi(x,Y) = -i\partial_x\theta(x,Y)$, we hereby used the expansion

$$\begin{aligned} e^{i\lambda\phi(x,Y+y/2)}e^{-i\lambda\phi(x,Y-y/2)} &\simeq 1 + i\lambda y\partial_Y\phi(x,Y) - \frac{1}{2}\lambda^2y^2(\partial_Y\phi(x,Y))^2 \\ &= 1 + \lambda y\partial_x\theta(x,Y) + \frac{1}{2}\lambda^2y^2(\partial_x\theta(x,Y))^2. \end{aligned} \tag{C.5}$$

A regularization in the form of $y \to y + a$ was introduced in Eq. (C.4), anticipating divergences for vanishing separations. Note, that since no term of the form $(\partial_x\phi)^2$ appears, only the combination vK will be renormalized by the Rashba SOC, while v/K remains unaffected. To identify the RG flow, we consider the action expanded up to first order in $\tilde{D}_\eta$, and use Eqs. (4.130) and (C.4), with $\lambda = 2\sqrt{K}$, to write

$$\begin{aligned} \mathcal{T}\exp\left[\int d\tau_1 d\tau_2 H_{\text{dis}}(\tau_1,\tau_2)\right] \simeq \frac{\tilde{D}_\eta}{2}\left(\frac{1}{\pi^2 aK}\right)\left(\frac{2\pi a}{L}\right)^{2K}\int \mathrm{d}x\,\mathrm{d}Y\,:(\partial_x\theta(x,Y))^2: \\ \times\,\mathcal{T}\int \mathrm{d}y\,\left(\frac{2\pi}{L}|y+a|\right)^{-2K}\left[1 - 4K + K\,(1+2K)\right] + \text{h.c.}. \end{aligned} \tag{C.6}$$

Time-ordering makes sure that the time difference is positive, $y \geq 0$. In addition to the contribution that has the form of the kinetic energy, we face an integral over the time distances y. Performing a contraction of y in the sense of Sec. 4.8, the above integral transforms into a factor of $2ad\ell\,(2\pi a/L)^{-2K}$. Again, as explained in Sec. 4.8, such a contraction embodies the effect of rescaling by an infinitesimal value $d\ell$. The missing piece was dropped, because it only represents an unimportant correction here. If we implemented it, instead of $d\ell$, we would get a factor of $1 + d\ell$. We find that upon rescaling, the first-order expansion in Eq. (C.6) eventually provides a term (another factor of two comes from the conjugate terms)

$$\mathcal{T}\exp\left[\int d\tau_1 d\tau_2 H_{\text{dis}}(\tau_1,\tau_2)\right] \simeq \left(\frac{2\tilde{D}_\eta v}{\pi^2 K}\right)(1-K)(1-2K)d\ell\int \mathrm{d}x\,\mathrm{d}\tau\,:(\partial_x\theta(x,\tau))^2:. \tag{C.7}$$

In the last step, we went back to imaginary time by $Y = v\tau$.
After re-exponentiation, the Rashba disorder thus contributes in first order to the renormalization of the product vK in H_{LL}, as (note that the fields were transformed back to $\theta \to \sqrt{K}\theta$),

$$\begin{aligned} -\frac{Kv(a(1+d\ell))}{2\pi} &= -\frac{Kv(a)}{2\pi} + \frac{4\tilde{D}_\eta}{2\pi^2}(1-K)(1-2K)v d\ell, \\ \frac{d}{d\ell}(Kv)(l) &= -\frac{4\tilde{D}_\eta}{\pi}(1-K)(1-2K)v. \end{aligned} \tag{C.8}$$

Using that v/K is not renormalized, the result can be rewritten in terms of K and v separately, as done in Eq. (4.133).
Importantly, adding the missing piece (see Sec. 4.8) does not seem necessary here [GCT14], as the RG already captures the correct non-interacting limit. A missing piece could still be implemented though, which would result in some corrections to Eq. (C.8). Here, however, we consider such corrections of minor importance, and Eq. (C.8) sufficient for the purpose of analyzing the physical picture. The reason why no missing piece is required here to obtain the correct limit, is again related to the fact that in first order, $\tilde{D}_\eta$ can not generate interaction terms of the type g_2 or g_4. The effect of Rashba disorder, in this order of the perturbation, can thus be understood as a renormalization of the effective Fermi velocity only.
Interestingly, the contraction in first order of $\tilde{D}_\eta$ never allows for terms of the form of generic inelastic SPB, proportional to $\partial_x^2\theta(x)e^{i\lambda\phi(x)}$. Formally, this is because we can not keep the exponential factor and, at the same time, expand it to gain another derivative. It therefore appears that to such a lowest order, Rashba disorder does not induce inelastic SPB, similar to what we have observed in Sec. 4.4 within a fermionic perturbation theory.

C.2. OPE in second order of D_η

Expanding the disorder action up to second order in $\tilde{D}_\eta$, we have with Eq. (4.130),

$$\begin{aligned} &\mathcal{T}\exp\left[\int \mathrm{d}\tau_1\ \mathrm{d}\tau_2\ H_{\mathrm{dis}}(\tau_1,\tau_2)\right] \\ &\simeq \frac{1}{2}\tilde{D}_\eta^2\frac{1}{(2\pi^2 a)^2}\left(\frac{2\pi a}{L}\right)^{4K}\sum_{a,b,c,d=1}^{N}\int \mathrm{d}x\ \mathrm{d}x'\ \mathrm{d}y_1\ \mathrm{d}y_2\ \mathrm{d}y_3\ \mathrm{d}y_4 \\ &\quad\times \mathcal{T}{:}\partial_x\theta_a(1)e^{i\lambda\phi_a(1)}{:}\times{:}\partial_x\theta_b(2)e^{-i\lambda\phi_b(2)}{:}\times{:}\partial_x\theta_c(3)e^{i\lambda\phi_c(3)}{:}\times{:}\partial_x\theta_d(4)e^{-i\lambda\phi_d(4)}{:}, \end{aligned} \tag{C.9}$$

where we used the notation $x_1 = x_2 = x$ and $x_3 = x_4 = x'$. Clearly, the OPE contains plenty of terms, but here we focus only on the possibility of TPB. Therefore, we aim at contracting two out of the four time variables. Time-ordering now is important, since it enforces a rearrangement of the operators. Focusing only on the terms mentioned above, we perform the respective time contractions in the process of the OPE, which results in

(with general coefficients λ),

$$\begin{aligned}
&\mathcal{T}{:}\partial_x\theta_a(1)e^{i\lambda\phi_a(1)}{:}\times{:}\partial_x\theta_b(2)e^{-i\lambda\phi_b(2)}{:}\times{:}\partial_x\theta_c(3)e^{i\lambda\phi_c(3)}{:}\times{:}\partial_x\theta_d(4)e^{-i\lambda\phi_d(4)}{:}\\
&=\mathcal{T}{:}\partial_x\theta_a(1)e^{i\lambda\phi_a(1)}{:}\times{:}\partial_x\theta_c(3)e^{i\lambda\phi_c(3)}{:}\times{:}\partial_x\theta_b(2)e^{-i\lambda\phi_b(2)}{:}\times{:}\partial_x\theta_d(4)e^{-i\lambda\phi_d(4)}{:}\\
&\simeq(2a(1+d\ell))^2h(x-x')^2\frac{1}{2^4}\mathcal{T}{:}e^{i\lambda\phi_a(x,y_1)}e^{i\lambda\phi_a(x',y_1)}{::}e^{-i\lambda\phi_b(x,y_2)}e^{-i\lambda\phi_b(x',y_2)}{:}\\
&\quad\times\Big[s_0(x-x')^2+2\lambda^2s_0(x-x')(u(1,2)+\tilde{u}(1,2))^2+(u_2(1,2)^2+\tilde{u}_2(1,2)^2)\\
&\quad+2\frac{\lambda^2}{4}(u_2(1,2)+\tilde{u}_2(1,2))(u(1,2)+\tilde{u}(1,2))^2+\left(\frac{\lambda}{2}(u(1,2)+\tilde{u}(1,2))\right)^4\Big].
\end{aligned}\tag{C.10}$$

Both position variables x, x' were kept, while contracting individually $y_3 \to y_1$ and $y_4 \to y_2$. The power-law functions $h, s_0, \tilde{u}$ and $\tilde{u}_2$ in principle take the same form as the functions h, s_0, u, u_2 given above, however, they arise from different contractions, and come with different arguments. Explicitly, we have (with Eq. (C.3)), $h(x-x') = h(1,2)|_{\lambda'=\lambda,\ y_1=y_2}$, $s_0(x-x') = s_0(1,2)|_{\lambda'=\lambda,\ y_1=y_2}$, and furthermore $\tilde{u}(1,2) = u(1,2)|_{y_1-y_2\to y,\ x_1-x_2\to x-x'}$ and $\tilde{u}_2(1,2) = u_2(1,2)|_{y_1-y_2\to y,\ x_1-x_2\to x-x'}$. In Eq. (C.10), the first term is expected to be the most dominant one, since all other terms decay with increasing time distances $y_1 - y_2$. In a lowest-order approximation, we therefore take into account only this first term, identifying a TPB-contribution of the form

$$\begin{aligned}
\mathcal{T}\exp\left[\int \mathrm{d}\tau_1\ \mathrm{d}\tau_2\ H_{\mathrm{dis}}(\tau_1,\tau_2)\right] &\simeq \frac{1}{2a^4}\left(\frac{\tilde{D}_\eta}{\pi^2K}\right)^2\left(\frac{2\pi a}{L}\right)^{8K}\sum_{a,b}\int \mathrm{d}x\ \mathrm{d}x'\ \mathrm{d}y_1\ \mathrm{d}y_2\ (1+2d\ell)\\
\times m\left(\frac{x-x'}{a}\right)\mathcal{T}{:}e^{i\lambda\phi_a(x,y_1)}e^{i\lambda\phi_a(x',y_1)}{::}e^{-i\lambda\phi_b(x,y_2)}e^{-i\lambda\phi_b(x',y_2)}{:}&+\text{h.c.}.
\end{aligned}\tag{C.11}$$

Here, the missing piece is kept, and turns out to be essential for the correct non-interacting limit. The dependence on the spatial distance is embodied in the form factor ($\lambda = 2\sqrt{K}$)

$$m\left(\frac{x-x'}{a}\right) = \left(\frac{(1-2K)-\left(\frac{x-x'}{a}\right)^2}{\left(1+\left(\frac{x-x'}{a}\right)^2\right)^{2-K}}\right)^2 . \tag{C.12}$$

Rescaling ϕ such that $\lambda = 2$ in Eq. (C.11), we obtain Eq. (4.137) of the main text.

D. Details about the calculation in Chap. 5

D.1. Derivation of the mixed spin correlations in Eq. (5.29)

In this section, we give a derivation of the spin-spin correlation functions of Eq. (5.29) in an equilibrium approach, following Refs. [VGG16, Väy16]. Generally, the average of an observable O can be written as (compare Sec. 3.2.1) $\langle O(t)\rangle = \mathrm{Tr}[\rho(t)O]/Z_0$. Here, $\rho(t)$ entails the full complexity of the system, as it evolves in time with the full Hamiltonian $H = H_0 + H_J$, where we use for now the most general Kondo coupling from Eq. (5.2). Calculating the average with respect to $\rho(t)$ will therefore be difficult, and we have to think of some simplifications. The simplest option was obviously to expand $\rho(t)$ in the coefficients J_{ij}, which to lowest order yields the Kubo formula. The solution for a general $\rho(t)$ can be found from the Heisenberg equation of motion,

$$\partial_t \rho(t) = i[\rho(t), H]. \tag{D.1}$$

Adapting to the notation of the above references, we now denote time-dependent operators in the interaction picture by $O_I(t) = e^{iH_0 t} O e^{-iH_0 t}$. In the interaction picture, we have $\langle O(t)\rangle = \mathrm{Tr}[\rho(t)O]/Z_0 = \mathrm{Tr}[\rho_I(t)O_I(t)]/Z_0$. In particular, $\rho_I(t) = e^{iH_0 t}\rho(t)e^{-iH_0 t}$, where we can use the fact that $\partial_t(\rho_I(t)) = [\partial_t\rho(t)]_I(t) + i[H_0, \rho(t)]$ to obtain from Eq. (D.1),

$$\partial_t(\rho_I(t)) = i[\rho_I(t), (H_J)_I(t)]. \tag{D.2}$$

This, in turn, leads us to the formal solution for ρ_I,

$$\rho_I(t) = \rho_0 + i\int_{-\infty}^{t} \mathrm{d}t' \, [\rho_I(t'), (H_J)_I(t')]. \tag{D.3}$$

For H_J, note the equivalency of $(S_i s_j)_I(t) = (S_i)_I(t)(s_j)_I(t) = S_i(s_j)_I(t)$, since the impurity spin remains time-independent. The time-dependent operator average then takes the form

$$\begin{aligned}\langle O(t)\rangle &= \frac{1}{Z_0}\mathrm{Tr}[\rho_I(t)O_I(t)] = \langle O(t)\rangle_0 + i\int_{-\infty}^{t} \mathrm{d}t' \, \mathrm{Tr}\left([\rho_I(t'), (H_J)_I(t')]O_I(t)\right)/Z_0 \\ &= \langle O(t)\rangle_0 + i\int_{-\infty}^{t} \mathrm{d}t' \, \left\langle [(H_J)_I(t'), O_I(t)]\right\rangle. \end{aligned} \tag{D.4}$$

In the last line, we used the cyclic permutation properties of the trace. The above expression is still exact, however, of a self-consistent form. Note that we arrive at the Kubo formula (see Eq. (3.14)), if we approximated $\rho(t)$ by ρ_0 in the last term on the right hand

side of Eq. (D.4), such that $\langle(\ldots)\rangle \to \langle(\ldots)\rangle_0$. We can use the general form of Eq. (D.4) to write the spin-spin correlation function as

$$\begin{aligned}\langle S_k(t){:}s_l(t){:}\rangle &= i\int_{-\infty}^{t} \mathrm{d}t'\ \langle\big[\,(H_J)_I\,(t'),(S_k{:}s_l{:})_I(t)\big]\rangle \\ &= i\sum_{ij} J_{ij}\int_{-\infty}^{t}\mathrm{d}t'\ \big(\frac{1}{2}i\sum_n \epsilon_{ikn}\,\langle S_n\{(s_j)_I(t'),{:}(s_l)_I(t){:}\}\rangle \\ &\quad + \frac{1}{4}\delta_{ik}\,\langle[(s_j)_I(t'),{:}(s_l)_I(t){:}]\rangle\,\big). \end{aligned} \tag{D.5}$$

Note that the unperturbed average vanishes, $\langle S_k(t){:}s_l(t){:}\rangle_0 = 0$, because of $\langle{:}s_l(t){:}\rangle_0 = 0$. We used the commutation relations in Eq. (5.3), as well as $[S_i s_j, S_k{:}s_l{:}] = \frac{1}{2}[S_i,S_k]\{s_j,{:}s_l{:}\} + \frac{1}{2}\{S_i,S_k\}[s_j,{:}s_l{:}]$, where $\{S_i,S_k\} = \frac{1}{2}\delta_{ik}$.
Next, two important approximations are made in order to obtain a practicable solution for the above mixed correlation functions. First, we assume that the electron spin and the impurity spin averages can be evaluated separately. Furthermore, the electron spin average is approximately taken with respect to the free system, which allows us to write above $\langle S_n(t')\{(s_j)_I(t'),{:}(s_l)_I(t){:}\}\rangle \simeq \langle S_n(t')\rangle\langle\{(s_j)_I(t'),{:}(s_l)_I(t){:}\}\rangle_0$. Formally, this is equivalent to approximating the density matrix by a direct product, $\rho_I(t') = \rho_S(t')\otimes\rho_0$, where ρ_S only acts on the magnetic moment S. Second, we estimate that $\langle S_n(t')\rangle \approx \langle S_n(t)\rangle$, which seems justified, as the electron spin correlations decay much faster with time than the impurity spin average [VGG16].
Using these two approximations, we arrive at

$$\begin{aligned}\langle S_k(t){:}s_l(t){:}\rangle &\simeq i\sum_{ij} J_{ij}\int_{-\infty}^{t}\mathrm{d}t'\ \big(\frac{1}{2}i\sum_n \epsilon_{ikn}\langle S_n(t)\rangle\langle\{(s_j)_I(t'),{:}(s_l)_I(t){:}\}\rangle_0 \\ &\quad + \frac{1}{4}\delta_{ik}\langle[(s_j)_I(t'),{:}(s_l)_I(t){:}]\rangle_0\big) \\ &= -\sum_{ij} J_{ij}\left(\sum_n \epsilon_{ikn}\langle S_n(t)\rangle \mathrm{Re}C_{jl} + \frac{1}{2}\delta_{ik}\mathrm{Im}C_{jl}\right), \end{aligned} \tag{D.6}$$

with a spin-spin correlation that takes the form of $C_{jl} = \int_{-\infty}^{t} dt'\langle(s_j)_I(t'){:}(s_l)_I(t){:}\rangle_0 = \int_0^\infty dt'\langle(s_j)_I(0){:}(s_l)_I(t'){:}\rangle_0$. This is Eq. (5.29) of the main text (the index "I" is dropped there for brevity, so $(s_j)_I(t) = s_j(t)$).

D.2. Explicit form of the Bloch parameters

The parameters $\gamma, \vec{h}$ and $\vec{c}$, making an appearance in the Bloch equations for $\langle\vec{S}\rangle$ in Eq. (5.41), take the form (here we use the general, and bare couplings J_{ij})

$$\gamma = -\begin{pmatrix} -\sum_{k\neq x}\left((J_{kx}^2+J_{ky}^2)\mathrm{Re}C_{xx} + J_{kz}^2\mathrm{Re}C_{zz}\right) \\ (J_{xx}J_{yx}+J_{xy}J_{yy})\mathrm{Re}C_{xx} + J_{xz}J_{yz}\mathrm{Re}C_{zz} \\ (J_{xx}J_{zx}+J_{xy}J_{zy})\mathrm{Re}C_{xx} + J_{xz}J_{zz}\mathrm{Re}C_{zz} \end{pmatrix}$$

$$\begin{pmatrix} (J_{xx}J_{yx}+J_{xy}J_{yy})\mathrm{Re}C_{xx} + J_{xz}J_{yz}\mathrm{Re}C_{zz} & (J_{xx}J_{zx}+J_{xy}J_{zy})\mathrm{Re}C_{xx} + J_{xz}J_{zz}\mathrm{Re}C_{zz} \\ -\sum_{k\neq y}\left((J_{kx}^2+J_{ky}^2)\mathrm{Re}C_{xx} + J_{kz}^2\mathrm{Re}C_{zz}\right) & (J_{yx}J_{zx}+J_{yy}J_{zy})\mathrm{Re}C_{xx} + J_{yz}J_{zz}\mathrm{Re}C_{zz} \\ (J_{yx}J_{zx}+J_{yy}J_{zy})\mathrm{Re}C_{xx} + J_{yz}J_{zz}\mathrm{Re}C_{zz} & -\sum_{k\neq z}\left((J_{kx}^2+J_{ky}^2)\mathrm{Re}C_{xx} + J_{kz}^2\mathrm{Re}C_{zz}\right) \end{pmatrix}, \tag{D.7}$$

$$\vec{h} = \begin{pmatrix} \frac{1}{2}\rho eV J_{xz} - (J_{zy}J_{yx} - J_{zx}J_{yy})\mathrm{Re}C_{xy} \\ \frac{1}{2}\rho eV J_{yz} + (J_{zy}J_{xx} - J_{zx}J_{xy})\mathrm{Re}C_{xy} \\ \frac{1}{2}\rho eV J_{zz} - (J_{yy}J_{xx} - J_{yx}J_{xy})\mathrm{Re}C_{xy} \end{pmatrix}, \tag{D.8}$$

$$\vec{c} = \begin{pmatrix} (J_{zy}J_{yx} - J_{yy}J_{zx})\mathrm{Im}C_{xy} \\ (J_{xy}J_{zx} - J_{zy}J_{xx})\mathrm{Im}C_{xy} \\ (J_{yy}J_{xx} - J_{xy}J_{yx})\mathrm{Im}C_{xy} \end{pmatrix}. \tag{D.9}$$

Assuming $J_{ij} = \mathrm{diag}(J_\perp, J_\perp, J_z)_{ij} + \delta J_{ij}$, those quantities can be expanded for small δJ, given that $\delta J_{ij} \ll J_\perp, J_z$. Hereby, we take into account only the lowest-order corrections to the δJ's. Furthermore, we lighten the notation by writing the running coupling constants $J_z(T,V), J_\perp(T,V), \delta J_{ij}(T,V)$, according to the RG flow of Eq. (5.38). To linear order in δJ, this leads, for instance, to ($\beta = 1/T$)

$$\begin{aligned} \vec{h} &\simeq \vec{e}_z \left(\frac{1}{2}\rho J_0 eV - J_0^2 \mathrm{Re}C_{xy}\right) + \begin{pmatrix} \frac{1}{2}\rho eV\delta J_{xz} + J_0\delta J_{zx}\mathrm{Re}C_{xy} \\ \frac{1}{2}\rho eV\delta J_{yz} + J_0\delta J_{zy}\mathrm{Re}C_{xy} \\ \frac{1}{2}\rho eV\delta J_{zz} - J_0(\delta J_{yy} + \delta J_{xx})\mathrm{Re}C_{xy} \end{pmatrix} \\ &= \vec{e}_z \frac{1}{2}\rho J_z(T,V) eV + \frac{1}{2}\rho eV \begin{pmatrix} \delta J_{xz}(T,V) \\ \delta J_{yz}(T,V) \\ \delta J_{zz}(T,V) \end{pmatrix}. \end{aligned} \tag{D.10}$$

Here, $\vec{e}_z$ is the unit vector in z-direction. Likewise, we find (for brevity we do not write explicitly the energy-dependence of the couplings $J_{ij}(T,V)$ in the following)

$$\begin{aligned} \gamma \simeq & \begin{pmatrix} \frac{\frac{eV}{2T}}{\tanh\frac{eV}{2T}} J_\perp^2 + J_z^2 & 0 & 0 \\ 0 & \frac{\frac{eV}{2T}}{\tanh\frac{eV}{2T}} J_\perp^2 + J_z^2 & 0 \\ 0 & 0 & 2\frac{\frac{eV}{2T}}{\tanh\frac{eV}{2T}} J_\perp^2 \end{pmatrix} \mathrm{Re}C_{zz} \\ & - \begin{pmatrix} -2\left(J_\perp \delta J_{yy} \frac{\frac{eV}{2T}}{\tanh\frac{eV}{2T}} + J_z \delta J_{zz}\right) & J_\perp(\delta J_{yx} + \delta J_{xy})\frac{\frac{eV}{2T}}{\tanh\frac{eV}{2T}} & J_\perp \delta J_{zx}\frac{\frac{eV}{2T}}{\tanh\frac{eV}{2T}} + J_z\delta J_{xz} \\ J_\perp(\delta J_{yx} + \delta J_{xy})\frac{\frac{eV}{2T}}{\tanh\frac{eV}{2T}} & -2\left(J_\perp \delta J_{xx}\frac{\frac{eV}{2T}}{\tanh\frac{eV}{2T}} + J_z\delta J_{zz}\right) & J_\perp \delta J_{zy}\frac{\frac{eV}{2T}}{\tanh\frac{eV}{2T}} + J_z\delta J_{yz} \\ J_\perp \delta J_{zx}\frac{\frac{eV}{2T}}{\tanh\frac{eV}{2T}} + J_z\delta J_{xz} & J_\perp \delta J_{zy}\frac{\frac{eV}{2T}}{\tanh\frac{eV}{2T}} + J_z\delta J_{yz} & -2J_\perp(\delta J_{xx} + \delta J_{yy})\frac{\frac{eV}{2T}}{\tanh\frac{eV}{2T}} \end{pmatrix} \\ & \times \mathrm{Re}C_{zz}\,, \end{aligned} \tag{D.11}$$

$$\vec{c} \simeq \vec{e}_z J_\perp^2 \frac{eV}{2T}\mathrm{Re}C_{zz} + \frac{eV}{2T}J_\perp \begin{pmatrix} -\delta J_{zx} \\ -\delta J_{zy} \\ \delta J_{xx} + \delta J_{yy} \end{pmatrix} \mathrm{Re}C_{zz}\,. \tag{D.12}$$

We used here, that $\mathrm{Im}C_{xy} = \mathrm{Re}C_{xx}\tanh\frac{eV}{2T}$ (see Eq. (5.30)). For simplicity, let us denote by $\gamma^{(0)}$ the first part of Eq. (D.11), which is of zeroth order in δJ, and its components $\gamma_\perp^{(0)}$ ($\gamma_z^{(0)}$) to be the first two (the third) term(s) on the diagonal. On the other hand, $\gamma^{(1)}$ is the first-order correction in δJ, and represents the second term in Eq. (D.11). An analogous notation holds for $\vec{h}^{(0)}$ and $\vec{h}^{(1)}$, as well as $\vec{c}^{(0)}$ and $\vec{c}^{(1)}$.
The steady-state impurity spin polarization, according to Eq. (5.41), eventually reads in

lowest order of δJ,

$$\begin{aligned}
\langle S_z\rangle &= \frac{1}{2}\tanh\frac{eV}{2T},\\
\langle S_x\rangle &= \langle S_z\rangle\,\frac{h_z^{(0)}\left(h_x^{(1)}+\frac{\delta J_{zy}}{J_\perp}\gamma_z^{(0)}-\gamma_{zy}^{(1)}\right)+\gamma_\perp^{(0)}\left(h_y^{(1)}-\frac{\delta J_{zx}}{J_\perp}\gamma_z^{(0)}+\gamma_{zx}^{(1)}\right)}{\left({h_z^{(0)}}^2+{\gamma_\perp^{(0)}}^2\right)},\\
\langle S_y\rangle &= \langle S_z\rangle\,\frac{h_z^{(0)}\left(h_y^{(1)}-\frac{\delta J_{zx}}{J_\perp}\gamma_z^{(0)}+\gamma_{zx}^{(1)}\right)-\gamma_\perp^{(0)}\left(h_x^{(1)}+\frac{\delta J_{zy}}{J_\perp}\gamma_z^{(0)}-\gamma_{zy}^{(1)}\right)}{\left({h_z^{(0)}}^2+{\gamma_\perp^{(0)}}^2\right)}.
\end{aligned} \tag{D.13}$$

Note that $\langle S_z\rangle$ is nonzero even in the absence of δJ, and can be expressed as $(c_z^{(0)}/\gamma_{zz}^{(0)})$. First-order corrections in δJ were thus neglected. In contrast, the averages $\langle S_{x,y}\rangle$ start from first order in δJ (compare with Eq. (5.27)).

D.3. Running couplings for $T_K \ll E \ll T^*$

At energies $T_K \ll E \ll T^*$, the exchange coupling H_{ex} becomes isotropic, $J(\ell) = J_\perp(\ell) \approx J_z(\ell)$, such that the RG flow simplifies. Furthermore, as we observe from Eq. (5.44), only certain combinations of the perturbative Kondo couplings enter into the average backscattering current. Therefore, to linear order in the perturbation, the scaling behaviour of the system can be fully described by the equations (compare with Eq. (5.7)) [Eri13]

$$\begin{aligned}
\frac{d}{d\ell}J &= \rho J^2,\\
\frac{d}{d\ell}\delta J &= -\rho J\delta J,
\end{aligned} \tag{D.14}$$

where δJ can be any of the combinations $(\delta J_{xx}-\delta J_{yy}), (\delta J_{xy}+\delta J_{yx})$ and $\sum_{i=x,y}(\delta J_{zi}+\delta J_{iz})$. In terms of energies, we obtain the solutions (see Eq. (5.10))

$$\begin{aligned}
J(E) &= \frac{J(T^*)}{1+\rho J(T^*)\log(E/T^*)} \sim \log^{-1}(E/T^*),\\
\delta J(E) &= \delta J(T^*) + \rho\delta J(T^*)J(T^*)\log(E/T^*).
\end{aligned} \tag{D.15}$$

We now have to replace in the bare couplings E_g by T^*, as the highest energy of the effective model. Note, that while the isotropic coupling J decreases logarithmically with the energy in this regime (see also Fig. 5.2), the perturbative couplings δJ actually increase logarithmically with energy.
An analysis of the backscattering current similar to the one above (for $E > T^*$), including a more exact energy crossover, could be realized in this energy regime as well. However, since the focus of interest is rather on the regime of high energies, we restrict ourselves to the qualitative conclusion that the expected correction to the backscattering current is proportional to a log squared, as was given in Eq. (5.23).

Acronyms

1D	one-dimensional
2D	two-dimensional
3D	three-dimensional
FGR	Fermi golden rule
FM	ferromagnetic impurity
LL	Luttinger liquid
MBS	Majorana bound state
N-S	normal-metal-superconductor (junction)
OPE	operator product expansion
QHE	quantum Hall effect
QSH	quantum spin Hall
RG	renormalization group
SC	superconductor
SOC	spin-orbit coupling
SPB	single-particle backscattering
TI	topological insulator
TPB	two-particle backscattering
TRS	time-reversal symmetry

Bibliography

[AF16] J. Alicea and P. Fendley. *Topological Phases with Parafermions: Theory and Blueprints*. Annual Review of Condensed Matter Physics, **7**, 119–139 (2016). doi:10.1146/annurev-conmatphys-031115-011336.

[Alc16] P. Alcorn. *Intel Xeon E5-2600 v4 Broadwell-EP Review*. `http://www.tomshardware.com/reviews/intel-xeon-e5-2600-v4-broadwell-ep,4514-2.html` (Mar 2016).

[AM76] N. W. Ashcroft and N. D. Mermin. *Solid State Physics*. Saunders (1976).

[And58] P. W. Anderson. *Absence of Diffusion in Certain Random Lattices*. Phys. Rev., **109**, 1492 (1958). doi:10.1103/PhysRev.109.1492.

[And70] P. W. Anderson. *A poor man's derivation of scaling laws for the Kondo problem*. J. Phys. C, **3**, 2436–2441 (1970). doi:10.1088/0022-3719/3/12/008.

[AR82] W. Apel and T. M. Rice. *Combined effect of disorder and interaction on the conductance of a one-dimensional fermion system*. Phys. Rev. B, **26**, 7063–7065 (1982). doi:10.1103/PhysRevB.26.7063.

[AS87] A. G. Aronov and Y. V. Sharvin. *Magnetic flux effects in disordered conductors*. Rev. Mod. Phys., **59**, 755–779 (1987). doi:10.1103/RevModPhys.59.755.

[AS10] A. Altland and B. Simons. *Condensed Matter Field Theory*. Cambridge University Press (2010). ISBN 9780521769754. doi:10.1017/CBO9780511789984.

[BB00] Y. M. Blanter and M. Büttiker. *Shot noise in mesoscopic conductors*. Phys. Rep., **336**, 1–166 (2000). doi:10.1016/S0370-1573(99)00123-4.

[BDR11] J. C. Budich, F. Dolcini, and P. Recher. *Phonon induced backscattering in helical edge states*. Phys. Rev. Lett., **108**, 086602 (2011). doi:10.1103/PhysRevLett.108.086602.

[BF04] H. Bruus and K. Flensberg. *Many-Body Quantum Theory in Condensed Matter Physics*. Oxford University Press (2004).

[BHZ06] B. A. Bernevig, T. L. Hughes, and S. C. Zhang. *Quantum Spin Hall Effect and Topological Phase Transition in HgTe Quantum Wells.* Science, **314**, 1757–1761 (2006). doi:10.1126/science.1133734.

[BKLB16] K. Bendias, M. Kessel, P. Leubner, and H. Buhmann. *Private communication* (2016).

[Blo33] F. Bloch. *Stopping power of atoms with several electrons.* Z. für Physik, **81**, 363 (1933).

[BR84] Y. A. Bychkov and E. I. Rashba. *Properties of a 2D electron gas with lifted spectral degeneracy.* JETP Letters, **39**, 78–81 (1984). doi:10.1088/0022-3719/17/33/015.

[BRW15] G. Bihlmayer, O. Rader, and R. Winkler. *Focus on the Rashba effect.* New Journal of Physics, **17**, 050202 (2015). doi:10.1088/1367-2630/17/5/050202.

[BTK82] G. E. Blonder, M. Tinkham, and T. M. Klapwijk. *Transition from metallic to tunneling regimes in superconducting microconstrictions: Excess current, charge imbalance, and supercurrent conversion.* Phys. Rev. B, **25**, 4515–4532 (1982). doi:10.1103/PhysRevB.25.4515.

[Büt86] M. Büttiker. *Four-terminal phase-coherent conductance.* Phys. Rev. Lett., **57**, 1761 (1986). doi:10.1103/PhysRevLett.57.1761.

[Büt88] M. Büttiker. *Absence of backscattering in the quantum Hall effect in multiprobe conductors.* Phys. Rev. B, **38**, 9375 (1988). doi:10.1103/PhysRevB.38.9375.

[Car96] J. Cardy. *Scaling and Renormalization in Statistical Physics.* Cambridge University Press (1996).

[CAS13] D. J. Clarke, J. Alicea, and K. Shtengel. *Exotic non-abelian anyons from conventional fractional quantum Hall states.* Nat. Comm., **4**, 1348 (2013). doi:10.1038/ncomms2340.

[CBD+12] F. Crépin, J. C. Budich, F. Dolcini, P. Recher, and B. Trauzettel. *Renormalization group approach for the scattering off a single Rashba impurity in a helical liquid.* Phys. Rev. B, **86**, 121106(R) (2012). doi:10.1103/PhysRevB.86.121106.

[Col15] P. Coleman. *Introduction to Many-Body Physics.* Cambridge university press (2015). ISBN 978-0-521-86488-6. doi:10.1017/CBO9781139020916.

[CPG00] S. Capponi, D. Poilblanc, and T. Giamarchi. *Effects of long-range electronic interactions on a one-dimensional electron system.* Phys. Rev. B, **61**, 410–417 (2000). doi:10.1103/PhysRevB.61.13410.

[CTD14] F. Crépin, B. Trauzettel, and F. Dolcini. *Evidence for Majorana bound states in transport properties of hybrid structures based on helical liquids.* Phys. Rev. B, **89**, 205115 (2014). doi:10.1103/PhysRevB.89.205115.

[CYO+12] J. G. Checkelsky, J. Ye, Y. Onose, Y. Iwasa, and Y. Tokura. *Dirac-fermion-mediated ferromagnetism in a topological insulator.* Nature Physics, **8**, 729–733 (2012). doi:10.1038/nphys2388.

[DD90] S. Datta and B. Das. *Electronic analog of the electro-optic modulator.* Appl. Phys. Lett., **56**, 665 (1990). doi:10.1063/1.102730.

[DKSD15] L. Du, I. Knez, G. Sullivan, and R.-R. Du. *Robust Helical Edge Transport in Gated InAs/GaSb Bilayers.* Phys. Rev. Lett., **114**, 096802 (2015). doi:10.1103/PhysRevLett.114.096802.

[Dol12] F. Dolcini. *Private communication* (2012).

[Dol17] F. Dolcini. *Interplay between Rashba interaction and electromagnetic field in the edge states of a 2D topological insu.* Phys. Rev. B, **95**, 85434 (2017). doi:10.1103/PhysRevB.95.085434.

[DRM+12] A. Das, Y. Ronen, Y. Most, Y. Oreg, M. Heiblum, and H. Shtrikman. *Zero-bias peaks and splitting in an Al-InAs nanowire topological superconductor as a signature of Majorana fermions.* Nat. Phys., **8**, 887–895 (2012). doi:10.1038/nphys2479.

[DSS16] G. Dolcetto, M. Sassetti, and T. L. Schmidt. *Edge physics in two-dimensional topological insulators.* Rivista del Nuovo Cimento, **39**, 113–154 (2016). doi:10.1393/ncr/i2016-10121-7.

[EK92] V. J. Emery and S. Kivelson. *Mapping of the two-channel Kondo problem to a resonant-level model.* Phys. Rev. B, **46**, 10812 (1992). doi:10.1103/PhysRevB.46.10812.

[Eri13] E. Eriksson. *Spin-orbit interactions in a helical Luttinger liquid with a Kondo impurity.* Phys. Rev. B, **87**, 235414 (2013). doi:10.1103/PhysRevB.87.235414.

[ESSJ12] E. Eriksson, A. Ström, G. Sharma, and H. Johannesson. *Electrical Control of the Kondo Effect at the Edge of a Quantum Spin Hall System.* Phys. Rev. B, **86**, 161103(R) (2012). doi:10.1103/PhysRevB.86.161103.

[FG96] M. P. A. Fisher and L. I. Glazman. *Transport in a one-dimensional Luttinger liquid.* arXiv:cond-mat/9610037 (1996).

[FK07] L. Fu and C. L. Kane. *Topological insulators with inversion symmetry.* Phys. Rev. B, **76**, 045302 (2007). doi:10.1103/PhysRevB.76.045302.

[FK08] L. Fu and C. L. Kane. *Superconducting Proximity Effect and Majorana Fermions at the Surface of a Topological Insulator*. Phys. Rev. Lett., **100**, 096407 (2008). doi:10.1103/PhysRevLett.100.096407.

[FK09a] L. Fu and C. L. Kane. *Josephson current and noise at a superconductor/quantum-spin-Hall-insulator/superconductor junction*. Phys. Rev. B, **79**, 161408(R) (2009). doi:10.1103/PhysRevB.79.161408.

[FK09b] L. Fu and C. L. Kane. *Probing Neutral Majorana Fermion Edge Modes with Charge Transport*. Phys. Rev. Lett., **102**, 216403 (2009). doi:10.1103/PhysRevLett.102.216403.

[FKM07] L. Fu, C. L. Kane, and E. J. Mele. *Topological Insulators in Three Dimensions*. Phys. Rev. Lett., **98**, 106803 (2007). doi:10.1103/PhysRevLett.98.106803.

[FN94] A. Furusaki and N. Nagaosa. *Kondo effect in a Tomonaga-Luttinger liquid*. Phys. Rev. Lett., **72**, 892 (1994). doi:10.1103/PhysRevLett.72.892.

[Fra13] E. Fradkin. *Field Theories of Condensed Matter Physics*. Cambridge University Press (2013).

[Fra16] B. H. Frank. *Google's new chip makes machine learning way faster*. `http://www.computerworld.com/article/3072652/cloud-computing/googles-new-chip-makes-machine-learning-way-faster.html` (May 2016).

[Fu11] L. Fu. *Topological crystalline insulators*. Phys. Rev. Lett., **106**, 106802 (2011). doi:10.1103/PhysRevLett.106.106802.

[FW16] Y. Fan and K. L. Wang. *Spintronics Based on Topological Insulators*. Spin, **6**, 1640001 (2016). doi:10.1142/S2010324716400014.

[GCT14] F. Geissler, F. Crépin, and B. Trauzettel. *Random Rashba spin-orbit coupling at the quantum spin Hall edge*. Phys. Rev. B, **89**, 235136 (2014). doi:10.1103/PhysRevB.89.235136.

[GCT15] F. Geissler, F. Crépin, and B. Trauzettel. *Evidence for broken Galilean invariance at the quantum spin Hall edge*. Phys. Rev. B, **92**, 235108 (2015). doi:10.1103/PhysRevB.92.235108.

[Gia91] T. Giamarchi. *Umklapp scattering and resisitivity in one-dimensional fermion systems*. Phys. Rev. B, **44**, 2905 (1991). doi:10.1103/PhysRevB.44.2905.

[Gia03] T. Giamarchi. *Quantum Physics in One dimension*. Clarendon Press, Oxford. International series of monographies on physics - 121 (2003).

[GKT17] F. Geissler, M. Kharitonov, and B. Trauzettel. *Backscattering in a helical liquid induced by Rashba spin-orbit coupling and electron interactions: locality and symmetry aspects.* In preparation (2017).

[GMP05] I. V. Gornyi, A. D. Mirlin, and D. G. Polyakov. *Dephasing and weak localization in disordered Luttinger liquid.* Phys. Rev. Lett., **95**, 046404 (2005). doi:10.1103/PhysRevLett.95.046404.

[GMP07] I. V. Gornyi, A. D. Mirlin, and D. G. Polyakov. *Electron transport in a disordered Luttinger liquid.* Phys. Rev. B, **75**, 085421 (2007). doi:10.1103/PhysRevB.75.085421.

[GNT04] A. Gogolin, A. Nersesyan, and A. Tsvelik. *Bosonization and strongly correlated systems.* Cambridge University Press (2004). ISBN 9780521617192.

[GR07] I. S. Gradsteyhn and I. M. Ryzhik. *Table of integrals, series and products, 7th edition.* Elsevier (2007).

[GS88] T. Giamarchi and H. J. Schulz. *Anderson localization and interactions in one-dimensional metals.* Phys. Rev. B, **37**, 325–340 (1988). doi:10.1103/PhysRevB.37.325.

[Hal81a] F. D. M. Haldane. *Effective harmonic-Fluid approach to low-energy properties of one-dimensional quantum fluids.* Phys. Rev. Lett., **47**, 1840–1843 (1981). doi:10.1103/PhysRevLett.47.1840.

[Hal81b] F. D. M. Haldane. *'Luttinger liquid theory' of one-dimensional quantum fluids. I. Properties of the Luttinger model and their extension to the general 1D interacting spinless Fermi gas.* J. Phys. C, **14**, 2585–2609 (1981). doi:10.1088/0022-3719/14/19/010.

[Hal82] B. I. Halperin. *Quantized Hall conductance, current-carrying edge states, and the existence of extended states in a two-dimensional disordered potential.* Phys. Rev. B, **25**, 2185–2190 (1982). doi:10.1103/PhysRevB.25.2185.

[Hal92] F. D. M. Haldane. *Varenna lectures, Proceedings.* arXiv:cond-mat/0505529 (1992).

[HQW+08] D. Hsieh, D. Qian, L. Wray, Y. Xia, Y. S. Hor, R. J. Cava, and M. Z. Hasan. *A topological Dirac insulator in a quantum spin Hall phase.* Nature, **452**, 970–974 (2008). doi:10.1038/nature06843.

[IG09a] A. Imambekov and L. I. Glazman. *Phenomenology of One-Dimensional Quantum Liquids Beyond the Low-Energy Limit.* Phys. Rev. Lett., **102**, 126405 (2009). doi:10.1103/PhysRevLett.102.126405.

[IG09b] A. Imambekov and L. I. Glazman. *Universal Theory of Nonlinear Luttinger Liquids*. Science, **323**, 228–231 (2009). doi:10.1126/science.1165403.

[ISG12] A. Imambekov, T. Schmidt, and L. Glazman. *One-dimensional quantum liquids: Beyond the Luttinger liquid paradigm*. Rev. Mod. Phys., **84**, 1253 (2012). doi:10.1103/RevModPhys.84.1253.

[KB62] L. P. Kadanoff and G. Baym. *Quantum statistical mechanics: Green's function methods in equilibrium and nonequilibrium problems*. W. A. Benjamin (1962).

[KDP80] K. v. Klitzing, G. Dorda, and M. Pepper. *New method for high accuracy determination of the fine structure constant based on quantized Hall resistance*. Phys. Rev. Lett., **45**, 494 (1980). doi:10.1103/PhysRevLett.45.494.

[KDS11] I. Knez, R.-R. Du, and G. Sullivan. *Evidence for Helical Edge Modes in Inverted InAs/GaSb Quantum Wells*. Phys. Rev. Lett., **107**, 136603 (2011). doi:10.1103/PhysRevLett.107.136603.

[Kel64] L. V. Keldysh. *Diagram technique for nonequilibrium processes*. Jetp, **20**, 1080 (1964). doi:10.1007/BF02724324.

[KF92a] C. L. Kane and M. P. A. Fisher. *Transmission through barriers and resonant tunneling in an interacting one-dimensional electron gas*. Phys. Rev. B, **46**, 15233 (1992). doi:10.1103/PhysRevB.46.15233.

[KF92b] C. L. Kane and M. P. A. Fisher. *Transport in a One-Channel Luttinger liquid*. Phys. Rev. Lett., **68**, 1220–1223 (1992). doi:10.1103/PhysRevLett.68.1220.

[KGCM14] N. Kainaris, I. V. Gornyi, S. T. Carr, and A. D. Mirlin. *Conductivity of a generic helical liquid*. Phys. Rev. B, **90**, 075118 (2014). doi:10.1103/PhysRevB.90.075118.

[KHR93] D. V. Khveshchenko, R. Hlubina, and T. M. Rice. *Non-Fermi-liquid behavior in two dimensions due to long-ranged current-current interactions*. Phys.Rev. B, **48**, 10766 (1993). doi:10.1103/PhysRevB.48.10766.

[Kit01] A. Y. Kitaev. *Unpaired Majorana fermions in quantum wires*. Physics Uspekhi, **44**, 131 (2001). doi:10.1070/1063-7869/44/10S/S29.

[Kit03] A. Y. Kitaev. *Fault-tolerant quantum computation by anyons*. Ann. Phys., **1**, 2–30 (2003). doi:10.1016/S0003-4916(02)00018-0.

[KM05a] C. Kane and E. J. Mele. *Quantum Spin Hall Effect in Graphene*. Phys. Rev. Lett., **95**, 226801 (2005). doi:10.1103/PhysRevLett.95.226801.

[KM05b] C. L. Kane and E. J. Mele. *Z_2 Topological Order and the Quantum Spin Hall Effect*. Phys. Rev. Lett., **95**, 146802 (2005). doi:10.1103/PhysRevLett.95.146802.

[Kni16] W. Knight. *Five Lessons from AlphaGo's Historic Victory*. `https://www.technologyreview.com/s/601072/five-lessons-from-alphagos-historic-victory/` (Mar 2016).

[Kon64] J. Kondo. *Resistance Minimum in Dilute Magnetic Alloys*. Prog. Theor. Phys., **32**, 37–49 (1964). doi:10.1143/PTP.32.37.

[Kor50] J. Korringa. *Nuclear magnetic relaxation and resonance line shift in metals*. Physica, **16**, 601–610 (1950). doi:10.1016/0031-8914(50)90105-4.

[KRB16] L. Kimme, B. Rosenow, and A. Brataas. *Backscattering in helical edge states from a magnetic impurity and Rashba disorder*. Phys. Rev. B, **93**, 081301 (2016). doi:10.1103/PhysRevB.93.081301.

[KWB+07] M. König, S. Wiedmann, C. Brüne, A. Roth, H. Buhmann, L. W. Molenkamp, X.-L. Qi, and S.-C. Zhang. *Quantum spin hall insulator state in HgTe quantum wells.* Science, **318**, 766–70 (2007). doi:10.1126/science.1148047.

[Lan57a] L. D. Landau. *Oscillations in a Fermi Liquid*. Soviet Phys. JETP, **5**, 101 (1957). doi:10.1016/B978-0-08-010586-4.50096-1.

[Lan57b] L. D. Landau. *The theory of a Fermi liquid*. Soviet Physics Jetp, **3**, 920 (1957). doi:10.1016/B978-0-08-010586-4.50095-X.

[Lau83] R. B. Laughlin. *Anomalous quantum Hall effect: An incompressible quantum fluid with fractionally charged excitations*. Phys. Rev. Lett., **50**, 1395–1398 (1983). doi:10.1103/PhysRevLett.50.1395.

[LBRS12] N. H. Lindner, E. Berg, G. Refael, and A. Stern. *Fractionalizing majorana fermions: Non-abelian statistics on the edges of abelian quantum hall states*. Phys. Rev. X, **2**, 041002 (2012). doi:10.1103/PhysRevX.2.041002.

[LHQ+08] C. Liu, T. L. Hughes, X.-L. Qi, K. Wang, and S.-C. Zhang. *Quantum Spin Hall Effect in Inverted Type II Semiconductors*. Phys. Rev. Lett., **100**, 236601 (2008). doi:10.1103/PhysRevLett.100.236601.

[Lin15] A. Linn. *Microsoft researchers win ImageNet computer vision challenge*. `https://blogs.microsoft.com/next/2015/12/10/microsoft-researchers-win-imagenet-computer-vision-challenge/#sm.0007nxg2okftdsn11bt1pl7fue786` (Dec 2015).

[LLN09] K. T. Law, P. A. Lee, and T. K. Ng. *Majorana Fermion Induced Resonant Andreev Reflection*. Phys. Rev. Lett., **103**, 237001 (2009). doi:10.1103/PhysRevLett.103.237001.

[LOB12] N. Lezmy, Y. Oreg, and M. Berkooz. *Single and multiparticle scattering in helical liquid with an impurity*. Phys. Rev. B, **85**, 235304 (2012). doi:10.1103/PhysRevB.85.235304.

[Lut63] J. M. Luttinger. *An Exactly Soluble Model of a Many-Fermion System*. J. Math. Phys., **4**, 1154 (1963). doi:10.1063/1.1704046.

[LvR+14] C. H. Li, O. M. J. van't Erve, J. T. Robinson, Y. Liu, L. Li, and B. T. Jonker. *Electrical detection of charge-current-induced spin polarization due to spin-momentum locking in Bi2Se3*. Nature Nanotechnology, **9**, 218–224 (2014). doi:10.1038/nnano.2014.16.

[LWF+15] T. Li, P. Wang, H. Fu, L. Du, K. A. Schreiber, X. Mu, X. Liu, G. Sullivan, G. A. Csáthy, X. Lin, and R.-R. Du. *Observation of a Helical Luttinger Liquid in InAs/GaSb Quantum Spin Hall Edges*. Phys. Rev. Lett., **115**, 136804 (2015). doi:10.1103/PhysRevLett.115.136804.

[Mac07] J. Maciejko. *An Introduction to Nonequilibrium Many-Body Theory*. Springer (2007).

[Mar05] T. Martin. *Noise in mesoscopic physics; Les Houches lecture notes*. arXiv:cond-mat/0501208 (2005).

[Mas95] D. L. Maslov. *Transport through dirty Luttinger liquids connected to reservoirs*. Phys. Rev. B, **52**, R14368 (1995). doi:10.1103/PhysRevB.52.R14368.

[Mas05] D. L. Maslov. *Fundamental aspects of electron correlations and quantum transport in one-dimensional systems*. arXiv:cond-mat/0506035v1 (2005).

[MB07] J. E. Moore and L. Balents. *Topological invariants of time-reversal-invariant band structures*. Phys. Rev. B, **75**, 121306(R) (2007). doi:10.1103/PhysRevB.75.121306.

[ML65] D. C. Mattis and E. H. Lieb. *Exact Solution of a Many-Fermion System and Its Associated Boson Field*. J. Math. Phys., **6**, 304–312 (1965). doi:10.1063/1.1704281.

[MLO+09] J. Maciejko, C. Liu, Y. Oreg, X.-L. Qi, C. Wu, and S.-C. Zhang. *Kondo Effect in the Helical Edge Liquid of the Quantum Spin Hall State*. Phys. Rev. Lett., **102**, 256803 (2009). doi:10.1103/PhysRevLett.102.256803.

[Moo65] G. E. Moore. *Cramming more components onto integrated circuits.* Electronics, **38**, 114–117 (1965).

[Moo75] G. E. Moore. *Progress In Digital Integrated Electronics.* IEEE, IEDM Tech Digest, pages 11–13 (1975).

[MS95] D. L. Maslov and M. Stone. *Landauer conductance of Luttinger liquids with leads.* Phys. Rev. B, **52**, R5539 (1995). doi:10.1103/PhysRevB.52.R5539.

[MSGL96] D. L. Maslov, M. Stone, P. M. Goldbart, and D. Loss. *Josephson current and proximity effect in Luttinger liquids.* Phys. Rev. B, **53**, 1548–1557 (1996). doi:10.1103/PhysRevB.53.1548.

[MZF+12] V. Mourik, K. Zuo, S. M. Frolov, S. R. Plissard, E. P. a. M. Bakkers, and L. P. Kouwenhoven. *Signatures of Majorana Fermions in.* Science, **336**, 1003 (2012). doi:10.1126/science.1222360.

[Nev15] A. H. Nevidomskyy. *Many-Body Physics: From Kondo to Hubbard.* E. Pavarini, E. Koch, and P. Coleman (Eds.), Verlag des Forschungszentrum Jülich (2015).

[NH79] D. R. Nelson and B. I. Halperin. *Dislocation mediated melting in two dimensions.* Phys. Rev. B, **19**, 2457–2484 (1979). doi:10.1103/PhysRevB.19.2457.

[Noz74] P. Nozières. *A "fermi-liquid" description of the Kondo problem at low temperatures.* J. Low Temp. Phys., **17**, 31–42 (1974). doi:10.1007/BF00654541.

[ORv10] Y. Oreg, G. Refael, and F. von Oppen. *Helical liquids and Majorana bound states in quantum wires.* Phys. Rev. Lett., **105**, 177002 (2010). doi:10.1103/PhysRevLett.105.177002.

[OTMS15] C. P. Orth, R. P. Tiwari, T. Meng, and T. L. Schmidt. *Non-Abelian parafermions in time-reversal-invariant interacting helical systems.* Phys. Rev. B, **91**, 081406 (2015). doi:10.1103/PhysRevB.91.081406.

[PBW03] C. S. Peça, L. Balents, and K. J. Wiese. *Fabry-Perot interference and spin filtering in carbon nanotubes.* Phys. Rev. B, **68**, 205423 (2003). doi:10.1103/PhysRevB.68.205423.

[Pon95] V. V. Ponomarenko. *Renormalization of the one-dimensional conductance in the Luttinger-liquid model.* Phys. Rev. B, **52**, R8666—-R8667 (1995). doi:10.1103/PhysRevB.52.R8666.

[QZ10] X.-L. Qi and S.-C. Zhang. *The quantum spin Hall effect and topological insulators.* Physics Today, **63**, 33–38 (2010). doi:10.1063/1.3293411.

[Ram07] J. Rammer. *Quantum field theory of non-equilibrium states*. Cambridge University Press (2007). ISBN 9780521874991. doi:10.1017/CBO9780511618956.

[RBB+09] A. Roth, C. Brüne, H. Buhmann, L. W. Molenkamp, J. Maciejko, X.-L. Qi, and S.-C. Zhang. *Nonlocal transport in the quantum spin Hall state*. Science, **325**, 294–7 (2009). doi:10.1126/science.1174736.

[RSOF+16] J.-C. Rojas-Sánchez, S. Oyarzún, Y. Fu, A. Marty, C. Vergnaud, S. Gambarelli, L. Vila, M. Jamet, Y. Ohtsubo, A. Taleb-Ibrahimi, P. Le Fèvre, F. Bertran, N. Reyren, J. M. George, and A. Fert. *Spin to Charge Conversion at Room Temperature by Spin Pumping into a New Type of Topological Insulator: α-Sn Films*. Phys. Rev. Lett., **116**, 096602 (2016). doi:10.1103/PhysRevLett.116.096602.

[Sak67] J. J. Sakurai. *Advanced Quantum Mechanics*. Addison-Wesley, Reading, MA (1967).

[SBGV+16] J. Sánchez-Barriga, E. Golias, A. Varykhalov, J. Braun, L. V. Yashina, R. Schumann, J. Minàr, H. Ebert, O. Kornilov, and O. Rader. *Ultrafast spin polarization control of Dirac fermions in topological insulators*. Phys. Rev. B, **93**, 155426 (2016). doi:10.1103/PhysRevB.93.155426.

[Sch18] W. Schottky. *Über spontane Stromschwankungen in verschiedenen Elektrizitätsleitern*. Ann. Phys., **57**, 541–567 (1918). doi:10.1002/andp.19183622304.

[Sch61] J. Schwinger. *Brownian Motion of a Quantum Oscillator*. J. Math. Phys., **2**, 407 (1961). doi:10.1063/1.1703727.

[Sch97] K. Schönhammer. *Interacting fermions in one dimension: The Tomonaga-Luttinger model*. arXiv:cond-mat/9710330v3 (1997).

[Sha94] R. Shankar. *Renormalization-group approach to interacting fermions*. Rev. Mod. Phys., **66**, 129–192 (1994). doi:10.1103/RevModPhys.66.129.

[Sim16] T. Simonite. *Moore's Law Is Dead. Now what?* `https://www.technologyreview.com/s/601441/moores-law-is-dead-now-what/` (May 2016).

[SJJ10] A. Ström, H. Johannesson, and G. I. Japaridze. *Edge Dynamics in a Quantum Spin Hall State: Effects from Rashba Spin-Orbit Interaction*. Phys. Rev. Lett., **104**, 256804 (2010). doi:10.1103/PhysRevLett.104.256804.

[SMHG99] O. A. Starykh, D. L. Maslov, W. Häusler, and L. I. Glazman. *Gapped Phases of Quantum Wires*. arXiv:cond-mat/9911286 (1999). doi:10.1007/3-540-46438-7_3.

[SND+14] E. M. Spanton, K. C. Nowack, L. Du, G. Sullivan, R.-R. Du, and K. A. Moler. *Images of Edge Current in InAs / GaSb Quantum Wells*. Phys. Rev. Lett., **113**, 026804 (2014). doi:10.1103/PhysRevLett.113.026804.

[SNK+14] Y. Shiomi, K. Nomura, Y. Kajiwara, K. Eto, M. Novak, K. Segawa, Y. Ando, and E. Saitoh. *Spin-electricity conversion induced by spin injection into topological insulators*. Phys. Rev. Lett., **113**, 196601 (2014). doi:10.1103/PhysRevLett.113.196601.

[Sól79] J. Sólyom. *The Fermi gas model of one-dimensional conductors*. Advances in Physics, **28**, 201–303 (1979). doi:10.1080/00018737900101375.

[SRvG12] T. L. Schmidt, S. Rachel, F. von Oppen, and L. I. Glazman. *Inelastic electron backscattering in a generic helical edge channel*. Phys. Rev. Lett., **108**, 156402 (2012). doi:10.1103/PhysRevLett.108.156402.

[SS95] I. Safi and H. J. Schulz. *Transport in an inhomogeneous interacting one-dimensional system*. Phys. Rev. B, **52**, R17040 (1995). doi:10.1103/PhysRevB.52.R17040.

[TFM11] Y. Tanaka, A. Furusaki, and K. A. Matveev. *Conductance of a helical edge liquid coupled to a magnetic impurity*. Phys. Rev. Lett., **106**, 236402 (2011). doi:10.1103/PhysRevLett.106.236402.

[THS95] S. Tarucha, T. Honda, and T. Saku. *Reduction of Quantized Conductance at Low-Temperatures Observed in 2 to 10 μm-long Quantum Wires*. Solid State Communications, **94**, 413–418 (1995). doi:10.1016/0038-1098(95)00102-6.

[TKND82] D. Thouless, M. Kohmoto, M. Nightingale, and M. Dennijs. *Quantized Hall Conductance in a Two-Dimensional Periodic Potential*. Phys. Rev. Lett., **49**, 405–408 (1982). doi:10.1103/PhysRevLett.49.405.

[Tom50] S.-I. Tomonaga. *Remarks on Bloch's method of sound waves applied to many-fermion problems*. Prog. Theor. Phys., **5**, 544–569 (1950). doi:10.1143/PTP.5.544.

[TSG82] D. C. Tsui, H. L. Stormer, and A. C. Gossard. *Two-Dimensional Magnetotransport in the Extreme Quantum Limit*. Phys. Rev. Lett., **48**, 1559 (1982). doi:10.1103/PhysRevLett.48.1559.

[Väy16] J. Väyrynen. *Private communication* (2016).

[VGG13] J. I. Väyrynen, M. Goldstein, and L. I. Glazman. *Helical edge resistance introduced by charge puddles*. Phys. Rev. Lett., **110**, 216402 (2013). doi:10.1103/PhysRevLett.110.216402.

[VGG16] J. I. Väyrynen, F. Geissler, and L. I. Glazman. *Magnetic moments in a helical edge can make weak correlations seem strong*. Phys. Rev. B, **93**, 241301(R) (2016). doi:10.1103/PhysRevB.93.241301.

[VGGG14] J. I. Väyrynen, M. Goldstein, Y. Gefen, and L. I. Glazman. *Resistance of helical edges formed in a semiconductor heterostructure*. Phys. Rev. B, **90**, 115309 (2014). doi:10.1103/PhysRevB.90.115309.

[VO11] J. I. Väyrynen and T. Ojanen. *Electrical Manipulation and Measurement of Spin Properties of Quantum Spin Hall Edge States*. Phys. Rev. Lett., **106**, 76803 (2011). doi:10.1103/PhysRevLett.106.076803.

[vS98] J. von Delft and H. Schoeller. *Bosonization for Beginners — Refermionization for Experts*. Ann. Phys., **7**, 225–305 (1998). doi:10.1002/(SICI)1521-3889(199811)7:4<225::AID-ANDP225>3.0.CO;2-L.

[Wal16] M. M. Waldrop. *More than Moore*. Nature, **530**, 144–147 (2016).

[WBZ06] C. Wu, B. A. Bernevig, and S.-C. Zhang. *The Helical Liquid and the Edge of Quantum Spin Hall Systems*. Phys. Rev. Lett., **96**, 106401 (2006). doi:10.1103/PhysRevLett.96.106401.

[Wil75] K. G. Wilson. *The renormalization group: Criticial phenomena and the Kondo problem*. Rev. Mod. Phys., **47**, 773 (1975). doi:10.1103/RevModPhys.47.773.

[Win03] R. Winkler. *Spin–Orbit Coupling Effects in Two-Dimensional Electron and Hole Systems*, volume 191. Springer Verlag (2003). ISBN 978-3-540-01187-3. doi:10.1007/b13586.

[Wra12] L. A. Wray. *Device Physics: Topological transistor*. Nature Physics, **8**, 705–706 (2012). doi:10.1038/nphys2410.

[WZ72] K. G. Wilson and W. Zimmermann. *Operator product expansions and composite field operators in the general framework of quantum field theory*. Commun. math. Phys., **24**, 87–106 (1972). doi:10.1007/BF01878448.

[XLCF16] H. Y. Xie, H. Li, Y. Z. Chou, and M. S. Foster. *Topological Protection from Random Rashba Spin-Orbit Backscattering: Ballistic Transport in a Helical Luttinger Liquid*. Phys. Rev. Lett., **116**, 86603 (2016). doi:10.1103/PhysRevLett.116.086603.

[XM06] C. Xu and J. E. Moore. *Stability of the quantum spin Hall effect: Effects of interactions, disorder, and Z_2 topology.* Phys. Rev. B, **73**, 045322 (2006). doi:10.1103/PhysRevB.73.045322.

[YLD94] Y. Yu, Y. M. Li, and N. D'Ambrumenil. *Bosonization for 2D Interacting Fermion Systems: Non-Fermi Liquid Behavior.* Mod. Phys. Lett. B, **8**, 59 (1994). doi:10.1142/S0217984994000078.

[ZCT15] N. T. Ziani, F. Crépin, and B. Trauzettel. *Fractional Wigner Crystal in the Helical Luttinger Liquid.* Phys. Rev. Lett., **115**, 206402 (2015). doi:10.1103/PhysRevLett.115.206402.

[ZvD00] G. Zaránd and J. von Delft. *Analytical calculation of the finite-size crossover spectrum of the anisotropic two-channel Kondo model.* Phys. Rev. B, **61**, 6918–6933 (2000). doi:10.1103/PhysRevB.61.6918.

Acknowledgement

I like to thank all my colleagues from the group TP IV in Würzburg, who created a very pleasant social and professional atmosphere, and in particular my supervisor Prof. Björn Trauzettel for continuous guidance and support. I further wish to acknowledge the persons I had the chance to collaborate with, or that assisted in various projects in the form of an active scientific exchange, to mention explicitly are François Crépin, Jan Budich, Nikolaos Kainaris, Thomas Schmidt, Jukka Väyrynen and Maxim Kharitonov. It was a pleasure to participate in international conferences and schools such as the Capri spring school, or the jointly organized ENB/VITI PhD meetings. The hospitality of the Karlsruhe Institute of Technology (Prof. Gornyi) and the Yale university (Prof. Glazman) is greatly appreciated. Financial support was thankfully granted by the DFG (SFB 1170 and SPP 1666), the Helmholtz Foundation (VITI), and the Elitenetzwerk Bayern (ENB graduate school on topological insulators).

List of publications

1. Jukka I. Väyrynen, Florian Geissler, and Leonid I. Glazman. *Magnetic moments in a helical edge can make weak correlations seem strong*, Phys. Rev. B, **93**, 241301(R) (2016)

2. Florian Geissler, François Crépin, and Björn Trauzettel. *Evidence for broken Galilean invariance at the quantum spin Hall edge*, Phys. Rev. B, **92**, 235108 (2015)

3. Florian Geissler, François Crépin, and Björn Trauzettel. *Random Rashba spin-orbit coupling at the quantum spin Hall edge*, Phys. Rev. B, **89**, 235136 (2014)

4. Florian Geissler, Jan Carl Budich, and Björn Trauzettel. *Group theoretical and topological analysis of the quantum spin Hall effect in silicene*, New J. Phys., **15** (2013) 085030